Formulation and characterization of siRNA embedded nanoparticles for pulmonary delivery

Inaugural dissertation

of the Faculty of Science,

University of Bern

presented by

Christoph Martin Zimmermann

from Germany

Supervisor of the doctoral thesis:

Prof. Dr. Paola Luciani

Department of Chemistry, Biochemistry and Pharmaceutical Sciences

Formulation and characterization of siRNA embedded nanoparticles for pulmonary delivery

Inaugural dissertation

of the Faculty of Science,

University of Bern

presented by

Christoph Martin Zimmermann

from Germany

Supervisor of the doctoral thesis:

Prof. Dr. Paola Luciani

Department of Chemistry, Biochemistry and Pharmaceutical Sciences

Accepted by the Faculty of Science.

Bern, 12.12.2022

The Dean

Prof. Dr. Marco Herwegh

To my parents and my wife

Abstract

Advancing existing or developing novel nanoparticle carrier systems is a crucial part of successful nucleic acid delivery for therapeutic purposes. The overall aim of nanoparticle formulations is to deliver their cargo to the site of action. During this procedure, nanoparticles need to show qualities to be internalized into the cell and release their cargo. Dependent on the application route and prior to cell uptake, nanoparticles can be transferred into a form of administration that improves conformation and leads to long-term storage stability.

The aim of this thesis is to identify various small interfering RNA (siRNA)-nanoparticle formulations as drug delivery systems with potential to target the lungs (Chapter I + II). Nanoparticles carrier systems comprised of polymers, lipids or a hybrid combination encapsulating nucleic acids and were formed using the concept of microfluidic mixing. The thesis can be separated into two main parts. The first part addresses the common dilemma of the endosomal escape problem by improving existing polymers through chemical modification (Chapter III), synthesizing a novel amphiphilic polymer (Chapter IV) and forming hybrid lipid polyplex nanoparticles (Chapter V). The second section focuses on the development of a spray-drying approach (Chapter VI) and the long-term storage under various conditions (Chapter VI) for siRNA-lipid nanoparticles (LNPs) based on an adapted Onpattro® formulation.

The endosomal release problem of polymeric nanoparticles was tackled looking at physicochemical nanoparticle characterization and *in vitro* performance assessment. Throughout Chapters III - V, sizes of 100 – 200 nm were reached, the zeta potential was kept neutral to positive, and the encapsulation efficiency of siRNA showed values > 90% resulting in an improved in vitro knockdown performance (> 50%) in comparison to polyethylene imine (PEI) polyplexes or triblock copolymer polyplexes cores.

The establishment of a spray drying platform for LNPs (Chapter VI) and subsequent drying for storage stability (Chapter VII) resulted in spray dried powders that maintained LNP integrity and stability by losing up to 15% of siRNA and lipid content. The aerodynamic properties showed ideal characteristics for pulmonary delivery with sizes of 3 µm. The *in vitro* performance reached knockdown levels of > 95% and a house keeping gene silencing of > 50% was established *ex vivo* in human precision cut lung slices.

In conclusion, this thesis should give an overview of several non-viral siRNA nanoparticles as nucleic acid delivery systems that on the one hand improve the endosomal escape problem of polymeric nanoparticles, and on the other hand are established for pulmonary delivery through a spray drying method.

Table of Content

Acknowledgements

I would like to express my sincere gratitude to my supervisors Prof. Dr. Paola Luciani and Prof. Dr. Olivia Merkel. Thank you for enabling a construct in which I was able to work on very exciting projects and be a part of two very special, kind and great groups. I appreciate all your help and advice that let me grow as a researcher and as a human being. I am very thankful to have presented my work at various conferences. I will never forget your support and understanding that you offered after my accident. Thank you very much!

I would like to thank the group members of Prof Luciani's Lab who welcomed me with open arms and helped me in any situation, particularly Lisa, Florian and Aymar.

The same gratitude goes to Prof Merkel's lab. Especially, Rima, Tobias, Lorenz, Bettina and Domizia created a working environment in which fun was paired with fruitful discussions. I learned a lot from you all and I would not be at this point without you! I will miss all the parties, fun and our „Stammtisch".

I want to thank Professor Dr. Gerhard Winter and Professor Dr. Wolfgang Friess for all the interesting scientific discussions and pleasant work environment. I am thankful to all PhD students from their groups who made work fun. It was a real shame that the pandemic hindered many trips to conferences but I will never forget the time that we had in Rotterdam and all the activities that we did together.

My biggest thank you belongs to my parents, Dr. Martin Zimmermann and Agneta Vesen-Zimmermann. You have given my all your support at every life step, and you have understood any decision that I have made. I was always able to count on your advice and help. I owe you so much!

Finally, I want to thank my wife, Sophie, who has been my rock. You always give me your endless support and understanding, especially if I had to work another weekend. I am so happy to have you! Thank you for everything!

A sarcastic thank you goes to the pandemic and COVID-19. Without you I would have never worked on a hot topic at the right time. Develping pulmonary therapeutics based on RNA-embedded nanoparticles enabled great collaborations and gives me the feeling that my PhD work has come at a serendipitous time.

Objectives of the thesis

Advancing existing or developing novel nanoparticle carrier systems is a crucial part of successful nucleic acid delivery for therapeutic purposes. The overall aim of nanoparticle formulations is to deliver their cargo to the site of action. During this procedure, nanoparticles need to show qualities to be internalized into the cell and release their cargo. Dependent on the application route and prior to cell uptake, nanoparticles can be transferred into an administration form that improves conformation and leads to long-term storage stability. Spray drying produces microparticle powders embedding nanoparticles keeping the cargos integrity and maintaining bioactivity for pulmonary application.

The aim of this thesis is to identify various small interfering RNA (siRNA)-nanoparticle formulations as drug delivery systems with potential to target the lungs. Nanoparticles carrier systems comprised of polymers, lipids or a hybrid combination encapsulating nucleic acids. The thesis can be separated into two main parts.

The first part addresses the common dilemma of the endosomal escape problem by improving existing polymers through chemical modification (Chapter III), synthesizing a novel amphiphilic polymer (Chapter IV) and forming hybrid lipid polyplex nanoparticles (Chapter V).

The second section focuses on the development of a spray-drying approach (Chapter VI) and the long-term storage under various conditions (Chapter VI) for siRNA-lipid nanoparticles (LNPs) based on an adapted Onpattro® formulation.

In more detail, **Chapter I** is separated into three parts. The first sections will give a short introduction to RNA interference and the discovery of small interfering RNA (siRNA). In addition, the need of a nucleic acid carrier system for drug delivery will be highlighted. The second part will explain the internalization pathway of nanoparticles linked to the endosomal escape problem. Two important aspects will be covered: What is the endosomal escape problem and what can be done to overcome it. The last section of the introduction will explain the process of spray drying. The importance of spray-drying to convert nanoparticles into pulmonary drug delivery systems with its advantages and disadvantages will conclude this chapter.

The concept of microfluidic mixing to form nanoparticles for pharmaceutical and medical application will be presented in **Chapter II**. A wide range of lipid-based, polymeric, hybrid and theranostic formulations will be covered. This chapter should give an overview of possibilities using microfluidic mixing.

Chapter III evaluates the use of an improved version of a triblock copolymer, PEG-PCL-PEI, which was already implemented as a non-viral siRNA carrier system in previous studies. Our approach consists of a microfluidic mixing method which leads to nanoparticle characterization and *in vitro* performance assessment. The main focus will be the improvement of endosomal release resulting in efficient gene downregulation.

A different approach tackling the endosomal escape problem is pursued in **Chapter IV**. We develop a novel amphiphilic poly(spermine acrylamides) polymer which represents a new class of sophisticated non-viral vectors for pulmonary siRNA delivery. Those nanoparticle systems undergo characterization, *in vitro* and *in vivo* tests. Results are compared to widely studied polyplexes based on polyethylene imine (PEI).

Rounding up the first part of the thesis and the endosomal release problem, **Chapter V** discusses the approach of coating a mediocre-working triblock copolymer, PEI-PCL-PEI, with various lipids. The idea follows the concept of using an existing polymeric nanoparticle system which faces endosomal release problems and improve its performance by addition of lipids. Lipids have shown to be successful

nanoparticle delivery systems and would help to improve the polyplex performance. The merging of both systems could disclose synergistic effects and create an efficient hybrid nanoparticle system. As for the previous chapter, a full characterization and *in vitro* testing of three different lipid coatings was performed.

The second part of the thesis deals with the spray drying of LNPs and its long-term storage at different conditions. **Chapter VI** describes the engineering of spray dried LNP powders in which an Onpattro®-derived nanoparticle system acted as the therapeutic agent. Prior to establishing the spray drying process, a novel dual emission fluorescence spectroscopy method helped to preselect the highest possible drying temperature and excipient solution maintaining LNP integrity and stability. Spray dried powders were characterized and tested for aerodynamic properties. The chapter is completed by evaluating *in vitro* performance and *ex vivo* downregulation in human precision cut lung slices (hPCLS).

Spray drying amorphous sugars, such as lactose, obtain residual moisture levels that can lead to degradation, chemical reactions or loss of efficacy. **Chapter VII** uses the spray drying approach from **Chapter VI** and applies a subsequent drying step to overcome those hurdles. A long-term storage for 3 months at 4 °C and 25 °C enables a comparative study to characterize powders and evaluate aerodynamic properties as a pulmonary delivery system. The *in vitro* performance consists of a protein downregulation in H1299 lung adenocarcinoma cells and a mRNA silencing approach in mucus excreting Calu-3 lung cancer cells.

In conclusion, this thesis should give an overview of several non-viral siRNA nanoparticles as nucleic acid delivery systems that on the one hand improve the endosomal escape problem of polymeric nanoparticles, and on the other hand are established for pulmonary delivery through a spray drying method.

Chapter I – Introduction

1. RNA interference (RNAi)

In 1998, researchers Fire and Melo discovered the RNA interference (RNAi) mechanism that enabled specific gene silencing by short, double-stranded fragments of RNA in *Caenorhabditis elegans*. [1, 2] The mechanism is shown in Figure 1. [3] Double stranded RNA (dsRNA) or exogenous short interfering RNA (siRNA) are internalized into the cytoplasma. Dicer enzymes bind to dsRNA and cleave the RNA into siRNA molecules at 20-25 base pair length. In a next step, a RNA-induced silencing complex (RISC) and its key protein Argonaute 2 (Ago2) binds to the siRNA. This complex cleaves the sense strand of the siRNA leaving the activated complex consisting of RISC, Ago2 and Antisense strand. Subsequently, messanger RNA (mRNA) is bound and cleaved which terminates the RNA interference process. As an additional benefit, the activated complex recycles to make use of further gene silencing opportunities.

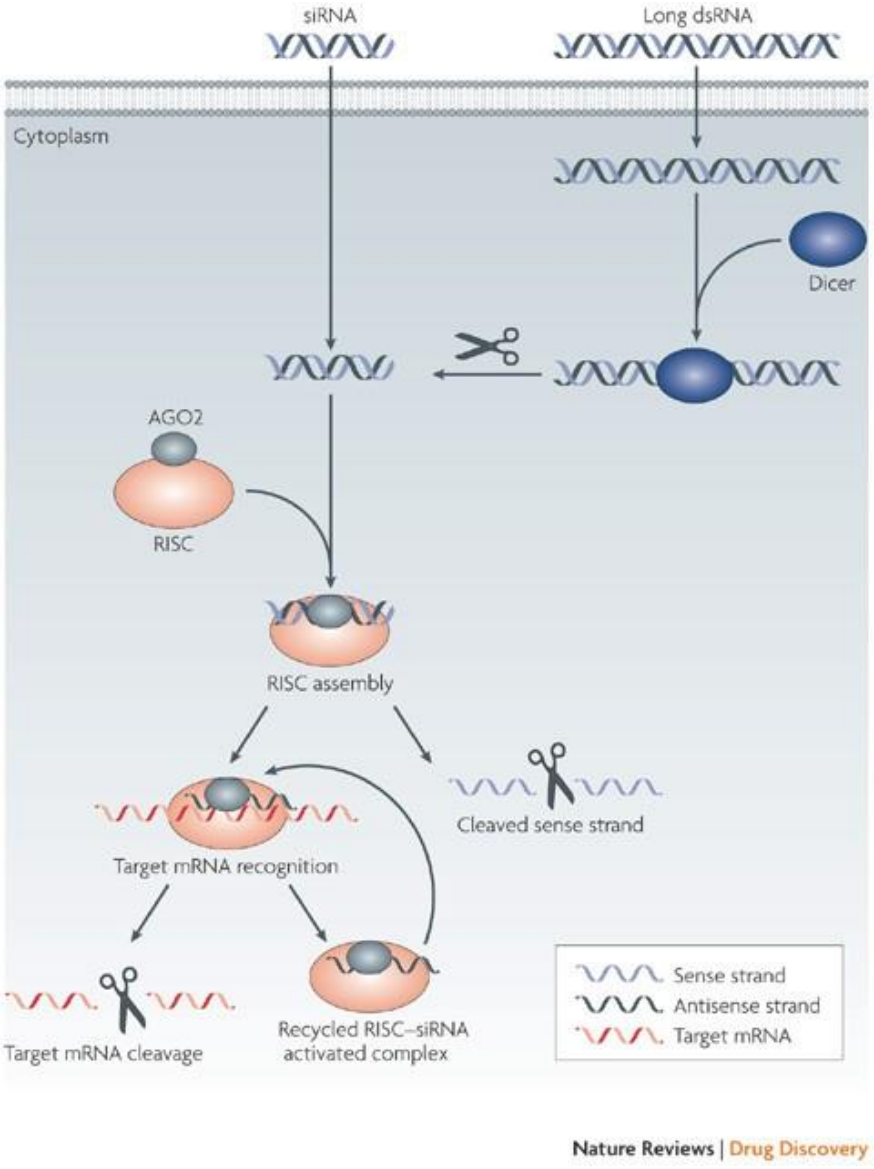

Figure 1 The mechanism of RNA interference (RNAi). Reprinted with permission of Whitehead et al., from 'Knocking down barriers: advances in siRNA delivery', Nat Rev Drug Discov, 8, 2009. [3]

This groundbreaking research paved the way for downregulating homologous mRNA, which to this day, holds an immense therapeutic potential. To induce RNAi effects, siRNA needs to enter the cytoplasm.

[4] Unfortunately, siRNA itself is unable to enter cells. The chemical structure of siRNA has been identified as the main reasons for hindering successful deliveries. siRNA is prone to degradation by nucleases, the negative charge of the phosphate backbone can be repelled by the negatively charged cell membrane, and the hydrophilic structure hinders the diffusion across cell membranes. [5, 6]

It was inevitable that effective carrier systems that encapsulate siRNA, enable nucleic acid protection, and induce cell internalization would be found. Non-viral vectors, such as polymeric or lipid nanoparticles, have proven to be successful options. [7] Despite the recent success in siRNA-based drug approvels by the Food and Drug Agency (FDA), under the names of Onpattro®, Givlaari®, Oxlumo™, Leqvio® and Amvuttra™, all drugs target liver and kidney diseases leaving several untouched therapeutic areas.

2. Endosomal Escape

Nanoparticles can cross the cellular membrane through multiple different entry routes which can be categorized into an endocytosis-based uptake pathway and a direct cellular entry pathway. [8] Research has shown that polymer- and lipid-based nanoparticles most commonly follow endocytosis to generate cell internalization. [9-11] In order to achieve nucleic acid induced therapeutic effects, nanoparticle systems need to escape the endosome to enter the cytosol, for RNA drugs, and the nucleus, for DNA drugs. [10] Several mechanisms have been studied and developed to overcome the hurdle of the endosomal escape problem, shown in Figure 2.

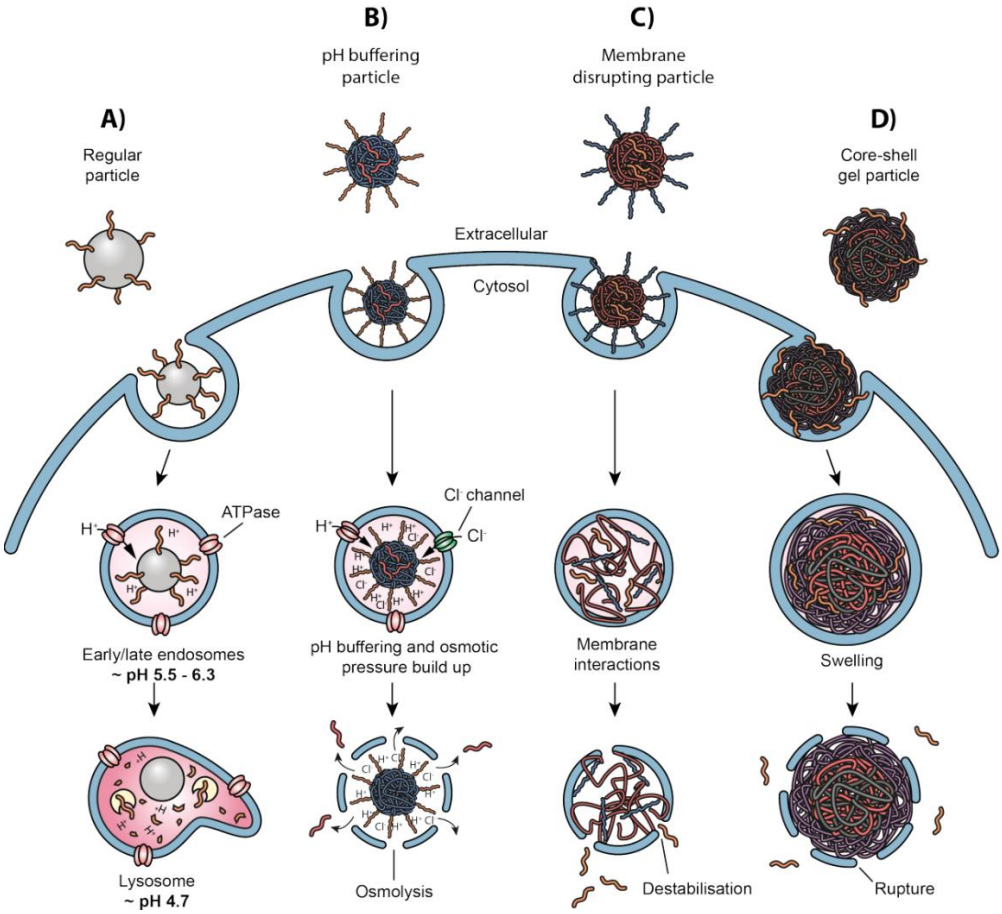

Figure 2 Endosomal escape mechanisms. A) Regular particle with no endosomal escape capabilities. B) pH buffering particle forcing osmolysis. C) Membrane disrupting particle. D) Particle swelling upon pH change. Reprinted with permission of Cupic et al., from 'Controlling endosomal escape using nanoparticle composition: current progress and future perspectives', Nanomedicine, 14, 2019. [12]

If a molecule or nanoparticle system cannot pursue an endosomal release after internalization, it will get stuck in the endosome and subsequentially trafficked into an acidic lysosome at pH 4.7 (Figure 2A).

The lysosomal compartment contains a range of enzymes, such as proteases, nucleases, esterases and lipases, whose main role is the degradation of any material. [11, 13] Therefore, nanoparticle carriers need to be engineered to overcome the endosomal escape problem. Figure 2B describes a common strategy to induce endosomal escape via the proton sponge effect based on the buffering capacity. [14, 15] Positively charged polymers or lipids can undergo pH buffering through protonation inside the acidic endosome (pH 5.5) which leads to an additional influx of protons and chloride counterions. The endosomal pressure will constantly rise which subsequently terminates in an osmolysis releasing the nanoparticle. Polymers and peptides have shown direct interaction with the endosomal membrane which leads to destabilization and hole formation for the therapeutic cargo to diffuse out of the endosome (Figure 2C). [16] Another way of inducing endosomal escape can be obtained by using core-shell gel particles which swell upon acidification forcing the membrane to rupture and releasing the cargo into the cytosol (Figure 2D). [17]

To improve the performance of polymer- or lipid-based nanoparticles, several approaches can lead to endosomal escape mechanisms, as seen in Figure 2. Either existing polymers or lipids are refined by addition of chemical modifications, or novel molecules are synthesized to use the benefit of a tailor-made approach precisely addressing the endosomal escape problem.

3. Spray drying siRNA-embedded nanoparticles

Spray drying is a procedure used in the chemical, pharmaceutical, cosmetic and food industry. In particular, inhalable powders are generated by spray drying. The process is appealing to laboratory and industrial setups because it enables rapid, continuous, reproducible, and scalable powder production in a single step. [18, 19]

Spray drying is also known as atomization drying which depends on a quick evaporation process of small water droplets through the impact of tempered air. The continuous process can be divided into three parts. First, the fluid is pumped through a nozzle into the drying chamber in which atomization of the fed material into small, micrometer-sized droplets occurs. Subsequently, the droplets dry fast in tempered air. Lastly, dried microparticles are separated from drying air by a cyclone and collected into a vessel. (Figure 3).

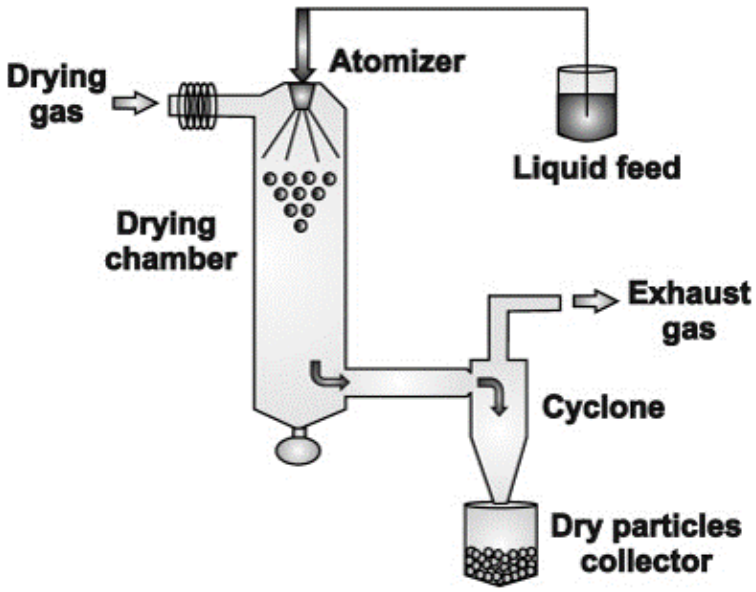

Figure 3 Spray drying process within a spray drying tower. Reprinted with permission of Sosnik et al., from 'Advantages and challenges of the spray-drying technology for the production of pure drug particles and drug-loaded polymeric carriers', Adv Colloid Interface Sci, 223, 2015. [19]

The design of the spray drying tower facilitates fine tuning of several process parameters. This includes the optimal setting of inlet and outlet temperature, flow rate of air stream, atomization pressure, spray drying speed and equipment design. [20] For instance, larger particle sizes will be obtained when combining the use of a high flow rate of the fluid feed with a large nozzle diameter. Conversely, a small nozzle diameter paired with a high atomization pressure will render in smaller particle sizes. [19]
The sprayed material comprises of solutions, suspensions, and emulsions which are usually sugar-, i.e. lactose, or sugar-alcohol-based, i.e. mannitol. Furthermore, the performance or morphology of the spray dried powder can be enhanced by the addition of amino acids, other sugars, inorganic substances, or salts.

The main advantages of spray drying are the improved chemical and physical stability of powders compared to liquid formulations as well as, process scalability and cost-effectiveness. [21, 22] Moreover, a broad spectrum of substances, including heat-sensitive molecules, can be dried without facing major adverse effects. [19, 23] Conversely, the main drawback of spray drying is the large yield loss of 30-80%. [24]
The aim of the spray drying process is the quick and product-protective production of a microparticle powder which facilitates pulmonary drug delivery characteristics while keeping the cargo integrity and demonstrating a long shelf-life stability.

Chapter II - Microfluidics for nano-pharmaceutical and medical applications

This chapter presents the first part of a book chapter that is submitted to Elsevier and peer reviewed: „Microfluidics for Cellular Applications“, editors U. Krühne, P. Luciani, G. Peroziello. Paperback ISBN: 9780128224823.

Author‘s contributions:

Friederike Adams,[a,c] Christoph M. Zimmermann [a,b], and Olivia M. Merkel [a]

F.A and C.M.Z wrote the paper and contributed equally to this work. O.M.M provided conceptual guidance and corrected the manuscript.

a. *Pharmaceutical Technology and Biopharmaceutics, Department Pharmacy, Ludwig-Maximilians-University Munich, Butenandtstr. 5-13, 81377 Munich, Germany*

b. *Pharmaceutical Technology, Department for Chemistry, Biochemistry and Pharmacy, University Bern, Freiestrasse 3, CH - 3012 Bern*

c. *Institute of Polymer Chemistry, Chair of Macromolecular Materials and Fiber Chemistry, University of Stuttgart, Pfaffenwaldring 55, 70569 Stuttgart, Germany Eberhard-Karls University of Tübingen, Geschwister-Scholl-Platz, 72074 Tübingen, Germany*

Key words: polymer, microfluidic mixing, polyplex, micelleplex, RNA therapeutics, siRNA delivery

Abstract

Microfluidic mixing techniques are versatile and facile tools for improving reproducible production of pharmaceutics on the one side and mimicking a complex cellular microenvironment on the other. In the first part of this chapter, a summary of nanoparticulate drug delivery systems synthesized by microfluidic mixing is given. Different nanocarrier systems such as polymers, lipids, or a combinatorial approach, known as hybrid systems, are discussed in terms of advantages and disadvantages. This overall aim of microfluidic platforms is to improve patient outcomes by detecting individual diseases and discovering tailor made therapies.

1. Introduction

After the approval of Doxil in 1995 and Abraxane in 2005, nanomedicine has become a popular field of research not only for improved therapeutic outcomes in oncology. The ongoing pharmaceutical and medical need of inventing and creating new drugs, cell-based approaches and manufacturing technologies has motivated the field of microfluidics. For decades, it has been known that microfluidics reduces production costs, shorten the production steps and time, while providing a production platform with reproducible outcomes. These favorable conditions explain the increased demand for microfluidic devices as all-rounders in drug development, production and screening as well as in cell culture application and tissue engineering.

This chapter will emphasize on the formation and utilization of nanoparticles for drug delivery and tissue engineering for pharmaceutical and medical applications. The first part will discuss the wide range of drug delivery systems produced using microfluidic devices. The second part will focus on *in vitro* experiments mimicking cell assays, native tissues, organs, or the entire body.

2. Nanoparticulate drug delivery systems for pharmaceutical application

Mixing plays an important role in generating appropriate drug delivery systems for pharmaceutical applications. Active pharmaceutical ingredients (APIs) show certain characteristics, such as hydrophobicity, hydrophilicity or thermolability, which need to be addressed choosing the most suitable delivery systems (Figure 1). Microfluidic mixing can be a conducive alternative to bulk mixing, particularly for the preparation of nanoparticle-based drug delivery systems. The microfluidic platform offers devices that are tailor-made, operating fast, reducing the overall costs, and becoming irreplaceable for the field of nanomedicine. Microfluidics increase the control over nanoparticle self-assembly to regulate the final nanoparticle size and size distribution, compactness, surface charge, drug loading efficiency, and release rate, which are all important properties for nanoparticle drug delivery systems. [25]

The microfluidic device plays a key role in implementing a new era for producing nanoparticle drug delivery systems. The key determinant for success of such mixing techniques is controlling the local mixing environment. While macroscopic mixing methods often result in heterogeneous particles with broad size distributions, rapid-mixing methods provide a high-throughput and continuous approach for synthesizing nanoparticles with control over size and its translation from the bench-scale to clinical volume. [25-29] As described in other book chapters, a vast variety of devices offers a multitude of choices regarding chip material (glass or polymer based), flow pattern (continuous flow, segmented flow, multi-inlet vortex mixer and micromixers), mixing system (active vs. passive) and the inner diameters and lengths. [30].

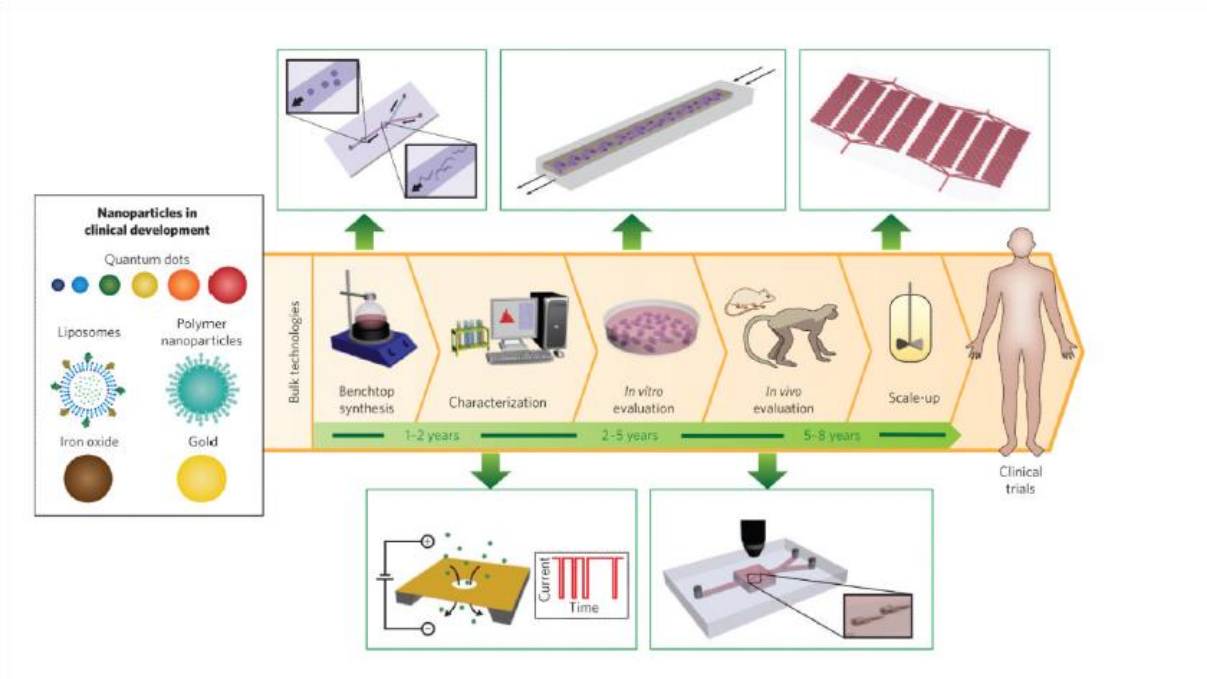

Figure 1 Microfluidic methods as improvements for nanoparticle production in clinical drug development. With permission from Ref. [31]. Copyright 2017, Elsevier.

This multitude of characteristics and combination possibilities makes the microfluidic device unique and allows to implement it practically anywhere. Due to the variety in structure and of different applications, as stated above, various approaches for creating nanoparticle drug delivery systems for pharmaceutical applications can be developed accordingly. In most nanomedicine approaches, the overall goal is drug encapsulation of small or biomolecules into particles with sizes around 100 nm or smaller (Figure 2). [32] Such small particles are preferred as natural defense mechanisms such as macrophages are known to detect and rapidly clear particles with sizes greater than approximately 250 nm. [33, 34]

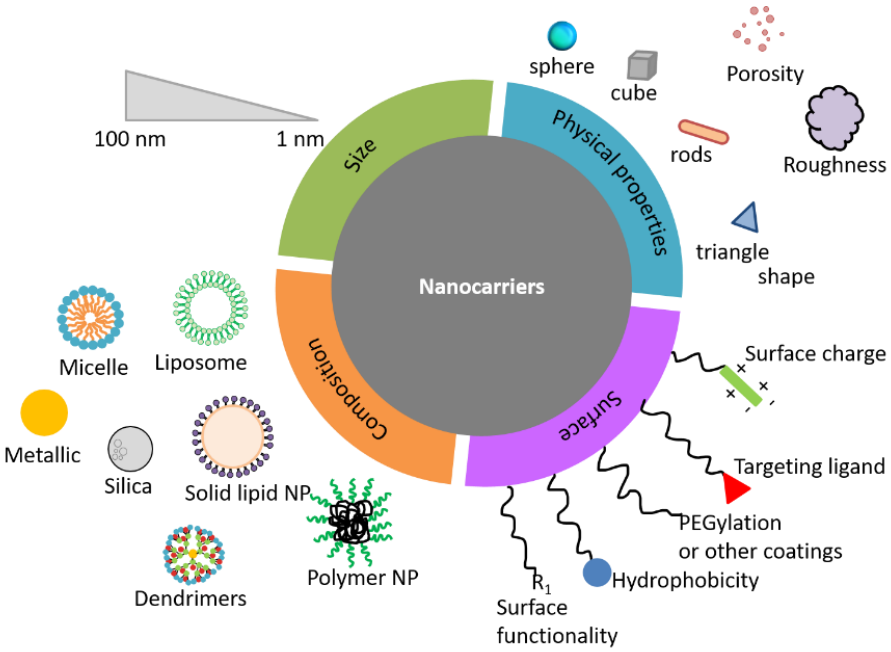

Figure 2 A summary of nanoparticle characteristics that have been explored to optimize nanocarriers for drugs.

The carrier material used for drug encapsulation can vary from polymers, lipids, inorganic materials to proteins or combinations of all the latter. If surface modification is desired, the surface is most commonly modified by linking poly(ethylene glycol) (PEGylation), changing the surface charge or binding targeting ligands. PEGylation increases colloidal stability and extends blood circulation, whereas a specific ligand is expected to enhance a specific cell targeting and binding effect. [35, 36] All these features are chosen to create a suitable and tailor-made drug delivery system adapted to the respective application.

2.1 Nanoemulsions

Preparing nanoemulsions is one of the most basic methods that can lead to the formation of nanoparticles which can be used in cosmetics, foods, and coating industries. Nanoemulsions are dispersions of two different liquids consisting of water, oil, and an emulsifier, in which hydrophilic or hydrophobic drugs can be solubilized. [37] The droplet size of the nanoemulsion varies from 5 to 500 nm. [38] Increasing the surfactant concentration can even decrease sizes. [39] Nanoemulsions can either be fabricated using low-energy approaches such as spontaneous emulsification or emulsion phase inversion methods. These types are inexpensive and simple to implement because they require no specialized equipment, and they are highly effective at producing small droplets for certain combinations of oils and emulsifiers. [40, 41] However, many oil or emulsifier types cannot be utilized in these approaches. Alternatively, high-energy approaches, which are based on homogenization, can be used. Microfluidic mixing offers a versatile set-up in which the mixing can be combined with high pressure homogenization in a one-step process to form nanoemulsion-based nanoparticles in a very efficient way. [41, 42] Microfluidics have been employed to generate stable nanoemulsions suitable for drug delivery, in which the oil and water suspensions are separately injected into the microfluidic chip forming an emulsion in procedures shown in Figure 3.

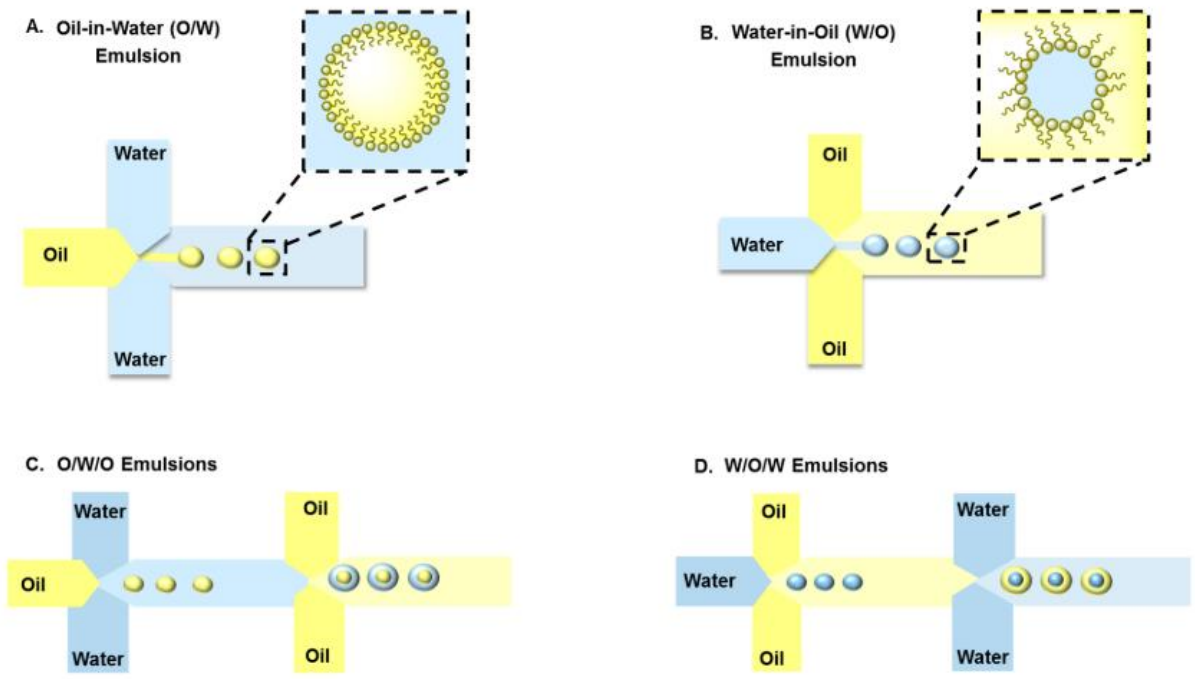

Figure 3 T-shaped microfluidic device for generating (A) oil in water (O/W), (B) water in oil (W/O), (C) oil in water in oil (O/W/O) and (D) water in oil in water (W/OW/) emulsions. With permission from Ref. [30] MDPI.

In comparison to traditional bulk emulsification, microfluidic devices are an alternative and versatile tool to generate uniform and size-controlled droplets in a nanometer scale. [30] An important feature of microfluidics is the ability to generate single, double, or multiple O/W, W/O, W/O/W and O/W/O emulsions. The flow rate of the continuous and dispersed phase controls the size, its distribution and number of droplets. [30] The formation of single, double or multiple emulsion based carriers can be achieved by combining cross-flow using X-, Y- or T-junctions, flow focusing and co-flow microfluidics. [43-45]

Bai et al. compared the use of single- and dual-chamber microfluidizers to produce nanoemulsions in regard to the emulsifier concentration and homogenization pressure on the resulting particle size. For both devices, keeping the homogenization pressure at 13 kpsi, the increase in emulsifier concentration, from 0 to 3 wt%, decreased the mean particle size from 230 nm to 110 nm. By comparing the size distribution between the two methods, it was shown, that the dual-channel method produced monomodal distribution, even at low emulsifier concentrations. However, the single-channel method produced bimodal distributions at all emulsifier concentrations. The influence on the homogenization pressure was determined using a 1 wt% emulsifier concentration. By increasing the pressure from 9 to 19 kpsi, the droplet diameter size was reduced from 1.3 µm before homogenization to 121 nm at the highest pressure. The dual-channel outperformed the single-channel in smaller particle sizes and monomodal distribution. Furthermore, the dual-channel method produced nanoemulsions at oil concentrations up to 50%. In comparison, the single-channel method was able to form nanoparticles at oil concentrations up to 10%. [41] This study shows that a dual-channel microfluidic device is more suitable for nanoparticle production based on nanoemulsions than single-channel or non-microfluidic methods. Their big advantage is that the production is performed in a single step. No premixing of the oil-water phase is necessary. Moreover, the separation of oil and water phase and merging the independent streams in a microfluidic device not only saves time and lowers the wasted materials, but also requires just a single pass of emulsion through the homogenizer, rather than multiple times for conventional homogenizers. [41]

In a recent study, Toprakciouglu et al. fabricated a T-junction droplet generator which was formed by using a two-step lithographic process to form a nanochannel-in-microchannel device. The generated droplets show monodisperse nanosized water-in-oil emulsions with controllable sizes ranging from 2500 ± 110 nm down to 51 ± 6 nm. They demonstrated that the control over the nanodroplet diameter can be achieved by varying the ratio between continuous to dispersed phase flow rate. Furthermore, they showed that adding a protein monomer to the dispersed phase will lead to protein self-assembly and consequently to the formation of protein nanogels under high temperatures. [46]

Summarizing, micro- or nanofluidic platforms provide support in various experimental set-ups to generate nanosized monodisperse nanoemulsions or nanodroplets. Their biggest advantage over general nanoemulsion fabrication is the control over the stream's flow rate resulting in tailor-made reproducible sizes and PDIs.

2.2 Liposomes

Liposomes have been investigated since the 1970s and are commonly used in cosmetics but also in clinical oncology, favored by their amphiphilicity and lipid arrangement mimicking the biological cell membrane. Liposomes consist of phospholipids and surfactants creating sizes ranging from ten nanometers to a few hundred micrometers, and they can be composed of a single shell, unilamellar or mulitlamellar shells. Due to their spontaneous assembly into spherical bilayers in aqueous environment, liposomes can be loaded with hydrophilic or hydrophobic molecules making them universally suitable for a broad range of cargoes. Common preparation methods, such as sonication, extrusion or high-pressure homogenization, allow for control over liposome size, lamellarity or drug encapsulation efficiency, but have to be performed in numerous subsequent steps. [30, 47, 48]

Liposomes show, in regard to their lipid bilayer mimicking biological membranes, a proficient encapsulation stability, non-toxicity, flexibility, biocompatibility and biodegradability. They can reduce the toxicity of the encapsulated agent as seen in Amphotericin B and Taxol. Furthermore, liposomes display the flexibility to be coupled with site-specific ligands to achieve active targeting. [49, 50] These characteristics paved the way for many liposomal-encapsulated drugs to target multiple diseases. [51] However, liposomes are also characterized by short shelf life and low physical stability, low encapsulation efficiency of certain APIs, and a rapid clearance from the bloodstream by phagocytic cells of the mononuclear phagocyte system (MPS). Moreover, liposomes show difficulties for scaling up and reaching clinical translation due to the batch-to-batch variability. [52-55]

To overcome these limitations, microfluidics help creating a single-step mixing set-up in which the liposome formation through confluence of aqueous and organic phases is concised. [56, 57] Microfluidic methods for forming liposomes consist of electroformation and hydration, extrusion, flow focusing, pulsed jetting, double emulsion templates, ice droplet hydration, transient membrane ejection and droplet emulsion transfer. [58-72] Out of all methods, flow focusing is most frequently used to form liposomes because of its simple set-up in which one substance inlet meets one or multiple solvent inlets enabling a smooth self-assembly process. Furthermore, smaller vesicles are formed and a high-throughput production is feasible. [73] Flow focusing is also favorable for delicate proteins or biomolecules because pulsed jetting, for instance, would create high shear stress which can cause aggregation and degradation of macromolecules. In addition, flow focusing can generate higher encapsulation efficiencies in comparison to ice droplet hydration, or double emulsion templates. [73]

The initial work on generating monodisperse liposomes using a flow focusing device was proposed by Jahn et al. in 2004. The microfluidic set-up consisted of three inlets, in which two rectangular aqueous buffer channels flew opposite of each other and a phospholipid plus fluorescent dye solution in isopropyl alcohol flew between the aqueous layers. Throughout the length of the device, the solvents were able to mix, and the alcohol diffused into the aqueous solution. During the process, the alcohol dilutes past a critical concentration to form liposomes spontaneously. The mean radius of the liposomes was found to decrease from 140 nm to 40 nm when the aqueous buffer to phospholipid flow rate ratio was increased from 5:1 to 50:1. Unfortunately, no information on the encapsulation efficiency of the fluorescent dye inside the liposomes was stated. [63]

Another example of using a hydrodynamic flow focusing device was published by Ran et al. They used the same one-step microfluidic method as Jahn et al. to form multifunctional liposomes. They encapsulated a fluorescence dye preparing three different formulations consisting of plain liposomes, PEGylated liposomes and folic acid-functionalized liposomes. The liposomes were formed by injecting the lipid-containing isopropanol solution to the central channel and adding phosphate buffer solution through two vertical channels. Increasing the flow rate ratio from 4:1 to 16:1 resulted in a decrease of liposomal size from 200 nm to 56 nm. Furthermore, these liposomes were stable in serum for at least 24 hours. [74]

Hamano et al. who used an automated microfluidic benchtop technology (NanoAssemblr® platform from Precision NanoSystems) to optimize curcumin loaded liposomes. [75] The advantage of using such benchtop systems lies in its easy and practical operation. Furthermore, this particular benchtop contains a cartridge with a microfluidic chip consisting of a Y-flow channel structure followed by a herringbone channel to increase diffusion and create a turbulent flow for particles to form. Most of the previously reported curcumin delivery systems suffered from low drug loading capacity, poor solubility and stability. [76, 77] Curcumin-liposomes, prepared with the above mentioned microfluidic system, exhibited a mean diameter of 120 nm with a low polydispersity index (<0.2) and superior loading capacity (17 wt. %) compared to other reported liposomal systems (<5 wt %). [78-80] Furthermore, the water solubility of curcumin was increased by 700-fold, leading to 8-20-fold increased systemic

exposure compared to the standard curcumin suspension formulation. When co-administered with cisplatin to tumor-bearing mice, such optimized curcumin-liposomes improved the antitumor efficacy of cisplatin in multiple mouse tumor models and decreased cisplatin-induced nephrotoxicity. [75]

Concluding, microfluidic mixing, especially flow focusing, helps to create monodisperse and reproducible liposomes of sizes below 100 nm and offers distinct advantages over macroscale or batch approaches. The biggest advantage is that by increasing the flow rate ratio between aqueous and alcoholic solution, the liposomal sizes decrease. However, the decrease is not linear, and a method optimization is important for every independent liposomal system.

2.3 Lipid nanoparticles

Lipid nanoparticle (LNP) delivery technology is a revolutionary development that has grown since its first approved drug formulation, AmBisome, in Europe in 1990 and enabled clinical translation of gene therapies. LNPs can deliver small molecules, siRNA, mRNA, DNA, or gene-editing complexes. [81-86] Most of all, the use of nucleic acids provides opportunities to treat diseases by silencing pathogenic genes, expressing therapeutic proteins, or correcting genetic defects. [87]

LNPs are solid particles at room and body temperature, consisting of solid lipids or a mixture of a solid lipid and a liquid lipid. In comparison, liposomes are spherical vesicles formed by phospholipids and other physiologic lipids. [88] LNPs can be produced by high-pressure homogenization, ultra-sonication, double emulsion or solvent injection method. All these methods follow LNP formation via the same steps: formation, size reduction, purification, and sterile filtration. In particular, size reduction via extrusion is a challenging process, particularly when nucleic acids are encapsulated in LNPs. [89, 90] Microfluidic mixing, involving its rapid mixing, merges the formation and size reduction into a single-step method. A water-miscible organic phase, i.e., ethanol that contains lipids, is mixed with an aqueous phase containing the respective small molecules or nucleic acids. Purification can be incorporated by using tangential flow filtration to remove the solvents, as well as any non-entrapped materials. Furthermore, a buffer exchange can be performed setting the needed pH value and stabilizing the formulation. [29, 91] It is favorable to use an organic solvent, such as ethanol, having a boiling point lower than water to easily remove or evaporate it in the last step. [82]

Chen et al. used a rapid microfluidic mixing system to form LNPs entrapping siRNA by introducing groove structures to the device. The method consisted of a stepwise ethanol dilution. Hence, an alcoholic solution of the lipid was mixed with an equal volume of aqueous siRNA solution. Hereby, water decreased the lipid solubility and promoted LNP self-assembly. Further dilution with aqueous solution reduced the ethanol content and prevented particle aggregation. Furthermore, a high reproducibility of nanoparticle sizes of 70 nm for flow rates above 200 µL/min was shown and the encapsulation efficiency was determined at 80%. [92] One example of successful LNP loading with siRNA via microfluidics was the biggest breakthrough of siRNA therapeutics resulting in the EMA (European Medicines Agency) and FDA (Food and Drug Association, USA) approval of Onpattro® (Patisiran) for the treatment of hereditary amyloidogenic transthyretin (TTR) amyloidosis. The LNPs were formed by combining an ethanolic lipid stream, consisting of an ionizable-lipid, DLin-MC3-DMA (hepatriaconta-6,9,28,31-tetraen-19-yl-4-(dimethylamino)butanoate), a phosphatidylcholine (1,2-disteraroyl-sn-glycero-3-phosphocholine, DSPG), cholesterol and a coating lipid (polyethylenglycol-dimyristolglycerol, PEG-DMG) with an acidic aqueous buffer containing siRNA in a microfluidic mixer with herringbone structure at a flow ratio of 1:1 (v/v). Maximum activity was exhibited at LNP-siRNA size of 80 nm. It was observed that smaller particles were less active because they were less stable and fusogenic, and larger particles (>100 nm) did not access hepatocytes. After formulation optimization, Patisiran underwent phase I – III clinical studies meeting all secondary endpoints. In fact, Patisiran did not only halt disease progression but even reversed it. [87, 93, 94] In a project using the same lipid phase at different molar ratios, Jyotsana et al. developed a reproducible ionizable cationic LNP system consisting

of an ionizable amino-lipid, entrapping siRNA for systemic delivery against the BCR-ABL fusion driver oncogene in chronic myeloid leukemia (CML). [95, 96] Highly efficient and non-toxic delivery of siRNA *in vitro* and *in vivo* with uptake of LNP-siRNA formulations in nearly 100% of bone marrow cells in a leukemia model was observed resulting in reduced leukemic burden in mice. [95] Importantly for industrial production, Belliveau et al. confirmed that scaling-up the microfluidic production process can be performed without losing batch quality. They combined six staggered herringbone mixers to obtain a total flow rate of 72 mL/min or a combined flux of 580 mg LNP/min (Figure 4). The siRNA entrapping LNPs obtained were produced at sizes between 54 nm and 28 nm and polydispersity indices as low as 0.05 and 0.08 based on dynamic lights scattering (DLS, number mode). The optimized formulations achieved 50% gene silencing in hepatocytes of mice. [97]

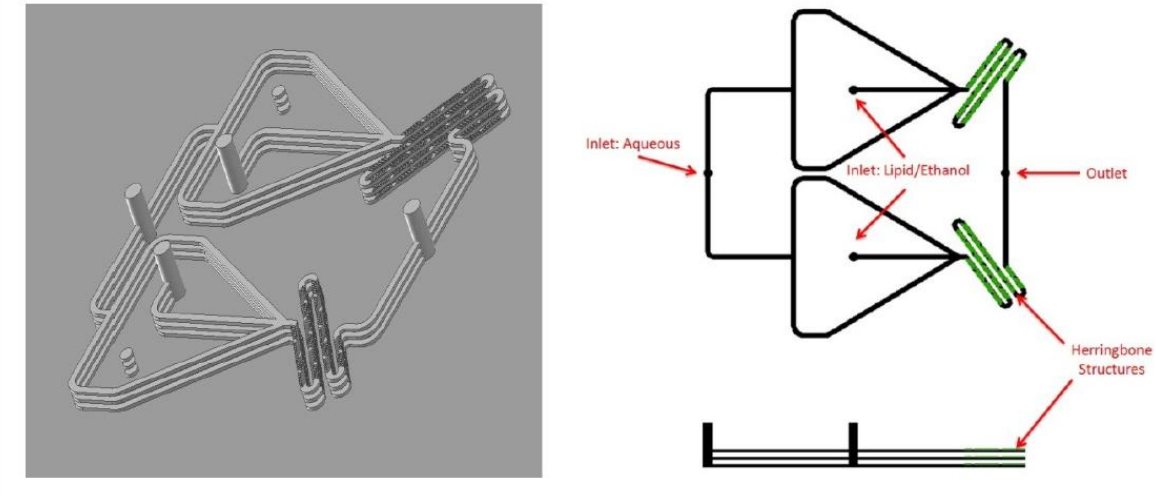

Figure 4 6x scaled-up microfluidic device for LNP formulation using a staggered herringbone mixing (SHM) system. With permission from Ref. [97]. Copyright 2012, The American Society of Gene & Cell Therapy.

The success of mRNA LNP formulations in the 2019/2020 SARS-CoV-2 pandemic would not have been possible without the microfluidic LNP formulation know-how available at Acuitas Therapeutics. [98] While the proprietary production procedures are not published, the advantages of RNA encapsulation in LNPs were described above.

As demonstrated in the examples discussed above, scalable production methods are available for microfluidic preparation of LNPs, and the influence of lipid compositions can be chosen to obtain particles with optimized uptake and endosomal escape properties. [99] For instance, ionizable lipids are used to reduce size and facilitate particle uptake. The use of cationic or ionizable lipids will also complex anionic molecules or nucleic acids to protect them from degradation. [99, 100] The LNP design parameters are influenced by microfluidic structure, flow rates and dilution of drug solution. In addition, LNP preparation can be fine-tuned to tailor particle modification, size, and encapsulation efficiency.

2.4 Polymeric nanoparticles

Polymers offer a big variety and diversity in design and synthesis which enables many possibilities for them to be integrated in a nanotechnology system. [101] Hence, polymers can be used to produce solid sphere nanoparticles, micelles, vesicular polymersomes, polyplexes, polymer-drug conjugates, and dendrimers. [102, 103] The preparation of polymeric nanoparticles is similar to the preparation of lipid nanoparticles and most commonly performed using emulsion and/or precipitation methods. The nanoparticle formation can be obtained using a one- or a two-step method. A one-step method does not require an emulsification process. Nanoparticles form through precipitation in conditions of spontaneous dispersion formation or self-assembly. In a two-step method, firstly an emulsified system is prepared

followed by precipitation or gelation of a polymer. Comparing both techniques reveals some advantages and disadvantages for each method. The biggest advantage of a one-step method is that the nanoprecipitation can be performed by using only three basic ingredients: the polymer, the polymer solvent, and the non-solvent, i.e., acetone. Hence, the experimental set-up can be developed further. The nanoparticle formation is obtained by a rapid diffusion after adding the polymer solution to the non-solvent. The resulting polymeric nanoparticle size is well defined around 200-300 nm and characterized by a narrow distribution. [104] On the other hand, a two-step method starting with an emulsification followed by precipitation, introduces a lot of variables to the experimental set-up which can be favorable, but can also add complexity. The droplet size range of the emulsion can vary from 10 µm to 10 nm depending on producing a macroemulsion or a microemulsion. In regard to the size and the chosen emulsion type, polydispersity can also vary amongst wide range between the different methods. Furthermore, stability plays an important role during emulsion formation and the time frames of stability can differ from a few seconds, in macroemulsions, to an infinite stability upon constant storage conditions in microemulsions, a thermodynamically stable system. Another big disadvantage is the amount of equipment that is needed, such as mechanical stirrers, high pressure homogenizers and colloid mills. [104] This process is followed by the precipitation and solvent extraction. Hence, many steps are needed to obtain polymeric nanoparticles and a simpler method that contains all different experimental steps in a single set-up, and still ensuring monodisperse sizes, would be favorable. Microfluidic mixing, in its tailor-made design simplifies all requirements. The following polymers are regularly used in microfluidic nanoparticle formation: polylactic-co-glycolic acid (PLGA), poloxamer, chitosan, hyaluronic acid, or alginates. [105-120]

Majedi et al. described that chitosan particle formation in an 2D-hydrodynamic flow focusing (2D-HFF) system was driven by pH changes in the aqueous environment. [121] The polymer solution was simply mixed with alkaline water (pH 9.0) to form nanoparticle sizes of sub 200 nm. It was shown that paclitaxel was encapsulated at an efficiency above 95%, and the nanoparticles conserved the drug's potency. In addition, the use of 3D-hydrodynamic flow focusing (3D-HFF) devices allowed to produce PLGA, PLGA-b-PEG and hydrophobically modified chitosan nanoparticles in the range of 20-350 nm given the advantages of 3D-coaxial flow with a more rapid and uniform mass transfer. [113, 122, 123] Further mixing techniques are the multi-inlet vortex mixer (MIVM) and confined-impinging jet mixers (CIJM). These methods have been used to improve the precipitation of PLGA-b-PEG with docetaxel and insulin. The advantage of these systems is rapid mixing driven by the collision of fluids under a high shear rate and an instant molecular diffusion among these fluids. Possible drawbacks could be shear stress causing aggregation of biomolecules such as insulin and potential increases in temperature which could negatively affect thermosensitive drugs and polymers. A particle size below 100 nm and a narrow size distribution (PDI < 0.2) were obtained both in case of insulin and docetaxel encapsulation. [31, 124]

Polyplexes, a sub-class of polymer-based nanoparticles, undergo spontaneous formation of oppositely charged molecules based on electrostatic interactions of polycations and negatively charged counterparts, i.e. nucleic acids.[125] Amongst polymer materials for nanoformulation and delivery of nucleic acids, cationic polymeric materials, i.e. polyethylenimine (PEI), PEI-derived-block copolymers, such as PEG-poly(caprolactone) modified PEI (PEG-PCL-PEI), chitosan or poly(β-amino esters) (PBAE) are well established as non-viral delivery systems. [34, 126-128] The polyplex formation reaction is commonly performed by bulk mixing and often results in batch-to-batch variability regarding polyplex size and polydispersity. [129, 130] Furthermore, polyplex formation via pipetting generates a lower polyplex concentration in suspension limiting *in vitro* and *in vivo* experiments. [131] Therefore, directed and controlled mixing as it can be performed in a microfluidic mixer has been discussed to offer an approach for overcoming such issues. Depending on the microfluidic device chosen for polyplex assembly, an aqueous solution containing nucleic acids or other active ingredients and an aqueous solution containing a polymer are directed at a certain flow rate. Their mixing ratio is usually shifted to

the polymer side generating a polymer excess and commonly positively charged polyplexes are obtained which facilitate cell uptake by adsorptive endocytosis. [132-134] Wilson et al. mixed polymer and plasmid DNA solution at a 1:1 v/v ratio in 25 mM sodium acetate in a self-built polydimethylsiloxane (PDMS) chip to generate PBAE/DNA complexes. [128] The obtained polyplexes showed sizes of around 100 nm, detected by nanoparticle tracking analysis (NTA). Uptake efficiency in over 70% of human glioblastoma cells (GB319) was obtained and no cell toxicity was detected in a cell proliferation assay (MTT), a colorimetric assay assessing cell metabolic activity. Subsequent lyophilization and storage at -20°C retained the sizes, its distribution and efficacy for at least three months. [128] In a different example of microfluidic polyplex assembly, Wang et al. prepared DNA polyplexes with cyclodextrin-grafted-PEI (CD-PEI) using a digital microfluidic droplet generator (DMDG). To obtain tailored nanoparticles, additional building blocks with specific ligands, such as arginylglycylaspartic acid (RGD) and/or a peptide derived from the transactivator of transcription (TAT) of the human immunodeficiency virus (HIV) were incorporated. The optimization resulted in a library of 648 nanoparticle formulations which were screened to detect the best transfection efficiency of plasmids. The best formulation consisted of 0.60 µM CD-PEI, 0.60 µM of TAT and 0.28 µM of RGD with sizes of 40 nm and a zeta potential of 3.7 mV, measured by DLS. Furthermore, the polyplexes kept their sizes at pH values ranging from 5.0 to 9.0 and over a time of 48 hours. The transfection efficiency (> 70%) of this formulation resulted in a superior behavior compared with Lipofectamine 2000 and RGD-PEI in all tested cell lines. [135] We showed recently that a decrease in size of siRNA/PEG-PCL-PEI from 260 nm (bulk mixing) to 122 nm (microfluidic mixing) may not affect their in vitro behavior in conventional cell culture but that in vivo smaller polyplexes, prepared by microfluidics, which were administered to the lung more efficiently silenced endogenous gene expression. [34] This observation was explained by the multitude of clearance mechanisms in the lung which smaller particles apparently escape more efficiently, while larger particles sediment faster in cell culture. Polyplexes of siRNA and PEG-PCL-PEI were later described to silence the DNA repair genes ERCC1 and XPF1 in lung cancer more efficiently than lipofectamine lipoplexes, leading to restored cisplatin sensitivity in previously cisplatin resistant lung cancer cells. [136]

Polyplexes have also shown to be successful delivery systems for peptide-based drug molecules. In a multi-inlet vortex mixer having four independent inlets, insulin-loaded nanoparticles were engineered by simultaneous infusion of water and aqueous solutions of chitosan, tripolyphosphate (TPP) and insulin. The insulin-loaded chitosan nanoparticles prepared via microfluidics showed smaller average particle sizes (45 nm), narrower size distributions and a higher encapsulation efficiency (90%) in comparison to the same particles prepared by drop wise addition (240 nm). Stability studies of nanoparticles produced via microfluidic mixing confirmed that physicochemical properties of reconstituted polyplexes, after lyophilization and storage at -20°C for 6 months, did not alter to freshly prepared polyplexes. Oral administration of the smaller insulin loaded chitosan nanoparticles in a rat model of type I diabetes resulted in an effective control of the blood glucose levels. [31, 137]

2.5 Hybrid nanoparticles

While improving the solubility of hydrophobic drugs via formulation in cyclodextrins or emulsions is commonly addressed by classic galenics, hydrophilic drug molecules with high solubility but poor permeability or drugs with low solubility and low permeability require efficient formulation for intracellular delivery. [138, 139] This is particularly important for nucleic acid based drugs such as siRNA, proteins, and some anticancer drugs such as docetaxel. [140, 141] The goal is to improve entrapment efficiencies and drug recovery rates to widen applications for drugs with low drug permeability. [142, 143] As discussed above, water-soluble polymers can encapsulate hydrophilic drugs and improve their drug delivery. If the drug molecules are charged such as nucleic acids or insulin, they can be encapsulated by charge-charge-interactions, but the biggest drawback of polyplexes is their

physical instability, aggregation, or dissociation in high salt environment. To further stabilize polyplexes, so-called lipid-polymer hybrid nanoparticles (LPHNP) can be formed by coating a polyplex core with a lipid shell. In comparison to polyplexes, the hybrid nanoparticle formation does not merely rely on electrostatic interactions creating a stable nanoparticle. [144-146] LPHNP can be produced through a two-step or single-step preparation method. In the two step-method, the polymeric core and the lipid shell are prepared separately and then merged by direct hydration, sonication or extrusion. [147-149] Nowadays, the single-step method is preferred mixing the polymer, lipid and the incorporated drugs to form the LPHNP via self-assembly using a microfluidic system. [150, 151]

In 2020, Tahir et al. compared LPHNP loaded with Sorafenib prepared via bulk nanoprecipitation or a microfluidic co-flow mixing technique with a glass capillary microfluidic device. [152] The morphological analysis of LPHNPs prepared by bulk nanoprecipitation revealed well-defined spherical nano-sized particles of 200 nm size with PDIs of 0.21-0.25. In contrast, core-shell morphology was observed in particles prepared by microfluidic mixing at sizes of 190-200 nm and PDIs below 0.16. The formulation indicated higher encapsulation efficiency (95% vs. 86-89%) and controlled release of Sorafenib from the particles as compared to the LPHNPs obtained by bulk nanoprecipitation. In addition, the colloidal stability, in vitro cytotoxicity, and cell growth inhibition studies of LPHNPs also demonstrated stability in biological media, biocompatibility and safety with enhanced anti-proliferative effects than free Sorafenib in breast cancer and prostate cancer cells. [152] A different approach was developed by Zhang et al. They used the microfluidic mixing technique to form controllable core-shell nanoparticles with polymer cores and lipid-monolayer- or lipid-bilayer-shells. The microfluidic device consisted of two stages. The first stage had three inlets. The main synthesis channel was fed with PLGA or lipid solution to undergo precipitation and form the core nanoparticle. The second stage comprised of a middle inlet-channel, to introduce the lipid or PLGA to the system, and a spiral synthesis channel. Both hybrid systems obtained sizes of just above 100 nm. However, lipid-bilayered particles require twice as much lipid than monolayered nanoparticles to completely cover the PLGA core. This results in lower flexibility, but also a more efficient cellular uptake and thus superior anticancer effects than bilayered particles. [153] Wei et al. used a multi-stage microfluidic device to form core-shell lipid-PCL-PEI-siRNA nanoparticles (LPS NPs). The chip is organized in a way that every part of the LNP NP will be added consecutively. The siRNA is compressed in a hydrophilic core of reverse PCL-PEI micelles coated with a neutral lipid membrane consisting of cholesterol, DOPE, a phosphatidylethanolamine, and DSPE-PEG, a phosphatidylglycerol modification. Uniform sizes of 120 nm, a PDI of 0.18 and encapsulation efficiencies of almost 98% were detected. In comparison, bulk mixing led to sizes of 200 nm, a PDI of 0.26 and 79% encapsulation efficiency. Furthermore, these LNP NPs demonstrated significant downregulation of mRNA and protein expression level both in vitro and in vivo. [154]

The possibility to merge the advantages of polymers and lipids results in great potential for hybrid nanoparticles to be a versatile nanoparticulate drug delivery toolbox for pharmaceutical applications. [101] In combination with microfluidic systems, a simple all-in-one formulation set-up will give enough flexibility to change and optimize physicochemical characteristics or drug loading efficiencies.

2.6 Theranostic nanoparticles

Theranostic nanoparticles combine a therapeutic and diagnostic application in one delivery system. The particle structure can consist of polymers, lipids or a hybrid combination and can incorporate multiple agents, such as therapeutic drugs and imaging agents. [155-158] These theranostic nanoparticles can also achieve specific targeting, enhanced blood circulation and enhanced penetration, as all nanoparticles discussed above. Surface modifications target specific cells or cellular markers to exploit their diagnostic aspects. A controlled or stimuli-driven release of the therapeutic agent is often required to account for the theranostic characteristics. The formation of theranostic nanoparticles occurs in the same way as polymeric, lipid or hybrid nanoparticles are formed. Precipitation is the nanoparticle

forming step. Microfluidics help to simplify the preparation procedure by incorporating a controlled flow to form uniform nanoparticles with diagnostic and therapeutic features. [157, 159]

Mosayebi et al. highlighted recent advances in microfluidic preparation from nanoparticle synthesis and functionalization steps to the final design considerations of physicochemical properties such as size and shape, composition, hydrophobicity, and surface charge (Figure 5). They incorporated magnetic nanoparticles (MNPs) as diagnostic means and modified the particles to evade the body's immune system targeting several different cancer types. Magnetic polarization and magnetophoretic mobility in a magnetic field form the basis of magnetic drug targeting. MNPs that respond to the magnetic field can be attracted to their targets. The applied magnetic field can keep the MNPs localized to their target sites. A wide range of synthetic routes such as wet chemistry, state-of-the-art microfluidic reactions, and biogenic routes, along with nanoparticle coating to stabilize the resulting MNPs can be incorporated. Additionally, key aspects of prolonging the half-life of MNPs via overcoming the sequential biological barriers are covered through unraveling the biophysical interactions at the bio–nano interface and propose a set of criteria to efficiently modulate MNPs' physicochemical properties. [160] Concepts of passive or specific targeting for successful cell internalization have been described in the literature for theranostic particles prepared by microfluidics. [31, 161] The unique properties of cancers can thus be exploited, and novel targeting ligands can be developed accordingly.

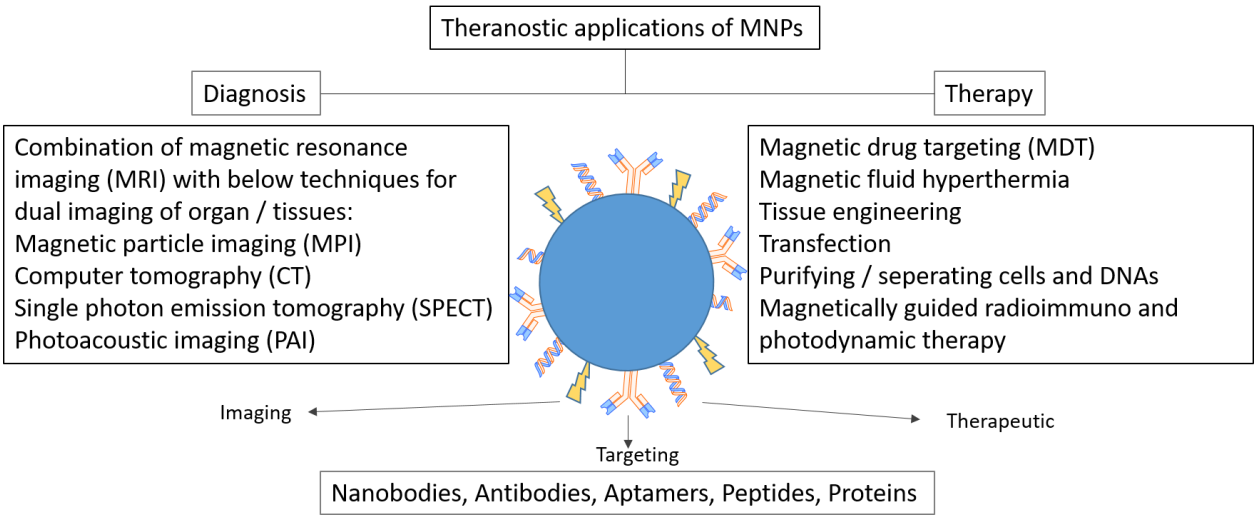

Figure 5 Theranostic applications of magnetic nanoparticles (MNPs)

Kim et al. used as 2D-hydrodynamic flow focusing technique to produce high density lipoprotein (HDL)-derived nanoparticles that were able to incorporate simvastatin, as a hydrophobic drug, as well as gold, iron oxide, quantum dots or fluorophores as diagnostic agents. Therefore, these HDL-particles can be considered a targeted delivery therapeutic and can be detected by computed tomography (CT), magnetic resonance imaging (MRI), or fluorescence microscopy. Their sizes varied from 30 nm to 10 nm, decreasing by increasing the Reynolds number.

Another example of a theranostic approach described hybrid nanoparticles prepared by microfluidic mixing as fine-tuned bone-seeking nanoparticles. The nanoparticles consisted of bisphosphonate conjugated PLGA chains co-encapsulating superparamagnetic iron oxide nanoparticles, as an MRI contrast agent, and paclitaxel, as the cytostatic therapeutic. It was shown that by reducing the flow ratio the particles sizes were decreased to 60-70 nm. These HNPs were labeled by fluorescein isothiocyanate (FITC), and the bisphosphonate part resulted in a strong affinity for hydroxyapatite, as demonstrated in an *in vitro* bone-binding assay, which was further supported by molecular dynamics simulation results. An in vivo proof of concept study verified the prolonged circulation of targeted microfluidic HNPs compared to non-targeted nanoparticles or targeted bulk-synthesized particles. Biodistribution as well

as noninvasive bioluminescence imaging experiments, by luciferin injection, showed high tumor localization and higher level of tumor suppression of the bone metastatic tumor using targeted microfluidic HNPs. [157]

Acknowledgement

The authors are thankful for funding by ELSE KRÖNER-FRESENIUS-STIFTUNG, grant number 2014_A299. This work was supported by the ERC Starting Grant ERC-2014-StG-637830.

Chapter III – Microfluidic formulation and evaluation of siRNA-triblock copolymer polyplexes

Author‘s contributions:

Christoph M. Zimmermann [a,b], Friederike Adams,[b,c] Paola Luciani [b] and Olivia M. Merkel [a]

F.A. synthesized the polymers. C.M.Z performed the experiments, evaluated the data and wrote the paper. C.Z and O.M.M conceived the presented idea and planned the experiments. P.L. and O.M.M supervised the work, provided conceptual guidance and corrected the manuscript.

d. *Pharmaceutical Technology, Department for Chemistry, Biochemistry and Pharmacy, University Bern, Freiestrasse 3, CH - 3012 Bern*

e. *Pharmaceutical Technology and Biopharmaceutics, Department Pharmacy, Ludwig-Maximilians-University Munich, Butenandtstr. 5-13, 81377 Munich, Germany*

f. *Institute of Polymer Chemistry, Chair of Macromolecular Materials and Fiber Chemistry, University of Stuttgart, Pfaffenwaldring 55, 70569 Stuttgart, Germany Eberhard-Karls University of Tübingen, Geschwister-Scholl-Platz, 72074 Tübingen, Germany*

Key words: polymer, microfluidic mixing, polyplex, micelleplex, RNA therapeutics, siRNA delivery

Abstract

Polyplexes have shown to be successful drug delivery systems, useful to encapsulate nucleic acids and to enable more precise targeting with a controlled release. However, reproducibility and scalability are major concerns in industrial preparation of polyplex formulations. Polyethylene imine (PEI)-based polyplexes facilitate siRNA complexation, cell internalization and endosomal escape. However, the excess positive charge can increase cytotoxicity and an inability to release nucleic acids leading to insufficient therapeutic effects. The addition of hydrophobicity and/or hydrophilicity can improve the polyplex' performance. PEI's performance can be improved covalently linking polycaprolactone (PCL) and polyethylene glycol (PEG) to it, generating block-copolymers. Tuning the polymer hydrophilic-hydrophobic balance, the particle's affinity for the cell membrane and leaving the endosome can be increased, the degradation rate slowed down, the polymer's solubility improved, aggregation is minimized, and colloidal stability increased.

This aim of this work was to test newly synthesized PEG-PCL-PEI (PPP) polymers as building block of polyplexes to improve the performance of physicochemical properties and *in vitro* compared to PEI-based polyplexes. Polyplex formation was established through aqueous microfluidic mixing using a Dolomite Micromixer® system and compared to direct pipetting. PPP polyplexes resulted in sizes < 100 nm at more homogeneous and smoother complexation. Furthermore, microfluidic mixing led to a more uniform charge distribution and increased colloidal stability. *In vitro* performance revealed a superior behavior of PPP- over PEI-based polyplexes. PPP polyplexes achieved a 3-fold increase in cell uptake and more than 50% gene silencing at no cytotoxic activity.

1. Introduction

Nucleic acids themselves lack the ability to be taken up into the cells and regulate cell expression because of rapid nuclease cleavage and renal and hepatic clearance. [162] Therefore, viral and non-viral carriers have been used to protect nucleic acids from degradation, minimize exposure to off-target cells and maximize delivery to on-target cells. [163] Non-viral systems, based on lipids or polymers, are more favorable because polymeric drug delivery systems have shown to be advantageous regarding safety profiles, mutagenicity and productions costs. [164] However, some biological hurdles, such as efficient cellular uptake, rapid endosomal escape of genetic cargo into the cytosol, and efficient nucleus localization, need to be overcome. [165, 166] Polyethyleneimine (PEI) is one of the most studied polymers used as a nucleic acid carrier system. Its structure consisting of a protonable amino group for every third atom enables the electrostatic complexation with negatively charged nucleic acids, such as siRNA, to form polyplexes. Even though PEI-based polyplexes facilitate cell internalization and endosomal escape, the excess positive charge leads to cell membrane damage followed by increased cytotoxicity and the inability to release their cargo renders in insufficient therapeutic effects. [167, 168] Studies have shown that the molecular weight and cationic densities influence the cytotoxicity while affecting transfection and endosomal escape behavior. [11] Low molecular weight PEI is less toxic but causes increased endosomal entrapment. Therefore, cationic polymers, such as PEI, face a dilemma associated with an efficiency versus toxicity trade-off which needs to be solved. [167] Synthesis of new polymers or modification of existing polymers delved into the problems of cationic polymers by improving biocompatibility and transfection performance at the same time. [169] The chemical toolbox enables various approaches of designing novel polymers, such as block addition, grafting or branching out. [170-172] Moreover, the integration of hydrophobic or hydrophilic groups has shown to refine the polyplex formation, impact the cellular uptake, facilitate cargo release and lower cytotoxicity. [170, 173] Hydrophobicity can be increased by adding amphiphilic polycaprolactone (PCL) blocks. PCL is biodegradable, biocompatible, increases the particles' affinity to adhere to the cell membrane and shows a slow degradation rate. [34, 174] However, increasing the hydrophobic part may lead to polymer insolubility in aqueous solutions. PEGylation, the addition of poly(ethylene glycol) (PEG), can help to

increase hydrophilicity and ensures an improvement in solubility of the polymer, minimizes its aggregation, increases colloidal stability and acts as a stealth agent to prevent macrophage clearance of nanoparticles. [175-178] On the other hand, high molecular PEG has shown to reduce cellular uptake and endosomal escape. [179] To overcome the hurdles that PEI polymers face, planning the synthesis of novel PEI-based polymers can lead to synergistic outcomes

In prior studies PEG-PCL-PEI (PPP) triblock copolymers were synthesized with the aim of combining the advantages of each individual component optimizing siRNA encapsulation and physicochemical properties as a nucleic acid drug delivery system. [170, 180-182] PPP helped to create polyplexes that promoted trans-membrane transport improving the transfection efficiency of nucleic acid-based nanoparticles. [170] The triblock copolymer mostly consisted of a hyper-branched 25 kDalton (kDA) PEI enabling endosomal buffering capacity and a proton-sponge effect promoting endosomal escape. The PCL block was kept to 342-800 Da, of which higher molecular weight PCL reduced cytotoxicity. PEG blocks were kept at 2 kDa as longer PEG-chain lengths can reduce cytotoxicity as well. [170, 183] The triblock copolymers demonstrated reduced cytotoxic effects at increased transfection efficiencies compared to hyper-branched PEI. Feldmann et al. used a PPP polymer consisting of 5 kDa PEG, 570 Da PCL and 25 kDA PEI to form siRNA polyplexes using a microfluidic mixing approach. [34] While direct pipetting is poorly suited to reproducibly generate uniform particles, microfluidic mixing uses the approach of molecular diffusion and turbulent mixing to rapidly form reproducible nanoparticle batches. [125, 184] Furthermore, a more homogeneous complexation could benefit from a more uniform charge distribution, increase in colloidal stability of nanoparticles, and improve transfection efficiency. [185] It was shown that the obtained nanoparticles resulted in smaller sizes at reduced size distribution and efficiently delivered siRNA *in vivo*. However, only one triblock copolymer was synthesized and the sizes of >120 nm at PDIs between 0.3 – 0.52 were worthy of improvement.

The aim of this work was to test newly synthesized PEG-PCL-PEI (PPP) polymers as building block of polyplexes by improving the previously stated polymers' performance using microfluidic mixing. The polymer composition was adapted reducing the molecular weight of PEG to 2 and 4 kDa, increasing PCL molecular weight to 1 and 2 kDa and using branched PEI at 10 kDa, respectively. Moreover, different grafting densities were synthesized as higher grafting degrees of the amphiphilic chains showed to enhance siRNA delivery *in vivo*. [181] We hypothesize an improvement of transfection efficiency by reducing the PEG content and increasing the hydrophobicity. Simultaneously, a less branched PEI at lower molecular weight should reduce its initial cytotoxicity by not affecting the endosomal escape. Physicochemical properties were tested, and targets were set at sizes of <100 nm and PDI values of about 0.2 at full siRNA encapsulation. Furthermore, *in vitro* performance was evaluated in the form of cell uptake, protein knockdown and cytotoxicity in adenocarcinoma cells H1299. PPP- should outperform PEI-polyplexes *in vitro* generating a gene knockdown of at least 50%.

2. Materials & Methods

2.1 Materials

Dicer substrate double-stranded siRNA targeting green fluorescent protein (DsiRNA EGFP, 25/27) (siGFP), scrambled, non-specific control (siNC) and amine modified siRNA labeled with succinimidyl ester (NHS) modified AF 488 (siAF488) (Life Technologies, Carlsbad, USA) were purchased from IDT (Integrated DNA Technologies, Inc., Leuven, Belgium). [186] Tris-EDTA buffer solution 100x (T9285), RPMI-1640 medium (R8758), fetal bovine serum (FBS) (F9665), penicillin-streptomycin (P/S) (P4333), G418 disulfate salt solution (G8168), Dulbecco's phosphate buffered saline (D-PBS) (D8537), methylthiazolyldiphenyl-tetrazoliumbromid (MTT) and 2,4,6-trinitrobenzene sulfonic acid (TNBS) were purchased from Sigma-Aldrich, a subsidiary of Merck KGaA (Darmstadt, Germany).

Black 96-well plates (10307451), were bought from Thermo Fisher Scientific (Schwerte, Germany). Micromixer® chip was bought from Dolomite Microfluidics, Blacktrace Holdings Ltd., Royston, UK.

2.2 Triblock copolymer PEG-PCL-PEI (PPP) synthesis

The synthesis of triblock copolymers based on methoxy-poly(ethyleneglycol)-block-poly(ε-caprolactone)-graft-branched-poly (ethylenimine) mPEG-b-PCL-g-br-PEI was performed as described before (Figure 1A). [170, 187-189] The components consisted of mPEG (2 000 and 4 000 g/mol), PCL (250, 1 000 and 2 000 g/mol) and branched PEI (10 000 g/mol). The grafting density was calculated using ^{1}H-NMR spectroscopy. Furthermore, the polymer's solubility in highly purified water (HPW) was examined after sterile filtration using a 0.22 µm syringe filter (Figure 1B).

A

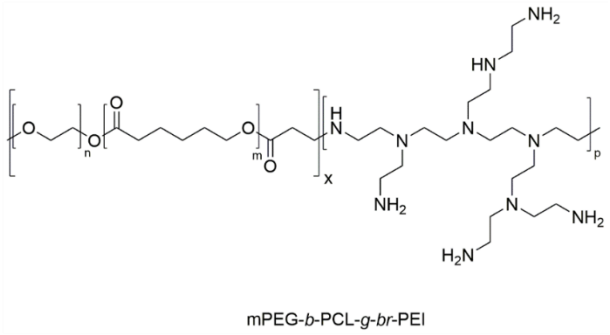

B

Polymer	Chemical structure	Solubility in water
PPP 1	$(PEG_{2k}PCL_{250})_{1.7}PEI_{10k}$	No problem
PPP 2	$(PEG_{2k}PCL_{2k})_{1.6}PEI_{10k}$	Insoluble
PPP 3	$(PEG_{4k}PCL_{2k})_{3.2}PEI_{10k}$	Slower
PPP 4	$(PEG_{2k}PCL_{1k})_{2.2}PEI_{10k}$	Insoluble
PPP 5	$(PEG_{2k}PCL_{1k})_{4.9}PEI_{10k}$	Slower

Figure 1 A) Chemical structure of triblock copolymer methoxy-poly(ethyleneglycol)-block-poly(ε-caprolactone)-graft-branched-poly (ethylenimine) (mPEG-PCL-g-br-PEI, PPP). B) Table overview of different triblock copolymers including the molecular weight of each individual component and the final grafting density (g).

2.3 TNBS assay for PEI quantification in PPP polymer

The total amount of PEI in triblock copolymer PPP can be calculated using the 2,4,6-trinitrobenzene sulfonic acid (TNBS) assay. Polymers were dissolved in HPW to get a concentration of 1 mg/mL. This concentration was diluted 200 times to reach a polymer concentration of 0.5 µg/100 µL. Subsequently, a PEI (1 mg/mL) standard curve was prepared by diluting 13.4 µL in 336.6 µL HPW. Further dilutions prepared a PEI mass range of (1.914 µg – 0.166 µg). An aliquot of 100 µL of each sample was pipetted into a transparent 96-well plate and mixed with 30 µL of 0.088% TNBS (w/V) in 0.1 M borax buffer. The plate was left for 1 h incubation under light exclusion. The absorbance was measured at 405 nm using a microplate reader (TECAN Spark, TECAN, Maennedorf, Switzerland). The data are shown as concentration of PEI (mg/mL) in comparison to the triblock copolymer PPP (1 mg/mL) and PEI amount detected via ^{1}H-NMR (Table 1).

Table 1 TNBS measurement results of PEI vs. calculated PEI concentration in various triblock copolymers PEG-PECL-PEI (PPP).

Polymer	TNBS – Conc. PEI (mg/mL)	Conc. PEI calculated (mg/mL)	Conc. PPP (mg/mL)
PPP 1	0.75	0.68	1.0
PPP 2	0.25	0.61	1.0
PPP 3	0.34	0.31	1.0
PPP 4	0.67	0.60	1.0
PPP 5	0.29	0.40	1.0

2.4 PEG-PCL-PEI (PPP) polyplex preparation

The polyplexes were formed by encapsulating siRNA in PPP polymers. Prior to the polyplex formation, all polymers were dissolved in highly purified water (HPW) to reach a concentration of 1 mg/mL. The amount of polymer needed was calculated by the following equation taking into account the PEI concentration found by the TNBS assay:

PEI (pg) = Mw (PEI) x siRNA nucleotides x N/P ratio x siRNA amount (pmol)

Mw (PEI): Molecular weight (Mw) of PEI's protonable unit is 43.04 g/mol. siRNA nucleotides: the number of nucleotides in siRNA sequence is 52, due to 25/27 base pairs. N/P ratio: the charge ratio between the cationic groups on the PEI molecule to the anionic phosphate in the RNA backbone.

All polyplex formulations consisted of 50 pmol siRNA (siAF488, siGFP, siNC). To form PPP polyplexes via microfluidic mixing, the hydrophobic Dolomite Micromixer®, was used. The set-up of the mixer enabled a polyplex formation as described before. [34] The flow rates were controlled by syringe pumps (KD Scientific Inc, USA) set to 1.0 mL/min. N/P ratios were set between 1 – 10, although all further experiments were performed using N/P ratio 6. The microfluidic chip was washed with HPW prior and with isopropanol after usage. PPP polyplexes were ready to be used directly after collection.

2.5 Hydrodynamic diameter and zeta (ζ) potential measurements of PPP polyplexes

Hydrodynamic diameters and polydispersity indices (PDI) of HLPNPs (70 µL, 500 pmol siRNA per mL) were measured, dispersed in highly purified water (HPW), in disposable cuvettes (Brand GmbH, Wertheim, Germany) using the Zetasizer Nano ZS instrument (Malvern Instruments Inc., Malvern, U.K.). All samples were detected at a backscatter angle of 173°. Results are presented as Z-average size (nm) ± SD and analyzed via polynomial fit. Zeta potentials were measured by Laser Doppler Anemometry (LDA) using a Zeta Cell (Zetasizer Nano series, Malvern, UK) containing a 6.5X dilution of the same 70 µL sample of HLPNP suspension in HPW. For each HLPNP formulation, measurements were presented as an average charge (mV) ± SD.

2.6 PPP polyplex encapsulation efficiency

A SYBR-Gold assay was performed to determine the siRNA encapsulation efficiency of PPP polyplexes. All samples were loaded with 50 pmol siRNA at N/P ratios 1-10, as described in 2.3. Firstly, 100 µL of each sample were transferred into a black 96-well plate, followed by the addition of 30 µL of 4x SYBR-Gold (Thermo Fisher Scientific). The plate was incubated for 10 min under light exclusion. Measurements were done using a FLUOstar Omega multi-mode microplate reader (BMG LABTECH GmbH, Ortenberg, Germany) at an excitation wavelength of 485/20 nm and an emission wavelength of 520/20 nm. siRNA samples served as a positive control to set the 100% value of free siRNA. Results were presented as the mean ± SD, n = 3.

2.7 *In vitro* characterization of PPP polyplexes

2.7.1 Cell Culture

The human non-small cell lung carcinoma cell line H1299 (ATCC CRL-5803) and the same cell line stably expressing enhanced green fluorescence protein (eGFP, H1299-GFP) were cultured in RPMI 1640 medium supplemented with 10% FBS, 1% P/S and additional 0.4% G418 for H1299-GFP cells. Cells were passaged every 3 days with 0.05% v/v trypsin and subcultured in 75 cm2 flasks. Cells were kept in a humidified atmosphere at 37 °C with 5% CO2.

2.7.2 *In vitro* uptake of PPP polyplexes in H1299 cells

For uptake experiments, amine modified siRNA (Integrated DNA Technologies, Coralville, USA) was labeled with succinimidyl ester (NHS) and linked to AF 488 (Life Technologies,Carlsbad, USA). PPP

polyplexes were prepared as described above loading 50 pmol siRNA. Lipoplexes were prepared with Lipofectamine (LF) 2000 at 50 pmol siRNA acting as a positive control. H1299 cells were seeded at a density of 50 000 cells per well in a 24-well plate (Thermo Fisher Scientific). Each well was filled with 500 µL medium and left for 24h incubation at 37°C and 5% CO2. Subsequently, cells were transfected with 100 µL of PPP polyplexes and left for another 24 h incubation time. As negative controls, blank samples were seeded and left untreated. Cells were harvested and washed three times before resuspension in 500 µL PBS/2 mM EDTA (Sigma-Aldrich). Samples were analyzed using an Attune NxT flow cytometer (Thermo Fisher Scientific) with 488 nm excitation and 530/30 nm emission filter. All PPP polyplex samples were gated by morphology for a minimum of 10 000 viable cells. Results are displayed as mean MFI values (%) ± SD, n = 3.

2.7.3 *In vitro* eGFP downregulation in H1299-GFP cells

The in vitro gene silencing efficiency of PPP polyplexes was evaluated by transfecting H1299-GFP cells with 50 pmol of siNC- and siGFP-loaded nanoparticles, prepared as described in 2.3. A 24-well plate was seeded at a density of 25 000 cells per well in 500 µL medium, incubated for 24 h at 37 °C and 5% CO2. Cells were transfected adding 100 µL of polyplexes to 400 µL of fresh culture medium, left for 48 h incubation at 37 °C and 5% CO2. At the end of the incubation time, cells were washed with PBS, trypsinized and collected and resuspended PBS with 2 mM EDTA. Samples were analyzed by flow cytometry (Attune® NxT, Thermo Fischer Scientific, Waltham, Massachusetts, USA), and the median fluorescence intensity (MFI) of GFP protein expression was measured by using a 488 nm excitation laser and the emitted light passing through a 530/30 nm band pass emission filter set was detected. All PPP polyplex samples were gated by morphology for a minimum of 10 000 viable cells. Results are displayed as mean MFI values (%) ± SD, n = 3.

2.7.4 *In vitro* cytotoxicity of PPP polyplexes in H1299 cells

Cell viability after transfection with PPP polyplexes was tested via an MTT assay as described previously. [32, 33] Briefly, 5 000 H1299 cells per well were seeded in 100 µL medium in a transparent 96-well plate (BioLite 96 well multidish, Thermo Fisher Scientific, Rochester, New York, USA). After 24 h, 10 µL of PPP polyplexes was added to 90 µL of prewarmed medium and pipetted to each well. The plate was incubated for another 24 h at 37 °C and 5% CO2. As a full viability control, cells were incubated in 100 µL medium only. At the end of incubation time, medium was aspirated and 200 µL of MTT containing medium (0.5 mg/ml in serum-free RPMI-1640 medium) was added to each well. The plate was incubated for another 3 h at 37 °C and 5% CO2. Subsequently, the cell culture medium was completely removed, and insoluble purple formazan crystals were dissolved in 200 µl DMSO. The plate was set on a horizontal shaker for 20 min for all crystals to dissolve. The absorbance was measured at 570 nm and corrected with background values measured at 680 nm, using a microplate reader (TECAN Spark, TECAN, Maennedorf, Switzerland). The data are shown as mean ± SD as percentage of viable cells in comparison to untreated cells representing 100% viability, n = 3.

2.8 Statistics, data analysis and presentation

All experiments were run in independent triplicates. Experimental data was analyzed for normality by running a D'Agostino & Pearson omnibus normality test. Statistical significance was analyzed using the One-Way ANOVA repeated measurements on the GraphPad Prism 5 software with Tukey's post-hoc test with $p>0.05$ considered not significant (ns), * $p<0.05$, ** $p<0.01$, *** $p<0.001$. Data presentation was performed using GraphPad Prism 5 data science packages. Data not fitting normality were excluded from presentation.

3. Results and Discussion

3.1 Physicochemical properties of PEG-PCL-PEI-based polyplexes

The preparation of PPP-based polyplexes via microfluidic mixing was performed via an aqueous phase mixing of a polymer stream and a siRNA stream. The layout of the microfluidic mixing chip ensured a rapid, turbulent mixing process, as described before. [34] As described in 2.2 and shown in Figure 1, various PPP polymers were synthesized. The block compositions were varied to have polymers with different hydrophobic and hydrophilic characteristics. The only constant was the PEI molecule at a branched layout and 10 kDa molecular weight. Prior to the mixing, the polymers PPP 1 – 5 needed to be dissolved in HPW. As seen in Figure 1B, PPP 2 and PPP 4 did not dissolve in water excluding them for polyplex formation and further evaluation. Those two polymers comprised of higher hydrophobicity having a PCL to PEG ratio of 1:1 (PPP 2) or 1:2 (PPP 4) at low grafting densities. However, polymers PPP 1, 3 and 5 were water soluble enabling polyplex formation at N/P ratio 6, shown in Table .

Table 2 Comparison of sizes, PDI and zeta potential of PPP-based polyplexes formed via direct pipetting or microfluidic mixing. All samples consisted of N/P ratio 6. Results are displayed as mean ± SD, n = 3.

	Direct pipetting			**Microfluidic mixing**		
	Size (nm)	**Polydispersity index (PDI)**	**Zeta potential (mV)**	**Size (nm)**	**Polydispersity index (PDI)**	**Zeta potential (mV)**
PPP 1	87.9 (± 3.5)	0.406 (± 0.017)	5.06 (± 1.48)	68.0 (± 8.1)	0.404 (± 0.022)	4.10 (± 0.18)
PPP 3	100.4 (± 2.8)	0.273 (± 0.004)	2.63 (± 0.74)	72.4 (± 0.9)	0.263 (± 0.010)	3.27 (± 0.48)
PPP 5	96.0 (± 5.0)	0.395 (± 0.080)	4.60 (± 0.97)	96.8 (± 0.4)	0.334 (± 0.004)	3.12 (± 0.39)

A size, PDI and zeta potential comparison between direct pipetting and microfluidic mixing of PPP polyplexes was obtained. Direct pipetting led to sizes of 87.9 – 100.4 nm. The PDI values varied from about 0.4 for PPP 1 and PPP 5 to 0.27 for PPP 3. Therefore, all polyplexes showed a wider size distribution when prepared by direct pipetting. The zeta potential was measured at +2.6 - +5 mV giving standard deviations of up to 1.5 mV. In comparison, the nanoparticle formation via microfluidic mixing resulted in smaller sizes for PPP 1 and PPP 3 polyplexes of 68.0 and 72.4 nm, respectively. Solely, PPP 5 polyplexes were not reduced in size but the standard deviation between batches was reduced from 5 nm to 0.4 nm. The target sizes of below 100 nm was reached as the optimal nanoparticle size is ranged between 10 nm, to prevent kidney clearance, and below 200 nm to enable microcapillary passage. [190] This underlines the smooth and reproducible complexation of polyplexes when formed with microfluidic mixing. [184, 185] Even though sizes of PPP 1 and PPP 3 polyplexes were reduced by 20 – 28 nm, the PDI remained similar. The PPP polymers might have already encapsulated the siRNA in the most efficient way, which would not have given much room of improvement for microfluidic mixing. PPP 5 polyplexes, however, narrowed their size distribution to 0.334 in comparison to 0.395 with direct pipetting. The zeta potentials remained slightly positive between 3.1 – 4.1 (± 0.18 – 0.48) mV. The reductions in standard deviation reveal the potential of microfluidic mixing to overcome batch-to-batch variability and increase reproducibility. Feldmann et al. used the same microfluidic mixing approach to form PEG-PCL-PEI/siRNA polyplexes at N/P 6 showing sizes of 168 nm, a PDI of 0.423 and a zeta potential of +5.6 mV at a flow rate of 1 mL/min. [34] The physicochemical properties of previous studies and of Table leave the impression that PPP polyplexes reached the limit in regards to size distribution Neither Feldmann et al., nor we were able to match PDI values of 0.2 or below. On the

one hand, the electrostatic interaction to form polyplex will always lead to broader size distributions than PLGA nanoparticles or other solid nanoparticle systems. [191] On the other hand, narrow sizes distributions are set at PDI values <0.2 and various studies have shown to produce PEI-based polyplexes at the target size distribution. [5, 192] Therefore, newly synthesized PPP polymers improved polyplex sizes and maintained PDIs and positive zeta potential through microfluidic mixing. A low positive zeta potential should induce cell uptake but keeping a reduced cytotoxicity. [193]

To prove and quantify the siRNA encapsulation efficiency of the PPP polyplexes, a SYBR-Gold assay was performed (Figure 2). N/P ratios of 1-10 were prepared via microfluidic mixing and SYBR-Gold dye was added. displays the siRNA complexation process of PEI-, PPP 1-, PPP 3- and PPP 5-based polyplexes at increasing N/P ratios. All polymers managed to encapsulate more than 90% of siRNA at N/P 2. This value was improved to encapsulation efficiencies of >95% from N/P 3 onwards. All three PPP polyplexes have shown successful encapsulation of siRNA, as well as adequate sizes and zeta potentials via microfluidic mixing to be tested as drug delivery systems.

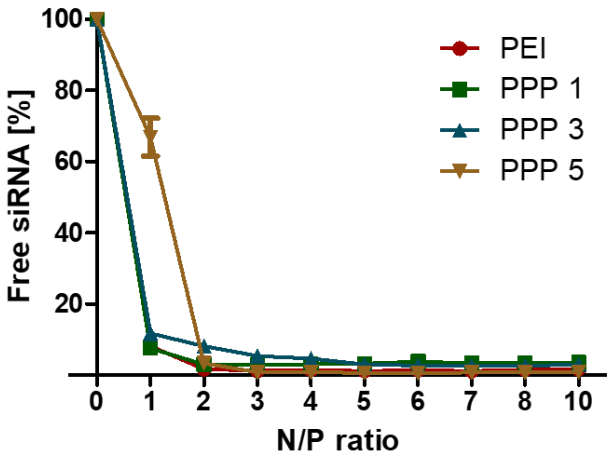

Figure 2 Encapuslation efficiency of PEI- and triblock copolymers (PPP 1, PPP 3 and PPP 5)-based polyplexes at various N/P ratios via SYBR-Gold assay. Polyplexes were prepared via microfluidic mixing. Results are displayed as mean ± SD, n = 3.

3.2 *In vitro* evaluation of PEG-PCL-PEI-based polyplexes

The in vitro performance of nanoparticle systems needed to be evaluated to classify triblock copolymer polyplexes as successful drug delivery systems. The uptake of nanoparticles into adenocarcinoma cells, H1299, was tested with all triblock copolymers and compared to Lipofectamine 2000 (LF), the positive control, and PEI-based polyplexes. Feldmann et al. have shown that there was no significant uptake improvement between hyper-branched PEI and PPP polymers, independent of direct pipetting or microfluidic mixing. [34] The aim was to achieve a better cellular uptake in comparison to branched PEI and at best as high as LF. As seen in Figure Figure 3, PEI polyplexes showed the lowest uptake of all nanoparticle systems. Even though PPP 1 polyplexes resulted in an increased uptake to PEI polyplexes, no statistical improvement was detected. However, PPP 3 and PPP 5 polyplexes showed a statistically significant uptake in comparison to PEI polyplexes that was almost as high as the uptake performance of LF lipoplexes. As mentioned above, amphiphilic PCL increases the polyplexes' affinity to adhere to the cell membrane and its hydrophobicity induces improved cell uptake. The differences in uptake performance can be explained by the molecular weights of PCL used for each individual PPP polymer. PPP 1 was composed of a 250 Da PCL block and showed a low grafting density of 1.7. This explained the weakest uptake performance of all PPP polymers. PPP 3 was synthesized with a 2 kDa PCL block and a grafting density of 3.2, giving the highest hydrophobicity of all PPP polymer. However,

the uptake performance did not exceed PPP 5 because the PEG block had a molecular weight of 4 kDa and high molecular PEG has shown to reduce cellular uptake. [179] The best performing polymer was PPP 5 consisting of a 1 kDa PCL and 2 kDa PEG at a grafting density of 4.9. The composition of lower PEG content, middle PCL weight and high grafting density enabled an uptake improvement to PEI polyplexes and almost reached the performance level of LF. Moreover, the newly synthesized PPPs outperformed the uptake performance shown from Feldmann et al.

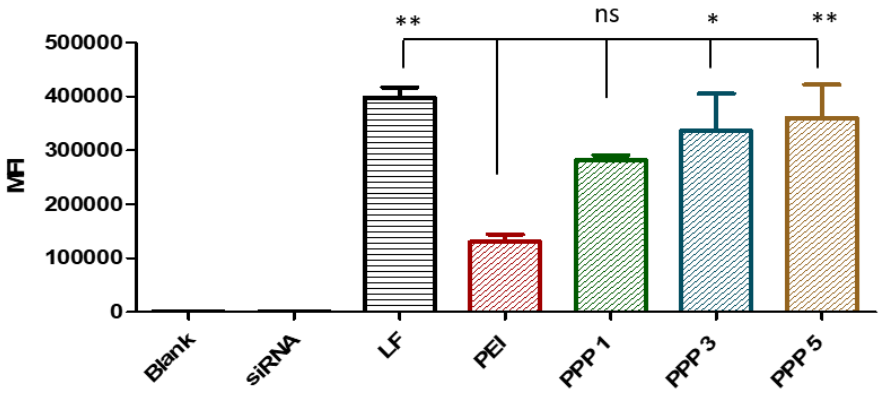

Figure 3 Uptake efficiency of triblock copolymers PPP1, PPP3 and PPP5 in comparison to PEI-based polyplexes and lipfectamine (LF) nanoparticles. Polyplexes were formed via microfluidic mixing encapsulating 50 pmol siAF488 at N/P ratio 6. Control values consisted of only medium (Blank) and non-encapsulated siRNA in medium (siRNA). MFI = Mean fluorescence intensity. Results are displayed as mean ± SD, n = 3.

The successful uptake of nanoparticle systems does not automatically imply a successful localization in the cytosol or nucleus, hence, a successful gene regulation. The cell uptake of nanoparticles occurs through endocytosis into endosomes. Subsequently, the particles leave the endosome to enter the acidic lysosomal compartment. [194] The endosomal escape is one of the most common hurdles of nanoparticles systems to successfully deliver their cargo to the target site. [10, 195] The structure of the triblock copolymer was chosen to use PEI to buffer the endosomal/lysosomal compartments leading to proton-sponge effect which is an osmotically induced swelling of the endosome. [196] Furthermore, PEI induces membrane thinning and pore formation causing endosomal escape. [11, 197, 198] Support of endosomal release was given by reducing the molecular weight of the PEG-block to 4 kDa and 2 kDa, respectively. A gene silencing evaluation was performed using siNC and siGFP encapsulated polyplexes to determine the endosomal release capability of PPP polyplexes and evaluate the GFP downregulation (Figure 4).

The positive control LF lipoplexes resulted in a very effective downregulation (>95%). PEI polyplexes silenced GFP for 40%. In comparison, PPP 1 and PPP 3 polyplexes did not improve the gene knockdown in H1299-GFP cells. PPP 1 resulted in 35% and PPP 3 in a 40% knockdown. Solely, PPP 5 managed to achieve a protein downregulation of more than 50% improving PEI's performance. Even though using the PPP improved the uptake of siRNA, it did not lead to an improved protein silencing. This can be explained by the endosomal escape dilemma, as stated above. This study used a PPP composition of 10 kDa branched PEI which was different to the 25 kDa hyperbranched PEI which was mainly evaluated in prior studies. [178, 180, 185] The buffering capacity and the ability to undergo the proton-sponge effect seemed to have adversely affected the polymers endosomal release. The triblock copolymers' composition was not able to synergize and outperform PEI.

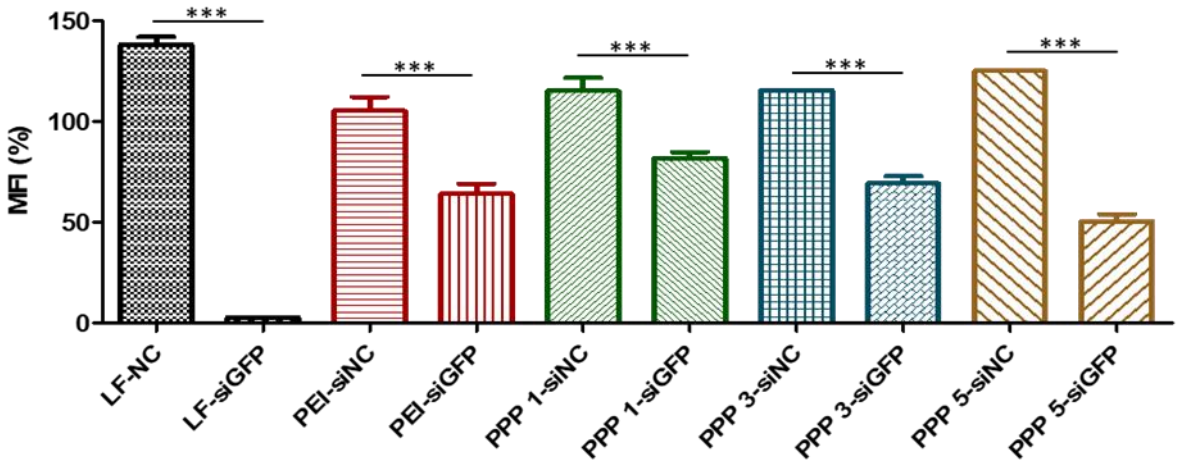

Figure 4 Knockdown efficiencies of LF-lipoplexes, PEI- and PPP- based polyplexes. Nanoparticles were formed via microfluidic mixing encapsulating 50 pmol siNC and siGFP at N/P 6. NC = negative control, GFP = green fluorescent protein. Results are displayed as mean ± SD, n = 3.

Figure 5 shows the cytotoxic effect of polyplexes in adenocarcinoma cells, H1299, via an MTT assay. Various N/P ratios were chosen to determine the impact of increased PPP polymer proportion on the cell viability. Up to N/P ratio 3, neither PEI-, nor PPP polyplexes revealed any cytotoxic behavior. At N/P 6, only PPP 5 reduced the cell viability to 85%. The other polyplexes did not affect the cell viability. Increasing the polymer content in the polyplexes led to a gradual increase in cell death from N/P 6 to N/P 15. At N/P 10, only PPP 1 polyplexes did not affect cell viability. All other polyplexes induced cell deaths of 10-20%. This range remained stable after another increase of polymer content to a N/P ratio of 15. In conclusion, the switch to a 10 kDa PEI and the addition of PCL and PEG blocks have helped to reduce the cytotoxic effect of PEI-based nanoparticle systems.

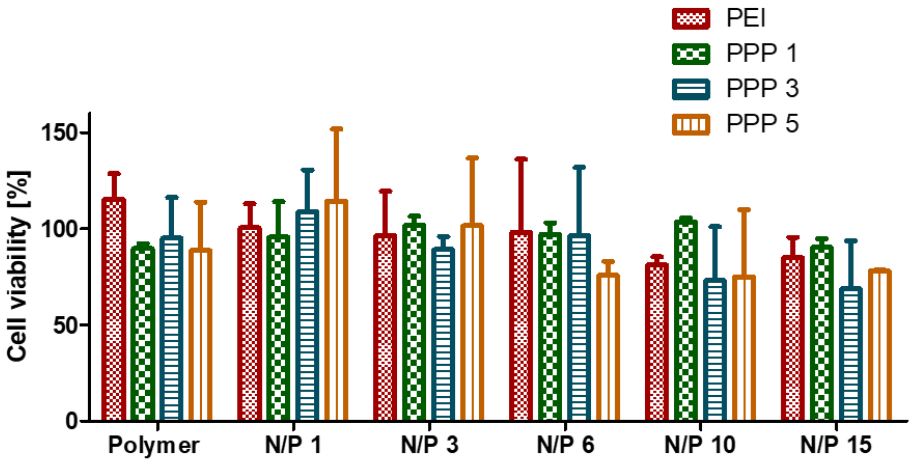

Figure 5 Cytotoxic evaluation of PEI- and PPP-based polyplexes at N/P ratios 1, 3, 6, 10 and 15. All samples were formed via microfluidic mixing having 50 pmol siRNA encapsulated. Results are displayed as mean ± SD, n = 3.

4. Summary & Conclusion

In this study we tested novel triblock copolymers, PEG-PCL-PEI (PPP), adapting the composition to optimize the polymer's siRNA complexation, physicochemical properties and *in vitro* performance as a nucleic acid drug delivery system. Prior studies served as a template to address PEIs weaknesses in cell uptake and cytotoxic effects. Various PPP compositions were synthesized to evaluate polyplex characteristics of hydrophobicity versus hydrophilicity, induced by the ratio between PCL and PEG block, or PEG versus PEI amount, influencing the endosomal release capability. Microfluidic mixing was the preferred polyplex formation method as it rapidly mixes polymers and siRNA to form

reproducible and homogeneous nanoparticle systems. In a comparison of polyplexes produced by direct pipetting against microfluidic mixing, latter method resulted in smaller sizes of 68.0 – 96.8 nm. A discrepancy between all PPP polyplexes was observed as PPP 5 polyplexes did not change in sizes using microfluidic mixing. However, PPP 1 and PPP 3 polyplex sizes were reduced by 20-28 nm. PDIs remained at 0.26 – 0.4 showing wider size distribution, independent of the formation method. Hence, the polymers' chemical composition to complex siRNA did already reach the performance limit which could not be improved by microfluidic mixing. The zeta potential reached the target of slightly positive values of +3 mV - +5 mV. These results go hand in hand with a prior mixing study of PPP polyplexes by Feldmann et al. [34] The polymer's composition of various PEG and PCL block weights and lengths confirmed the hypothesis of improving the cellular uptake by increasing hydrophobicity. All PPP polyplexes outperformed PEI. PPP 3 and PPP 5 almost managed to reach a cell uptake which was as good as the golden standard Lipofectamine 2000. Unfortunately, this trend was not seen in the gene silencing experiment. Only PPP 5 managed to knock GFP down at about 50% which was a slight improvement to the performance of PEI-based polyplexes. Therefore, the polyplexes seem to face an endosomal escape problem. The reduction in PEI mass and branching benefited a low cytotoxicity but came to the cost of a reduced endosomal escape.

In conclusion, the idea to improve PEIs' performance and overcome its weaknesses by adding hydrophobicity and colloidal stability through creation of a triblock copolymer PEG-PCL-PEI was well thought. Results of physicochemical properties and uptake behavior underline the superiority of the PPP over PEI. However, the transfection did not lead to sufficient outcomes because of the existing endosomal release problem. Further optimization of finding the right composition of the PPP polymer would be necessary. Another idea could be to synthesize a triblock copolymer PEI-PCL-PEI leaving out PEG. The loss in hydrophilicity can be overcome by adding PEI endings which would increase the buffering capacity and proton-sponge effect leading to an improved endosomal release. An important fact that needs to be considered when working with PPP is the long-term storage and composition. The chemical structure reveals amines close to ester bonds which could undergo aminolysis leading to degradation and loss in effectiveness.

Chapter IV – Amphiphilic poly(spermine acrylamides): A new class of sophisticated non-viral vectors for pulmonary siRNA delivery

This chapter is prepared for submission and peer review as:

„Amphiphilic poly(spermine acrylamides): A new class of sophisticated non-viral vectors for pulmonary siRNA delivery"

Author‘s contributions:

Friederike Adams,[a,b] Christoph M. Zimmermann,[a,d] Domizia Baldassi,[a] Thomas M. Pehl,[c] Philipp Weingarten,[a] Iris Kachel,[a] Moritz Kränzlein,[c] and Olivia M. Merkel[a]

F.A., T.M.P., P.W., I.K. and M.K. synthesized and characterized the polymers. C.M.Z performed the nanoparticle characterization and in vitro experiments. D.B. performed the in vivo experiments. C.M. Z. and F.A. evaluated the data and wrote the manuscript. F.A., C.M.Z, O.M.M conceived the presented idea and planned the experiments. O.M.M supervised the work, provided conceptual guidance and corrected the manuscript.

g. *Pharmaceutical Technology and Biopharmaceutics, Department Pharmacy, Ludwig-Maximilians-University Munich, Butenandtstr. 5-13, 81377 Munich, Germany*

h. *Institute of Polymer Chemistry, Chair of Macromolecular Materials and Fiber Chemistry, University of Stuttgart, Pfaffenwaldring 55, 70569 Stuttgart, Germany Eberhard-Karls University of Tübingen, Geschwister-Scholl-Platz, 72074 Tübingen, Germany*

i. *WACKER-Chair of Macromolecular Chemistry, Catalysis Research Center, Department of Chemistry, Technical University Munich, Lichtenbergstr. 4, 85748 Garching bei München (Germany)*

j. *Pharmaceutical Technology, Departement for Chemistry, Biochemistry and Pharmacy, University Bern, Freiestrasse 3, CH - 3012 Bern*

Key words: pulmonary delivery, siRNA delivery, poly(spermine acrylamide), radical polymerization, post-polymerization functionalization, nanomedicine, non-viral vectors

Abstract

RNA interference by small interfering RNA (siRNA) is an efficient strategy to silence genes. However, clinically relevant, and targeted application of siRNA still faces several challenges since siRNA is a negatively charged macromolecule. Consequently, suitable carriers for siRNA must be developed in which the synthesis of spermine-based, brushed poly(acrylamides) is reported herein. Polymers are prepared via polymerization of N-acryloxysuccinimide, an active ester of acrylic acid. The active ester was converted into spermine-based pendant groups by reaction with a spermine-derivative. Copolymerizations with hydrophobic decylacrylamide, which has an excellent balance of hydrophobicity and size, are employed to increase the hydrophobicity of the polymers and to obtain amphiphilic materials. After deprotection of the primary and secondary amino groups of spermine-containing side chains, these polymers are observed to have high potential as siRNA delivery agents for pulmonary delivery. Polymers showed excellent siRNA encapsulation to obtain perfectly sized polyplexes at very low N/P ratios. Hydrophobic segments improved siRNA uptake to cancer cells due to an enhanced compatibility of the amphiphilic polymers with the plasma membrane. In vitro 2D and 3D cell culture and in vivo experiments revealed superior properties of amphiphilic spermine-copolymers in delivery of siRNA to lung cells in comparison to commonly used transfection agents showing a perfect balance between efficient polyplex formation, toxicity, and siRNA delivery efficiency.

1. Introduction

RNA mediated targeted inactivation of genes, known as RNA interference (RNAi), is an established technique for the investigation of cellular processes in vivo and is increasingly being suggested for the potential treatment of a plurality of diseases such as respiratory disorders (e.g. severe acute respiratory syndrome viruses or asthma), rheumatic diseases, brain diseases or degenerative disorders. [199-215] Since artificially synthesized siRNAs can be introduced into cells by transfection, in principle sequence-specific cleavage of any target mRNA can be achieved via a complementary siRNA. [216-221] Despite intensive research, to date, FDA has approved five siRNA agents: Onpattro®/patisiran, Givlaari®/givosiran, Oxlumo™/lumasiran, Leqvio®/inclisiran, and Amvuttra™/vutrisiran; all targeting liver-specific diseases, which shows the lack of current therapy in specific targeting of siRNA therapeutics beyond the liver, especially when administered intravenously. [4, 222, 223] Local administration routes can improve the performance of in vivo RNAi. Intranasal or intratracheal delivery to airway and alveolar epithelium can enhance delivery efficiency of siRNA regarding respiratory disorders without the need for active targeting combined with the advantage of reduced doses compared to systemic administration. Thus, less systemic side effects are expected, and interactions with serum proteins can be avoided. Due to administration directly to nose or mouth, direct access to target lung epithelial cells is facilitated which are essential target cell types in a variety of pulmonary diseases (e.g., cystic fibrosis, chronic obstructive pulmonary disease, asthma, lung cancer, pulmonary fibrosis, influenza, or SARS corona viruses). [216-220, 224-226] Despite several advantages of pulmonary administration, major barriers of respiratory delivery are mucociliary clearance, the presence of mucus and clearance of particles by macrophages. [227] In the context of pulmonary delivery, polymers can be advantageous over other non-viral vectors to protect and transport negatively charged siRNA due to their higher encapsulation efficiencies of nucleic acids, combined with a better reproducibility of the formed siRNA/polymer-complexes (polyplexes) and their improved stability in lung surfactants. [227, 228] In addition, these polycationic polymers can be synthesized on a large scale and generally exhibit higher biocompatibility than viral vectors. [229] The development of polymers overcoming low transfection efficiencies of non-viral systems combined with minimal cytotoxicity remains to be the greatest barrier of successful non-viral nucleic acid delivery. [230, 231] Spermine is a biogenic polyamine with great potential in nucleic delivery as it is found as a polycation at all pH values, however,

it shows only low ability to condense siRNA due to its low molecular weight. It is produced biosynthetically from the amino acids arginine and ornithine via polycationic intermediates putrescine and spermidine regulated by several enzyme classes such as oxidases, transferases, synthases and decarboxylases, making spermine-containing polymers potentially biodegradable. [232-235] Although the first gene transfer in mammalian cells was performed by Szybalksa and Szybalksi in 1962 with spermine, spermine polymers still remain rare in literature. [236] To the best of our knowledge, spermine-containing polymers for RNA delivery are restricted to oligomeric and low-molecular weight forms, modification of precursors with low numbers of spermine molecules or linear spermine-polymers that solely bear secondary amines hindering efficient nucleic acid delivery. [237-249] However, for all these examples, excellent toxicity profiles have been reported.

Since high molecular weight and branched polymers often have beneficial transfection efficiencies, we herein report on novel high molecular weight, brushed spermine-based polyacrylamides synthesized via facile free-radical polymerization of N-acryloxysuccinimide (NAS), an active ester monomer. Post-polymerization functionalization with a modified spermine-species and deprotection led to poly(spermine acrylamides) P(SpAA) with increased molecular-weights which still contain a high density of secondary and primary amines. To boost the non-specific cellular uptake, enhanced interaction of hydrophobic groups with the plasma membrane by binding of amphiphilic compounds to lipid membranes can be exploited to consequently also result in higher transfection efficiencies. [229, 250, 251] Additionally, hydrophobic modifications with alkyl chains have been reported to decrease cytotoxicity of cationic polymers. [252, 253]

To investigate the impact of different hydrophobic fractions on siRNA delivery, copolymers with varying ratios of spermine acrylamide (SpAA) units (cationic) and hydrophobic units, derived from N-decylacrylamide (DAA), were synthesized. This hydrophobic monomer, which has an excellent balance of hydrophobicity and size, has received little attention for drug delivery applications. Only very few reports are published in the current literature in which DAA was used for micellar approaches. [254-256] The obtained homopolymers P(SpAA) 1-3 and copolymers P(SpAA-co-DAA) 1-3 showed different molecular weights and molar ratios of DAA ranging from 0-60 mol%. Polymers were fully characterized and achieved excellent siRNA encapsulation to obtain perfectly sized polyplexes at low polymer excess. In vitro 2D and 3D cell culture experiments and in vivo experiments revealed superior properties of amphiphilic P(SpAA-co-DAA) in delivery of siRNA to lung cells showing a perfect balance between polyplex formation, toxicity, and siRNA delivery efficiency.

2. Experimental section

2.1 Materials and Methods for Polymer Synthesis and Characterization of Polymer-Samples:

All reactions were carried out under nitrogen atmosphere using standard Schlenk techniques. All glassware was heat dried under vacuum prior to use. Unless otherwise stated, all chemicals were purchased from Sigma-Aldrich, Acros Organics, or TCI and used as received. Hyperbranched polyethylenimine (PEI, 25 kg/mol) was obtained from BASF (Ludwigshafen, DE). Solvents for polymerization were used in an anhydrous form unless otherwise stated.

NMR spectra were recorded on a Bruker AVIII-300, AVIII-400, a Avance III HD Bruker BioSpin 400 or AVIII-500 Cryo spectrometer at Ludwig-Maximilians University Munich or Technical University of Munich in the respective NMR facilities.

Unless otherwise stated, 1H- and 13C-NMR spectroscopic chemical shifts δ are reported in ppm. δ (1H) is calibrated to the residual proton signal, δ (13C) to the carbon signal of the solvent. Deuterated solvents were obtained from Sigma-Aldrich, Deutero or Eurisotop.

Elemental analysis was measured at the Laboratory for Microanalysis of the Central Analytics of the Faculty of Chemistry and Pharmacy, Ludwig-Maximilians-University Munich, on an Elementar vario EL or Elementar vario micro cube.

ESI-MS analysis was performed using a Thermo Finnigan LTQ FT Ultra Fourier Transform ion cyclotron resonance mass spectrometer in positive ionization mode. The resolution was set to 100,000 at 400 m/z. Depending on the respective measurement, mass ranges from 50 to 2000 u were detected. The spray capillary voltage on the IonMax ESI head was 4 kV, the heater capillary temperature 250 °C, the nitrogen sheath gas flow 20 and the sweep gas flow 5 units.

Molecular weights and polydispersities of polymers were measured via size exclusion chromatography (SEC) with samples of 3-5 mg/ml concentration either on a Varian 390-LC at 30 °C equipped with two PL Gel 5 µm Mixed C columns using a refractive index detector (RI detector) with chloroform as eluent relative to polystyrene standards or on an Agilent PL-GPC 50 equipped with two PL-Polargel-M columns and an RI detector at 30°C using a mixture of DMF and 0.025 mol/l lithium bromide as eluent relative to poly(methyl methacrylate) (PMMA) depending on the solubility of the polymers.

2.1.1 Buffering capacity.

Acid-base titration studies over pH values ranging from 12 to 2 were performed to determine the buffering capacity of the studied polymers. In brief, an aqueous polymer solution with a concentration of 1 or 5 mg/mL was prepared and the pH was adjusted to 12 to 11.5 with 0.1 M NaOH. Subsequently, the solution was titrated with 0.1 M HCl and pH change was measured after every 50 µL addition, until the pH of the polymer solutions decreased to a constant pH of 2-3. The pH value was monitored with a pH-meter and an electrode at 25 °C (Fisherbrand accumet AB150, Fisher Scientific GmbH, Schwerte, Germany).

2.1.2 Critical Micelle Concentration (CMC).

The measurement of the CMC of the studied polymers was carried out according to literature. [257] A Nile red stock solution was prepared by dissolving the dye in DMSO at a concentration of 0.794 mg/mL. Multiple stock solutions of each polymer were prepared in high purity water, then combined with the Nile red stock solution and additional water high purity water was added to provide the final concentrations to obtain a concentration series of each polymer. The solutions were sonicated for 30 min at 35 °C and incubated at 25 °C for 5 h. After incubation, the solutions were transferred to a black 96-well microplate (Microplate, PS 96 well, Black, Fluotrac, Greiner Bio-One, Frickenhausen, Germany). Excitation/emission wavelengths of 485/636 nm were used measured on a microplate reader (TECAN Spark, TECAN, Maennedorf, Switzerland).

2.2 Materials and Methods for Cell Culture:

Highly purified water (HPW) was provided by Ludwig-Maximilians-University Munich. HEPES (4-(2-hydroxyethyl)-1-piperazineethanesulfonic acid), sodium acetate, Heparin sodium salt, Thiazolyl blue tetrazolium bromide (MTT), RPMI-1640 Medium, Fetal Bovine Serum (FBS), Penicillin-Streptomycin solution, Dulbecco's Phosphate Buffered Saline (PBS), Trypsin-EDTA solution 0.05%, L-glutamine solution 200 mM, dimethyl sulfoxide (DMSO) and Geneticin (G418) disulfate solution were purchased from Sigma-Aldrich (St. Louis, MO, USA). NCI-H1299 (human non-small cell lung carcinoma) cell line, green fluorescent protein (GFP) reporter cell line-NCI-H1299 (human non-small cell lung carcinoma) and L929 cells (subcutaneous tissue fibroblasts) were purchased from ATCC (Manassas, VA, USA). SYBR Gold Dye, Lipofectamine 2000 Transfection Reagent, AlexaFluor 488 (AF488) dye were purchased from Life Technologies (Carlsbad, California, USA). HyClone trypan blue solution 0.4% in phosphate buffered saline was obtained from FisherScientific (Hampton, New Hampshire, USA). Amine modified GFP siRNA (5′ - pACCCUGAAGUUCAUCUGCACCACcg, 3′ -

ACUGGGACUUCAAGUAGACGGGUGGC) and scrambled siRNA (5′ - pCGUUAAUCGCGUAUAAUACGCGUat, 3′ - CAGCAAUUAGCGCAUAUUAUGCGCAUAp) were purchased from Integrated DNA Technologies (Coralville, IA, USA) (indication of modified nucleotides: “p” denotes a phosphate residue, lower case letters are 2′-deoxyribonucleotides, capital letters are ribonucleotides, and underlined capital letters are 2′-O-methylribonucleotides).

NCI-H1299 cells (human non-small cell lung carcinoma cells) and L929 cells (mouse subcutaneous tissue fibroblasts) were cultured in RPMI-1640 media supplemented with heat inactivated FBS (10%) and Penicillin-Streptomycin (1%). GFP reporter cell line-NCI-H1299 was cultivated in RPMI-1640 media supplemented with heat inactivated FBS (10%), Penicillin-Streptomycin (1%) and 0.4% (v/v) Geneticin (G418). The plasmid for GFP expression contains an antibiotic resistance for Geneticin to enable the selection of stably expressing GFP cells. All cells were subcultured, maintained, and grown in an incubator under humidified air with 5% CO2 at 37 °C.

2.2.1 Preparation of Polyplexes

To prepare polymer-siRNA complexes (polyplexes), aqueous polymer stock solutions (1 mg/mL) were diluted with freshly, sterile filtered HEPES buffer (pH 7.4) to predetermined concentrations. Afterwards, the polymer solution was added to a defined amount of siRNA in a microcentrifuge tube and vigorously mixed to obtain polyplexes at various N/P ratios. An incubation time of one hour facilitated a stable polyplex formation. The N/P ratio is defined as the molar ratio between the polymers’ amine groups (N) and the siRNA’s phosphate groups (P). The amount of polymer needed to obtain different N/P ratios was calculated according to following equation:

m (polymer in pg) = n siRNA (pmol) x protonable unit (g/mol) x N/P x number of nucleotides siRNA.

Hyperbranched PEI (25 kg/mol, Lupasol® WF, BASF, Ludwigshafen, Germany) has a protonable unit of 43.1 g/mol. The number of nucleotides of 25/27mer siRNA is set to 52. Lipofectamine polyplexes were prepared according to the manufacturer’s protocol.

2.2.2 Size and Zeta (ζ)-Potential Analysis by Dynamic Light Scattering and Laser Doppler Anemometry

Particle size, polydispersity index (PDI) and zeta potential of polyplexes were measured using a Zetasizer Nano ZS (Malvern Instruments, Malvern, UK). After 1-hour incubation time, 100 µl of freshly prepared polyplexes were used for particle size and PDI measurements. Zeta potentials were measured using a Zeta Cell (Zetasizer Nano series, Malvern, UK) containing a 6.5X dilution of the same 100 µl sample of polyplex suspension. Results are expressed as mean ± standard deviation (n = 3; the diameter was averaged over three independent values consisting each of 15 measurements).

2.2.3 siRNA encapsulation Assay by SYBR Gold assay

SYBR Gold assay was used to evaluate the capacity of the polymers to condense siRNA at various N/P ratios as previously described. [237] For each batch, 100µl of polyplex solution was transferred to a black FLUOTRAC 96 well plate (Greiner Bio-One, Frickenhausen, Germany). A 4X SYBR Gold solution (30 µL) was added to each well and the plate was incubated for 10 min in the dark. The fluorescence signal was determined using a fluorescence plate reader (TECAN Spark, TECAN, Maennedorf, Switzerland) at 485 nm and 535 nm excitation and emission wavelengths. Analogue procedure with free siRNA was used as 100% value. Measurements were performed in triplicates and results are shown as mean values ± standard deviation (n = 3).

2.2.4 Heparin Assay

Heparin assays were used to determine the stability of the polyplexes at a physiologically relevant pH 7.4, as well as at pH 4.5 representing the late endosome. N/P ratio of 7 was chosen for all polymer-

siRNA polyplex formations for testing the stability against increasing amounts of heparin (0, 0.1, 0.25, 0.5, 0.75 and 1.0 international Unit (1 IU = 4.926 µg heparin sodium salt). All polyplexes were formed as described in the preparation of polyplexes. The samples at pH 7.4 were prepared in 100 µL 10 mM HEPES buffer, while the samples measured at pH 4.5 were prepared in 100 µL sodium acetate buffer. Samples were prepared as described for the SYBR gold assay with the exception of adding 10 µL of heparin solution at various concentrations (0 - 1.0 IU per well) and incubated for another 30 minutes before adding the SYBR Gold solution. The fluorescence was measured at 485 nm and 535 nm excitation and emission wavelengths using a microplate reader (TECAN Spark, TECAN, Maennedorf, Switzerland). The experiments were run in triplicates and results were analyzed as described before for the SYBR Gold assay.

2.2.5 MTT Assay

Cytotoxicity of free polymers (PEI, P(SpAA)1-3 and P(SpAA-co-DAA)1-3) was tested via an MTT Assay as described previously. [258, 259] 5,000 L929 cells per well were seeded in a transparent 96 well plate (BioLite 96 well multidish, Thermo Fisher Scientific, Rochester, New York, USA). After 24 hours, different stock concentrations of free polymers were diluted in 10 mM HEPES buffer (pH 7.4) to a final volume of 10 µL. This volume was added to 90 µL of prewarmed RPMI-1640 medium to obtain polymer concentrations of 5, 10, 15, 25, 50 and 100 µg/mL. The cell medium of every well was aspirated and 100 µl of polymer containing media was added to each well and incubated for 24 hours at 37 °C and 5% CO2. As a positive control, cells were incubated in 100 µL consisting of 10 µL 10 mM HEPES buffer (pH 7.4) and 90 µL medium. After 24 hours, media was aspirated and 100 µl of MTT containing medium (0.5 mg/ml in serum-free RPMI-1640 medium) was added to each well. Cells were incubated for another 3 hours in the incubator. Subsequently, the cell culture medium was completely removed and insoluble purple formazan crystals, converted from water soluble MTT by metabolically active mitochondria, [260] was dissolved in 200 µl DMSO. The absorption was measured at 570 nm, corrected with background values measured at 680 nm, using a microplate reader (TECAN Spark, TECAN, Maennedorf, Switzerland). Data is shown as mean ± SD from three independent experiments that were run in duplicates as percentage of viable cells in comparison to untreated cells representing 100% viability. IC 50 values were calculated by plotting the concentration on a logarithmic axis against cell viability using OriginPro 2019b software (OriginLab, Northampton, Massachusetts, USA).

2.2.6 Quantification of Cellular Uptake by Flow Cytometry

Flow cytometry was used to quantify the in vitro cellular uptake of polyplexes. Amine modified siRNA was labeled with the fluorescence dye Alexa Fluor 488 (siAF488) following the manufacturer´s protocol and purified by ethanol precipitation and spin column binding as described previously. [180] NCI-H1299 cells were seeded in 24 well plates at a density of 50,000 cells per well and incubated for 24h at 37 °C and 5% CO2. For all uptake experiments, negative controls consisted of cells treated with free siRNA (siAF488), while positive control cells were transfected with Lipofectamine 2000-siAF488 lipoplexes, which were prepared according to the manufacturer's protocol. Cells were transfected with positive and negative controls and polyplexes containing 100 pmol siAF488 for 24 hours. After incubation, medium was aspirated, cells were washed with prewarmed PBS and detached using 0.05% trypsin-EDTA. RPMI-1640 medium was added to all samples and spun down at 400G for 5 minutes using a centrifuge (Heraeus Megafuge 16R, Thermo Fisher Scientific, Osterode am Harz, Germany). Medium was aspirated without taking out the cell pellet. Samples were washed two times with PBS and resuspended in 500 µl PBS/2 mM EDTA. Median fluorescence intensities (MFI) were analyzed using an Attune NxT Acoustic Focusing Cytometer (Thermo Fisher Scientific, Waltham, Massachusetts, USA) by exciting the siRNA-AF488 at 488 nm and measuring the fluorescence signal with an 530/30 nm emission filter. Subsequently, trypan blue quenching was used to exclude surface fluorescence signals of not completely internalized siRNA-complexes and MFI of samples was measured again. Data

is shown from two independent experiments that were run in duplicates, each sample consisting of a minimum of 10,000 viable cells. Three-way ANOVA with Bonferroni mean comparison ($p > 0.05$ considered not significant (ns); $*p < 0.05$, $**p < 0.01$, $***p < 0.001$ considered significantly different) was performed with OriginPro 2019b software (OriginLab, Northampton, Massachusetts, USA).

2.2.7 *In vitro* eGFP Knockdown

To determine if polyplexes can efficiently knockdown protein levels in cells, the green fluorescent reporter gene (eGFP) was intended to be silenced by siRNA (siGFP) comprised polyplexes. 25,000 NCI-H1299/eGFP cells per well were seeded in 24 well plates in 500 µl RPMI-1640 + 0.4% G418 medium and grown for 24 h at 37 °C in humidified atmosphere with 5% CO_2. As positive control, Lipofectamine 2000-siGFP lipoplexes formulated with 100 pmol of siRNA against eGFP and as negative control poly - and lipoplexes containing 100 pmol of scrambled siRNA (siNC) were used. Nanoparticle formation was followed as described for the preparation of polyplexes. Cells were transfected with siGFP-polyplexes for 48 h at 37 °C in humidified atmosphere with 5% CO_2. Subsequently, cells were trypsinized and prepared for flow cytometry measurements as described for cellular uptake experiments. MFIs of samples were quantified using an Attune Cytometer (Thermo Fisher Scientific, Waltham, Massachusetts, USA) with an 488nm excitation laser and an 530/30 nm emission filter. Data is shown from two independent experiments that were run in duplicates, each sample consisting of a minimum of 10,000 viable cells. Three-way ANOVA with Bonferroni mean comparison ($p > 0.05$ considered not significant (ns); $*p < 0.05$, $**p < 0.01$, $***p < 0.001$ considered significantly different) was performed with OriginPro 2019b software (OriginLab, Northampton, Massachusetts, USA). Results are shown as percentage of knockdown in comparison to the expression level in negative controls of each polymer.

2.3 Methods for Air-Liquid Interface (ALI) Cell Culture:

2.3.1 Materials

Eagle´s Minimum Essential Medium (EMEM), Trypsin 0.25%, PBS, Tween 20 and formaldehyde solution were purchased from Sigma Aldrich (St. Louis, MO, USA). Rhodamine phalloidin, 4′,6-diamidino-2-phenylindole (DAPI), and AF488-wheat germ agglutinin were obtained from Life technologies. FluorSave was purchased from Merck Millipore. Transwell® polyester cell culture inserts (6.5 mm, 0.4 µm pore) were purchased by Corning. PneumaCult™ ALI medium was obtained by STEMcell technology.

2.3.2 Culturing conditions

Calu3 cells were maintained in EMEM medium supplemented with 10% FBS and 1% P/S. Cells were cultivated in 75 cm2 and split with 0.25% trypsin/EDTA solution. Cells were maintained at 37°C and 5% CO2.

Calu3 cells were seeded at a density of 250,000 cells onto uncoated Transwell® polyester cell culture inserts (6.5 mm, 0.4 µm pore, Corning, USA) in 100 µl of medium, while 700 µl were added to the basolateral chamber. After 72 hours, apical medium was removed from the inserts to obtain ALI conditions, while the basolateral medium was replaced with 200 µl of PneumaCult™ ALI medium (STEMcell technology, Vancouver, Canada) and replaced every two days. Experiments were performed after TEER values ≥ 300 Ω*cm2 were reached as measured by EVOM epithelial volt/ohm meter (World Precision Instruments, Sarasota, USA).

2.3.3 Phalloidin staining

For microscopy experiments, amine modified siRNA was labeled with succinimidyl ester (NHS) modified AlexaFluor647 (Life Technologies, Carlsbad, USA) according to the manufacturer´s protocol and purified via ethanol purification to obtain the resulting AF647-siRNA, as previously described. [180] Calu3 monolayers were transfected with 100 pmol AF647-siRNA/P(SpAA-co-DAA)3 polyplexes

at N/P 5 for 24 h. Afterwards, monolayers were fixed in 4% PFA for 15 minutes, washed three times with PBS and permeabilized with PBS + 0.3% Tween 20 for 10 minutes. Cells were then incubated with rhodamine phalloidin (Life technologies, Carlsbad, USA) for 60 minutes. Finally, nuclei were stained with 4′,6-diamidino-2-phenylindole (DAPI) (Life technologies, Carlsbad, USA) at a concentration of 0.5 µg/ml for 15 minutes and washed two times with PBS. Samples were then mounted on glass slides using FluorSave reagent (Merck Millipore, Billerica, USA) prior to analysis with a SP8 inverted scanning confocal microscope (Leica Camera, Wetzlar, Germany). The images were exported from the Leica Image Analysis Suite (Leica) and processed with the Fiji distribution of ImageJ.

2.3.4 Mucus staining

Calu3 monolayers were transfected with 100 pmol AF647-siRNA/P(SpAA-co-DAA)3 polyplexes at N/P 5 for 24 h. Once the incubation time was completed, cells were incubated for 15 minutes with AF488-wheat germ agglutinin (WGA) (Life technologies, Carlsbad, USA) at 37 °C and 5% CO2, washed with PBS twice and mounted on glass slides using Fluorsave. Monolayers were then immediately analyzed with a SP8 inverted scanning confocal microscope (Leica Camera, Wetzlar, Germany). The images were exported from the Leica Image Analysis Suite (Leica) and processed with the Fiji distribution of ImageJ.

2.3.5 qPCR

Calu3 monolayers were transfected with 100 pmol siGAPDH/P(SpAA-co-DAA)3 polyplexes at N/P 5 and respective siNC as negative control for 24 h at 37 °C and 5% CO2. Lipofectamine lipoplexes were prepared as positive control. Cells were then lysed, and RNA was isolated using the PureLink RNA mini kit (Thermo Fischer Scientific, Waltham, USA) according to the manufacturer's protocol with additional DNase digestion. Afterwards, cDNA was synthetized using the high-capacity cDNA synthesis kit (Applied Biosystems, Waltham, Massachusetts). For qPCR, cDNA was diluted 1:10 and run with primers for GAPDH (Qiagen, Hilden, Germany) as well as β-actin (Qiagen, Hilden, Germany) for normalization. Cycle thresholds were acquired by auto setting within the qPCRsoft software (Analytic Jena, Jena, Germany). Values are given as mean ± SEM with n = 3. Two-way ANOVA with Bonferroni mean comparison ($p > 0.05$ considered not significant (ns); * $p < 0.05$, ** $p < 0.01$, *** $p < 0.001$ considered significantly different) was performed with OriginPro 2019b software (OriginLab, Northampton, Massachusetts).

2.4 Methods for *in vivo* studies:

2.4.1 Animals

All animal experiments were carried out according to the German law of protection of animal life and approved by an external review committee for laboratory animal care.

Female Balb/c mice were purchased form Charles River Laboratories and used at 5 weeks of age. Mice were intratracheally instilled (under ketamine/xylazine anaesthesia) with 2 nmol siRNA/P(SpAA-co-DAA)3 polyplexes at N/P 5 prepared in 50 µl 5% glucose as well as with siRNA/PEI polyplexes prepared in 50 µl 5% glucose. As negative control, animals were administered with 5% glucose only. After 48 h, mice were sacrificed and bronchoalveolar lavage fluid (BALF) as well as blood was collected.

BALF was obtained by lavaging lungs with 1 ml PBS/protease inhibitor and stored at -80 °C. The concentration of interleukins in BALF was determined using the mouse LEGENDplex ELISA kit (BioLegend, San Diego, California). Values are given as mean ± SEM with n= 4 for treatment with PEI or P(SPAA-co-DAA)3 polyplexes and n = 2 for untreated mice. One-way ANOVA with Bonferroni mean comparison ($p > 0.05$ considered not significant (ns); * $p < 0.05$, ** $p < 0.01$, *** $p < 0.001$

considered significantly different) was performed with OriginPro 2019b software (OriginLab, Northampton, Massachusetts).

Additionally, lung cell suspensions were prepared as previously reported. [261] Lung cell suspension were counterstained with BB515 labelled rat anti-mouse CD45 (30-F11, 1:40, BD Biosciences, Franklin Lakes, New Jersey), pacific orange labelled F4/80 (1:100, Invitrogen, Waltham, Massachusetts), BV421 labelled anti-tubulin Beta 3 (1:100, BioLegend, San Diego, California), anti-prosurfactant protein C (1:100, Abcam), mouse anti-rabbit PE-Cy7 (1:200, Santa Cruz Biotechnology), anti-uteroglobin antibody (1:100, Abcam) and mouse anti-rabbit AF594 (1:200, Invitrogen, Waltham, Massachusetts) following the manufacturer's protocol. The analysis was performed on a Cytek Aurora (Cytek Biosciences, Fremont, California). The different populations of leukocytes (CD45+), macrophage/monocytes (F4/80+), Type II pneumocytes (proSPC+), ciliated cells (tubulin beta +) and club cells (uteroglobin +) were gated and the MFI of siRNA-AF647 in the different cell populations was quantified. Values are given as mean ± SEM with n= 2 for treatment with PEI or P(SPAA-co-DAA)3 polyplexes.

2.5 Buffering capacity

In the past years, a multitude of different polymers ranging from bio-based polymers such as chitosan and poly(L-lysine) to synthetic ones like polyethylenimine (PEI) and polymethacrylates were tested as non-viral vectors for gene and nucleic acid therapy. Studies on structure-function relationships revealed a necessity of positively charged amines in which the structure and density of amines impacted the transfection efficiency. A higher density of amines and thus a higher charge provoke a higher efficiency, but also a higher toxicity. [229] An important property of polycations is their buffering capacity to facilitate endosomal escape of siRNA. Due to the buffering capacity of amine-containing polymers, endosomes can be destabilized which is often explained by the "proton-sponge effect". The residual non-protonated amino groups of the polymers after complexation with siRNA are protonated due to a lower pH in the endosome causing the disruption of the membrane, release of the genetic material into the cytoplasm, and successful transfection. [15, 262]

Amongst the polymers used for nucleic acid delivery, branched PEI is one of the most widely used polymers. It shows a superior transfection efficiency, due to its high buffering capacity caused by its branched polymer architecture. With primary, secondary and tertiary amino groups exhibiting pKa values distributed over the entire physiological pH range (10 to 4), it still has a good buffering capacity in the acidic environment of endo-lysosomes thus acting as a proton sponge. [15, 262] However, as a consequence thereof, it also causes high cytotoxicity, which is associated with limitations and concerns in in vivo applications and with restrictions in clinical trials. [263]

The basic capacity of spermine-polymer P(SpAA)3 and spermine-molecule 4, both with a ratio of primary/secondary/tertiary amines = 1/2/0, was investigated by performing an acid/base titration with 0.1M HCl. It was compared to hyperbranched PEI with a molecular weight of 25 kg/mol and a ratio of primary/secondary/tertiary amines of 1/1.1/0.7 (indicated by the manufacturer, BASF, Ludwigshafen, Germany). Additionally, spermine (primary/secondary/tertiary amines = 2/2/0) was investigated to compare the results with the spermine polymers with respect to changes in basicity when one primary amine is converted to an amide. The resulting titrations curves were illustrated by plotting the pH value versus the amount of added acid (A1, Figure S1). In these measurements, polymers with higher buffering capacities required larger amounts of HCl for the alteration of the pH value of the solution. As presented, PEI has a substantial buffering capacity over almost the whole pH range. The buffering capacity at the pH values higher than 9 is mainly attributed to the primary and secondary amines with the reported pKa values of 8-9, whereas the buffering capacity at lower pH values, especially in the range of 5.5-7, might be associated to the tertiary amines with the pKa values of 6-7, which is in accordance with literature. [264] Spermine itself is known to induce pH buffering. Since the same amount of substance (in mol)

was used regarding each protonable unit, the buffering capacity of P(SpAA)3, 4 and spermine was found to be better than that of PEI in the region of pH 11 to pH 6. The P(SpAA)3 and the small modified spermine molecule 4 showed similar buffering capacities, with the latter performing slightly better, revealing the similarity of both structure with regards to the ratio of primary and secondary amines. Having the highest percentage of primary amines, spermine performed best in the pH region of 11-6. Due to the absence of tertiary amines, a lower buffering capability is observed for P(SpAA)3, 4 and spermine in the pH region of 5 to 2.

Taking into account, that coiling in polyplexes of the brushed polymers might further lower the pKa value of the sterically hindered secondary amines, these results suggest, that within the experimental pH range of 5−8, spermine polymers offer a buffering ability, which can facilitate endosomal escape.

2.6 Critical micelle concentration

The critical micelle concentration (CMC) is defined as the concentration of amphiphilic molecules required for the spontaneous formation of micelles. It is a determining factor for applications of amphiphilic polymers, including drug delivery, as it predicts the micelle-forming capacity and stability of polymeric micelles. Hence, P(SpAA)3 and P(SPAA-co-DAA) 1-3 solutions in water with increasing concentration were prepared. Using the water-insoluble Nile red, a fluorogenic dye that undergoes an increase of fluorescence intensity when encapsulated in the hydrophobic core of a micelle, CMC values were determined by plotting the concentration of the polymer versus the fluorescence of Nile red. [257]

Homopolymer P(SpAA)3 was barely able to encapsulate small amounts of Nile Red when using concentrations of 0.1 mg/mL or more, but only a very low fluorescence was observed (A1, Figure S2). It seems, that the hydrophobic backbone of the polymer led to negligible amphiphilic properties. In contrast, copolymers P(SPAA-co-DAA) 1-3 that bear different percentages of hydrophobic comonomer DAA can encapsulate considerable amounts of Nile Red. In detail, the CMC decreased from 0.24 mg/mL determined for P(SPAA-co-DAA)1 (17% DAA units) nearly six-fold to 0.041 mg/mL for P(SPAA-co-DAA)3 bearing 57% hydrophobic monomer units (A1, Figures S3 – S5). This value is within the same range or even lower than values reported for hydrophobically-modified PEI systems. [265-269] In addition, not only the CMC decreased with increasing amounts of hydrophobic moieties, also the fluorescence value increased significantly indicating that higher amounts of Nile red were encapsulated. Consequently, copolymers P(SPAA-co-DAA) 1-3 seemed to be promising candidates with amphiphilic properties that can enhance cellular uptake and stability of polyplexes.

3. Physico-chemical characterization of siRNA-polyplexes

3.1 siRNA encapsulation ability

SYBR Gold assay was used to evaluate the capacity of the polymers to condense siRNA at various concentrations. An excellent condensation of siRNA is needed to protect siRNA and to ensure cellular uptake while preventing enzymatic degradation. The synthesized positively charged polymers can electrostatically interact with negative charges of phosphate groups in siRNA which is quantified using the fluorescent dye SYBR Gold. Apart from P(SpAA)1-3 and P(SpAA-co-DAA) 1-3, hyperbranched PEI (25 kg/mol) and spermine were used for comparison reasons. In a first comparison, the same concentrations of polymers per siRNA were used, due to different protonable units, to compare polyplexes prepared with the same amount of polymer (Figure 1). However, taking the higher molecular weight of the spermine-polymer repeating units into account, amine concentration is lower in comparison to PEI when using the same amount of polymer. All polymers and spermine were able to condense siRNA in which more efficient encapsulation was observed with increased concentrations, due to higher amounts of positively charged amines facilitating more electrostatic interactions with siRNA. Spermine showed a relatively low siRNA encapsulation ability with a constant value of approximately 4% free siRNA (or detectable siRNA on the surface of the complexes) even at high

concentrations attributed to the rigid siRNA-structure and the low molecular weight of spermine compared to the spermine polymers. Homopolymers P(SpAA)1 and P(SpAA)3 showed full encapsulation at about 1.0 µg polymer per µg siRNA, whereas P(SpAA)2 showed a slightly better encapsulation. Due to the higher number of amines in PEI using same concentrations, siRNA encapsulation is more efficient leading to full encapsulation at weight ratios above 0.4 µgpolymer/µgsiRNA. In matters of N/P ratio this would be a value of 3 regarding the protonable unit of PEI which is in accordance with SYBR gold assays of hyperbranched PEI (25kDa) performed in literature. [270] The N/P ratio is defined as the numbers of amines in the polymer divided by the number of siRNA phosphate groups. Regarding that commonly used number, P(SpAA)1-3 show full encapsulation already at N/P of 1, showing the excellent encapsulation ability of these polymers (A1, Figure S6). An extensive use of free amine groups can be avoided that can provoke high toxicities. In comparison to similar systems, such low N/P ratios for fully condesing siRNA were neither reported for spermine/siRNA complexes nor for hydrophobically-modified PEI/siRNA systems. [237, 240, 241, 244, 249, 271-273]

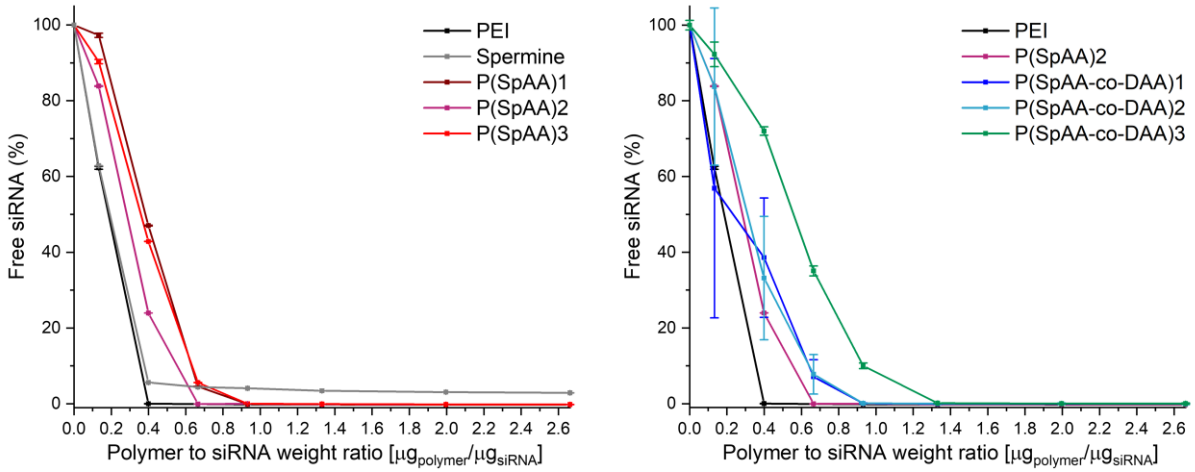

Figure 1 siRNA encapsulation profiles of polyplexes as measured by SYBR Gold assay at various polymer to siRNA weight ratios. 100% values are represented by the determined fluorescence of uncondensed siRNA (data points indicate mean, n = 3).

Copolymers P(SpAA-co-DAA)1 and P(SpAA-co-DAA)2 showed comparable profiles with a sufficient encapsulation of siRNA at concentrations of 1.0 µg polymer per µg siRNA. Furthermore, the P(SpAA-co-DAA)3 copolymer required a higher concentration for a complete encapsulation of siRNA due to high amounts of hydrophobic subunits that do not contribute to electrostatic interactions between amines and siRNA. siRNA encapsulation based on N/P ratio showed that also copolymers can encapsulate siRNA at an N/P ratio of one or higher (A1, Figure S6). From these results, it can be concluded that hydrophobic segments in the polymer do not negatively influence electrostatic interactions of siRNA and amines, as was already observed in literature in which hydrophobic modification led to less efficient siRNA encapsulation than with the unmodified PEI-counterpart at the same N/P ratio. [271, 273]

3.2 Size and zeta(ζ)-potential analysis

Not only the full encapsulation of siRNA, but also size and charge of polyplexes play a major role in successful delivery of the payload. Particle sizes, polydispersity indices (PDI) and zeta potentials of polyplexes were measured using dynamic light scattering (DLS) and laser Doppler anemometry (LDA).

Comparing polyplexes, formed with the same concentration of polymers using three different concentrations (c1 = 5.603 µg/mL, c2 = 7.844 µg/mL, c3 = 11.206 µg/mL polymer representing N/P ratios of 5, 7 and 10 for PEI), all polyplexes were small with slightly positive zeta potentials. These results indicate optimal siRNA encapsulation already at low polymer excess with low to moderate

polydispersities (A1, Figure S7). Solely, P(SPAA-co-DAA)3 was not able to fully encapsulate siRNA at a low concentration of c1; which equals an N/P ratio of 0.75 for this polymer. Incomplete encapsulation is concluded based on the negative zeta-potentials and large, polydisperse particles. Since more phosphate groups are present than nitrogen atoms at such a low N/P ratio, full condensations are rather uncommon. Additionally, spermine was not able to form polyplexes at all concentrations owing to its low molecular weight. Incompletely encapsulated siRNA on the surface of the polyplex causes negative zeta potentials as well as a detection of "free" siRNA as already shown for SYBR gold assays with spermine. Zeta-potentials of PEI-polyplexes were slightly positive to neutral at all concentrations even if those concentrations are comparably high for PEI in matters of N/P ratio (NP = 5 (c1), 7 (c2) and 10 (c3)). All other spermine-polymers showed similar or higher zeta-potentials, confirming that poly(spermine acrylamides) were able to fully encapsulate siRNA already at low concentrations (equals N/P ratio of about 1) and higher concentrations (NP = 1.5 to 2.2). No correlation between sizes and zeta potentials with increasing concentrations was found, as sizes remained small for all polyplexes with full siRNA encapsulation.

To further analyze sizes, polydispersities and zeta potentials with regard to the number of nitrogen atoms per polymer, measurements with all polymers were conducted at N/P ratios of 2, 5 and 7 which are relevant descriptors for in vitro experiments (Figure 2). Since PEI does not show full encapsulation of siRNA at N/P ratio of 2, zeta potentials for these polyplexes were negative and polyplexes showed increased sizes and polydispersities. Polyplexes from poly(spermine acrylamides) displayed efficient siRNA encapsulation at low N/P ratios with small polyplexe sizes between 70 and 130 nm and positive zeta potentials (3 – 23 mV), indicating that these polymers can form optimal particles already at exceptionally low N/P ratios. Advantageously, the use of low polymer excess helps avoiding unwanted side or toxic effects due to a low number of amines present in the system. Polyplexes from P(SpAA)1, P(SpAA)3, P(SPAA-co-DAA)1 and P(SPAA-co-DAA)2 formed at N/P ratios of 2 showed very slightly positive zeta potentials indicating a low amount of excess positive charges. With increasing N/P ratios, zeta potentials became more positive while sizes remained around 100 nm for these polymers. For all polyplexes, polydispersities were low to moderate with values raging between 0.13 and 0.37, with P(SPAA-co-DAA)3 forming the most monodisperse polyplexes (PDI = 0.14 - 0.23) at all tested N/P ratios, most likely due to its most amphiphilic character. Smaller as well as similar to higher sizes were reported in literature for amphiphilic PEI-polyplexes in comparison to the parent PEI indicating that the ability for a dense packaging of siRNA is individual for each cationic system. [271, 274] However, reported polyplex sizes for similar systems were mostly higher than our reported sizes of around 100nm. [273-275]

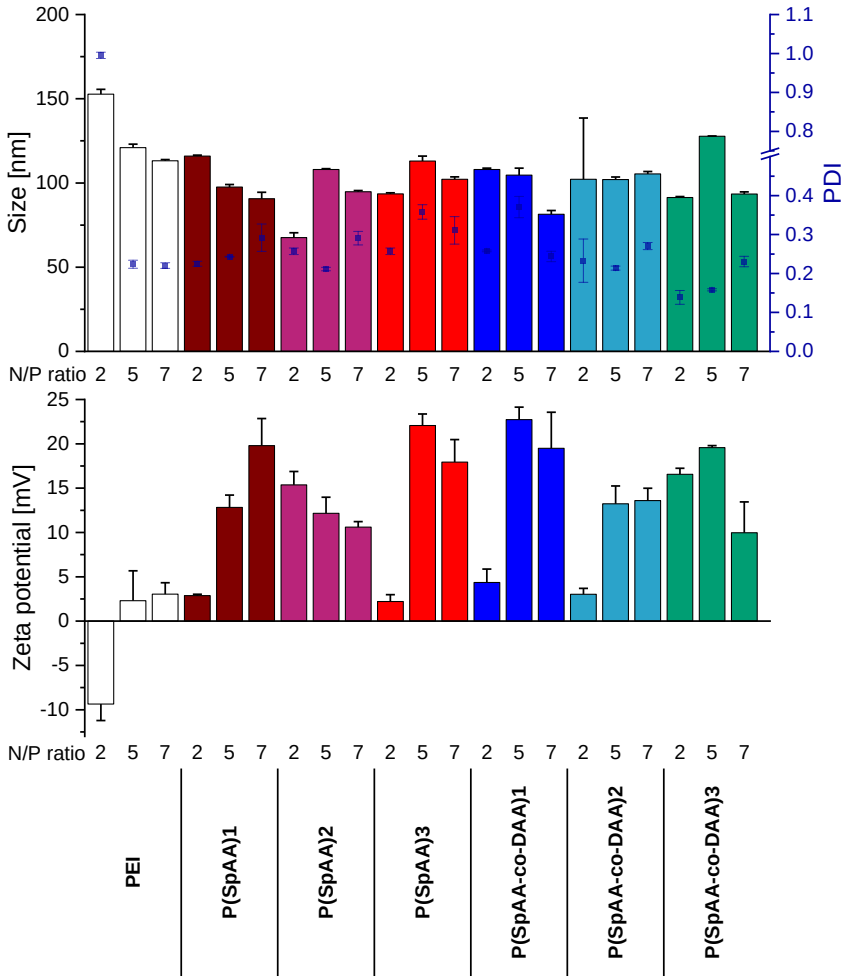

Figure 2 Dynamic light scattering and laser Doppler anemometry measurements of polyplexes formed with PEI, P(SpAA) 1-3 and P(SpAA-co-DAA) 1-3 (Top) Hydrodynamic diameters (left y-axis), polydispersity indices (PDI, right y-axis) and (B) zeta potentials of polyplexes at N/P ratios of 2, 5, and 7 (data points indicate mean ± SD, n = 3).

3.3 Stability of polyplexes

To evaluate polyplex stability in the presence of competing polyanions under neutral and acidic conditions, a heparin-modified SYBR gold competition assay was performed to estimate the behavior in cell culture medium or serum as well as intracellular stability. The ability of P(SpAA)1-3 and P(SpAA-co-DAA)1-3 to protect siRNA in the presence of increasing concentrations of polyanionic heparin under physiologically relevant conditions of the cytoplasm (pH 7.4) was tested (Figure 3, top). siRNA displacement at pH 7.4 from P(SpAA) polyplexes was not observed at low heparin concentrations and reached maximum release of less than 20% at high concentration of 1.00 I.U. heparin per well. P(SpAA)1 and P(SpAA)2 showed slightly better stability at pH 7.4 than P(SpAA)3 reflected by a higher concentration of heparin necessary to replace initial amounts of siRNA. In comparison, PEI formed more loosely assembled polyplexes as higher amounts of siRNA (up to 30%) were released generally, and siRNA replacement took place already at low concentrations of heparin. Similar observations were made for polyplexes with spermine at low heparin concentrations. At high concentrations of 1.00 I.U. heparin per well, a release of up to 80% siRNA was detected from unstable polyplexes formed with spermine which corroborates our earlier findings and investigations on low-

molecular weight oligospermines. [237] P(SpAA-co-DAA) copolymers showed less effective siRNA complexation at higher heparin concentration than homopolymers. Polyplexes from P(SpAA-co-DAA)2 and 3 started to release siRNA at a concentration of 0.25 whereas P(SpAA-co-DAA)1 formed more stable polyplexes with concentrations of 0.50 I.U. of heparin necessary to displace small amounts of siRNA. At high heparin concentration, all polyplexes from copolymers release between 35 and 55% siRNA. Even if this release is higher than for the homopolymers and a low release would be preferred to confirm a high protection ability at pH 7.4, similar values were observed for other polycationic systems [237, 250]

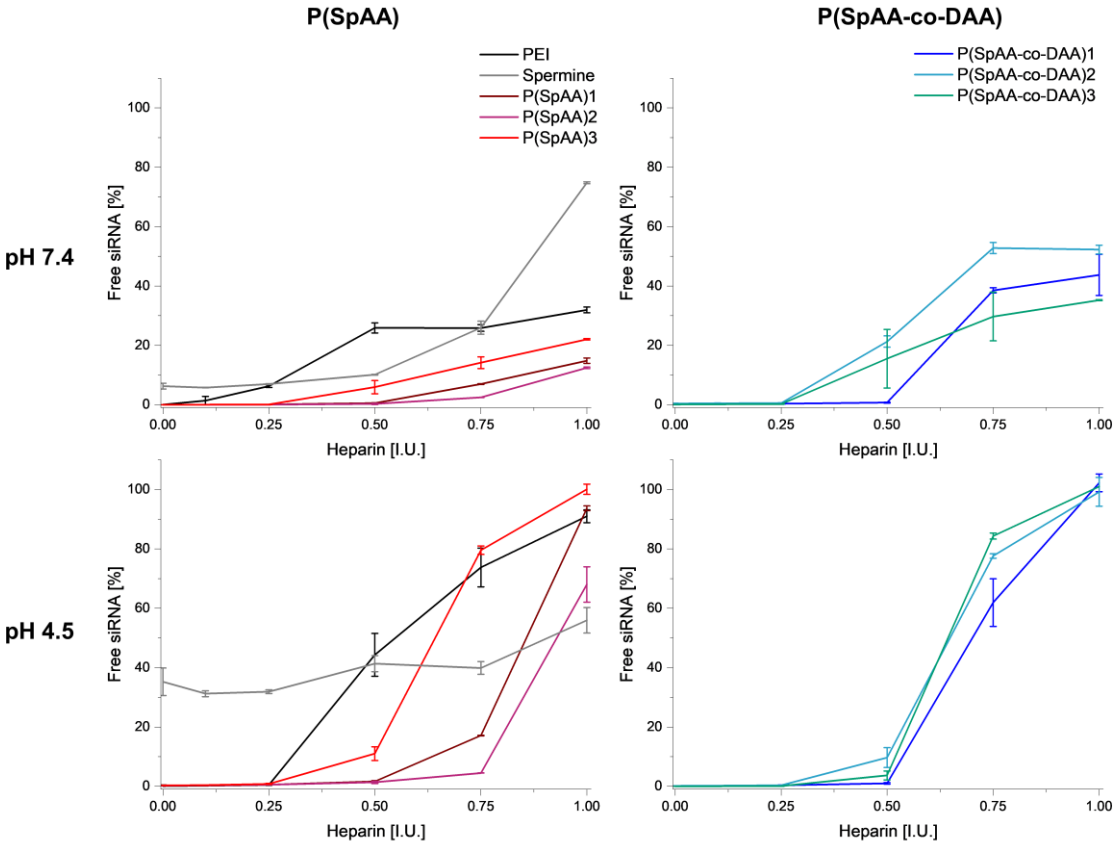

Figure 3 Release profiles of siRNA from PEI, Spermine, P(SpAA) 1-3 and P(SpAA-co-DAA) 1-3 polyplexes at N/P 7 as a function of heparin concentration (0.0 - 1.0 I.U. heparin per well, 1 I.U. = 4.9 µg) at pH 7.4 (top) and pH 4.5 (bottom).

Additionally, siRNA release ability under acidic conditions (pH 4.5), mimicking the endosomal compartment, was analyzed using a different buffer system (Figure 3, bottom). siRNA was more easily released from P(SpAA) and PEI polyplexes reaching almost 100% release for P(SpAA)2 and 70-90% for P(SpAA)1, P(SpAA)3 and PEI due to higher amount of protonated amines causing an elevated charge repulsion. A similar behavior was observed using copolymers, with all copolymers releasing 100% siRNA at high heparin concentrations, indicating suitable siRNA release abilities. Spermine, on the other hand, is not able to form any stable polyplexes at pH 4.5.

It seems, that amphiphilic copolymers P(SpAA-co-DAA) 1-3 and homopolymer 3 form less stable polyplexes which release siRNA even more efficiently than PEI. These polyplexes might be less stable due to lower charge density or higher steric hindrance caused by the hydrophobic subunits, which in turn also helps to release the payload at lower pH values in the endo-lysosomal compartment probably due to further destabilization caused by charge repulsion of additionally protonated amine groups.

4. *In vitro* performance of polyplexes in lung cells

4.1 Cellular uptake in H1299 cells

Initial experiments indicated that spermine-containing polyacrylamides are suitable for siRNA delivery regarding siRNA encapsulation efficiency and physicochemical characteristics. To further test their ability to mediate internalization into H1299 human non-small cell lung carcinoma cells, cellular uptake of Alexa Fluor 488-labeled siRNA was quantified by flow cytometry determining the median fluorescence intensity (MFI). Incubation times of 24 h were chosen, and polyplexes from P(SpAA) 1-3, P(SpAA-co-DAA)1-3 and PEI with fluorescent siRNA at N/P ratios of 2, 5 and 7 were analyzed. Trypan blue treatment, which was additionally applied in order to exclude extracellular fluorescent signals caused by cell surface-bound siRNA, resulted in insignificantly lower MFI values for all tested polyplexes, indicating that negligeable amounts of polyplexes were only attached to the outer cell membranes (Figure 4 and 5).

PEI polyplexes showed similar uptake abilities independent from the used N/P ratio. For P(SpAA) 1-3 homopolymers, the fluorescence signals of cellularly internalized siRNA-AF488 decreased from N/P ratios of 2 to 7 (Figure 4). Independent of this observation, significantly higher uptake was reached at all N/P ratios of the three homopolymers in comparison to PEI-mediated siRNA uptake. Highest uptake was reached with P(SpAA)3 at N/P 2 which was about 6-times higher than observed in PEI-mediated uptake experiments. P(SpAA)1, the lowest performing homopolymer, still induced more than three-fold cellular uptake of fluorescent siRNA even at N/P 7, highlighting that all P(SpAA) homopolymers are able to outperform commonly used PEI at all tested N/P ratios.

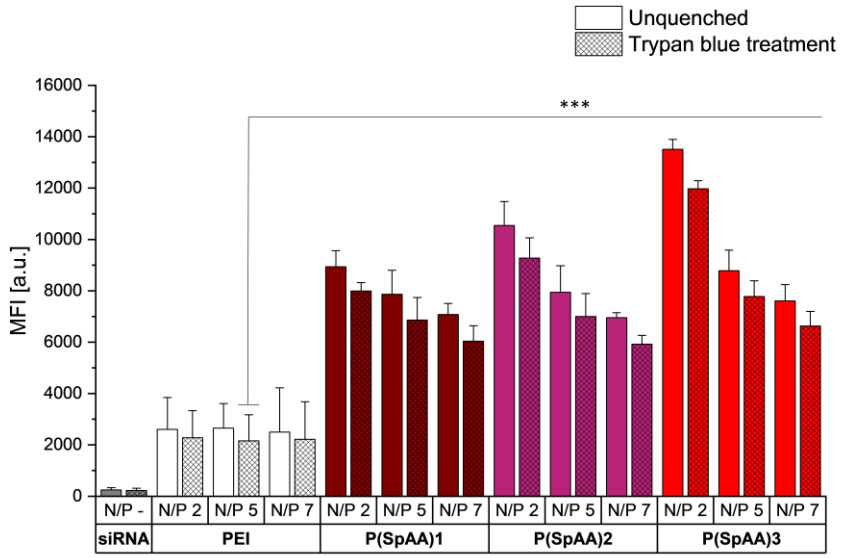

Figure 4 Cellular uptake of polyplexes made of AF488-labeled siRNA with PEI or P(SpAA) 1-3 at N/P ratios of 2,5 and 7 after 24 h of incubation, as quantified by flow cytometry performed with and without trypan quenching and presented as median fluorescence intensity. Cells treated with free siRNA served as negative control. Significance levels shown in comparison to PEI uptake. Lipofectamine as positive control was omitted for clarity.

Similar trends were observed for copolymers P(SpAA-co-DAA)1-3 (Figure 6). All polyplexes induced higher cellular uptake in comparison to PEI-polyplexes with a correlation with the hydrophobic fraction of the polymer on the MFI, however without any clear influence of the N/P ratio. The copolymer with the lowest hydrophobic ratio (P(SpAA-co-DAA) 1) induced between 3 and 4-times higher uptake compared to PEI polyplexes, which is in the same range as the homopolymers. With higher hydrophobic fraction, copolymers further enhanced cellular uptake of Alexa Fluor 488-labeled siRNA. P(SpAA-co-DAA)2 polyplexes formed at N/P 2 and 5 reached performance insignificantly different from positive

control Lipofectamin (LF). Remarkably, P(SpAA-co-DAA)3 polyplexes formed at N/P 2 were able to outperform “gold standard” Lipofectamin in our experiments and additionally induced 10-times higher cellular uptake of siRNA in comparison to PEI. To the best of our knowledge, none of the previously hydrophobically-modified PEI-polyplexes or spermine-containing polyplexes were able to outperform 25 kg/mol hyperbranched PEI by this far especially at such low N/P ratios of 2-7. [271, 276, 277]

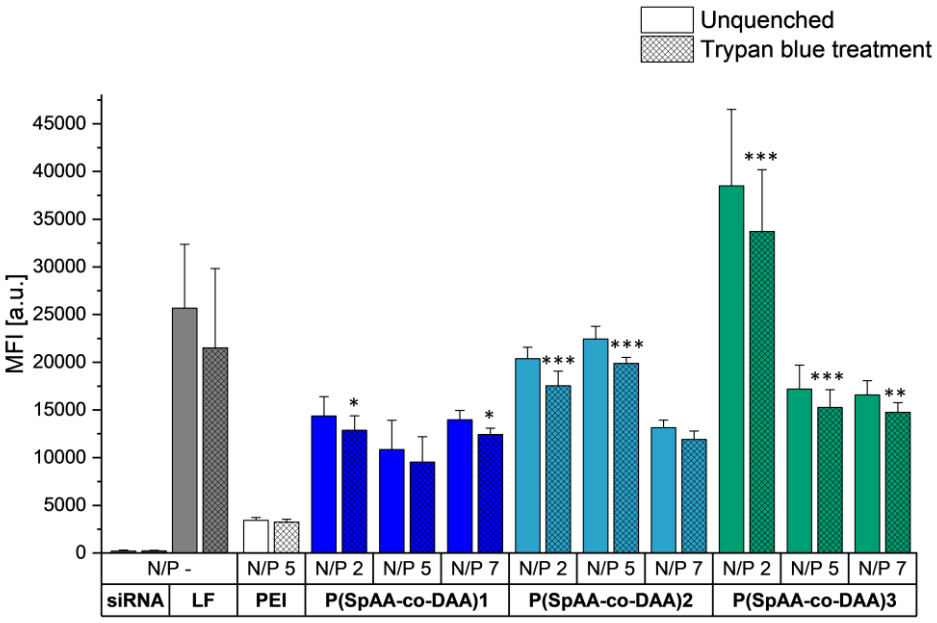

Figure 5 Cellular uptake of polyplexes made of AF488-labeled siRNA with PEI at N/P 5 or P(SpAA-co-DAA) 1-3 at N/P ratios of 2, 5 and 7 after 24 h of incubation, as quantified by flow cytometry performed with and without trypan quenching and presented as median fluorescence intensity. Cells treated with free siRNA served as negative control, whereas Lipofectamine (LF) lipoplexes served as positive control. Significance levels shown in comparison to PEI uptake.eGFP knockdown in H1299 cells.

To evaluate the gene silencing efficiency of spermine-acrylamide polyplexes on the protein level, H1299/eGFP cells were utilized that express the ‘enhanced green fluorescent protein’ reporter gene (eGFP). Based on *in vitro* cellular uptake experiments, H1299/eGFP cells were transfected with PEI, P(SpAA)2, P(SpAA-co-DAA)2 or P(SpAA-co-DAA)3 polyplexes formulated with siRNA against eGFP (siGFP) or with scrambled siRNA (siNC) as negative control using N/P ratios of 2, 5 or 7 to determine optimal parameters for efficient protein knockdown (A1, Figure S8). As positive control, Lipofectamin 2000 lipoplexes were used. After treatment, the median fluorescence intensity of eGFP in each sample was quantified via flow cytometry after 48 hours of incubation. Polyplexes containing siNC did not reduce the MFI of GFP, proving that protein knockdown is not attributed to the polymeric system or any non-specific effects. All siGFP-polyplexes from spermine-polyplexes were able to provoke eGFP knockdown between 20 and 47%, however with P(SpAA-co-DAA)2 polyplexes at N/P 5 showing statistically insignificant knockdown ability. Whereas PEI solely showed a significant knockdown at N/P ratios of 5 and 7 with up to 36% eGFP knockdown, P(SpAA-co-DAA)3 showed a constant knockdown after 48h of 47 to 40% at all tested N/P ratios even without chloroquine treatment (often used to induce endosomal release of siRNA). [278, 279] These findings emphasize that P(SpAA-co-DAA)3 polyplexes efficiently escape the endosome. Consequently, polyplexes with P(SpAA-co-DAA)3 can be used at various N/P ratios without drastic effects on their performance allowing less optimization steps and thus also reduced costs.

4.2 Staining and GAPDH knockdown in ALI culture

Following validation of cellular uptake mediated by poly(spermine acrylamide)(siRNA polyplexes in vitro, further evaluation of uptake and knockdown abilities in a more in vivo relevant context was performed using air-liquid interface (ALI) cultures of lung epithelial cancer cells.

Mucus staining of Calu3 cells in ALI cultures was performed by WGA-AF488 staining of the mucus layer (A1, Figure S10). Polyplexes were prepared using P(SpAA-co-DAA)3 and fluorescently labeled AF647-siRNA at an N/P ratio of 5. After 24 hours of incubation time, AF647-siRNA can be found below the mucus layer indicating successful polyplex transport across mucus.

Cell uptake was visualized by staining of Calu3 cells in the presence of fluorescent siRNA (Figure 6, left and A1, Figure S9). Nuclei were stained by DAPI (blue), and the cytoskeleton was stained using rhodamine-labeled phalloidin. For 24 hours, cells were incubated with the same polyplexes as described above. Confocal microscopy confirmed that siRNA was located in the cytoplasm of Calu3 cells, confirming cellular uptake of polyplexes.

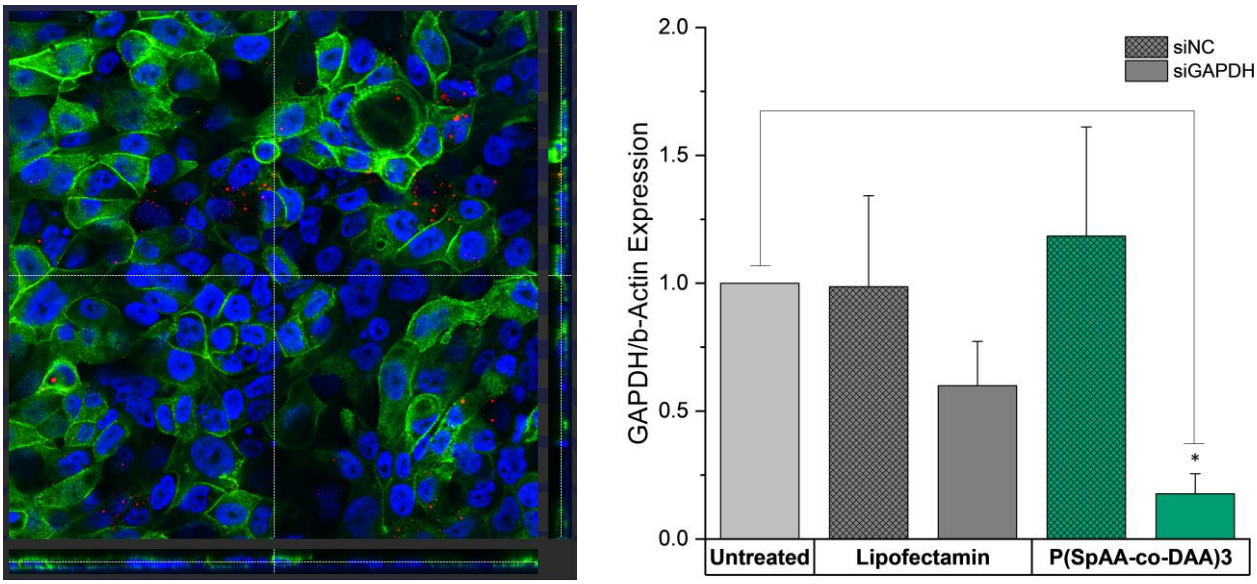

Figure 6 (Left) Orthogonal view of phalloidin staining of Calu3 cells at ALI. Incubation time: 24 h; Blue: DAPI (nuclei); Green: Rhodamine-labelled Phalloidin (cytoskeleton); Red: AF647-siRNA. (Right) GAPDH gene knockdown of P(SpAA-co-DAA)3 polyplexes using an N/P ratio of 5 in Calu3 cells grown in ALI cultures after 24 h transfection. 100 pmol hGAPDH siRNA were used. Blank samples consisted of Calu3 monolayers treated with 5% glucose only. The positive control consisted of Lipofectamine 2000 (LF) lipoplexes with 100 pmol hGAPDH siRNA. GAPDH expression was quantified by real time PCR and normalized to β-actin expression. Data points indicate mean ± SD (n=3).

The ability of spermine-acrylamides to silence an endogenously expressed gene in Calu3 monolayers, after successful mucus diffusion and cellular uptake, was additionally tested. Cells were transfected with P(SpAA-co-DAA)3 polyplexes containing siRNA against the housekeeping gene GAPDH (siGAPDH) or scrambled sequence siRNA (siNC as negative control) at N/P 5 for 24 h. Negative controls consisted of blank cells that were treated with 5% glucose only, while positive control cells were transfected with Lipofectamine 2000. GAPDH gene expression was quantified by real time PCR and normalized to β-actin gene expression (Figure 6, right). Calu3 cells that were transfected with P(SpAA-co-DAA)3/siGAPDH polyplexes showed higher levels of gene knockdown when compared to the blank cells or those that were treated with P(SpAA-co-DAA)3/siNC polyplexes. Lower levels of reduced GAPDH gene expression were also observed in comparison to cells that were treated with LF/siGAPDH, indicating that P(SpAA-co-DAA)3 polyplexes are able to efficiently deliver siRNA to lung epithelial cells in an in vitro model of the lung, resulting in efficient gene knockdown. In more in vivo-like models such as ALI cultures, especially when mucus is present, lipofectamine is shown not to be as effective as

in standard in vitro experiments since pulmonary surfactants inhibit lipofection, [228] while polyplexes from P(SpAA-co-DAA)3 can still efficiently mediate a target gene downregulation. Additionally, lipofectamine cannot be employed in in vivo experiments due to its toxicity. Just recently, Merkel et al. tested hyperbranched PEI and a highly efficient virus-inspired polymer for endosomal release (VIPER) in the same ALI-culture setup and it was shown that both polymers induce less (PEI) or similar (VIPER) GAPDH knockdown than P(SpAA-co-DAA)3. [280] Thus, P(SpAA-co-DAA)3 is a very promising candidate for safe and efficient siRNA delivery to lung cells via pulmonary delivery routes.

5. Toxicity experiments

MTT assays were used to colorimetrically evaluate cell proliferation as well as the viability of the cells treated with all spermine-containing homo- and copolymers and PEI. Mitochondrial activity in L929 mouse fibroblasts was assessed after 24 h of incubation using different polymer concentrations. Results are presented as the percentage of cell viability compared to untreated control cells. IC50 values were calculated by plotting cell viability and concentration of polymers on a logarithmic scale using a sigmoidal model fit (A1, Figure S11). [281] All spermine polymers affected the cell viability less than PEI (25 kg/mol, IC50 = 19.05 μg/mL), and IC50 values for the spermine polymers were observed to be between 25 and 71 μg/mL. P(SpAA-co-DAA)3 showed the lowest toxicity with regards to the IC50 value, most likely due to the lowest number of free amine groups when using the same polymer mass concentrations which is in accordance with previous studies in which hydrophobically modified PEIs affected the cell viability less than the respective unmodified cationic motif. [266, 274, 282] These results are very promising, especially considering that all spermine-polymers had much higher molecular weights than the tested PEI. In general, cytotoxicity correlates directly with molecular weight of polyamines. [283] Therefore, lowering the molar mass of poly(spermine acrylamide) homo and copolymers could have an additional beneficial effect on their biocompatibility.

To further test the toxicity of the newly developed polycationic polymers in a more relevant setup when used for pulmonary siRNA delivery, immune and cytokine responses of polyplexes from PEI and P(SpAA-co-DAA)3 at an N/P ratio of 5 were analyzed in mice. Bronchoalveolar lavage fluid (BALF) and BALF cells were collected after mice were intratracheally treated with PEI or P(SpAA-co-DAA)3/siRNA polyplexes, and levels of various cytokines were quantified in a multiplex-ELISA (Figure 7).

For most of the tested cytokines, P(SpAA-co-DAA)3 treated mice showed similar or lower levels of inflammation than untreated mice (IL-23, IL-27, IFN-y, IL-12p70, IL-10, IFN-b). In some cases, the values were below the detection limit (IL-1a, GM-CSF).

Solely, IL-1b, IL-6, TNF-a and IL-17A levels were slightly, but not significantly higher after P(SpAA-co-DAA)3 polyplex treatment, and MCP-1 values showed a 6-fold increase. At the administered concentration, PEI/siRNA complexes showed similarly low proinflammatory effects, with an increased IL-23 level (not significant) and without increasing the secretion of MCP-1. In case of some cytokines, levels were lower after treatment with P(SpAA-co-DAA)3 as compared to PEI polyplexes. Taking into account that previous comparable in vivo inflammation studies of poly(ethylenimine) for pulmonary delivery revealed that in vivo cytokine releases were generally higher with amphiphilic PEIs than with unmodified polymers, such generally low levels of cytokines of amphiphilic P(SpAA-co-DAA)3 indicate that spermine-polymers are a safe and biocompatible delivery system. [177, 284]

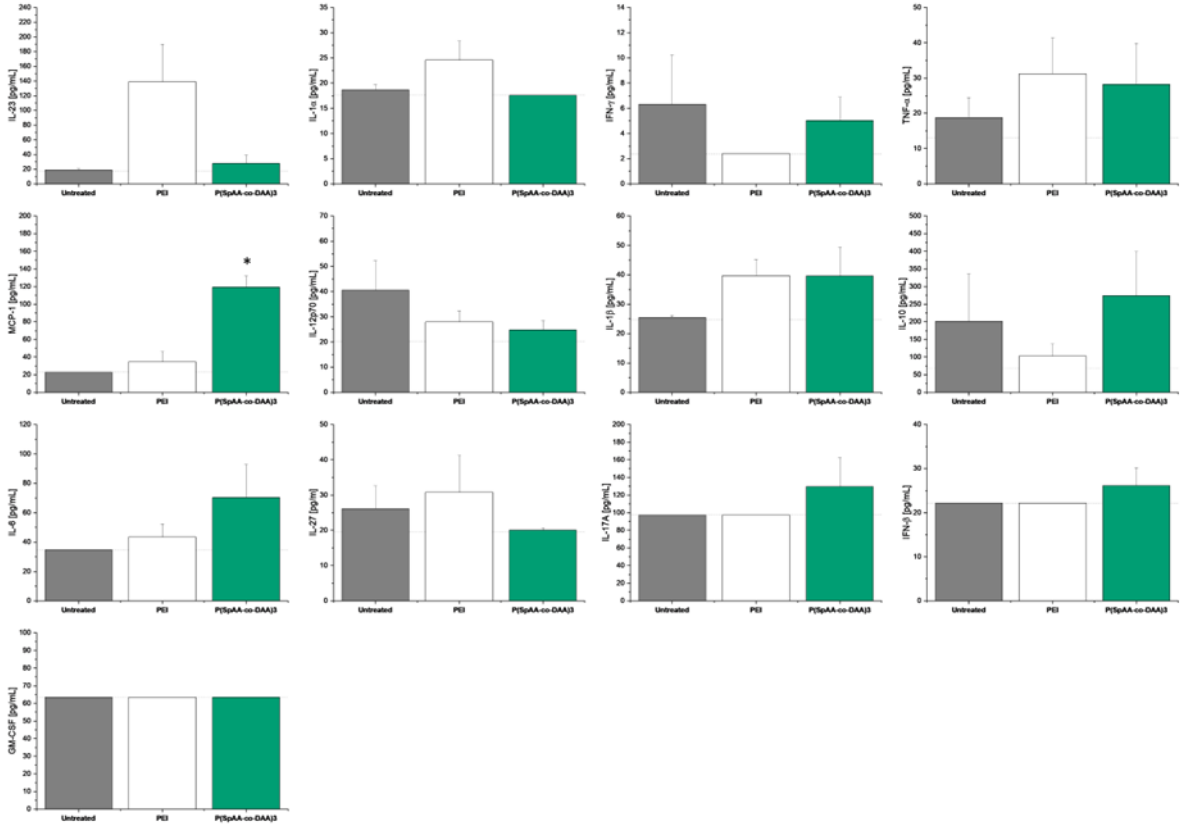

Figure 7 Cytokine release in BALF after intratracheal instillation of siRNA polyplexes using PEI or P(SpAA-co-DAA)3 at an N/P ratio of 5. Data represent mean ± SEM (n= 4 for treatment with PEI or P(SPAA-co-DAA)3 polyplexes and n = 2 for untreated mice); significantly increased cytokine levels compared to control were marked with an asterisk (*$p < 0.05$). Detection limit: dotted line.

6. Distribution of P(SpAA-co-DAA)3-siRNA polyplexes in lung cells

Epithelial cells are considered as essential target cell types in a variety of pulmonary diseases. [224-226] To quantify the in vivo distribution of P(SpAA-co-DAA)3/siRNA polyplexes in different lung cell types, BALB/c mice were intratracheally administered with 2 nmol of polyplexes loaded with AF647-labeled siRNA. After 48 h, bronchoalveolar lavage fluid (BALF) was collected while lungs were further processed to obtain a single cell suspension. Different types of lung cells were counterstained with specific markers to quantify the fate of polyplexes after pulmonary administration. P(SpAA-co-DAA)3/siRNA polyplexes were mainly taken up by two cellular subsets: type II pneumocytes and macrophages proving that siRNA can reach the site of action when being transported by spermine-polymers after intratracheal administration to lung (Figure 8). The cellular uptake observed in type II pneumocytes was higher (not significantly) than uptake to macrophages. Since Alveolar macrophages are the initial cellular defense in the deep lungs against foreign substances, uptake by these cell types is not surprisingly, nevertheless, total macrophage clearance was avoided since small polyplexes of around 100nm were administered. Similar observations were recently made by Merkel et al. with PEI and VIPER/siRNA polyplexes. [280]

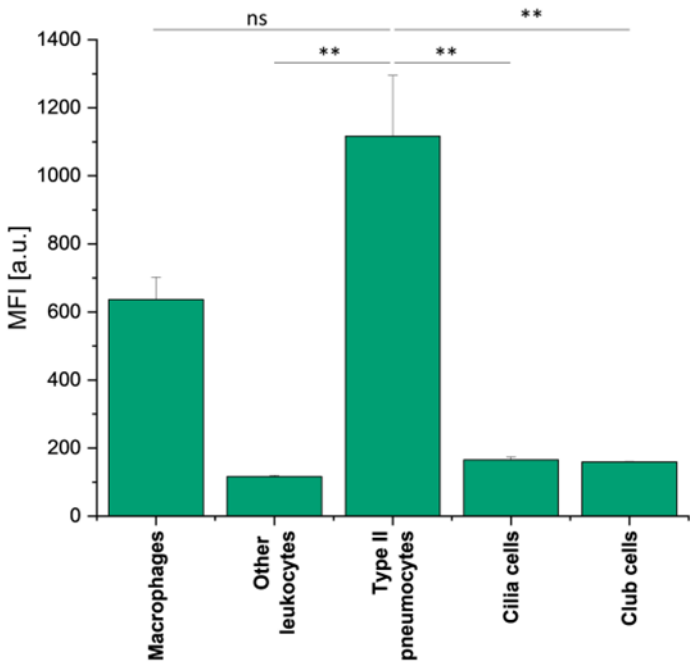

Figure 8 In vivo P(SpAA-co-DAA)3/siRNA polyplex distribution in lung cells using P(SpAA-co-DAA)3 at an N/P ratio of 5. Cellular uptake of in different lung cell populations was quantified by flow cytometry. Data points indicate mean ± SEM.

7. Conclusion

The research regarding carrier systems for siRNA delivery has caught a lot of attention, since it offers a promising therapeutic approach by downregulation of disease-related genes via RNA interference. Especially polyamine-containing polymers are considered promising delivery systems due to their electrostatic interactions with siRNA, leading to high loading efficacy and protecting the payload from the degrading environment. However, the development of polymers with high transfection efficiencies and minimal cytotoxicity remains to be the greatest barrier of successful non-viral nucleic acid delivery. In this study, the approach of using the endogenous, cationic molecule spermine as pendant groups in polyacrylamides was examined. In an effort to improve the transfection ability by increasing the molecular weight, a protocol to synthesize brushed poly(spermine acrylamides) via free-radical polymerization of the active ester N-acryloxysuccinimide was developed. To evaluate the impact of different hydrophobic content in the polymer chain for further enhancement in cellular uptake, copolymerizations of NAS and N-decylacrylamide were performed. The monomer reactivity ratios of each monomer were determined in copolymerizations using Fineman-Ross technique showing a compositional drift from DAA to NAS units within the polymer chain. The active ester monomer was converted into spermine-based pendant groups by reaction with Tri-boc spermine followed by deprotection of the amine groups resulting in poly(spermine acrylamide) and poly(spermine acrylamide-co-N-decylacrylamide) polymers. A set of three different homopolymers and three copolymers with varying molecular weights and ratios of hydrophobic DAA-units were obtained. Critical micelle concentration studies were conducted confirming self-assembly into micelles at low concentrations. siRNA condensation ability and physicochemical characteristics, i.e., particle size, size distribution and zeta potential, were determined showing that all synthesized polymers were able to form uniform polyplexes with siRNA at favorable sizes of around 100 nm in hydrodynamic diameter supplemented by narrow size distributions at very low N/P ratios. These results in combination with slightly positive zeta-potentials and desired buffering-capacities indicate optimal conditions for efficient encapsulation and siRNA release. All homo- and copolymers showed an improved cellular uptake in lung carcinoma cells compared to hyperbranched 25 kg/mol PEI. P(SpAA-co-DAA)3, with a ratio of 43% cationic and 57% hydrophobic monomer subunits, mediated a better cellular uptake than “gold standard”

lipofectamine and a 10-fold higher uptake than induced with PEI polyplexes under similar conditions. Efficient endosomal escape and siRNA release was tested using air-liquid interface studies to examine the efficiency in pulmonary siRNA delivery to lung cells. P(SpAA-co-DAA)3 induced a significant knockdown outperforming PEI and Lipofectamine in ALI-cultured Calu3 cells. In vivo studies, regarding biodistribution and cytotoxic effects in the lung after intratracheal injection verified that P(SpAA-co-DAA)3 treated mice showed similar or lower levels of most tested cytokines than untreated mice and that P(SpAA-co-DAA)3 polyplexes efficiently reached type II pneumocytes, club and cilia cells in the lung. These findings qualify the newly described spermine based homo- and copolymers as promising pulmonary nucleic acid agents for therapeutic applications in lung diseases such as respiratory viral infections, asthma, or COPD.

Acknowledgements

The authors acknowledge support from the European Research Council (ERC-2014-StG – 637830), from the Bavarian Research Foundation (AZ-1449-20C) and from the Center for NanoScience at LMU Munich. F.A. is grateful for funding from the Federal Ministry of Education and Research (BMBF) and the Baden-Württemberg Ministry of Science, Research and Art as part of the Excellence Strategy of the German Federal and State Governments. M.K. is grateful for the PhD scholarship from the Studienstiftung d. dt. Volkes.

Chapter V – Design and characterization of lipid-polyplex hybrid nanoparticles for siRNA delivery

This chapter is prepared for submission and peer review as:

„Design and characterization of lipid-polyplex hybrid nanoparticles for siRNA delivery "

Author‘s contributions:

Christoph M. Zimmermann [a,b], Rosario Milazzo, Benjamin Winkeljann [b,c], Paola Luciani [a] and Olivia M. Merkel [b]

C.M.Z and R.M. performed the experiments and evaluated the data. C.M.Z wrote the manuscript. C.M.Z, B.W., P.L. and O.M.M. conceived the presented idea and planned the experiments. B.W., P.L. and O.M.M supervised the work, provided conceptual guidance and corrected the manuscript.

a. *Pharmaceutical Technology, Department for Chemistry, Biochemistry and Pharmacy, University Bern, Freiestrasse 3, CH - 3012 Bern*

b. *Pharmaceutical Technology and Biopharmaceutics, Department Pharmacy, Ludwig-Maximilians-University Munich, Butenandtstr. 5-13, 81377 Munich, Germany*

c. *Center for NanoScience (CeNS), Ludwig-Maximilians-University Munich, 80799 Munich, Germany*

Key words: polymer, lipid, hybrid nanoparticle, RNA therapeutics, siRNA delivery, novel therapeutic option

Abstract

Lipid-polymer hybrid nanoparticles can be used as a nucleic acid delivery system improving the characteristics of polymer-based nanoparticle systems. Cationic polymers, such as polyethylene imine (PEI) and its derivatives, form tightly packed polyplexes that might face endosomal release problems. Chemically tunable lipid coatings can overcome those hurdles by destabilization of the lipid bilayer structure of the cell membrane or using pH-sensitivity. Additionally, lipids facilitate excellent biocompatibility, biomimicking properties, and chemical tunability. Hybrid nanoparticle systems combine synergistic features from both worlds resulting in an improved nanoparticle delivery system.

The aim of the study was to identify a hybrid nanoparticle system to be produced in a one-step microfluidic method with improved physicochemical properties, stability, and in vitro performance with respect to its polyplex precursor. Polyethylene imine-polycaprolactone-polyethylene imine (PEI-PCL-PEI), a triblock copolymer, served as the complexation agent for siRNA while 1,2-Dioleoyl-sn-glycero-3-phosphocholine (DOPC), 1,2-dioleoyl-3-trimethylammonium-propane (DOTAP) and 4-(dimethylamino)-butanoic acid, (10Z,13Z)-1-(9Z,12Z)-9,12-octadecadien-1-yl-10,13-nonadecadien-1-yl ester (DLIN-MC3-DMA) were used for lipid coating. The microfluidic mixing setup was defined by the respective N/P ratio and flow rate ratio (FRR) between siRNA, polymer and lipid. The target values were set at a size of 150 nm, PDI of ≤ 0.2, a positive zeta potential, encapsulation efficiency of >95% and a gene silencing efficiency of >50%. Results show that hybrid-lipid-polyplex nanoparticles (HLPNP) coated with DOPC and DOTAP reached the set targets for physicochemical properties and siRNA encapsulation. However, DOTAP-coated HLPNP did neither improve their respective polyplex uptake performance, nor did they mediate more than 40%. Gene silencing efficacy. On the other hand, D-LIN-coated HLPNPs achieved all set target values and successfully silenced enhanced green fluorescence protein (eGFP) expression in vitro by 60% compared with 30% for the respective polyplex formulation.

1. Introduction

Polymeric nanoparticle systems have shown great potential to successfully encapsulate nucleic acids, such as DNA and RNA, as therapeutic drug delivery systems. [11, 177, 181, 285, 286] Especially, short interfering RNA (siRNA) therapeutics have opened new possibilities for treatment options due to a reversible gene knockdown approach. Cationic polymers, such as poly(ethylene) imine (PEI) or its modifications, form polyplexes with negatively charged RNA demonstrating effectiveness *in vitro* and *in vivo*. [34, 287-289] Even though electrostatic interactions are advantageous producing polyplexes of smaller sizes and positive charges facilitate cell internalization, as well as inducing an endosomal buffering capacity to promote endosomal escape, the inability to release siRNA and cell membrane damage can lead to insufficient therapeutic effects and increased cytotoxicity. [167, 290] Moreover, polyplexes face wider polydispersity causing poor reproducibility and adding towards its effectiveness.

Polymer architecture created a pool of various modifications to improve biocompatibility and transfection performance. [286, 291] Numerous modifications were synthesized having polycaprolactone (PCL) and/or poly(ethylene) glycol (PEG) linked to increase hydrophobicity or hydrophilicity. Several studies on PEI modifications showed improvements in sizes and uptake performances in comparison to PEI-polyplexes. However, one of the biggest hurdles remains to be the endosomal release. [177, 179, 181] This can be overcome by searching for a new polymer modification, as abovementioned, or to make use of the advantages of lipids as nanocarrier systems. They account for amphiphilicity and mimick the biological cell membrane which enables a proficient encapsulation stability, non-toxicity, flexibility, biocompatibility and biodegradability. [49, 50, 292] The approach of forming lipid-polymer hybrid nanoparticles can combine the synergies of both to improve existing polyplex systems. Previous studies have shown that combining lipids and polymers can lead to higher

stability of nanoparticles, a much higher transfection and improve circulatory half-lives. [293-295] Various lipids and phospholipids were used for structure enhancement ranging from positively charged lipids (1,2-dioleoyl-3-trimethylammonium-propane, DOTAP), helper lipids (1,2-dioleoyl-sn-glycero-3-phosphocholine, DOPC), and ionizable lipids (4-(dimethylamino)-butanoic acid, (10Z,13Z)-1-(9Z,12Z)-9,12-octadecadien-1-yl-10,13-nonadecadien-1-yl ester, DLIN-MC3-DMA). The addition of helper lipids can lead to an enhancement of transfection activity of lipid nanoparticles through destabilization of the lipid bilayer structure in cell membranes. [50] Ionizable lipids found their breakthrough in the siRNA-LNP formulation of Onpattro®. The pH-sensitivity of ionizable lipids is beneficial for nucleic acid delivery, especially in vivo, because at a neutral pH the ionizable lipids have less interactions with the anionic membranes of blood cells which improves the biocompatibility of lipid nanoparticles. In addition, entering the endosome, resulting in a lower pH value, protonates the lipids which increases the positive charge promoting membrane destabilization and facilitating endosomal release. [296, 297]

Despite the vast variety and promising characteristics of lipid-polymer hybrid nanoparticles, traditional methods of particle formation lack batch reproducibility and the translation into large-scale production. [152, 298] Most common methods of preparing hybrid nanoparticle systems consist of two-steps or one-step. Two step methods prepare nanoparticles via nanoprecipitation, emulsification-solvent evaporation or high-pressure homogenization. Generally, hybrids are formed by the addition of preformed polymeric nanoparticles to a dried lipid film or lipid vesicles. The final assembly is achieved by the input of external energy via ultrasonication or vortexing. In a single-step method, nucleic acid and polymer are dissolved together and the lipid is dissolved in water. Lipids are heated and the polymer/nucleic acid solution is added dropwise. [299] Both attempts are time, energy, and material intense. Microfluidic mixing is an alternative technology for nanoparticle production offering a precise, rapid, and cost-effective regulation, as well as a wide set-up variety. [300] It can act as a single-step method in which the polymeric-, nucleic acid- and lipid-stream are mixed in the same microfluidic chip. Either the components are added continuously in the same stream, or the layout allows a polymer nanoparticle formation in one chip circuit, followed by a subsequent lipid coating in another circuit on the same chip. The company Dolomite Microfluidics have found a Micromixer® chip which displays two circuits, each of them having mixing chambers increasing the turbulent flow. Feldmann et al. and our group (Chapter 2) have previously used this particular chip to improve polyplex formation of siRNA encapsulation in a triblock copolymer (PEG-PCL-PEI). [34] However, only one circuit was used leaving room for exploration of lipid-polymer hybrid nanoparticle formation.

The aim of this study was to establish a single step microfluidic formulation of hybrid-lipid-polyplex nanoparticles (HLPNPs) based on a PEI-PCL-PEI triblock copolymer, used for siRNA encapsulation, with a lipid coating. For the latter, either a zwitterionic lipid, DOPC, a positively charged lipid, DOTAP, or an ionizable lipid, DLIN-MC3-DMA, were utilized. The purpose of the coating was to improve the polyplex performance, especially, regarding the in vitro performance. The set target parameters consisted of a size of 150 nm, a PDI of about 0.2 and a positive zeta potential. A size range below 200 nm is advisable to avoid nanoparticle clearance by renal and hepatic pathways. [301] siRNA encapsulation over >95% and nanoparticle stability at pH 7.4 is expected. The in vitro uptake of HLPNPs should be comparable or better than that of polyplexes without significant cytotoxicity. The in vitro gene silencing performance of HLPNPs should exceed 50% for better performance than observed with polyplexes. Overall, the lipid coating should verify the formation of a hybrid nanoparticle system to improve the polyplex performance. This study's findings provide an approach to enhance the performance of polymers as non-viral delivery systems by simply coating with a lipid using a single-step sequential microfluidic mixing set-up.

2. Materials & Methods

2.1 Materials

Dicer substrate double-stranded siRNA targeting green fluorescent protein (DsiRNA EGFP, 25/27mer) (siGFP), scrambled, non-specific control (siNC) and amine modified siRNA labeled with succinimidyl ester (NHS) modified AF 488 (siAF488) (Life Technologies, Carlsbad, USA) were purchased from IDT (Integrated DNA Technologies, Inc., Leuven, Belgium) (A2, Table S1) [237, 270, 302, 303]. Tris-EDTA buffer solution 100x (T9285), RPMI-1640 medium (R8758), fetal bovine serum (FBS) (F9665), penicillin-streptomycin (P/S) (P4333), G418 disulfate salt solution (G8168), Dulbecco's phosphate buffered saline (D-PBS) (D8537), methylthiazolyldiphenyl-tetrazoliumbromid (MTT), heparin porcine salt, were purchased from Sigma-Aldrich, a subsidiary of Merck KGaA (Darmstadt, Germany). 1,2-Dioleoyl-sn-glycero-3-phosphocholine (DOPC), 1,2-dioleoyl-3-trimethylammonium-propane (DOTAP) and 4-(dimethylamino)-butanoic acid, (10Z,13Z)-1-(9Z,12Z)-9,12-octadecadien-1-yl-10,13-nonadecadien-1-yl ester (DLIN-MC3-DMA; D-LIN, A2, Figure S1) were bought from Avanti Polar Lipids (Alabaster, USA). Black 96-well plates (10307451) were bought from Thermo Fisher Scientific (Schwerte, Germany). Micromixer® chips were bought from Dolomite Microfluidics, Blacktrace Holdings Ltd. (Royston, UK).

2.2 Preparation of hybrid lipid-polyplex nanoparticles (HLPNPs) via microfluidic mixing

LPHNPs consist of a polyplex core, which forms via electrostatic attraction between positively charged polymer and negatively charged siRNA, and a lipid coating (Table 1). The polyplexes were formed using a triblock copolymer consisting of two polyethylenimine termini and a polycaprolactone center block (polyethyleneimine-polycaprolactone-polyethylenimine, PEI-PCL-PEI). The polymer was synthetized as described before and dissolved in acetone to reach a stock concentration of 1 mg/mL. Subsequently, to enable an aqueous mixing in the microfluidic chip, the polymer stock solution was transferred by dropwise addition under magnetic stirring to a 10 mM 4-(2-Hydroxyethyl)piperazine-1-ethanesulfonic acid (HEPES) buffer solution (pH 7.4) for acetone evaporation. Prior to the polyplex formation, the amount of polymer needed was calculated by the following equation taking into account a PEI ratio of 2/3 within the triblock copolymer:

PEI (pg) = MW (PEI) x siRNA nucleotides x N/P ratio x siRNA amount (pmol)

MW (PEI): Molecular weight (MW) of PEI's protonable unit is 43.04 g/mol. siRNA nucleotides: the number of nucleotides in the 25/27mer siRNA sequence is 52. N/P ratio: the charge ratio between the protonable groups in the PEI molecule to the anionic phosphate in the RNA backbone.

All polyplex formulations consisted of an siRNA (siAF488, siGFP, siNC) concentration of 1000 pmol/mL. To form polyplexes and hybrid lipid-polyplex nanoparticles, microfluidic mixing in the Micromixer® was performed. The microfluidic set-up consisted of two mixing circuits with three inlet positions. The mixing procedure was performed in a single-step of aqueous solutions to form the polyplexes. Subsequently, the lipid coating was added in the second circuit. The flow rates were controlled by syringe pumps (KD Scientific Inc, USA). Formation of polyplexes was approached in two different manners. Either, polyplexes were formed by loading polymer and siRNA solutions into syringes and setting the same flow rate of 0.5 mL/h. N/P ratios of 7, 10 and 14 were investigated. Or, the flow rate ratio (FRR) was adapted by fixing the polymer flow rate to 0.5 mL/h and decreasing the siRNA flow rate 6-fold or 8-fold. Hence, the final siRNA concentration was always 1000 pmol/mL. N/P ratios of 7 and 14 were prepared. The microfluidic chip was washed with 10 mM HEPES buffer solution prior and after use. The lipid coating of the polyplexes was performed in the second mixing circuit of the Micromixer® chip. Different lipids were used to form the HLPNPs. Zwitterionic lipid DOPC and positively-charged lipid DOTAP were used to establish a hybrid system. D-LIN was used to further optimize the HLPNP system. All lipids were dissolved in a mixture of methanol and ethanol (1:1) to

obtain a 1 mg/mL stock solution. Adapted from a previous study, a solvent displacement was achieved by adding the lipid solution dropwise to a stirring 10 mM HEPES buffer solution. The mixture was left stirring for 30 min to let the organic solvent to evaporate. [304] The polyplex stream was guided into the second circuit to mix with the lipid solution. Various FRR of 1:1, 1:4 and 1:8 were investigated keeping the polyplex to lipid ratio at 1:1 (Table 1). This led to a final siRNA concentration of 500 pmol/mL within the HLPNPs.

Table 1 Polymer, siRNA and lipids concentrations for different samples synthesis

Sample	**Abbreviation**	**N/P ratio**	**FRR**	**Polymer** [µg/mL]	**siRNA** [pmol/mL]	**Lipid** [µg/mL]
PP N/P 7	PP 1	7	6:1	23.52	1000	/
PP N/P 14	PP 2	14	6:1	47.04	1000	/
DOPC N/P 14	HLPNP 1	14	1:1	23.52	500	23.52
DOTAP N/P 7	HLPNP 2	7	1:1	11.76	500	11.76
DOTAP (2x) N/P 7	HLPNP 3	7	1:1	11.76	500	23.52
DOTAP N/P 14	HLPNP 4	14	1:1	23.52	500	23.52
D-LIN N/P 7	HLPNP 5	7	1:1	11.76	500	11.76
D-LIN N/P 14	HLPNP 6	14	1:1	23.52	500	23.52

2.3 Hydrodynamic diameter and zeta (ζ) potential measurements of HLPNPs

Hydrodynamic diameters and polydispersity indices (PDI) of HLPNPs (70 µL, 500 pmol siRNA per mL) were measured, dispersed in highly purified water (HPW), in disposable cuvettes (Brand GmbH, Wertheim, Germany) using the Zetasizer Nano ZS instrument (Malvern Instruments Inc., Malvern, U.K.). All samples were detected at a backscatter angle of 173°. Results are presented as Z-average size (nm) ± SD and analyzed via polynomial fit. Zeta potentials were measured by Laser Doppler Anemometry (LDA) using a Zeta Cell (Zetasizer Nano series, Malvern, UK) containing a 6.5X dilution of the same 70 µL sample of HLPNP suspension in HPW. For each HLPNP formulation, measurements were presented as an average charge (mV) ± SD.

2.4 Atomic force microscopy (AFM) measurements of HLPNPs

AFM was performed using the Multimode AFM (Veeco, Plainview, USA) to assess the size and morphology of the HLPNPs. For AFM size and morphology measurements, HLPNPs were prepared as mentioned above via microfluidic mixing. A volume of 20 µL (500 pmol siRNA/mL) HLPNP suspension was added to a glass coverslip and let dry. DOTAP and DOPC lipid coatings of HLPNPs were compared.

2.5 Nanoparticle tracking analysis (NTA) for HLPNPs

NTA measurements were performed using the NanoSight NS300 (Malvern Instruments Inc., Malvern, U.K.). Polyplexes and HLPNPs, at concentrations of 500 pmol siRNA/mL, were prepared via microfluidic mixing, as mentioned above. DOTAP was used at N/P ratios of 7 and 14 for HLPNP formation. Samples were injected using a syringe and five regions were recorded and analyzed for 1 min.

2.6 Transmission electron microscopy (TEM) measurements of HLPNPs

Transmission electron microscopy was used in order to assess the size and morphology of HLPNPs. For TEM analysis, HLPNPs were formed using DOPC and DOTAP, as described above, at final siRNA concentrations of 500 pmol/mL and an N/P ratio of 14. A volume of 5 µL of samples were added dropwise to an activated copper-coated grid and air-dried for 5 min. The excess liquid was removed using filter paper and 10 µL of staining solution (2 % phosphotungstic acid (m/V) in HPW) was added. Subsequently, the staining agent was removed and washed three times with 10 µL of HPW. HLPNPs were imaged using a FEI TECNAI G2 200kV s-Twin microscope (FEI Titan Themis, Hillsboro, USA).

2.7 Co-localization of HLPNP components via confocal microscopy

For confocal microscopy experiments, an AlexaFluor488 (AF488) labeled siRNA and a Liss Rhod (Avanti Polar Lipids, Michigan, United Stated) –linked DOPC lipid were used for HLPNP formation. To evaluate the co-localization of polymer and lipid within the same HLPNP system, 20 µL of HLNPs solution was pipetted on a glass slide and observed under the SP8 Inverted scanning confocal microscope (Leica Camera, Wetzlar, Germany). The pinhole was set to 1AU and a 63x oil objective was used. The images were exported from the Leica Image Analysis Suite and processed with the Fiji distribution of ImageJ. Co-localization was calculated by determining the Pearson coefficient.

2.8 HLPNP encapsulation efficiency and stability

To determine siRNA encapsulation efficiencies of polyplexes and HLPNPs, a SYBR-Gold assay was performed. All samples were loaded with 50 pmol siRNA at N/P ratios 7 and 14. Furthermore, sample formation was adjusted by changing the FRR or the composition, as mentioned under 2.2. First, 100 µL of each sample were transferred into a black 96-well plate, followed by the addition of 30 µL of 4x SYBR-Gold Nucleic Acid Gel Stain (Thermo Fisher Scientific). The plate was incubated in the dark for 10 min. Measurements were conducted on a SPARK® multimode microplate reader (TECAN Group Ltd., Maeneedorf, Switzerland) at an excitation wavelength of 485/20 nm and an emission wavelength of 520/20 nm. Samples with only siRNA were prepared, treated and measured in the same way as all the other samples. Fluorescence of free siRNA was used as a control for 100% free siRNA. Results were presented as the mean ± SD, n = 3.

To compare the stability of formed nanoparticle systems, polyplexes and HLPNPs were exposed to a heparin solution. Heparin, a polyanion, competes with the negatively charged nucleotides to bind to the cationic polymer thus allowing to examine a potential siRNA release. In brief, various heparin concentrations at 1.0, 0.75, 0.5 and 0.25 international units (IU) in 10 µL were prepared. Then, 100 µL of HLPNP samples were added to each well of a black 96-well plate, followed by the addition of 10 µL heparin solution at various concentrations. The plate was left to incubate for 30 min. Subsequently, a SYBR-Gold assay was run as above mentioned. Results are shown as mean ± SD, n = 3.

2.9 *In vitro* characterization of HLPNPs

2.9.1 Cell Culture

The human non-small cell lung carcinoma cell line H1299 (ATCC CRL-5803) and the same cell line stably expressing enhanced green fluorescence protein (eGFP, H1299-GFP) was cultured in RPMI 1640 medium supplemented with 10% FBS, 1% P/S and additional 0.4% G418 for H1299-GFP cells. Cells were passaged every 3 days with 0.05% v/v trypsin and subcultured in 75 cm2 flasks. Cells were kept in a humidified atmosphere at 37 °C with 5% CO2.

2.9.2 *In vitro* uptake of HLPNPs in H1299 cells

For uptake experiments, amine modified siRNA (Integrated DNA Technologies, Coralville, USA) was labeled with succinimidyl ester (NHS) modified AF 488 (Life Technologies,Carlsbad, USA) . HLPNPs

were prepared at a concentration of 500 pmol siRNA-AF488 per mL at different N/P ratios as described in 2.2. Lipoplexes were prepared with Lipofectamine 2000 as positive control. Per well, 50,000 H1299 cells were seeded in 24-well plates (Thermo Fisher Scientific) with 500 µL medium and left for 24h incubation at 37°C and 5% CO2. Then, cells were transfected with 100 µL of samples and left for another 24 h incubation time. As negative controls, blank samples were seeded and left untreated. Cells were harvested and washed three times before resuspension in 500 µL PBS/2 mM EDTA (Sigma-Aldrich). Samples were analyzed using an Attune® NxT flow cytometer (Thermo Fisher Scientific) with 488 nm excitation and 530/30 emission filter. All LNPs samples were gated by morphology for a minimum of 10,000 viable cells. For trypan blue quenching, one half of each sample was washed with 0.4% trypan blue to mask any signal originating from extracellular fluorescence. Results are displayed as mean MFI values (%) ± SD, n = 3.

2.9.3 *In vitro* GFP downregulation in H1299-GFP cells

To evaluate the in vitro gene silencing efficiency of HLPNPs, H1299-GFP cells were seeded in a 24-well plate at a density of 25,000 cells per well in 500 µL medium incubated for 24 h at 37 °C and 5% CO2. Cells were transfected with 100 µL of HLPNPs at a concentration of 500 pmol/mL and added to 400 µL of fresh culture medium left for 48 h incubation at 37 °C and 5% CO2. At the end of the incubation time, cells were washed with PBS, trypsinized and collected. After centrifugation at 400 rcf for 5 min, the supernatant was discarded, and the cell pellet was washed two times in PBS before being resuspended in PBS with 2 mM EDTA. Samples were analyzed by flow cytometry (Attune NxT, Thermo Fischer Scientific, Waltham, Massachusetts, USA), and the median fluorescence intensity (MFI) of GFP protein expression was measured by using a 488 nm excitation laser and the emitted light passing through a 530/30 nm band pass emission filter set was detected. All HLPNPs samples were gated by morphology for a minimum of 10,000 viable cells. Results are displayed as mean MFI values (%) ± SD, n = 3.

2.9.4 *In vitro* cytotoxicity of HLPNPs in H1299 cells

Cell viability after transfection with HLPNPs was tested via an MTT assay as described previously. [258, 259] Briefly, 5,000 H1299 cells per well were seeded in 100 µL medium in a transparent 96-well plate (BioLite 96 well multidish, Thermo Fisher Scientific, Rochester, New York, USA). The samples were prepared at a concentration of 500 pmol/mL as described in 2.2. After 24 h, 90 µL of prewarmed medium was added to each well and supplemented with 10 µL of sample, respectively. The plate was incubated for 24 h at 37 °C and 5% CO2. As a full viability control, cells were incubated in 100 µL medium only. After 24 h, the media was aspirated and 200 µL of MTT containing medium (0.5 mg/ml in serum-free RPMI-1640 medium) was added to each well. Cells were incubated for another 3 h at 37 °C and 5% CO2. Subsequently, the cell culture medium was completely removed, and insoluble purple formazan crystals were dissolved in 200 µl DMSO. The plate was set on a horizontal shaker for 20 min for all crystals to dissolve. The absorbance was measured at 570 nm, corrected with background values measured at 680 nm, using a microplate reader (TECAN Spark, TECAN, Maennedorf, Switzerland). The data are shown as mean ± SD as percentage of viable cells in comparison to untreated cells representing 100% viability, n = 3.

2.10 Statistics, data analysis and presentation

All experiments were run in independent triplicates. Experimental data was analyzed for normality by running a D'Agostino & Pearson omnibus normality test. Statistical significance was analyzed using the One-Way ANOVA repeated measurements on the GraphPad Prism 5 software with Tukey's post-hoc test with $p>0.05$ considered not significant (ns), * $p<0.05$, **$p<0.01$, ***$p<0.001$. Data presentation was performed using GraphPad Prism 5 data science packages. Data not fitting normality were excluded from presentation.

3. Results and Discussion

3.1 Characterization of physicochemical properties of DOPC- and DOTAP-coated HLPNPs

Hybrid nanoparticles consisted of a polyplex core made of the triblock copolymer PEI-PCL-PEI and a lipid coating. The HLPNP formation was achieved using a single-step microfluidic mixing method to simplify the production by keeping a high reproducibility and quality. The Micromixer set-up allowed a premixing of the polyplex in one circuit before coating the polyplex with the lipid in the other circuit. All components were dissolved or transferred into an aqueous solution keeping the mixing procedure as simple as possible. At a neutral pH of 7.4, the PEI ends of the triblock copolymer have protonated nitrogen groups enabling the electrostatic attraction and binding with the negatively charged siRNA. Various polyplex samples were tested by adapting the N/P ratio from 5, 7 and 10 to 20, while keeping the FRR at 1:1 (Table 2).

Table 2 Size, polydispersity index (PDI) and zeta potential of polyplexes, DOPC-coated and DOTAP-coated HLPNPs after microfluidic mixing. Polyplexes consist of siRNA complexed with PEI-PCL-PEI polymer. Results are displayed as mean ± SD, n = 3.

Sample	Abbreviation	N/P ratio polyplex	FRR polyplex	Polyplex-lipid ratio	Size (nm)	PDI	Zeta potential (mV)
Polyplex	-	5	1:1	-	113.4 ± 5.6	0.373 ± 0.034	-14.4 ± 7.5
	-	7	1:1	-	123.2 ± 1.2	0.237 ± 0.005	-3.85 ± 0.55
	-	10	1:1	-	869.4 ± 467.2	0.305 ± 0.394	-4.90 ± 0.89
	-	20	1:1	-	65.13 ± 0.15	0.199 ± 0.014	-1.48 ± 0.47
Polyplex	-	7	1:1	-	123.2 ± 1.2	0.237 ± 0.005	-3.85 ± 0.55
	-		4:1	-	87.7 ± 2.96	0.121 ± 0.024	-0.65 ± 1.73
	PP 1		6:1	-	96.9 ± 1.28	0.201 ± 0.026	9.42 ± 7.29
	-		8:1	-	88.1 ± 0.72	0.130 ± 0.007	5.46 ± 9.24
	PP 2	14	6:1	-	101.6 ± 7.3	0.211 ± 0.039	16.00 ± 2.92
DOPC hybrid	-	7	6:1	1:1	157.4 ± 21.9	0.379 ± 0.070	-13.71 ± 6.54
	HLPNP 1	14	6:1	1:1	210.9 ± 0.6	0.233 ± 0.005	0.31 ± 2.07
DOTAP hybrid	HLPNP 2	7	6:1	1:1	147.9 ± 15.1	0.227 ± 0.045	-2.73 ± 0.36
	HLPNP 3	7	6:1	1:2	198.2 ± 0.2	0.204 ± 0.012	2.42 ± 1.30
	HLPNP 4	14	6:1	1:1	107.6 ± 6.6	0.212 ± 0.014	7.04 ± 8.14

This first screening revealed a wide range of sizes from 65 nm at N/P 20 to 869 nm at N/P 10. N/P ratios 5 and 7 gave sizes of 113 to 123 nm, a range that fits the target values of <150 nm. The PDIs varied from 0.2 to 0.373. Despite that wide size distribution obtained, the zeta potential showed a negative value throughout all samples. That means, the siRNA is not complexed within the polyplex and negative charge is detected at the outer layer of the nanoparticle. Our findings seemed to suggest that the flow speed at which the polymer solution and the siRNA solution meet might be too high. To overcome the

negative zeta potential, the FRR was changed to a slower siRNA stream but keeping the same polymer solution flow rate of 0.5 mL/h. The siRNA concentration was increased to keep the final polyplex concentration constant at 1000 pmol/mL. The N/P ratio of 7, instead of N/P 20, was chosen as it gave the best first set of data by keeping in mind that a lower polymer amount will induce lower positive charge, and therefore, less cytotoxicity. [193] The increasing FRR of 4:1, 6:1 and 8:1 stabilized the polyplex sizes at round 87-97 nm. The PDI was reduced to 0.121 – 0.201 showing a narrow size distribution of polyplexes. Reaching a PDI value of 0.2 or lower fulfills the target values and matches literature values. [305] In addition, the increase in FRR resulted in a more positive zeta potential. Starting with a neutral value of -0.65 mV for FRR 4:1, a gradual increase in FRR to 6:1 and 8:1 resulted in zeta potentials of 9.4 mV and 5.5 mV, respectively. The neutral zeta potential value of FRR 4:1 is generally not favorable for nanoparticle systems because the lack of electrostatic repulsion could lead to particle aggregation. [306] Changing the FRR from 6:1 to 8:1 should result in additional positive charge, however, the zeta potential dropped by almost half. This decrease can be explained by the dynamic electrostatic interaction within the polyplex that constantly forms and deforms the nanoparticle structure until an equilibrium is reached. [307] Furthermore, shifting the ratio between siRNA- and polymer flow can influence the complexation efficiency. Therefore, the FRR of 6:1 was chosen to be used for further polyplex formations implying most suitable physicochemical properties. For the same reason, though room for improvement, the N/P ratios for polyplex formation were set to 7 and 14. The polyplex formation at N/P 14 led to adequate sizes of around 100 nm, a PDI value of 0.21 and a zeta potential of +16 mV. Hence, PP 1 and PP 2 are favored for all further hybrid coating experiments. In a comparable polyplex formation study by Feldmann et al. using the same microfluidic setup but a different triblock copolymer, PEG-PCL-PEI, their polyplexes at N/P 6 resulted in bigger sizes of 122 - 168 nm and polydisperse PDI values of 0.3 – 0.52. Two major discrepancies included a constant FRR of 1:1 and much higher flow rates of 0.5 – 2 mL/min which can explain the values yet worthy for improvement. [34] Therefore, the adjustment of the FRR has already proven to be successful in forming a polyplex system of sizes at around 100 nm and narrower size distributions of ≤0.2.

DOPC-coated (HLPNP 1) and DOTAP-coated (HLPNP 2, 3, 4) hybrid nanoparticles maintained a polyplex core at N/P ratios 7 and 14 and had a lipid FRR of 1:1. Only in the case of DOTAP, a double lipid amount, resulting in a FRR of 1:2 (HLPNP 3), was evaluated as well. The zwitterionic lipid DOPC exhibiting an overall neutral charge should set the DOPC-coated HLPNPs' zeta potential to about 0 mV. For DOPC-coated hybrids at N/P 7, bigger sizes of 157 nm and PDI values of 0.379 were obtained. The zeta potential resulted in a negative value of -13.7 mV which can be explained by a disruption of the hybrid construct externalizing the nucleic acid and disqualifying this hybrid system for microfluidic formation. In comparison to N/P 7, HLPNP 1 resulted in a neutral zeta potential of +0.3 mV at sizes of 210 nm and PDI values of 0.233. This affirms the assumption that a coating with the neutrally charged DOPC can lead to a zeta potential around 0 mV. The results from DOPC-coated HLPNPs at N/P 7 could rise the question if the hybrid systems are proper hybrids, or if the microfluidic coating led to a disruption or even a co-existence of polyplexes and lipid nanoparticles. Figure S2 (A2) shows the DLS measurements of DOPC-lipids in comparison to HLPNP 1. The distribution profiles differ from each other and most importantly, DOPC-coated HLPNPs show a single size distribution peak indicating that a monodisperse hybrid system is detected. To confirm these results, a confocal microscopy measurement to co-localize siRNA embedded polyplexes and DOPC lipid was performed. As seen in Figure 1, a co-localization of siRNA (red) and Liss Rhod PE linked DOPC lipid (green) led to color change to yellow. The Pearson coefficient, quantifying the co-localization, was calculated at 0.558 meaning a strong positive correlation was observed. [308] Therefore, the DOPC-coated HLPNPs at N/P 14 were considered promising candidates as a nucleic acid carrier and will be further evaluated.

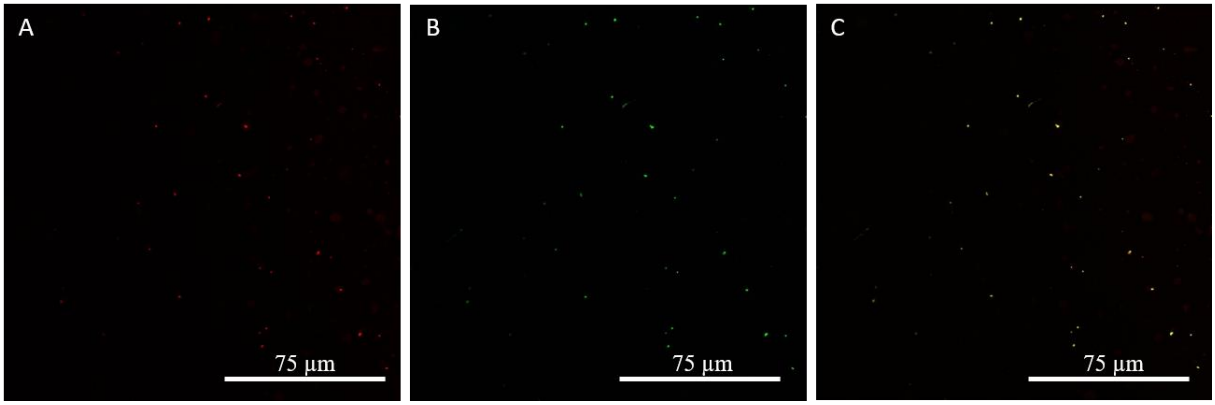

Figure 1 Confocal pictures of HLPNPs. A) siRNA-AF488 (red), B) Liss Rhod PE linked DOPC lipid (green) and C) siRNA-lipid co-localization (yellow).

A second HLPNP formulation was tested using the positively charged lipid DOTAP to coat the polyplex nanoparticles. The decision was led by the assumption that a positively charged lipid will increase the positive zeta potential which in conclusion would stabilize the hybrid system and improve the transfection efficiency. The sizes of DOTAP-coated HLPNPs at N/P 7, single and double amount of lipid, and N/P 14, differed widely from 107 nm up to 198 nm. The obtained sizes were verified by NTA measurement of N/P 7 and N/P 14 DOTAP-coated HLPNPs resulting in sizes of 134 nm and 86 nm, respectively (A2, Figure S3). This big size range did not affect the PDI which remained around 0.2 – 0.23. However, the zeta potential varied from -2.7 – +7 mV showing that the positive charge of DOTAP does not have a severe impact on the overall charge of the HLPNPs. The positive charge of DOTAP is most likely partially directed towards the siRNA and partially towards the outside of the HLPNPs. Therefore, the overall charge does not appear to be highly positive.

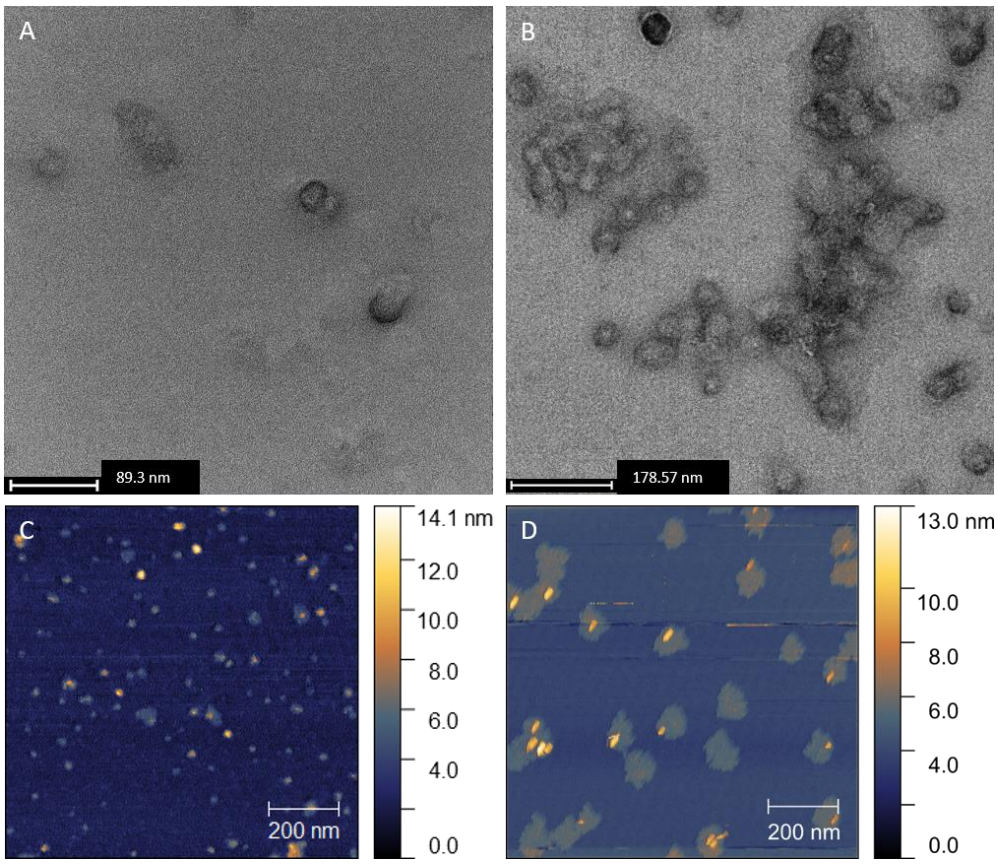

Figure 2 Morphology and sizes of HLPNPs at a N/P ratio of 14 and a polyplex to lipid FRR of 1:1. TEM pictures of A) HLPNP 4 (DOTAP) and B) HLPNP 1 (DOPC). AFM measurement of C) HLPNP 4 (DOTAP) and D) HLPNP 1 (DOPC).

All hydrodynamic measurements of freshly prepared DOPC- and DOTAP-coated HLPNPs varied widely between N/P 7 and 14, as seen via DLS. Therefore, TEM and AFM measurements were done to evaluate the morphology of fresh nanoparticles and to confirm their size. TEM pictures in Figure 2A and B show round-shaped nanoparticles. In Figure 2A, HLPNP 4 showed sizes of about 70 nm, whereas HLPNP 1 showed aggregates and sizes of 200 nm and more. In Figure 2C, the AFM measurement of HLPNP 4 displayed sizes of about 70 nm in good agreement with the TEM results. HLPNP 1 showed sizes of up to 200 nm which substantiates the results of DLS and TEM (Figure 2D). As mentioned above, the neutral charge of DOPC-coated HLPNPs (HLPNP 1) favors the aggregation.

The zeta potential of a nanoparticle system is just one indicator for the complexation of the siRNA. Another approach is to test the encapsulation efficiency by SYBR-Gold assay. Figure 3 showed a quantification of the amount of free siRNA of all microfluidic produced polyplexes and HLPNPs. In Figure 3A, the different FRR for polyplex formation were examined resulting in almost full encapsulation of the siRNA. Polyplexes of N/P 7 and 14, as well as DOPC- and DOTAP-coated HLPNPs showed encapsulation efficiencies of more than 99% exceeding the set target of 95% and most PLGA-based hybrid nanoparticles (Figure 3B). The HLPNP stability can be observed performing a heparin competition assay using the presence of heparin as a large polyanion to effectively compete with the polyplexes and hybrid complex.

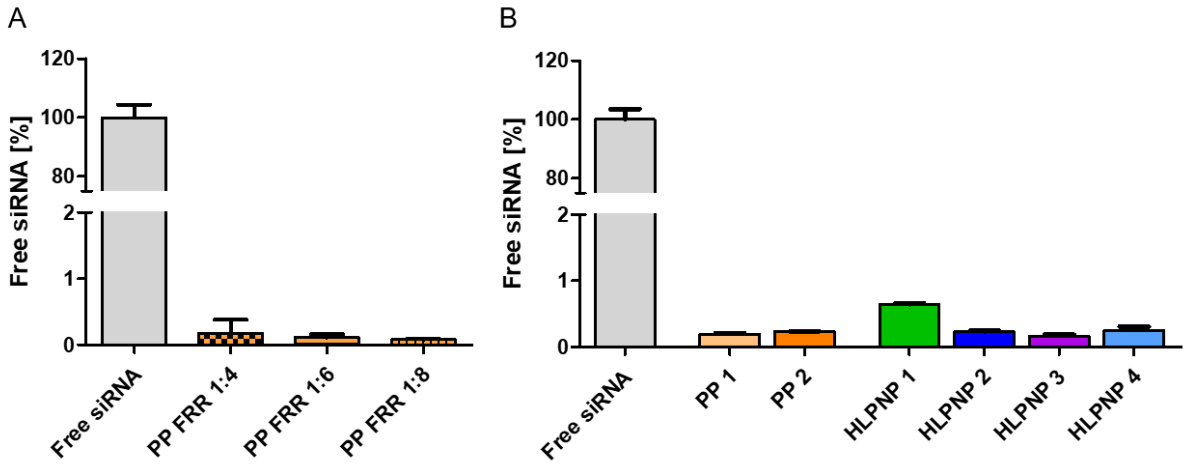

Figure 3 Encapsulation efficiency using the SYBR-Gold assay. A) Detection of siRNA complexation within polyplex nanoparticles at N/P 7 (PP) and various FRR. B) Comparison of siRNA encapsulation between polyplexes (PP 1-2) and DOPC- and DOTAP-coated hybrid nanoparticles (HLPNP 1-4). Results are displayed as mean ± SD, n = 3.

Figure showed that all samples resulted in an increased amount of free siRNA of 20-40% by gradually adding more heparin up to 1 I.U. HLPNP 2 seemed to have the weakest complexation of siRNA at 40% free siRNA which underscores the negative zeta potential observed. All other DOTAP-coated HLPNPs (HLPNP 3 and 4) displayed 20% of free siRNA. Hence, the nucleic acids tighter packed in the hybrid particles than the corresponding polyplex nanoparticles indicating that the lipid coating improves the nanoparticle properties. In conclusion, the siRNA was complexed inside the various HLPNPs, and all nanoparticle systems fulfilled quality criteria to be tested in an *in vitro* environment.

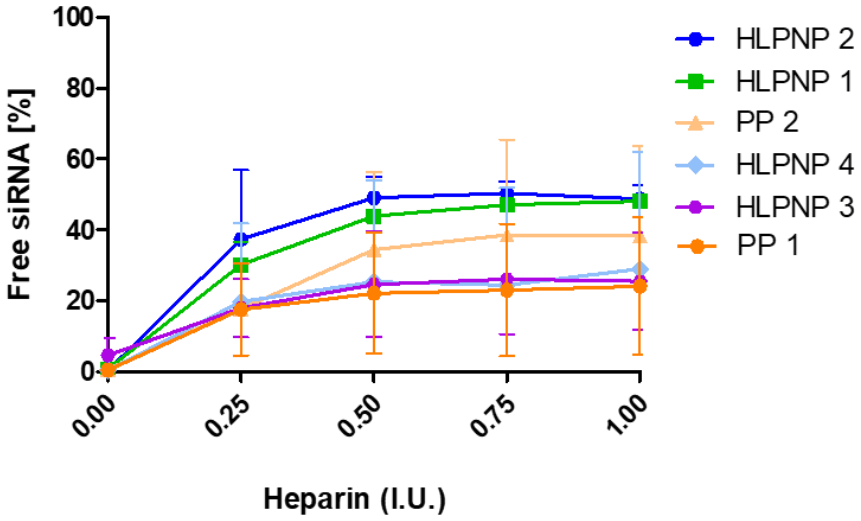

Figure 4 Polyplex (PP 1-2) and HLPNPs (1-4) stability evaluation using a Heparin-SYBR-Gold assay at pH 7.4. Results are displayed as mean ± SD, n = 3.

3.2 In vitro evaluation of DOPC- and DOTAP-coated HLPNPs

The in vitro performance of polyplexes and HLPNPs was tested by examining cytotoxic effects after transfection and the uptake behavior in H1299 cells. If the HLPNP systems should find clinical application as drug delivery system, they must not show any cytotoxic effects. Figure 5A examined the nanoparticles' cytotoxicity using a MTT assay in H1299 cells. No statistically significant cytotoxicity was observed using any of the polyplexes (PP 1 and PP 2) and HLPNPs 1-4. Figure 5B shows the mean fluorescence intensity (MFI) of all samples as they were detected non-quenched and quenched with trypan blue. Nanoparticles might stick to the cell membrane without internalizing into the cell resulting in a surface fluorescence signal. To avoid a false-positive uptake detection, cell membranes are dyed with trypan blue to detect absolute uptake intensities. [309] HLPNP 1 had half the uptake intensity of the corresponding polyplexes at N/P 14 (PP 2), whereas HLPNP 4 maintained the same uptake behavior. PP 1 resulted in a similar uptake value as PP 2 and HLPNPs 2-4. Therefore, the uptake seems to be independent of the surface charge of the nanoparticles. HLPNP 2's uptake value was slightly lower than its preformed polyplexes. One reason was the highest leakage in siRNA for this composition as revealed in the heparin competition assay. In addition, a slight negative zeta potential could have caused a cell membrane repulsion. leading to a reduced uptake. The only formulation that increased the uptake performance was HLPNP 3, which consisted of a double amount of DOTAP-lipid.

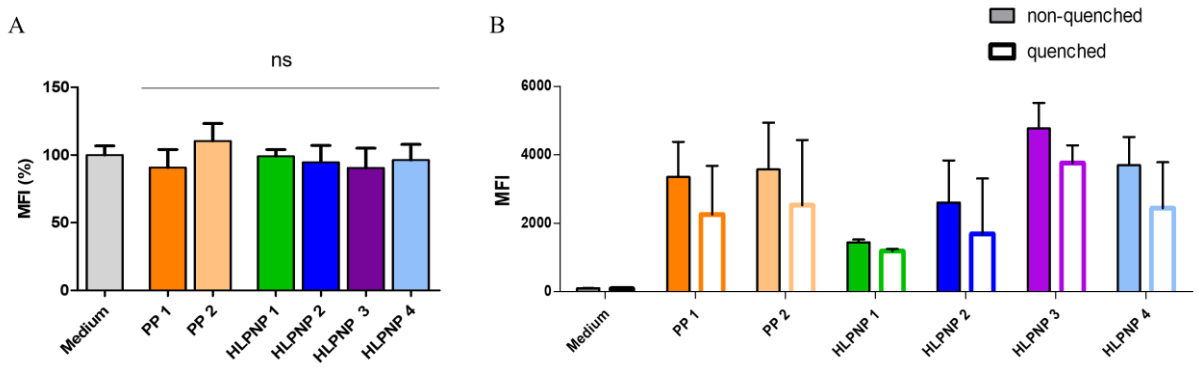

Figure 5 *In vitro* evaluation of siRNA embedded nanoparticles via microfluidic mixing. A) Cytotoxicity evaluation of polyplexes and HLPNPs in H1299 cells. B)) Uptake behavior of polyplexes (PP 1-2), DOPC-coated (HLPNP 1) and DOTAP-coated HLPNPs (HLPNP 2-4) in H1299 adenocarcinoma cells. Nanoparticle compositions found in Table 2. Results are displayed as mean ± SD, n = 3.

A-combination of a positive zeta potential, bigger particle sizes and sufficient hybrid nanoparticle stability were identified as the contributing reasons. Overall, the uptake performance of polyplexes PP 1and PP 2 were only improved by one hybrid formulation (HLPNP 3) but decreased by HLPNP 1 and HLPNP 2. These results underline the complexity of lipid-coating in aqueous environment via microfluidic mixing.

The uptake behavior alone does not imply that a carrier system can efficiently release its cargo to the cell interior. A gene silencing evaluation can help to understand if a cargo is released at its designated point, i.e., to downregulate protein expression. Figure 6 presents the knockdown data of all polyplexes (PP 1 + 2) and HLPNP 2-4 in H1299 cells expressing the enhanced green fluorescence protein (H1299-GFP). HLPNP 1 (DOPC coating) was excluded because of its insufficient prior performance. Polyplexes and hybrid nanoparticles were formed having scrambled siRNA (siNC) and GFP-targeting siRNA (siGFP) encapsulated. Samples with scrambled siRNA were used as negative control. The knockdowns resulted in a non-significant gene silencing of about 10% throughout all samples. Only HLPNP 4 showed a 40% knockdown efficiency. This overall poor performance can be explained by the endosomal escape problem. [10, 195] Polyplexes are considered to escape the endosomes via the proton sponge effect, which is an osmotically induced swelling of the endosome. This is triggered by the proton buffering capacity of the polyplexes, ultimately resulting in rupture of the endosomal membrane. [196] Furthermore, protonation of polymers will cause polymer swelling because of the electrostatic repulsion between the protonated polymers that show an enhanced electrostatic interaction with the endosomal membrane. Molecular dynamic simulation has shown that membrane adsorption of polymer under tension, in case of osmotic swelling and size increase, lowers the critical stress required to disrupt the endosomal membrane. [310] To evaluate if this is occurring, polyplexes and HLPNPs are transfected with chloroquine which induces an endosomal release. [311] A highly significant knockdown of >90% was observed for all samples. Therefore, all polyplex and hybrid nanoparticle systems got stuck in the endosome and did not release their siRNA cargo effectively. One the one hand, a stable nanoparticle structure, tightly encapsulating the nucleic acid, is helping nanoparticle transfection. On the other hand, this tight formation could hinder the siRNA to be released from the endosome. Furthermore, an increase in size could have led to the reduced critical stress to disrupt the endosomal membrane. Despite sufficient physicochemical properties and nanoparticle stability, DOPC- and DOTAP-coated hybrid nanoparticle systems did not improve the performance of their polyplex precursor.

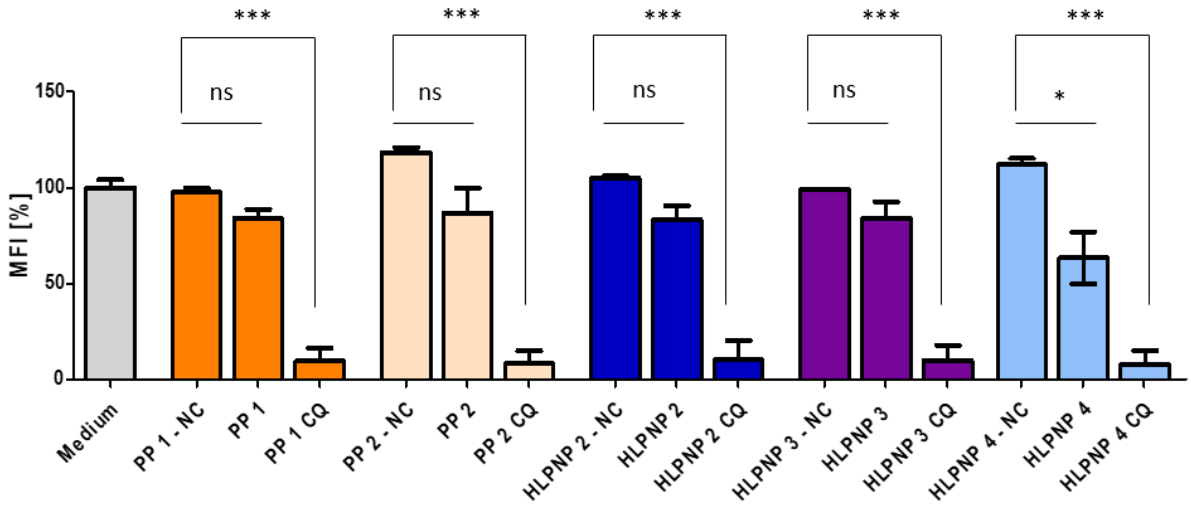

Figure 6 Knockdown efficiencies of polyplexes (PP 1-2) and DOTAP-coated HLPNPs (HLPNP 2-4). NC = negative control siRNA (siNC). All other HLPNPs had siGFP encapsulated. CQ = chloroquine treatment, forcing endosomal release. Exact nanoparticle compositions found in Table 1. Results are displayed as mean ± SD, n = 3.

3.3 Optimization of HLPNP systems using DLIN-MC3-DMA lipid

Hybrid nanoparticles based on DOPC- and DOTAP-coating showed good physicochemical properties but could not exceed in their in vitro performance concluding not to be used as siRNA delivery systems. Therefore, a different approach was chosen by using the ionizable lipid DLIN-MC3-DMA which is widely used in the formation of lipid nanoparticles. [312-314] In lipid nanoparticles (LNPs), the ability of ionizable lipids, such as DLIN, to form destabilizing non-bilayer structures at acidic pH is the major factor for their efficient endosomal release and nucleic acid cytosolic delivery. [315] Hence, the coating with DLIN-MC3-DMA could help tackling the endosomal release problem.by inducing the disruption of the endosomal membrane. The procedure of D-LIN coated nanoparticle formation remained as above-mentioned and the first approach determined the sizes, PDIs and zeta potentials of HLPNP 5 + 6. As shown in Table 3, the D-LIN-coated nanoparticle sizes were measured between 178 – 217 nm. The PDI resulted in size distribution of 0.2, which have been the best and most consistent values of all polyplexes and hybrid nanoaprticles. The zeta potential results confirmed the previous values of 0 - +5 mV. This was expected because DLIN-MC3-DMA is not charged at physiological pH. However, as discussed above, the neutral charge could have caused the particle's increased size. In comparison to DOPC- and DOTAP-coated HLPNPs, the newly formed D-LIN hybrids showed similar sizes and charge values, independently of the N/P ratio of the polyplex cores.

Table 3 Size, polydispersity index (PDI) and zeta potential of freshly prepared D-LIN-coated hybrid nanoparticles (HLPNP 5-6) via microfluidic mixing. Results are displayed as mean ± SD, n = 3.

Sample	Abbreviation	N/P ratio polyplex	FRR polyplex	Polyplex-lipid ratio	Size (nm)	PDI	Zeta potential (mV)
DLIN-MC3-DMA	HLPNP 5	7	1:6	1:1	217.3 ± 10.6	0.200 ± 0.070	-0.84 ± 0.55
(D-LIN) hybrid	HLPNP 6	14	1:6	1:1	178.2 ± 0.3	0.197 ± 0.026	5.81 ± 7.98

Another important comparison between polyplexes and D-LIN HLPNPs was assessed by evaluating the encapsulation efficiency and performing a hybrid stability assay. The D-LIN hybrid encapsulation efficiency of siRNA was detected at 99% for N/P ratios 7 and 14 (Figure 7A). These results match the encapsulation results displayed in section 3.1 which also detected about 99% encapsulation for DOPC- and DOTAP-based HLPNPs (Figure 3A). This underscores the effectiveness of the hybrid system to keep the siRNA complexed. In an in vivo environment many proteins and anions interact with the nanoparticles making them a target for disruption. Hence, the heparin competition assay tries to mimic the interaction. D-LIN-coating (HLPNP 5+6) led to an improvement of siRNA complexation in comparison to polyplexes. The amount of released siRNA from the polyplex, detected at 20-40%, was reduced to 10-18% (Figure 7B). The results highlight the newly formed D-LIN hybrid nanoparticles as stable siRNA delivery systems that outperform the previously formed DOPC- and DOTAP-coated HLPNPs.

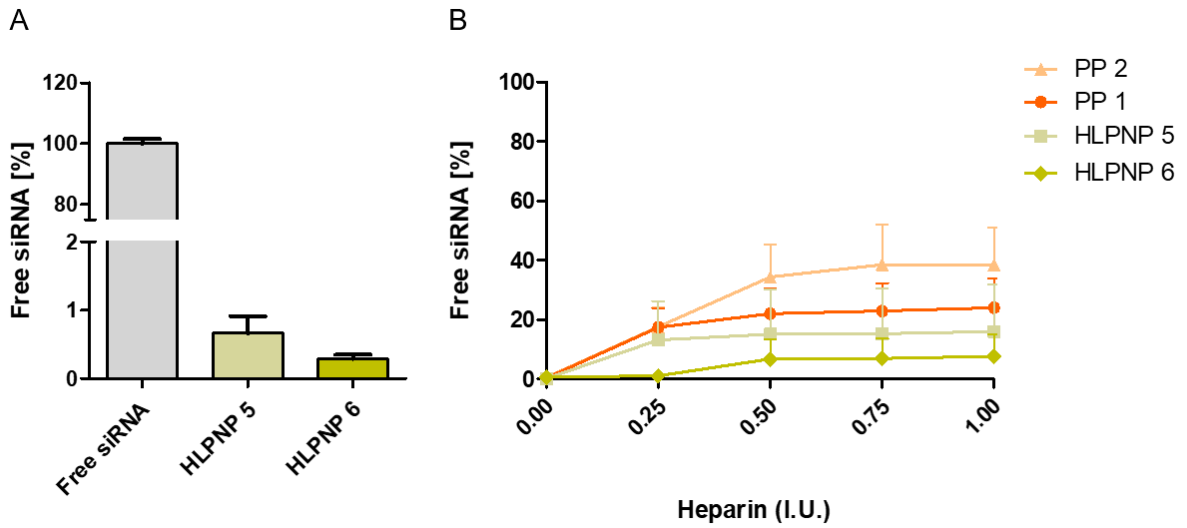

Figure 7 Encapsulation efficiency and HLPNP stability using the SYBR-Gold assay. A) Detection of siRNA complexation for HLPNP 5 + 6. B) Comparison of heparin competition assay on polyplexes (PP 1 + 2) and D-LIN-coated nanoparticles (HLPNP 5 + 6). Results are displayed as mean ± SD, n = 3.

The physicochemical property testing of D-LIN-coated HLPNPs was followed by performance assessment in an in vitro environment. It is noteworthy, that all D-LIN-coated nanoparticles (HLPNP 5 + 6) did not induce cytotoxicity (Figure 8A). The uptake performance of HLPNPs 5 + 6 underperformed PP 1 and PP 2. In comparison, DOTAP-coated nanoparticles (HLPNP 2-4) achieved an uptake level which was at least as good as PP 1 and PP 2 or even exceeded their value as seen for HLPNP 3. As seen with HLPNP 2-4, trypan blue quenching led to a reduced MFI value of D-LIN hybrids (HLPNP 5-6), in comparison to the non-quenched detection. Especially, HLPNP 5 obtained a very low uptake level below 500 MFI. In comparison to PP 1, HLPNP 5 resulted in a non-quenched reduction of 6-fold and a quenched reduction of 4-fold. (Figure 8B). In summary, D-LIN-coated HLPNPs were not as efficiently taken up by H1299 cells as their polyplex precursors.

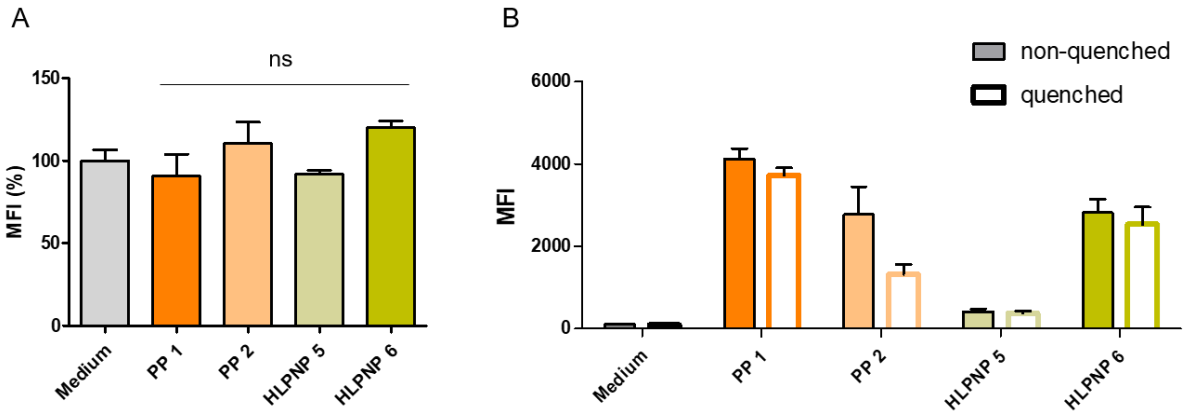

Figure 8 *In vitro* evaluation of polyplexes (PP 1 + 2) and D-LIN-coated nanoparticles (HLPNP 5 + 6). A) Cytotoxicity evaluation of in H1299 cells. B) Uptake behavior in H1299 adenocarcinoma cells. Results are displayed as mean ± SD, n = 3.

However, as already discussed, the advantage of ionizable lipids lies within their chemical characteristics to promote an endosomal escape at an acidic environment. The gene silencing efficiency of D-LIN-coated hybrids (HLPNP 5-6) was evaluated targeting H1299-GFP cells. Despite the decreased uptake of HLPNP 5 + 6 with respect to their polyplex precursors, an improved knockdown was noticed. PP 1 and PP 2 showed GFP knockdowns of 20-30% whereas D-LIN-coated hybrids improved the knockdown level to 30% for HLPNP 5 and over 60% for HLPNP 6 (Figure 9). In comparison to DOPC- and DOTAP-coated hybrid nanoparticles, only HLPNP 4 reached a 40% knockdown. In a study by Wei

et al., a 50% downregulation of EGFR mRNA using siRNA in PEI-PCL polyplexes coated with DOPE lipid was obtained. [154] Our HLPNP 6 was able to outperform the hybrid formulation and HLPNP 4, respectively. A valid comparison can be drawn because Wei et al. used a similar one-step microfluidic set-up in and a polyplex core that should be improved in performance by lipid coating.

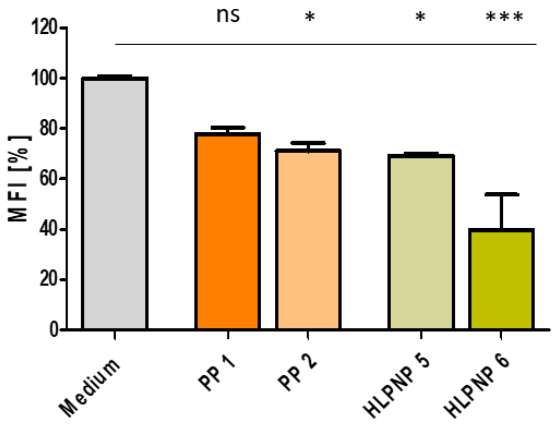

Figure 9 Knockdown efficiencies of polyplexes (PP 1 + 2) and D-LIN-coated nanoparticles (HLPNP 5 + 6). All HLPNPs were encapsulated with siGFP. Results are displayed as mean ± SD, n = 3.

The use of the ionizable lipid D-LIN seemed to improve the endosomal release of HLPNP 5 + 6. However, the N/P ratio of 7, leading to a lower D-LIN amount as seen in Table 1, did not improve uptake behavior and only led to a slight significant knockdown improvement. Therefore, a minimum amount of ionizable lipid might be required to induce a sufficient cell uptake and endosomal release.

4. Summary & Conclusion

The urge to find novel and efficient nucleic acid delivery systems is a constant demand. Nucleic acid delivery systems based on polymers and lipids fulfill the specifications that carriers need to deliver its cargo to the designated destination. Nevertheless, the production processes of polyplexes or lipid nanoparticles comprise of multiple and even time-consuming steps. Our approach aimed at finding a hybrid nanoparticle system that merges and uses the synergies of polymer- and lipid-based nanoparticles to successfully encapsulate and delivery siRNA to adenocarcinoma cells. Microfluidic mixing was chosen for nanoparticle formation as a rapid and reproducible set-up. After finding the right mixing parameters for polyplexes and hybrid nanoparticles, all HLPNPs resulted in sizes of 100-200 nm, However, this particle size is still in the range of being useful for nucleic acid delivery without being cleared by renal or hepatic pathways. Throughout the fine-tuning of the mixing parameters, the nanoparticles' zeta potential was moved from a negative to a positive value. This was important to enable a cell membrane attraction and not triggering a repulsion. The in vitro transfection of all hybrid nanoparticles did not induce any cytotoxic effects. The uptake performance of our HLPNPs, however, varied between DOPC-, DOTAP and D-LIN coated hybrid systems. HLPNP 1 (DOPC-coated) showed the weakest uptake performance of all three lipid coatings. Thus, it was excluded from further evaluation. DOTAP-coated hybrid nanoparticles (HLPNP 2-4) kept the uptake behavior of their polyplex precursors, or even outperformed them in the case of HLPNP 3. However, only HLPNP 4 managed to significantly downregulate the green fluorescence protein for 40%. The internally set target value of 50% gene knockdown was not reached. Forcing endosomal release of siRNA with chloroquine led to a 90% gene knockdown, confirming the hypothesis that HLPNPs remained confined in the endosome. In addition, a strong complexation stability, as seen in the heparin assay, might have hindered the siRNA to be released in the cytosol. In case of D-LIN-MC3-DMA-coated HLPNPs, the targeted physicochemical properties of sizes around 150 nm and a positive zeta potential were met. The positive charge should not cause membrane activity or side effects; hence, the hemolysis of the hybrid

nanoparticle systems should be evaluated in future experiments to generate a complete dataset of D-LIN-coated HLPNPs. The uptake behavior was slightly reduced for HLPNP 6 (N/P 14) but drastically reduced for HLPNP 5 (N/P 7), suggesting that the microfluidic mixing of HLPNP 5 and its precursor PP 1 rearrange the nanoparticle composition resulting in a worsened uptake behavior. However, the knockdown efficiency was improved for both N/P ratios resulting in a GFP-knockdown of 60% at N/P 14. As shown for DOTAP-coated HLPNPs, D-LIN coating did not render in cytotoxicity.

In conclusion, if polymer-based nanoparticles show limitations regarding the in vitro performance, it is worthwhile to form hybrid nanoparticles to use the advantages of lipids to improve the hybrid nanoparticles' behavior. In our case, the formation of HLPNPs with a D-LIN coating at N/P 14 (HLPNP 6) using microfluidic mixing, as a quick, reliable, and reproducible method, proved to improve the knockdown efficiency drastically by retaining physicochemical properties and siRNA complexation. Further optimization of the D-LIN-coated HLPNPs could be obtained by investigating the N/P ratio or FRR or using other ionizable lipids to find the best possible HLPNP formation. Additional evaluation of hybrid nanoparticle stability would be essential to classify this coating approach as a long-term drug delivery system. The heparin competition assay was a first implication of the siRNA complexation ability of HLPNPs. However, it reflected only a single time point which was placed after preparation. A long-term storage of polyplexes and their corresponding HLPNPs could gain more insight about the hybrid nanoparticles' suitability as a nucleic acid drug delivery system.

Acknowledgements

The authors thank Rebecca Schlatterer and Bizan Balzer from the University of Freiburg for supporting this project and for providing AFM measurements.

Chapter VI – Spray drying siRNA-lipid nanoparticles for dry powder pulmonary delivery

This chapter is published as:

Christoph M. Zimmermann [a,i], Domizia Baldassi [a], Karen Chan [b,c], Nathan B.P. Adams [d], Alina Neumann [d], Diana Leidy Porras-Gonzalez [e], Xin Wei [e], Nikolaus Kneidinger [f], Mircea Gabriel Stoleriu [g], Gerald Burgstaller [e], Dominik Witzigmann [b,c,h], Paola Luciani [i], Olivia M. Merkel [a,e,], 2022. Spray drying of siRNA-lipid nanoparticles for dry powder pulmonary delivery. Journal of Controlled Release, 351, pp. 137-150.

a. D*epartment of Pharmacy, Pharmaceutical Technology and Biopharmacy, Ludwig-Maximilians Universität München, 81377 Munich, Germany*
b. *Department of Biochemistry and Molecular Biology, University of British Columbia, 2350 Health Sciences Mall, Vancouver, BC V6T 1Z3, Canada*
c. *NanoMedicines Innovation Network (NMIN), 2350 Health Sciences Mall, Vancouver, BC V6T 1Z3, Canada*
d. *Nanotemper Technologies GmbH, Flößergasse 4, 81369 Munich, Germany*
e. *Institute of Lung Health and Immunity (LHI) and Comprehensive Pneumology Center (CPC) with the CPC-M bioArchive, Helmholtz Munich, Member of the German Center for Lung Research (DZL), Munich, Germany*
f. *Department of Medicine V, University Hospital, LMU Munich, Member of the German Center for Lung Research (DZL), Munich, Germany*
g. *Center for Thoracic Surgery Munich, Ludwig-Maximilians-University of Munich (LMU) and Asklepios Pulmonary Hospital, Marchioninistraße 15, 81377 Munich and Robert-Koch-Allee 2, 82131 Gauting, Germany*
h. *NanoVation Therapeutics Inc., 2405 Wesbrook Mall 4th Floor, Vancouver V6T 1Z3, Canada*
i. *Department of Chemistry, Biochemistry and Pharmacy, University Bern, Freiestrasse 3, Bern, Switzerland*

Author contributions:

C.M.Z. performed most of the experiments, evaluated the data and wrote the paper. N.BP.A. and A.N. performed the novel dual emission fluorescence spectroscopy measurments. D.L.P-G, X.W., N.K., M.G.S. and G.B. provided the knowledge and tissue material of hPCLS. D.B. helped performing the hPCLS experiments. C.M.Z and O.M.M. conceived the presented idea and planned the experiments. K.C., D.W., P.L. and O.M.M. supervised the work, provided conceptual guidance and corrected the manuscript.

The published article can be accessed online via:

https://doi.org/10.1016/j.jconrel.2022.09.021

Key words: lipid nanoparticles, LNP, Onpattro®, RNA therapeutics, siRNA delivery, spray drying, pulmonary delivery, respiratory diseases, human precision-cut lung slices, formulation screening

Graphical Abstract

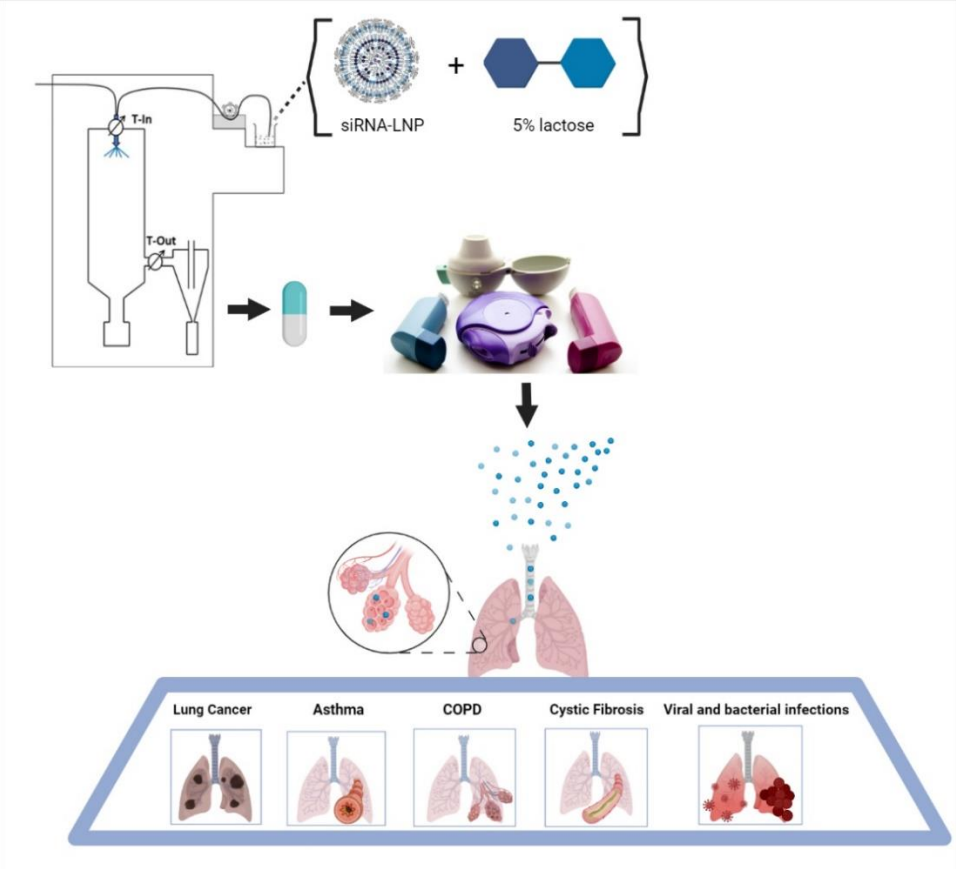

Abstract

While all the siRNA drugs on the market target the liver, the lungs offer a variety of currently undruggable targets which could potentially be treated with RNA therapeutics. Hence, local, pulmonary delivery of RNA nanoparticles could finally enable delivery beyond the liver. The administration of RNA drugs *via* dry powder inhalers offers many advantages related to physical, chemical and microbial stability of RNA and nanosuspensions. The present study was therefore designed to test the feasibility of engineering spray dried lipid nanoparticle (LNP) powders. Spray drying was performed using 5% lactose solution (m/V), and the targets were set to obtain nanoparticle sizes after redispersion of spray dried powders around 150 nm, a residual moisture level below 5%, and RNA loss below 15% at maintained RNA bioactivity. The LNPs consisted of an ionizable cationic lipid which is a sulfur-containing analog of DLin-MC3-DMA, a helper lipid, cholesterol, and PEG-DMG encapsulating siRNA. Prior to the spray drying, the latter process was simulated with a novel dual emission fluorescence spectroscopy method to preselect the highest possible drying temperature and excipient solution maintaining LNP integrity and stability. Through characterization of physicochemical and aerodynamic properties of the spray dried powders, administration criteria for delivery to the lower respiratory tract were fulfilled. Spray dried LNPs penetrated the lung mucus layer and maintained bioactivity for >90% protein downregulation with a confirmed safety profile in a lung adenocarcinoma cell line. Additionally, the spray dried LNPs successfully achieved up to 50% gene silencing of the house keeping gene GAPDH in *ex vivo* human precision-cut lung slices at without increasing cytokine levels. This study verifies the successful spray drying procedure of LNP-siRNA systems maintaining their integrity and mediating strong gene silencing efficiency on mRNA and protein levels both *in vitro* and *ex vivo*. The successful spray drying procedure of LNP-siRNA formulations in 5% lactose solution creates a novel siRNA-based therapy option to target respiratory diseases such as lung cancer, asthma, COPD, cystic fibrosis and viral infections.

1. Introduction

The lungs are the most vulnerable internal organ to infection and injury from the external environment because of its constant exposure to particles, chemicals, and infectious organisms in ambient air. Respiratory diseases impose an immense worldwide health burden. Altogether, >1 billion people suffer from either acute or chronic respiratory conditions. [316] Chronic respiratory diseases such as asthma, chronic obstructive pulmonary disorder (COPD), cystic fibrosis and lung cancer made up >545 million cases in 2017. Noteworthy, this number increased by almost 40% from 1990 to 2017. [317] Since the start of the Covid-19 pandemic in 2019, an increased number of pulmonary dysfunctions on top of all other pulmonary diseases was noted [318], followed by an inevitable increasing demand for novel pulmonary therapies being locally applied to the site of action. RNA therapeutics are promising for the treatment of respiratory diseases, and nucleic acid-based therapy have been studied for COPD or asthma therapies. [189, 319-321] In comparison to conventional therapeutic approaches using proteins, peptides, small molecules or monoclonal antibodies, RNA therapeutics provide high selectivity, potency, and the possibility of personalized therapy. [322, 323] Small interfering RNA (siRNA) as one class of RNA therapeutics inhibits gene expression to improve or cure disease symptoms, underlying pathologic mechanisms, and viral infections. [324] However, siRNAs are negatively charged macromolecules that do not bind to the cell surface and do not permeate through the cell membrane. Furthermore, challenges such as nuclease degradation, off-target gene silencing and immune-stimulating effects need to be addressed and resolved. [325] To overcome these limitations, siRNAs are encapsulated in a vast variety of materials including lipids, polymers, inorganic materials, proteins, and combinations of the above. Lipid-based carrier systems mimicking the composition of pulmonary surfactant, or the cell membrane enhance the ability to overcome the lungs' biological barriers and reduce toxicity and antigenicity. [326, 327]

One of the biggest breakthroughs of siRNA therapeutics was the approval of the first siRNA-LNP drug, Onpattro® (Patisiran) by the FDA (Food and Drug Association, USA) and EMA (European Medicines Agency). Onpattro® consists of lipid nanoparticles (LNPs) encapsulating siRNA in its lipid matrix to treat hereditary amyloidogenic transthyretin (TTR) amyloidosis. [29, 313] The target is the liver after intravenous administration. Recently, LNP technology has also enabled the rapid development and approval of mRNA-based vaccines against COVID-19. [328] These types of LNPs consist of phospholipids, cholesterol, polyethylene glycol-conjugated lipids, and ionizable helper lipids. Ionizable helper lipids bind to anionic RNA to enable efficient encapsulation and promote endosomal escape following internalization into the target cell. [329] The major advantage of LNP technology is its adaptability to different siRNA payloads as its physicochemical properties remain similar. [330] Therefore, LNP formulations can potentially be pursued to deliver therapeutic cargoes *via* different administrative routes for the treatment of a large variety of diseases.

The lungs are one of the most complex organs and offer advantages of local, over systemic, delivery such as noninvasive access and a large alveolar surface area. [331] Furthermore, the administered dose can be reduced for local effects compared to systemic delivery, resulting in decreased side effects. Regarding RNA delivery to the lungs, the absence of serum proteins on the air-side keeps the nuclease activity relatively low. [181] Therefore, drugs can most effectively be delivered by inhalation and are immediately available to the lungs. [200, 332] In order to deliver drugs or nanoparticles to the lungs, incorporation into microparticles with aerodynamic diameters between 1 and 5 μm are required. The matrices of these particles need to consist of excipients, such as FDA-approved lactose or mannitol, which readily dissolve upon contact with the lung fluid to release their cargo. [333-335] During the spray drying process, two main stress factors applied to the product are heat and shear forces which may tear the nanoparticle structure and result in degradation of the cargo. To avoid a negative impact on the quality of nanoparticles, appropriate sugar excipients need to be selected and the process parameters

need to be optimized. Another important aspect that needs to be considered is the restricted outlet temperature range for thermolabile drugs. [336] siRNAs are prone to degrade at about 90 °C, and Onpattro-like LNPs have shown phase transition temperatures of 38 °C with a gradual phase transition. [337] Furthermore, during the development of novel dosage forms for lung administration, lung deposition, retention, dissolution, metabolism and toxicity of spray dried microparticles need to be tested. [338]

The aim of this study was to transfer LNP formulations based on an updated Onpattro® composition but consisting of a neutral, positively or negatively charged helper lipid (nLNP, (+)LNP and (-)LNP) into a successful spray dried powder at maintained physicochemical properties and siRNA integrity for pulmonary application. The target range was set to obtain sizes after redispersion of around 150 nm, a residual moisture level below 5%, and RNA loss below 15% at maintained RNA bioactivity. A novel dual emission fluorescence spectroscopy method was used to simulate the stability of LNPs in different excipient solutions (PBS, lactose, mannitol and trehalose) at different temperatures. This prescreening to find the best combination of LNPs, excipients and temperatures for the spray drying process, supersedes the necessity for a trial-and-error approach. Quantification of siRNA and lipid concentration of LNPs after redispersion of spray dried powders underlines a quality criterion which should always be carried out to avoid performance loss or increased material costs. The particles' performance and siRNA integrity were tested *in vitro* in lung cancer cells expressing enhanced green fluorescent protein (eGFP), and *ex vivo* in human precision-cut lung slices (hPCLS) targeting the house keeping gene GAPDH. The findings of this study provide unique insights into the possibility of spray drying siRNA embedded LNPs and maintaining their bioactivity while keeping optimal properties for pulmonary delivery.

2. Materials & Methods

2.1 Materials

Dicer substrate double-stranded siRNA targeting green fluorescent protein (DsiRNA EGFP, 25/27) (siGFP), dicer substrate double-stranded siRNA targeting the house-keeping gene GAPDH (DsiRNA GAPDH) (siGAPDH) and scrambled, non-specific control (siNC) were purchased from IDT (Integrated DNA Technologies, Inc., Leuven, Belgium) (A3, Table S1). [237, 270, 302] Cholesterol, tris-EDTA buffer solution 100× (T9285), RPMI-1640 medium (R8758), fetal bovine serum (FBS) (F9665), penicillin-streptomycin (P/S) (P4333), G418 disulfate salt solution (G8168), Dulbecco's phosphate buffered saline (D-PBS) (D8537), isopropanol for molecular biology, methylthiazolyldiphenyl-tetrazoliumbromid (MTT), D-mannitol, HEPES buffer 1 M, Triton X- 100, MISSION® siRNA fluorescent universal negative control #1, cyanine 4 (SIC005) and cholesterol quantitation kit were purchased from Sigma-Aldrich, a subsidiary of Merck KGaA (Darmstadt, Germany). PEG-DMG, DSPC, DSPG and DOTAP were bought from Avanti Polar Lipids, Alabaster, USA. The ionizable cationic lipid is a sulfur-containing analog of DLin-MC3-DMA (pKa 6.3–6.6) defined by the structure shown in Figure S1 (A3). [339] InhaLac®230, lactose monohydrate for dry powder inhalers, was purchased from Meggle Group (Wasserburg, Germany). Quant-it™ RiboGreen DNA reagent, chloroform as molecular biology reagent, black and white 96-well plates (10307451), TRIzol reagent, Power SYBR™ green PCR master mix and Aquastar® water standard oven 1% were bought from Thermo Fisher Scientific (Schwerte, Germany). Pumpsil® tubings were bought from Watson-Marlow GmbH (Rommerskirchen, Germany) and had an inner diameter and a thickness of 1.6 mm. Lysing matrix D 2.0 mL tubes and D(+)-trehalose were purchased from VWR International GmbH (Ismaning, Germany). White 96 well PCR plate and 0.2 mL PCR tubes were purchased from Biozym Scientific GmbH (Hessisch Oldendorf, Germany). AL-crucibles at 40 µL (ME-26763) for DSC measurements were bought from Mettler Toledo (Fürstenfeldbruck, Germany). High sensitivity capillaries (PR-C006) produced by NanoTemper Technologies GmbH were used for all formulation screening measurements.

2.2 Preparation of lipid nanoparticles (LNPs) entrapping siRNA

LNP-siRNA formulations had a lipid composition based on the clinically approved Onpattro® formulation and were prepared as previously described [29, 297, 313]. Briefly, lipid components (ionizable cationic lipid, helper lipid, cholesterol, and PEG-DMG) at molar ratios of 50:10:38.5:1.5 mol% were dissolved in ethanol to a concentration of 10 mM total lipid. Different helper lipids, *i.e.* 1,2-distearoyl-*sn*-glycero-3- phosphocholine (DSPC), 1,2-dioleoyl-3-trimethylammonium-propane (DOTAP), and 1,2-distearoyl-sn-glycero-3-phospho-(1′ -rac-glycerol) (DSPG), were used to enable formation of LNP-siRNA systems with near neutral [nLNP], positive [(+)LNP], and negative [(-)LNP] zeta potential, respectively. Purified siRNA (siNC, siGFP and siGAPDH) was dissolved in 25 mM sodium acetate pH 4 buffer to achieve an N/P ratio of 3, which is the charge ratio between the ionizable cationic head group on the lipid to the anionic phosphate in the RNA backbone. The two solutions were mixed through a T-junction mixer at a total flow rate of 20 mL/min, and a flow rate ratio of 3:1 *v*/v (aqueous:organic phase). The resulting LNP suspension was subsequently dialyzed overnight against PBS pH 7.4, sterile filtered (0.2 μm), and concentrated to 1.0 mg/mL siRNA.

2.3 siRNA loading of preformed LNPs for thermal stability measurements

10 nmol MISSION® siRNA Fluorescent Universal Negative Control #1, Cyanine 5 (Cy5-siRNA) was diluted to 1000 μg / μL in 10 mM HEPES buffer pH 7.4 and used as a stock in all experiments. To load preformed LNPs, Cy5-siRNA was diluted 1:10 in 25 mM sodium acetate buffer pH 4. Afterwards, 1.2 μL LNP, 0.7 μL 100 μg / mL Cy5-siRNA and 1.4 μL 25 mM sodium acetate buffer pH 4 were gently mixed and incubated at room temperature in the dark for 5 min. LNPs were then diluted in 97 μL final formulation buffer (PBS, 5% mannitol, 5% trehalose or 5% lactose) and incubated for additional 30 min at room temperature in the dark before being further analyzed.

2.4 Thermal stability of LNPs

A novel and highly sensitive method was used to characterize environmental changes experienced by Cy5-labelled siRNA within different LNPs in regards to their excipient buffer and temperature. The system used was a prototype instrument developed by NanoTemper Technologies GmbH to monitor a dedicated dual-emission optical system. Detection channels were used at LED excitation of 570 nm and emission detection with two filters simultaneously, one at 640 +/- 20 nm and one at 697 +/- 29 nm.

2.4.1 Fluorescence spectral detection of LNP spectral shift

Experiments were performed in a JASCO FP-8300 Fluorescence Spectrometer with a PCT-818 Peltier Temperature Controller controlled by the Spectra Manager 2.0 (JASCO Deutschland GmbH, Pfungstadt, Germany). For each sample, 100 μL LNP suspension was loaded into a quartz microcuvette and fluorescence spectra was recorded at an excitation wavelength of 590 ± 20 nm and the fluorescence emission was recorded at a wavelength between 620 and 725 nm, with a 10 nm bandgap, 1 nm step, 0.2 s integration time, using high sensitivity, with 4 accumulations per scan. The emission spectra were recorded as the temperature ramped from 20 °C to 90 °C, at a ramp rate of 2 °C / min, with scans taken every 10 °C.

2.4.2 Fluorescence based temperature stability scans

Thermal stability experiments were performed in coated high sensitivity capillaries (PR-C006) on a prototype instrument equipped with dual emission optics (NanoTemper Technologies GmbH, Munich, Germany). Each data point requires 10 μL of sample. For each ratiometric reading, the fluorescence was recorded simultaneously at 650 nm and 670 nm after excitation with an amber LED. For fluorescence stability experiments, data were recorded in a modified version of Pr. Control. The excitation power was set to 100% and scans were performed from 15 °C to 110 °C, with a 1 °C / min ramp rate. The

temperature stressing experiments were performed in a modified version of Pr.TimeControl, with the temperatures as indicated in the figures, and a temperature ramp rate of 7 °C / min.

2.5 Spray drying of LNPs

For production of spray dried LNPs, a B-290 spray drying tower (Büchi Labortechnik, Flawil, Schweiz) was used. Pumpsil Tubing 1.6 mm × 1.6 mm (Watson Marlow Tubing, Falmouth, UK) with a pump rate of 1.4 mL/min was chosen. Nitrogen functioned as atomizing gas, whereas drying gas was air. In order to avoid dust and other airborne particles, both nitrogen gas and air were filtered through a 0.2 µm PTFE membrane pore. Pressurized air was used to ensure sufficient heating of the air supply and to avoid overheating of the Büchi's vacuum pump. The aspirator was set to 70% and vacuum ranged from - 40 mbar to - 35 mbar. The airflow was set to 40 mm corresponding to 473 NL/h. The inlet-temperatures (T-In) were set to 100 °C and 120 °C resulting in measured outlet-temperatures (T-Out) of accordingly 62 °C and 72 °C ± 2 °C, respectively. Each individual stock solution of LNP-siRNA formulations was diluted to a concentration of 30 µg siRNA in 5000 µL of a specified solvent (highly purified water (HPW) with lactose (InhaLac) at 5% *w*/*V*, sterile filtered). This resulted in an siRNA to sugar concentration of 0.12 µg siRNA/mg lactose.

2.6 Loss detection after spray drying of LNPs

2.6.1 siRNA quantification

The Quant-IT™ Ribogreen assay was adapted as described in Walsh et al. [340] Briefly, LNPs were either freshly prepared or redispersed as described above. For each reading, 50 µL of samples was transferred in a black 96-well plate and filled to 100 µL with 2% Triton X-100 solution. A siRNA standard curve was pipetted at 25.0, 10.0, 5.0 and 2.5 µL of a stock solution (20 µg/mL) resulting in final concentration of 2.5, 1.0, 0.5 and 0.25 µg/mL, respectively. The plate was incubated at 37 °C for 30 min in a shaking incubator. Upon the addition of the Ribogreen reagent at a 1:100 dilution, the fluorescence intensities were measured at an excitation wavelength of 480 nm and an emission wavelength of 525 nm. The siRNA loss was quantified by normalizing the siRNA amount of spray dried samples to the siRNA amount of fresh LNP samples.

2.6.2 Cholesterol quantification

The cholesterol quantification method was performed following the Cholesterol Quantitation Kit product information sheet (Sigma-Aldrich). To construct the standard curve, 20 µL of a 2 µg/µL cholesterol standard solution was diluted with 140 µL of the cholesterol assay buffer resulting in a 0.25 µg/µL stock solution. Amounts of 0, 4, 8, 12, 16 and 20 µL were pipetted into a clear 96 well plate, and each well was replenished to 50 µL by addition of cholesterol assay buffer. To measure the cholesterol content of the test samples, 50 µL per sample were transferred into the well plate. Since the cholesterol amount was unknown, each individual sample was diluted several times and replenished to 50 µL with cholesterol assay buffer. Subsequently, the Reaction Mix at 50 µL/well was prepared and added to each well. The plate was protected from light and placed in a shaking incubator for 60 min at 37 °C. The cholesterol concentration was determined by measuring the absorbance at 570 nm.

2.7 Hydrodynamic diameter and zeta (ζ) potential measurements of LNPs

Hydrodynamic diameters and polydispersity indices (PDI) were measured in disposable cuvettes (Brand GmbH, Wertheim, Germany) using the Zetasizer Nano ZS instrument (Malvern Instruments Inc., Malvern, U.K.). To measure the size and PDI of spray dried formulations after redispersal, approximately 8.33 mg of spray dried LNP powder was dissolved in 100 µL HPW. This equates to 1 µg of siRNA (10 µg siRNA/ mL). For comparison, fresh LNPs (c = 1 mg/mL) were diluted in 5% lactose to reach a concentration of 10 µg siRNA/mL. All samples were detected at a backscatter angle of 173°. Results are presented as average size (nm) ± SD. Zeta potentials were measured by Laser Doppler

Anemometry (LDA) using a Zeta Cell (Zetasizer Nano series, Malvern, UK) containing a 6.5× dilution of the same 100 µL sample of LNP suspension. For each LNP formulation, measurements were presented as an average charge (mV) ± SD.

2.8 Residual water content – Karl Fischer titration

The residual water content for spray dried LNPs in 5% lactose (*w*/*V*) was determined by weighing 10 mg powder of each LNP sample into 2R vials. A 1% water standard was equally prepared with approximately 40–50 mg powder. Empty vials served as blank values. For coulometric measurements, an Aqua 40.00 Karl Fischer Autosampler-Titrator with corresponding software from Analytik Jena AG (Jena, Germany) was used. The oven was heated to 100 °C, and the final drift was set to <10.0 µg/min. Blank measurements were run and automatically subtracted from the standards and samples. Residual moisture measurements were considered valid if the 1% water standard measurement resulted in a value between 0.9 and 1.1%. Results are presented as mean residual moisture (%) ± SD.

2.9 Differential scanning calorimetry (DSC)

For calorimetric measurements 5 to 10 mg of spray dried LNPs were weighed into AL-crucibles at 40 µL volume and closed. The reference was an empty crucible. The reference and samples were inserted into the oven at a set point of 25 °C. Measurements were taken with a DSC 214 Polyma (Erich NETZSCH GmbH & Co. Holding KG, Selb, Germany) starting from 0 °C with a ramp of 8 °C/min until temperature reached 200 °C for all spray dried LNP formulations in 5% lactose (*w*/*V*) and spray dried 5% lactose (w/V). Data was analyzed using the Proteus Analysis software.

2.10 Scanning electron microscopy (SEM)

Scanning electron microscopy (SEM) is used to determine the geometric diameter and morphology of spray dried powders. A small amount of spray dried LNPs was placed on top of a stub covered with double-sided carbon tape. The stub was then coated with carbon under vacuum for 40 s. The microparticles were examined imaged using a FEI Helios G3 UC (Thermo Fisher Scientific, Schwerte, Germany).

2.11 Aerodynamic properties of spray dried LNPs

For the analysis of the aerodynamic properties of spray dried powders, procedures specified in the monograph 2.9.18, apparatus E, of the European Pharmacopoeia was performed using a next generation impactor (NGI) from Copley Scientific (Nottingham, UK). The measurement procedure was adapted as previously described. [189] Spray dried LNP powder was transferred into 2–3 hydroxypropylmethylcellulose capsules. Each capsule was loaded into a Handihaler® (Boehringer Ingelheim Pharma GmbH & Co. KG, Ingelheim, Germany) and hole-punched. Every capsule was discharged twice with a 5 s interval between the two actuations. Following the application of the Handihaler®, the same procedure as in 2.6.1. was performed. Every stage of the NGI was washed with 2% Triton-X buffer. The induction port (IP) was washed with 5 mL and the pre-separator (PS) was pre-filled with 15 mL 2% Triton-X buffer. The small cups were filled with 2 mL 2% Triton-X buffer, whereas the greater cups were filled with 4 mL 2% Triton-X buffer solution. All parts were cautiously shaken and placed on a horizontal shaker for 20 min. A standard curve of fresh siRNA was prepared and topped up to 100 µL with 2% Triton-X buffer. As a control, fresh LNPs, at siRNA concentration of 10 µg/mL, similar to the redispersed samples, were prepared in 2% Triton-X buffer. Three aliquots of 100 µL from each stage were used for further analysis. All samples were pipetted to a black 96-well plate and put into a shaking incubator for 60 min at 37 °C. Upon the addition of Ribogreen reagent at a 1:100 dilution, the fluorescence intensities were measured at an excitation wavelength of 480 nm and an emission wavelength of 525 nm. The mass median aerodynamic diameter (MMAD), geometric standard deviation (GSD), fine particle dose (FPD), fine particle fraction (FPF) and powder recovery

(%) were calculated as described in the European Pharmacopoeia considering fine particles at sizes below 5 μm MMAD.

2.12 Mucus penetration assay of spray dried LNPs

The mucus penetration of fresh *versus* spray dried LNPs was adapted from Casciaro et al. [341] Briefly, 75 μL of artificial mucus was transferred onto 8 μm pore polycarbonate membrane Transwell® inserts submerged in 300 μL of acceptor medium in a 24-well plate. Afterwards, 5 mg of spray dried LNPs was redispersed in HPW (0.6 μg siRNA / 100 μL) and labelled with 1 μL 1,1-dioctadecyl-3,3,3,3-tetramethylindodicarbocyanine solution (DiD) solution, acting as a fluorescence lipid marker. The same procedure was performed to assess diffusion of fresh LNPs at the same concentration. Hence, 100 μL of samples was deposited on artificial mucus. Non-deposited samples were stored for 24 h under light exclusion for further fluorimetric analysis as a comparable value. Simulated interstitial lung fluid (SILF) was used as acceptor media for mucus diffusion experiments and placed on the bottom of the well, respectively. SILF was carefully prepared according to the instructions provided by Moss et al. [342] At scheduled time intervals (0.5, 1, 2, 4 and 24 h), the acceptor medium was collected, pipetted to a 96 well plate and quantified by spectrofluorimetric analysis at excitation wavelength of 520 nm and an emission wavelength of 635 nm. Values were calculated by normalizing each mucus deposited sample value to the non-deposited and stored DiD-LNPs. The results are reported as percentage (%) of total LNPs permeated over time.

2.13 *In vitro* characterization of spray dried LNPs in a lung cell line

2.13.1 Cell culture

The human non-small cell lung carcinoma cell line H1299 (ATCC CRL-5803) stably expressing enhanced green fluorescence protein (eGFP) was cultured in RPMI 1640 medium supplemented with 10% FBS, 1% P/S and 0.4% G418. Cells were passaged every 3 days with 0.05% *v*/v trypsin and subcultured in 75 cm2 flasks. H1299-GFP cells were kept in a humidified atmosphere at 37 °C with 5% CO2.

2.13.2 *In vitro* GFP protein downregulation

To evaluate the *in vitro* gene silencing efficiency, H1299-GFP cells were seeded in a 24-well plate at a density of 2.5 × 104 cells per well in 500 μL medium at 37 °C and 5% CO2. Fresh LNPs of different helper lipids were prepared at concentrations of 1 μg/mL and 10 μg/mL in 5% lactose (*w*/*V*). Comparably, 0.833 mg and 8.333 mg of spray dried LNPs encapsulating siNC or siGFP, were resuspended in 100 μL HPW resulting in equal concentrations as aforementioned. The day after, 100 μL of each sample was added to 400 μL of fresh culture medium and incubated for 24 h at 37 °C and 5% CO2. The medium was then discarded and replaced with 500 μL of fresh medium, and the plates were further incubated for another 24 h. At the end of the incubation time, cells were washed with PBS, trypsinized and collected. After centrifugation at 400 rcf for 5 min, the supernatant was discarded and the cell pellet was washed two times in PBS before being resuspended in PBS with 2 mM EDTA. Samples were analyzed by flow cytometry (Attune® NxT, Thermo Fischer Scientific, Waltham, Massachusetts, USA), and the median fluorescence intensity (MFI) of GFP protein expression was measured by using a 488 nm excitation laser and the emitted light passing through a 530/30 nm band pass emission filter set (BL-1H) was detected. All LNPs samples were gated by morphology for a minimum of 10,000 viable cells. Results are displayed as mean MFI values (%) ± SD.

2.13.3 *In vitro* cytotoxicity of spray dried LNPs

Cell viability after transfection with spray dried LNPs (neutral, positive and negative LNPs) was tested *via* an MTT Assay as described previously. [258, 259] Shortly, 5000 H1299-GFP cells per well were seeded in 100 μL medium onto a transparent 96-well plate (BioLite 96 well multidish, Thermo Fisher

Scientific, Rochester, New York, USA). The samples were prepared by redispersing 0.833 mg (1 µg siRNA) and 8.33 mg (10 µg siRNA) of spray dried powders in 100 µL of HPW. After 24 h, 90 µL of prewarmed medium was added to each well and supplemented with 10 µL of sample, respectively. Thus, siRNA concentrations of 1.0 and 10.0 µg/mL were added for each LNP sample. The plate was incubated for 24 h at 37 °C and 5% CO2. As a full viability control, cells were incubated in 100 µL of liquid consisting of 10 µL sterile 5% lactose solution (m/V) and 90 µL medium. After 24 h, the media was aspirated and 200 µL of MTT containing medium (0.5 mg/mL in serum-free RPMI- 1640 medium) was added to each well. Cells were incubated for another 3 h at 37 °C and 5% CO2. Subsequently, the cell culture medium was completely removed, and insoluble purple formazan crystals, converted from water soluble MTT by metabolically active mitochondria, were dissolved in 200 µL DMSO. [260] The plate was set on a horizontal shaker for 20 min for all crystals to dissolve. The absorbance was measured at 570 nm, corrected with background values measured at 680 nm, using a microplate reader (TECAN Spark, TECAN, Maennedorf, Switzerland). The data are shown as mean ± SD as percentage of viable cells in comparison to untreated cells representing 100% viability.

2.14 *Ex vivo* gene silencing of spray dried LNPS in human precision-cut lung slices (hPCLS)

2.14.1 Human tissue, ethics statement and hPCLS

Human tissue was obtained from the CPC-M bioArchive at the Comprehensive Pneumology Center (CPC), from the University Hospital Großhadern of the Ludwig-Maximilian University (Munich, Germany) and from the Asklepios Biobank of Lung Diseases (Gauting Germany). Participants provided written informed consent to participate in this study, in accordance with approval by the local ethics committee of the Ludwig-Maximilians-Universit¨at Munich, Germany (Project 19–630). Precision-cut lung slices (PCLS) were prepared as described before. [343-345] Briefly, PCLS were prepared from tumor-free peri-tumor tissue. The lung tissue was inflated with 3% agarose solution and solidified at 4 °C. Afterwards, 500 µm-thick slices were cut from tissue blocks using a vibration microtome (HyraxV50) (Karl Zeiss AG, Oberkochen, Germany). PCLS were cultured in DMEM F-12 medium supplemented with 0.1% FBS. Prior to the experiments, PCLS were cut by means of a biopsy puncher into 4 mm-diameter PCLS punches.

2.14.2 LNP transfection, nucleic acid extraction and qPCR

For the gene silencing of hPCLS cells, LNPs loaded with siGAPDH and siGFP were spray dried in 5% lactose. The spray dried powder was redispersed to reach a concentration of 10 µg siRNA/mL. 100 µL of each sample was added to a well consisting of three PCLS punches in 500 µL medium, respectively. The plate was incubated for 24 h at 37 °C and 5% CO2. Once the incubation time was completed, the RNA extraction was performed by homogenizing the hPCLS punches in 1 mL TRIzol using a Fast Prep 24 Tissue Lyzer (M.P. Biomedicals, Irvine, California, USA). The samples were incubated for 5 min at room temperature. Subsequently, 0.2 mL of chloroform was added, and each tube was vigorously mixed, followed by another incubation at room temperature for 3 min. Afterwards, samples were centrifuged at 11000 rcf for 15 min at 4 °C. The aqueous phase containing RNA was transferred into a new tube. Next, 500 µL of isopropanol was added and incubated for 10 min at room temperature before another centrifugation at 11000 rcf for 10 min at 4 °C was run. The supernatant was discarded, and the pellet was washed with 1 mL of ice-cold 75% ethanol followed by centrifugation at 7500 rcf for 5 min at 4 °C. The supernatant was discarded and the RNA pellet was resuspended in 30 µL of RNase free water. The RNA concentration and purity were quantified by RT-qPCR. In brief, cDNA was synthesized from total RNA using high-capacity cDNA synthesis kit (Applied Biosystems, Waltham, Massachusetts, USA). The obtained cDNA was then diluted 1:10, and a qPCR was performed using the SYBR™ Green PCR Master Mix (Thermo Fischer Scientific, Waltham, Massachusetts, USA) with primers for human GAPDH and β-actin (Qiagen, Hilden, Germany) for normalization. Cycle thresholds were acquired by auto setting within qPCRsoft software (Analytik Jena AG, Jena, Germany). Three individual batches of

spray dried LNPs (siGAPDH and siGFP) were tested on three individual donor hPCLS samples. The GAPDH silencing results are reported in the mean percentages (%) normalized to siGFP values ± SEM.

2.14.3 Cytokine secretion from hPCLS

To assess the toxicity of the spray dried LNPs toward human lung tissue, the levels of 12 pro-inflammatory cytokines in the supernatant of the treated hPCLS was determined using the human LEGENDplex Inflammation Panel 1 kit (BioLegend, San Diego, USA) according to the manufacturer's protocol. Briefly, 25 µL samples of supernatant were diluted with the supplied assay buffer and incubated with the supplied beads for 2 h. After washing the beads, they were incubated for 1 h with the detection antibodies, and the fluorophore was added. After further incubation, the beads were washed and diluted in PBS/EDTA buffer for analysis on an Attune® NxT flow cytometer. Cytokine levels were determined relative to a standard curve obtained with a standard supplied by the manufacturer.

2.15 Statistics, data analysis and presentation

All experiments were run in independent triplicates. Experimental data was analyzed for statistical significance using the One Way or Two Way ANOVA repeated measurements on the GraphPad Prism 5 software with either Bonferroni or Dunnetts post-hoc test with $p > 0.05$ considered not significant (ns), * $p < 0.05$, ** $p < 0.01$, *** $p < 0.001$. Data analysis was performed using Python (3.8.8) using the ipython (v7.29.0), matplotlib (v3.5.0), numpy (v 1.20.3), seaborn (v 0.11.2) and GraphPad Prism 5 data science packages. Analysis routines and algorithms were specifically written to analyze dual emission fluorescence traces.

3. Results and Discussion

3.1 LNP stability using dual emission fluorescence spectroscopy

Lipid based nanoparticles are most commonly spray dried at comparably low temperatures because the lipid component acts as a limiting factor showing phase transition temperatures at about 55 °C for the used helper lipids. [346] In comparison, when spray drying polymer-based nanoparticles, the polymers can resist much higher temperatures having melting points over 100 °C. In this case, the cargo might face degradation or melting before the polymer does. [189] Therefore, spray drying lipids requires a maximum temperature which does not melt the lipid layers while still reducing the moisture levels to a sufficient level in the produced powders, as this is important for avoiding agglomeration and microbial growth. However, the residual moisture level depends on the excipient used and the temperature applied. It has been shown that spray dried powders based on crystalline excipients such as mannitol can be obtained with very low residual moisture level below 0.5%. In comparison, amorphous sugars such as lactose and trehalose ensue higher residual moisture levels of 3–5% after spray drying. [347-349] Here, we used a new dual-emission epifluorescence setup to screen all LNP formulations at different temperatures and in different excipient solutions to avoid a trial-and-error approach of selecting spray drying temperatures and finding suitable excipient solutions (A3, Figure S2). The fluorescence-based stability measurements were found to be highly sensitive when characterizing environmental changes experienced by fluorophore-labelled siRNA within LNP formulations. Since the Cyanine 5 (Cy5) dye is very sensitive to environmental changes, its fluorescence emission is red shifted with a 6 nm peak shift from 660 to 666 nm upon encapsulation within a lipid nanoparticle (LNP) (A3, Figures S3-S5). Instead of measuring the full emission spectrum, the fluorescence is recorded simultaneously only at two pre-selected wavelengths, 670 nm and 650 nm, with photon-multiplier-tubes (PMTs), which greatly enhance sensitivity. The small hypsochromic (blue-) or bathochromic (red-) shifts of the emission peak of the fluorescent dye are translated into large changes in the 670 / 650 nm ratio (A3, Figure S6). These changes are then monitored as a function of temperature, either online, or after temperature stressing. Therefore, we expected to obtain information through fluorescence emission about the LNPs' stability related to temperature applied and excipient used. All LNP samples were produced encapsulating Cy5-

siRNA and monitored for a change in fluorescence ratio while heating the samples from 15 °C to 110 °C. LNPs were prepared in either a control PBS buffer, or in 5% mannitol, 5% trehalose and 5% lactose solution (m/V) (A3, Figure S7). The behavior of the LNPs when subjected to a melting curve is more difficult to interpret than a standard nanoDSF analysis of protein melting. Proteins have sharp melting curves where the maximum of the first derivative of the melting curve can provide a Tm of melting. LNPs, where the lipids and cholesterols have wider glass transitions as opposed to defined transition temperatures, as points of denaturing, lead to less defined curves. [337] While melting events are somewhat visible in PBS, in the sugar solutions the melting events occur over a much larger temperature range. The first derivatives of each curve were analyzed and plotted in Figure S8 (A3). The inflection temperatures (*T*i) do not accurately represent the stability of the LNPs, as visual inspection of the data shows that the nLNPs in 5% trehalose are likely to be more stable than an inflection of approx. 20 °C indicates. Visually, it appears that LNPs in 5% lactose and 5% mannitol seem to be more stable than in PBS or 5% trehalose. An alternative approach to observe LNP behavior was sought, which would also align with spray drying methods. Here, LNPs were subjected to four temperatures (41 °C, 51 °C, 62 °C, 72 °C) mimicking the elevated outlet temperatures in a spray dryer, and then returned to the original temperature (A3, Figure S9A). As the LNPs are heated, the ratio, and therefore the environment experienced by the Cy5-siRNA irreversibly changes. This change is quantified by the difference between the initial ratio (*Ri*) and final ratio (*R*I) measurements, determined using the simple equation $\Delta R = Ri - Rf$ (A3, Figure S10B). The change in Δ*R* was determined for each LNP formulation, at each temperature and in each excipient solution as summarized in Fig. 1. Looking at the ΔR alone, (+)LNPs appear to be the most stable LNP in every dispersant measured. (-)LNPs are the least stable. An issue that arose was that in some cases of LNP and dispersant combination, the ratio value for the LNP was not greatly different from the Cy5-siRNA in solution (A3, Figure S10B) – suggesting that the buffer changes lead to a different conformation of the LNP during formation. Furthermore, (-)LNPs encapsulating negatively charged siRNA might experience repulsion effects, thus leading them to be less stable than (+)LNPs. To provide a more holistic view, ΔR was plotted against initial ratio and the marker sizes used to indicate the temperature stress (Figure 2). The plots allow us to visualize a region of stability in the upper left-hand corner of each plot, with larger shifts in initial ratio and lower Δ*R* at increasing stress temperature easily observed for LNPs in 5% mannitol and 5% lactose, while PBS and 5% trehalose show higher Δ*R* values trending higher as the stress temperatures increases and lower initial ratios. Moreover, applying a temperature of up to 72 °C seemed not to have an influence of the LNPs stability in 5% lactose and 5% mannitol solutions (m/V). In the previous studies by Freitas and Müller, solid lipid nanoparticles were successfully spray dried at outlet temperatures of 50–60 °C using mannitol, trehalose or lactose as the excipient solution. However, the particles were not carrying any cargo, and no *in vitro* or *in vivo* work was performed. [350] Of the different excipient solutions tested, 5% mannitol and 5% lactose solutions were most effective at stabilizing the LNPs at the temperatures tested. Comparing these two excipient solutions more closely, the 5% lactose solution stabilized the different LNPs more efficiently at chosen temperatures. Furthermore, the Δ ratio within each LNP formulation remained lower than in the LNPs prepared in 5% mannitol solution. Hence, it seems favorable to use 5% lactose as an ideal excipient solution for spray drying of LNP formulations. In regards to the LNP carriers, the thermal stressing of LNPs up to 72 °C did not lead to any reduction of stability. RNA stability was not assessed, however. In conclusion, the highest possible temperatures, 62 °C and 72 °C, were selected for spray dry all LNP formulations in 5% lactose solution (m/V).

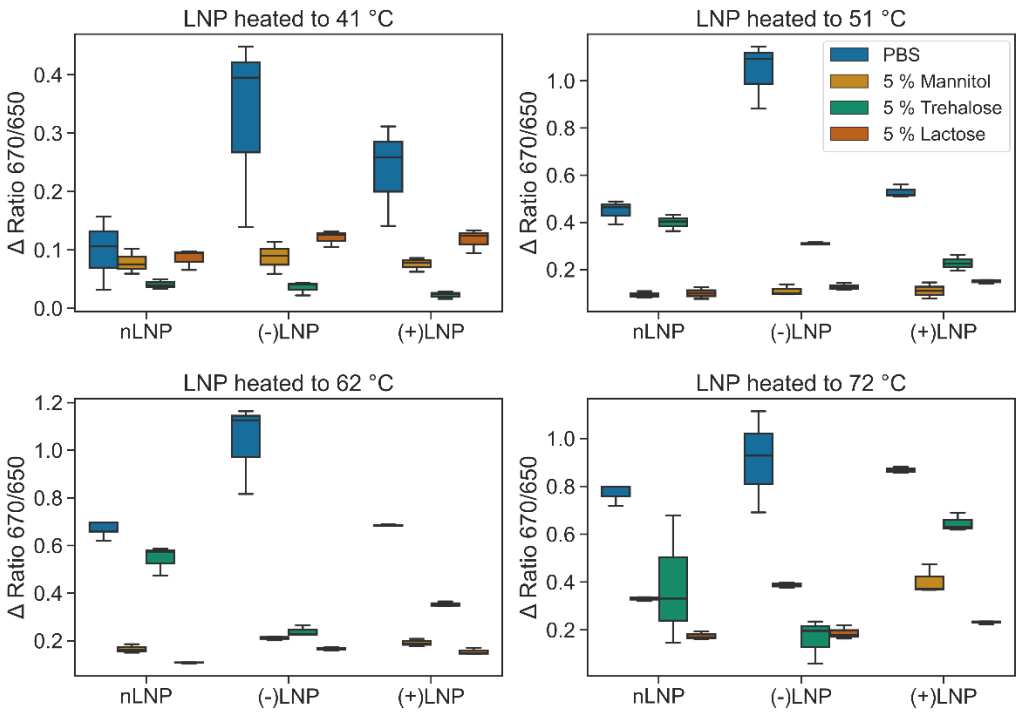

Figure 1 Box plots of the Δ R values observed by each LNP in different buffers (as indicated by colored legends) and hold temperatures).

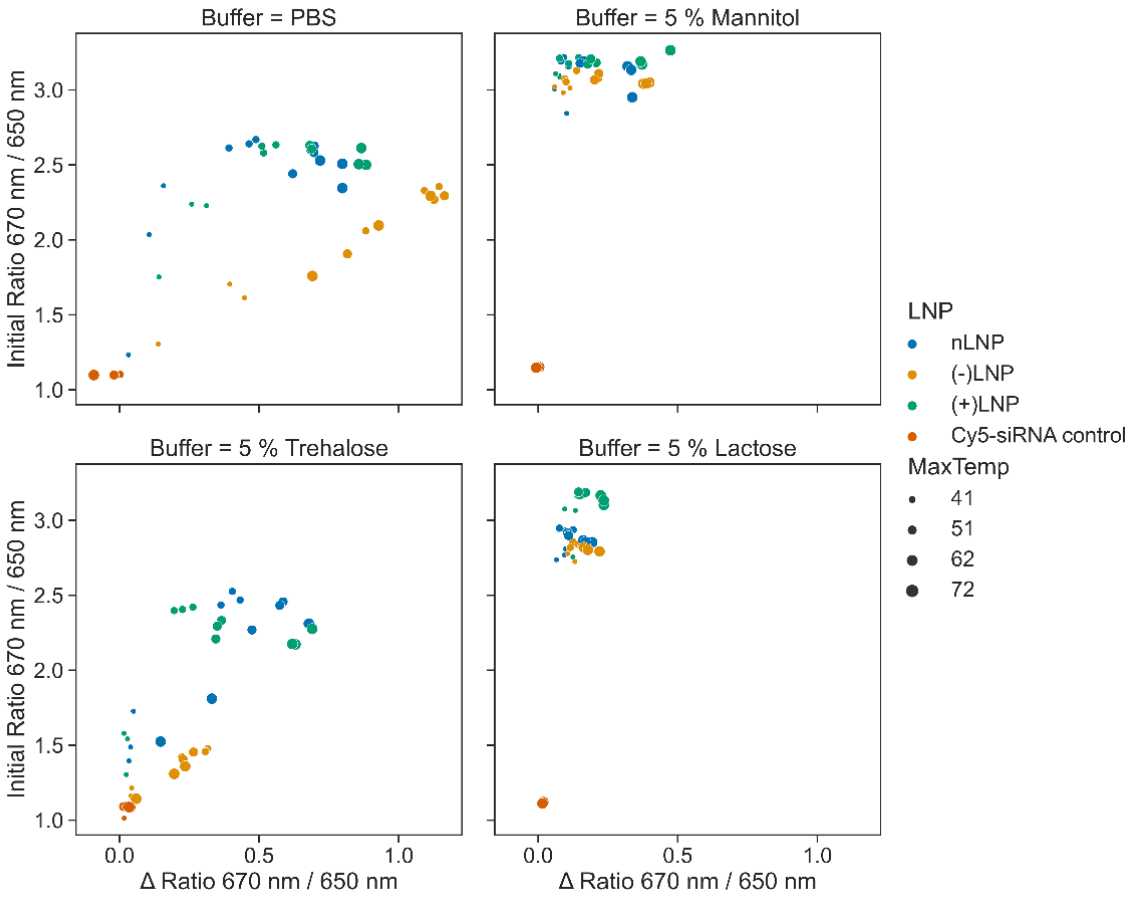

Figure 2 Stability plot shows stability of LNPs in each excipient buffer condition. The ΔR is plotted against initial ratio in each buffer condition, with the color indicating LNP and the size of marker stating the temperature the LNPs were stressed at. The top left quadrants represent the most stable environments.

3.2 Characterization of spray dried LNPs

3.2.1 Losses during spray drying

Spray drying of LNPs was performed in a Büchi B-290 spray drying tower applying inlet temperatures of 100 °C and 120 °C resulting in outlet temperatures of 62 °C and 72 °C, respectively. In order to ascertain whether the spray drying process results in LNP- and subsequently siRNA losses, the respective amounts were measured before and after spray drying. When spray dried at 62 °C outlet temperature, none of the LNP formulation showed high siRNA or LNP losses of >30%. The siRNA losses were shown to be 7.5–14.0% (Figure 3A). The cholesterol detection assay resulted in 3.85–9.54% LNP losses (Figure 3B). There were no significant differences between the lipid and the siRNA losses observed between the three LNP formulations. However, even though the dual emission fluorescence-based stability measurements were performed at the outlet temperature of 72 °C (Tin = 120 °C), this temperature led during the spray drying process to visual destruction of LNP samples. Only a very low amount of powder was collected showing streaks in the collection vial indicating that the LNP formulation had started to melt. Analysis of the small amount of collected powder showed high cholesterol losses over 80% (Figure 3B**)**. Accordingly, the maximum temperature suitable for spray drying LNPs was set at an inlet temperature of 100 °C, resulting in an outlet temperature of 62 ± 2 °C.

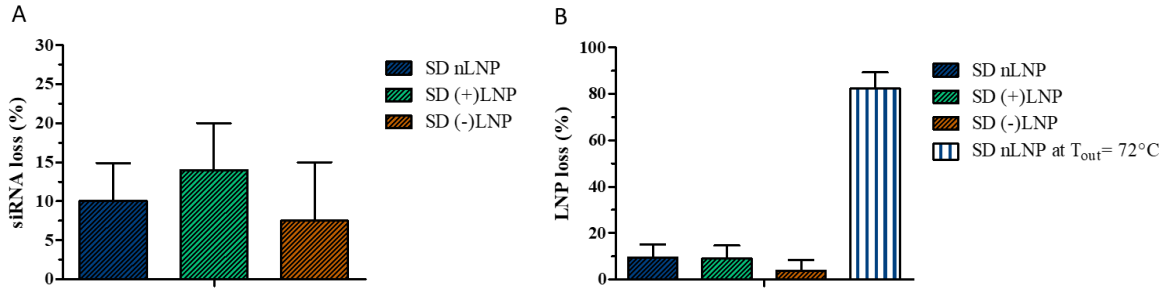

Figure 3 2 Quantification of the losses of A) siRNA and B) cholesterol after spray drying of LNPs in 5% lactose solution (m/V) at an outlet temperatures of 62°C. A nLNP loss at outlet temperature of 72°C is shown in B). Each bar shown as mean ± standard deviation, n=3. SD stands for spray dried.

3.2.2 Physicochemical properties of spray dried LNPs

Besides heat, spray drying exerts shear forces on LNP-siRNA systems and could melt, disassemble, destroy or merge LNPs. Therefore, DLS measurements were performed before and after spray drying to visualize any possible effects. Subsequently, spray dried microparticles, having the LNPs embedded, were dissolved in HPW for LNP redispersion to mimic impaction and matrix excipient dissolution in the lungs. As demonstrated in Figure 4, *Z*-average values of freshly LNPs prepared in 5% lactose (m/V) and redispersed LNPs from spray dried powders did not show any statistical differences. Also, differences in PDI were not observed except for redispersed nLNPs. Here, the PDI increased slightly by keeping the sizes similar to before spray drying. However, we recognized higher PDI values which may be explained to some extent by sugar monomers that change the size distribution of the particles. It was shown by Weinbuch et al. that monomers of sugar and sugar alcohol are detected by DLS in highly concentrated solutions. [351] Furthermore, by measuring the size of redispersed spray dried 5% lactose solution, without any LNP cargo, we detected particle structures at 200 nm size and a PDI of over 0.3. It is expected that the sugar matrix does not instantly dissolve. By diluting the obtained lactose solution further, the count rate dropped and no significant peaks were detected (data not shown). Furthermore, a PEG-DMG loss from the LNP formulation could potentially explain the increased PDI and zeta potential changes.

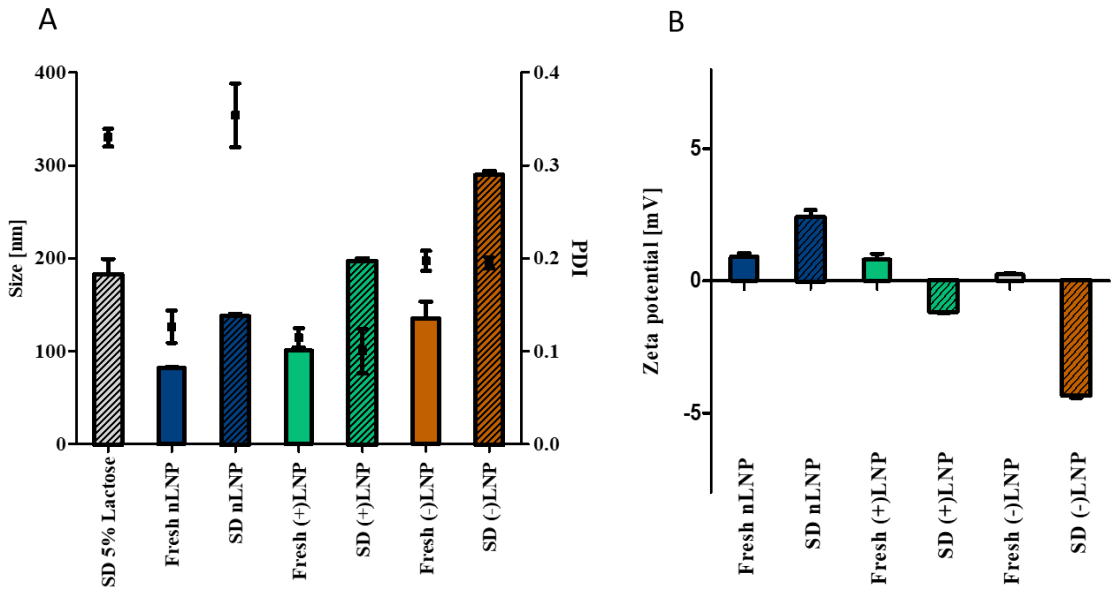

Figure 4 A) DLS measurements of freshly prepared (full colored bars) and redispersed (shaded colored bars) LNPs. PDI is indicated by black squares. LNP formulations with neutral, positive or negative charge and spray dried (SD) 5% lactose were redispersed in HPW after spray drying at 62°C outlet temperature and compared to freshly prepared LNPs in 5% lactose solution. B) Zeta potential measurements of fresh and spray dried LNPs in 5% lactose solution via LDA. Mean ± standard deviation, n=3.

In summary, LNP size and distribution were not affected by spray drying and remained comparable to the freshly prepared samples. The zeta potential of LNPs, on the other hand, is dictated by their helper lipid. Neutral DSPC, positively charged DOTAP and negatively charged DSPG were implemented into the LNP structure to facilitate different characteristics. However, by spray drying LNPs in 5% lactose solution (m/V), the zeta potential of positively and negatively charged LNPs was reduced. It was therefore investigated in the following experiments whether the decreased zeta potentials changed *in vitro* cellular uptake.

As seen in Table 1, the average amount collected for all LNP formulations was around 65% yield at a maximum of 250 mg spray dried powder. This is in line with the expectations from a Büchi B-290 spray dryer which is stated to achieve a yield of about 70% and is ranked at the upper end of collected yield in comparison to literature values. [352, 353] Another important parameter that needs to be tested is the residual moisture.

Table 1 Residual moisture recovered spray dried mass and yield of LNPs spray dried with 5% lactose (w/V) at an outlet temperature of 62°C.

Name	SD mass (mg)	SD yield (%)	Residual moisture (%)
SD 5% Lactose	192.06 ± 3.44	76.83 ± 1.37	4.90 ± 0.01
SD nLNP	160.89 ± 5.69	64.36 ± 2.28	4.01 ± 0.79
SD (+)LNP	164.15 ± 4.35	65.66 ± 1.74	4.12 ± 0.53
SD (-)LNP	164.69 ± 3.55	65.87 ± 1.42	3.56 ± 0.40

Spray dried powders should show low residual moisture levels in order to allow for storage stability. Although it was discussed above that residual moisture may act as a plasticizer stabilizing LNPs during

the spray drying process, it could nonetheless cause microparticle aggregation lead to microbial growth and RNase contamination. Therefore, the moisture content of all formulations was measured by Karl Fischer titration. The results show that for all LNP formulations, independent of the charge of the LNP and the drying temperature, the residual moisture levels were 3.5–4%. Interestingly, spray drying 5% lactose solution without any LNPs showed a slightly higher residual moisture level of 4.9%. However, the differences are not significant and are in line within previously reported literature values. [347]

Lactose often solidifies upon spray drying into an amorphous state. This was detected by DSC of spray dried 5% lactose solution in comparison to all other spray dried LNP formulations (Figure 5). In addition to the hygroscopic nature of lactose, the reason for the formation of amorphous structures is the fast drying step which does not provide sufficient time for lactose molecules to arrange into an ordered structure with subsequent crystal nucleation and growth. This explanation is supported by the molecule's crystallization temperature of around 110 °C and melting points ranging from 150 °C to 180 °C. [354] All of the lactose formulations showed glass transitions at temperatures between 47 °C and 56 °C corresponding to their residual moisture content (Table 1). [347, 355, 356] This temperature (Tg) is important for stability predictions during storage as amorphous solid forms are thermodynamically unstable and tend to crystallize if stored close to or above Tg. [357] The amorphous state of the formulation is favorable for LNP preservation. Therefore, when storing these products at 4 °C or room temperature for a longer period of time, high Tg values are necessary. The final Tg of a formulation, however, is closely linked to the water content: the higher the residual moisture the lower Tg. Also, with a lower residual moisture content degradation processes are less likely to occur. [358] It is therefore of interest to further decrease the amount of residual moisture in lactose formulations to avoid nucleation and degradation processes over time and in order to maintain the amorphous state of the formulation. (See Table 2.) When administration of spray dried powders application is envisioned *via* the pulmonary route, their morphology and particle sizes need to be examined. Aerodynamic sizes of 1–5 µm are considered ideal for inhalation because >50% of particles of an aerodynamic size of 3 µm deposit in the alveolar region.

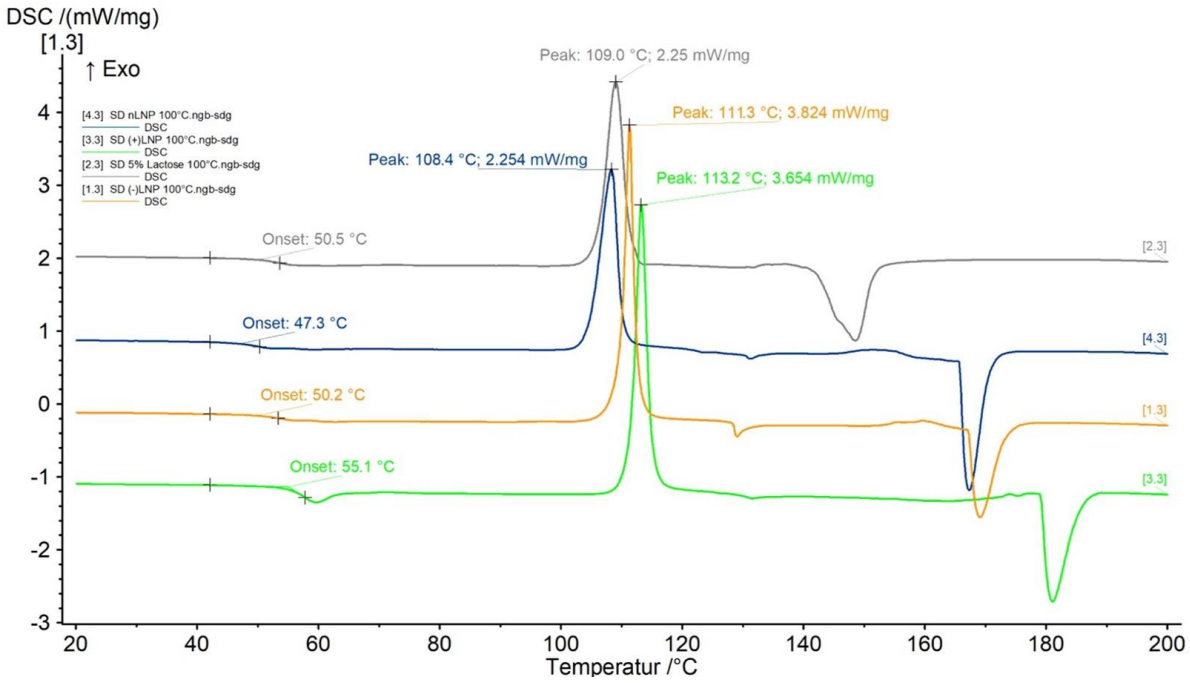

Figure 5 DSC measurements of lactose formulations spray dried at an outlet temperature of 62°C: 1.3) SD (-)LNP (brown), 2.3) SD 5% lactose (grey), 3.3) SD (+)LNP (green), 4.3) SD nLNP (blue).

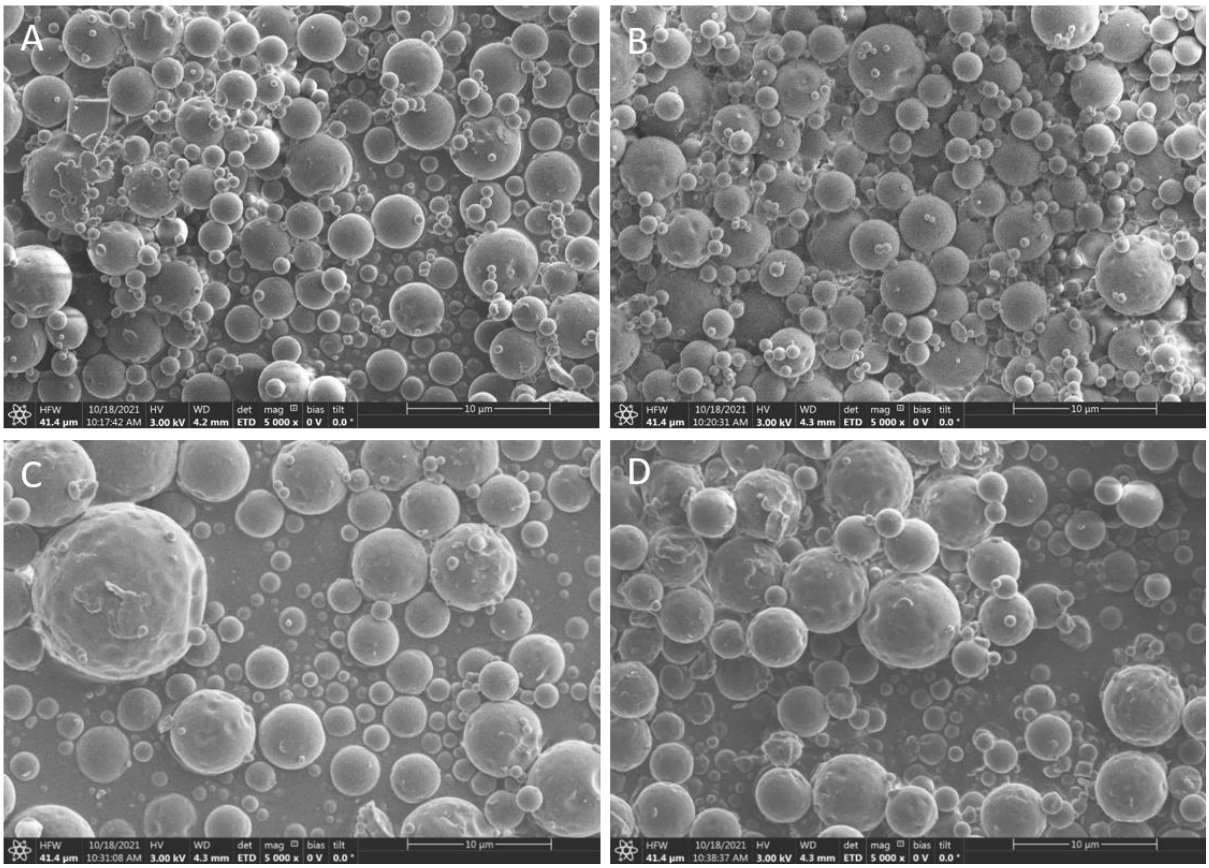

Figure 6 SEM pictures of spray dried A) 5% lactose solution, B) nLNP formulation, C) (+)LNP formulation and D) (-)LNP formulation. All samples were spray dried in 5% lactose solution at 62°C outlet temperature.

If the particle sizes are smaller than 3 µm, an 80% chance of reaching the lower airways and a 50–60% chance of deposition in the alveoli is given. [359-361] Therefore, the optimal aerodynamic size for deep lung deposition after pulmonary delivery is around 3 µm. For local effects, aerodynamic particles sizes around 5–7 µm can as well be acceptable. To determine whether the spray dried particles in this study fit these criteria, they were imaged using SEM. The geometric median diameters (GMD) which reveal the actual visual particle size. As seen in Fig. 6, spray drying of all LNP formulations with 5% lactose solution resulted in smooth round microparticles of sizes below 10 µm. In Figure 6A, spray dried 5% lactose, and 6B, spray dried nLNPs, showed a GMD size range from particles of 2–7 µm, whereas, (+) LNPs and (-)LNPs were slightly larger with 3–9 µm (Figures 6C and D). For porous materials, geometric sizes commonly exceed the aerodynamic diameter, which was therefore examined experimentally. [362] Furthermore, the residual moisture has a direct impact on the particles' size with higher water content resulting in more particle aggregation and bigger GMD values accordingly.

3.2.3 Aerodynamic performance of spray dried LNPs

The aerodynamic performance of each spray dried LNP formulation was measured using an NGI. The mass median aerodynamic diameters (MMAD) of all powders present sizes of 2.85–2.9 µm with standard deviations of 0.07–0.42 µm. These results position the spray dried LNP formulations at aerodynamic sizes of about 3 µm which was discussed as the optimal particle size range for lower respiratory delivery targeting a wide field of pulmonary diseases such as COPD, or respiratory viruses, *e. g.*, influenza or SARS-CoV-2. This is underlined by the fact that the geometric standard deviation (GSD) remains low at 2 µm. Reaching a fine particle fraction (FPF, defined as particles under 5 µm in diameter) of almost 30% is a very good value that is in line with the geometric diameter results obtained from SEM pictures. The FPF can be improved by reducing the residual moisture of spray dried LNPs to narrow down the size distribution, GSD, of spray dried powders and avoid particle agglomerates. This

can be achieved by drying the spray dried powder in a subsequent drying step at a lower inlet temperature to reduce the heat stress on the product. The temperature should not be increased since the spray drying temperature was already set to an upper threshold value keeping the LNPs integrity.

Table 2 Microparticle characteristics of spray dried LNP formulations in 5% lactose solution at an outlet temperature of 62 °C using a Next Generation Impactor (NGI). DD: dose delivered, FPD: fine particle dose, FPF: fine particle fraction, MMAD: mass median aerodynamic diameter, GSD: geometric standard deviation.

	nLNP	(+)LNP	(-)LNP
DD (µg)	2.37 ± 0.85	2.62 ± 0.31	2.66 ± 0.70
FPD (µg)	0.70 ± 0.27	0.74 ± 0.13	0.73 ± 0.10
FPF (%)	29.5 ± 0.60	28.1 ± 1.70	28.1 ± 3.80
MMAD (µm)	2.85 ± 0.07	2.85 ± 0.35	2.90 ± 0.42
GSD (µm)	1.96 ± 0.02	2.01 ± 0.05	2.01 ± 0.16
Recovery (%)	71.1 ± 28.1	82.9 ± 4.50	86.8 ± 17.3

The fine particle dose (FPD) expresses the FPF value in an absolute mass. Therefore, 0.74 µg siRNA were delivered at sizes below 5 µm out of 2.6 µg siRNA applied, known as dose delivered (DD). The overall recovery rate ranged from 71.1% to 86.8%. Some losses could have been caused by an insufficient clearance of capsules using the Handihaler device. Furthermore, depending on the surface charge of the LNPs, a difference in electrostatic charge was noticeable that could have led to higher adhesion of powders to the walls of capsules, induction port and pre-separator. The conclusion can be drawn that for all the different powders, regardless of their different LNP cargo, optimal microparticulate characteristics for pulmonary application were achieved.

3.3 Mucus penetration of spray dried LNPs

For efficient delivery of spray dried powder to the lungs, a few hurdles need to be overcome. First, the nano-in-microparticles need to be redispersed in lung fluid quick enough to dissociate into nanoparticles. Second, the nanoparticles need to pass the lung fluid as quickly as possible before the fluid is renewed and all particles are washed away. To mimic this scenario, we performed a mucus penetration study, in which we compared the penetration ability of freshly prepared LNPs in 5% lactose solution with spray dried LNPs redispersed in HPW. By taking into account the LNPs zeta potential which remained neutral for all LNP formulations in 5% lactose solution (m/V), LNPs are expected to pass the mucus layer without diffusion restrictions due to charge interactions. [363] As seen in Figure 7, 65–90% of the freshly prepared LNPs penetrate the mucus layer, whereas only 20–40% of the spray dried LNP penetrate the mucus. This higher amount of penetration for freshly prepared LNPs can be explained by referring to the sizes of redispersed LNPs which lets us assume that the sugar matrix was not fully dissolved resulting in bigger nanoparticle sizes. Moreover, the spray dried LNPs were still immobilized inside the sugar matrix not being able to pass the mucus layer as efficiently as freshly prepared LNPs. It is noteworthy, that the negatively charged, (-)LNPs, showed the least efficient mucus diffusion both as freshly prepared or spray dried particles. Comparing our results to the literature, a negatively charged particle should pass through the negatively charged mucus more efficiently because of charge repulsion.

A positively charged particle would interact with the negative mucus charge and be hindered in diffusion. A neutral charged particle would pass the mucus layer but not as efficiently as the negative ones. [341, 363] Freshly prepared (+)LNPs show mucus penetration characteristics of 90% which contradicts the charge theory. However, low nanoparticle sizes and near to neutral zeta potential in 5% lactose solution can explain its efficient mucus penetration. Spray dried nLNPs showed the highest penetration at 40%. In conclusion, the spray dried LNPs are capable of penetrating a lung mucus layer in order to reach the lung cells to release the siRNA cargo even if to a lesser extent than their freshly prepared counterparts.

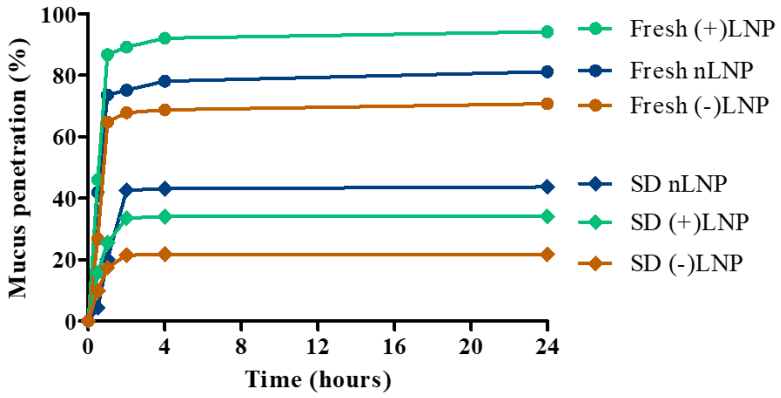

Figure 7 Mucus penetration assay of fresh LNPs vs spray dried (SD) LNPs. The time points were chosen at 0h, 0.5h, 1h, 2h, 4h and 24h.

3.4 *In vitro* characterization of spray dried LNPs

For siRNA delivery it is fundamental to maintain the molecule's bioactivity throughout the spray drying and storage process. Since the outlet temperature of 62 °C is not close to the degradation temperature of siRNAs and no severe losses of LNPs or siRNA were detected as abovementioned (Figure 3), the bioactivity of the LNPs was expected to be intact. Therefore, the gene silencing efficiency of spray dried LNPs (nLNP, (+)LNP and (-)LNP) of the enhanced green fluorescence protein expressing H1299 (H1299-GFP) cells were tested. All LNPs had an siRNA against GFP (siGFP) encapsulated. Furthermore, for comparison, another set of LNPs was prepared with scrambled, negative-control siRNA (siNC). Freshly prepared LNPs were dispersed in 5% lactose solution (m/V), whereas spray dried LNPs were redispersed in HPW. The specific amount of fresh LNPs and spray dried LNPs was chosen to transfect the cells at an siRNA concentration of 1 µg/mL (55.7 nM siGFP/ siNC) and 10 µg/mL (557 nM siGFP/siNC), respectively. As other controls, spray dried 5% lactose solution was redispersed in HPW and free siRNA in the same amount was added to the cells. As seen in Figures 8A and B, all LNPs having siGFP encapsulated show a highly significant GFP downregulation effect on the protein level. The downregulation ranged from approximately 80% for freshly prepared nLNPs at 1 µg/mL to >95% downregulation of fresh (+)LNPs at 10 µg/mL. All control values showed no gene knockdown effect. Hence, the gene silencing efficiency is RNAi mediated and a result of the complementary siRNA sequence. At 1 µg siRNA/mL, Figure 8A, freshly prepared nLNPs performed least efficiently of all LNP formulations with 80% downregulation, in comparison to 90% knockdown of spray dried nLNPs.

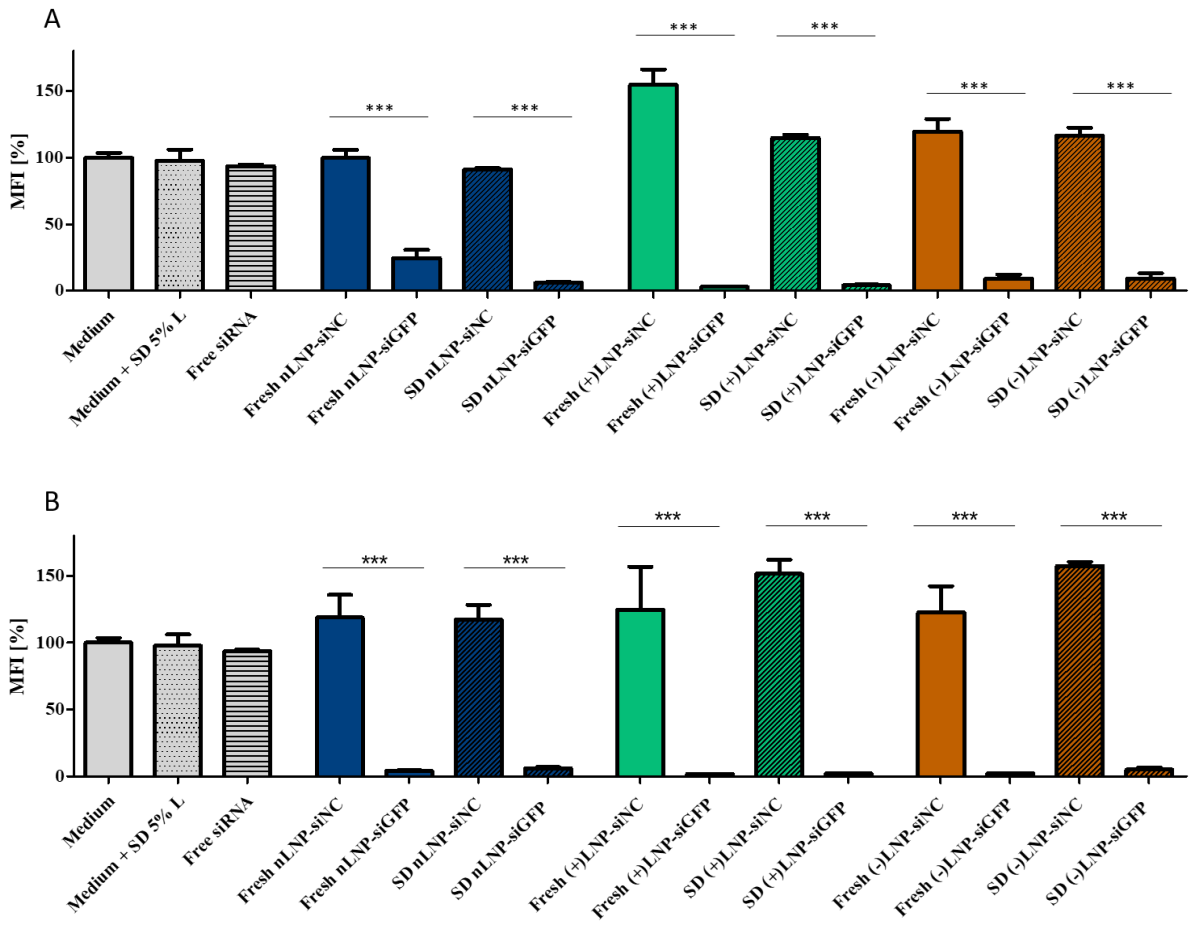

Figure 8 In vitro gene silencing effect of enhanced green fluorescent protein (eGFP) within a H1299-eGFP expressing cell line. Different siRNA concentrations were tested: A) 1 µg/mL , B) 10 µg/mL. Samples are plotted as follow: freshly prepared LNPs in full colored bars, spray dried LNPs in shaded colored bars. Bars show the mean fluorescent intensities (MFI) of the eGFP as a percentage relative to the untreated sample (grey, unpatterned bar).

This difference can be explained by the charge difference of freshly prepared LNPs in comparison to redispersed spray dried LNPs. More positively charged nanoparticles show a greater interaction with the cell membrane through attractive electrostatic interactions with negatively charged phospholipids or membrane proteins, and subsequently lead to a higher cell uptake. [193, 364] Therefore, a higher eGFP knockdown can be the result of the aforementioned with an increased amount of siRNA entering the cells. (-)LNPs showed 90% gene silencing and were outperformed with >95% performance by (+)LNPs. By increasing the siRNA amount 10-fold, the gene silencing effect increased throughout all LNP formulations to values >90% (Figure 8B). The negative control, scrambled siRNA values remained above 100% for each LNP formulation reflecting a highly significant gene silencing effect. To compare the LNP formulations against each other, (+)LNPs outperformed the other two formulations, even at lower siRNA concentrations. This observation can be explained by (+)LNPs entering the cell more easily and releasing higher amounts of siRNA from the endosome. [365] The 5% lactose solution should not interfere with the charges since the cells were cultivated in 400 µL cell medium and 100 µL of redispersed LNPs. This dilution could have enhanced the dissolution of LNPs out of the sugar matrix. Noteworthy, the gene silencing effects do not differ between freshly prepared and spray dried LNPs, and a knockdown on protein level was successfully achieved. This underlines the excellent characteristics of the LNPs which did not change after the spray drying process. To compare our results to previous studies, Jensen et al. spray dried DOTAP modified PLGA nanoparticles loaded with siRNA in mannitol at an outlet temperature of 30 °C to obtain hybrid dry powder formulations. Performing eGFP knockdown experiments in H1299-GFP cells resulted in a maximum silencing of 73%. [366] This knockdown result was one of the highest found in literature but not close to our outcome for the hybrid

system spray dried at low temperatures. In another study, Karve et al. spray dried mRNA embedded hybrid nanoparticles at an outlet temperature of 46–50 °C. Neither *in vitro,* nor *in vivo* work was performed and the attempt to spray dry lipid particles without polymer pre-encapsulation resulted in a recovery rate of 1–2%. [367] The temperature increase came in cost of the recovery rate. Adding a polymer to stabilize the system helped the authors to create a more feasible system. This confirms the difficulty of spray drying lipid nanoparticles at the highest possible temperatures while keeping the composition and bioactivity of the cargo. To the best of our knowledge, we are the first to report a successful eGFP knockdown of over 95% after spray drying of Onpattro®-derived LNPs at an outlet temperature of 62 °C. Neither different spray dried lipid based nanoparticle systems, nor hybrid or polymeric nanoparticulate systems have shown a similar eGFP *in vitro* activity.

To exclude any toxic effects originated from LNP formulations, a cytotoxicity evaluation *via* an MTT assay was performed. All samples show no toxic effects and results are not statistically significantly different for freshly prepared LNPs *vs.* spray dried LNPs, apart from (+) LNP at a siRNA concentration of 10 µg/mL (Figure 9). This cytotoxic effect of about 35% could result from combining the positive LNP charge with a high amount of sugar being added to the cells. As discussed in literature and shown for many nanoparticulate systems, high positive charges cause increased toxicity to the cells. [193, 368] By increasing the siRNA amount by 10 fold, we also increased the (+)LNP amount. This could cause an increased impact of positive charge to the cell membrane leading to cell disruption and cell death. Furthermore, an increasing amount of sugar can cause increased osmotic effects on the cells, inevitably, resulting in the same outcome. However, all other LNP formulations, redispersed after spray drying, do not show any cytotoxic effects. Hence, the main cytotoxic reason results from its positive charge. In summary, it was determined that a siRNA concentration of no higher than 10 µg/mL was necessary for achieving adequate gene knockdown, and higher concentrations were likely to increase the risk of cytotoxicity.

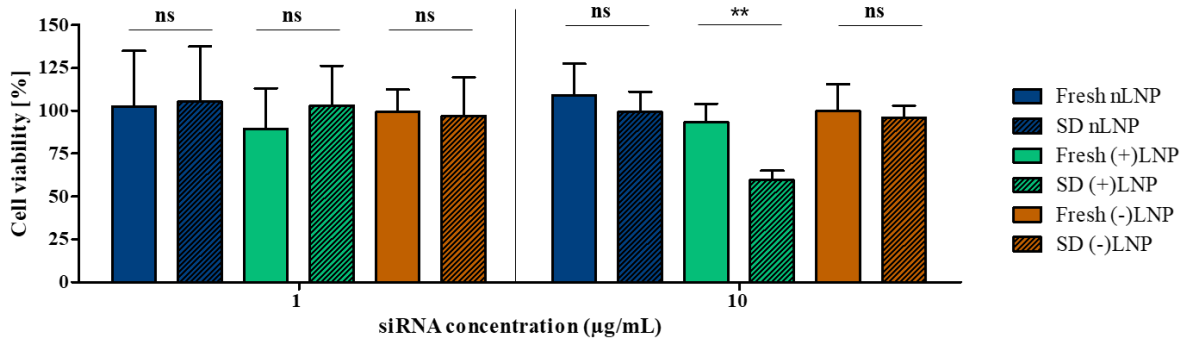

Figure 9 In vitro cytotoxicity evaluation via a MTT assay in H1299-eGFP cells. The siRNA concentrations were set at 1 µg/mL and 10 ug/mL for all samples. Samples are plotted as follow: freshly prepared LNPs in full colored bars, spray dried LNPs in shaded colored bars.

3.5 Ex vivo activity of spray dried LNPs in human precision-cut lung slices (hPCLS)

Human PCLS represent complex *ex vivo* 3D tissue culture models closely mimicking the anatomy and physiology of the lungs by maintaining the structure and cellular diversity. Furthermore, by closing the translational gap between *in vitro* and *in vivo* models, PCLS enable the study of respiratory diseases such as allergic asthma, COPD, IPF and viral infections and can act as a more sophisticated nucleic acid delivery model to the lungs. [369-376] Following the investigation of successful gene silencing on the protein level using spray dried LNPs, human precision cut lung slices (hPCLS) of individual donors were used to evaluate the gene knockdown efficiency of LNPs on the mRNA level. Human PCLS were transfected at siRNA concentrations of 10 µg/mL using redispersed spray dried LNP formulations targeting the house keeping gene GAPDH (siGAPDH). As a reference control, spray dried LNP-siGFP formulations were used to rule out any off-target effects. Untreated control hPCLS were treated with

medium and 5% lactose solution only. Figure 10 shows the normalization of GAPDH mRNA by the mRNA levels of β-actin and all values being normalized against LNP-siGFP values. The hPCLS treated with spray dried LNPs-siGAPDH showed significant reduction of GAPDH expression for each LNP formulation tested. The knockdown results ranged from 35% in (-)LNPs to 50% in (+)LNPs. The nLNP formulation showed a silencing efficiency of 45%. Figure S11 (A3) underlines that no statistically significant inflammatory effects were observed after transfection of hPCLS with different LNPs based on the level of twelve different proinflammatory cytokines. As stated in the *in vitro* protein silencing experiment, the (+)LNPs outperformed the other LNP formulations demonstrating their drug delivery potential for pulmonary administration. The overall performance of LNPs being able to reduce the mRNA level up to 50% underlines the LNPs' preservation of bioactivity and transfection efficiency after spray drying. Most importantly, the LNP formulations did mediate a level of *ex vivo* gene knockdown that has not been observed before with spray dried LNP delivery systems targeting the lungs. In comparison, Ruigrok et al. reported approximately 50% gene silencing of GAPDH in murine PCLS using non-spray dried Accell siRNA not using a nanocarrier delivery system [376]. As discussed in the beginning, naked siRNAs cannot cross the cell membrane sufficiently and need to be protected from heat stress during the spray drying process, hence, a galenic packaging of the cargo is necessary. Moreover, pulmonary administration is most commonly achieved *via* nebulization or dry powder inhalation. Furthermore, the LNPs' stability to retain the siRNA after spray drying highlights robustness and manifoldness of LNP formulations for pulmonary application systems. Those aspects underline the complexity of spray drying of LNP-siRNA formulations for silencing of GAPDH RNA levels emphasize the relevancy of spray dried LNPs as a promising therapy for the treatment of respiratory diseases such as asthma, COPD, lung cancer, cystic fibrosis or viral infections.

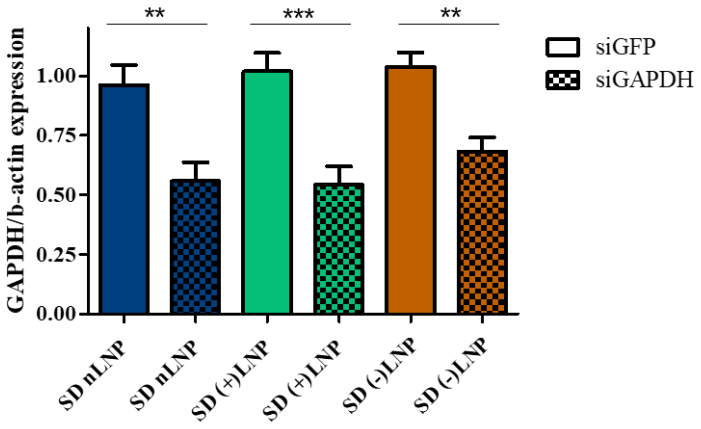

Figure 10 Ex vivo knockdown of house-keeping gene GAPDH. Human precision cut lung slices (hPCLS) were transfected at 10 µg siRNA / mL with spray dried LNPs encapsulating either siGAPDH or siGFP. All values were expressed as a percentage in comparison to the baseline values of samples treated with LNP-siGFP. Mean ± standard deviation, n=3.

4. Conclusion

In this study, we established a spray drying setup that allows RNA-loaded lipid nanoparticle systems to be spray dried at the highest possible temperature while retaining the LNP structure, cargo integrity and maintaining bioactivity and gene silencing efficiency. The detection of thermal stability of LNPs using the dual emission fluorescence-based method enabled a prescreening of different LNP formulations in different excipient solutions and at different temperatures. It was beneficial to test LNP stabilities near the lipids' phase transition temperatures to understand whether a spray drying process would damage the LNP composition or lead to cargo leakage. In addition, it enabled measurements of low sample volume and wide temperature ranges to simulate heat stress on the individual LNP systems during spray drying. These results led to a preselection of spray drying parameters including the best suitable excipient solution. Therefore, spray drying was performed in 5% lactose solution (m/V) in combination

with a maximum spray drying inlet temperature of 100 °C (62 °C outlet temperature). Quantification measurements of spray dried LNPs resulted in low losses underlining the preservation of siRNA and LNPs. The spray dried microparticles demonstrate optimal physicochemical and aerodynamic properties for pulmonary administration to the lower respiratory tract. Spray dried LNP formulations were able to successfully pass an artificial mucus layer similarly found in human lungs. Efficient gene silencing on the protein level was achieved *in vitro* in an adenocarcinoma cell line showing very good cellular compatibility. Spray dried LNPs efficiently silenced the house keeping gene GAPDH in *ex vivo* human lung tissues. In conclusion, our research confirms the successful spray drying of LNP-siRNA formulations to create a novel siRNA-based therapy to target respiratory diseases such as lung cancer, asthma, COPD, cystic fibrosis and viral infections.

Acknowledgements

The authors thank Prof Pieter Cullis for supporting this collaborative project and for providing the LNP formulations. We gratefully acknowledge the provision of human biomaterial and clinical data from the CPC-M bioArchive and its partners at the Asklepios Biobank Gauting, the Klinikum der Universität München and the Ludwig-Maximilians- Universität München. The authors would like to acknowledge technical support from Shubankar Ambike, Technische Universität München, and Ulrich Wilk and Jana Pöhmerer, Group of Prof Ernst Wagner at Ludwig- Maximilians-Universität München. The authors acknowledge Prof Marco Ciufolini and Dr. Fariba Saadati for providing the sulfur-containing lipid. This project was funded by the European Research Council (ERC-StG 637830 and ERC-PoC-101069308 to O.M.M.)

Chapter VII – Evaluation of storage conditions on spray dried siRNA-LNPs before and after subsequent drying

This chapter is prepared for submission and peer review as:

„Evaluation of storage conditions on spray dried siRNA-LNPs before and after subsequent drying "

Author‘s contributions:

Christoph M. Zimmermann [a,b], Paola Luciani [a] and Olivia M. Merkel [b]

C.M.Z performed the experiments, evaluated the data and wrote the manuscript. C.M.Z and O.M.M. conceived the presented idea and planned the experiments. P.L. and O.M.M supervised the work, provided conceptual guidance and corrected the manuscript.

a. *Pharmaceutical Technology, Department for Chemistry, Biochemistry and Pharmacy, University Bern, Freiestrasse 3, CH - 3012 Bern*

b. *Pharmaceutical Technology and Biopharmaceutics, Department Pharmacy, Ludwig-Maximilians-University Munich, Butenandtstr. 5-13, 81377 Munich, Germany*

Key words: lipid nanoparticles, LNP, Onpattro®, RNA therapeutics, siRNA delivery, spray drying, pulmonary delivery, subsequent drying, storage, shelf life

Abstract

An ideal world would have pharmaceutical drugs at an infinite shelf life, no susceptibility to degradation, chemical reactions or loss of efficacy. In reality, these processes occur making it desirable to extend a drugs' shelf life. Nucleic acid based drugs are most commonly stored in an aqueous solution making it vulnerable to microbial growth and degradation processes. Drying procedures, such as lyophilization and spray drying, help to reduce the products' residual moisture by increasing the products' shelf life and stability. The present study was designed to evaluate a 90-days storage of spray dried siRNA-LNPs at 4 °C and 25 °C. An updated Onpattro® composition consisting of a positively charged helper lipid was used as the LNP carrier system. In addition, all LNP samples were subsequently dried in the spray drying tower for 20 min. Physicochemical properties measurements of spray dried and subsequently dried LNPs resulted in sizes of 180 nm, PDI values of 0.1-0.15 and zeta potentials of +3 mV. Spray drying resulted in residual moisture levels of 3.6 - 4% and was reduced by subsequent drying to 2.8 - 3.1%. Aerodynamic properties showed discrepancies between the storing conditions. MMADs remained at 2.8 µm at storing conditions of 4 °C, whereas an increase to 5 µm at 25 °C was observed. Subsequent drying led to sizes of 3.6-3.8 µm, independent of the storing conditions. Spray dried LNPs maintained bioactivity for > 95% protein downregulation confirming no cytotoxic effects in a lung adenocarcinoma cell line. Furthermore, the spray dried and subsequently dried LNPs stored for 3-months at 4 °C and 25 °C achieved up to 50% gene silencing of the house-keeping gene GAPDH by addition to the mucus layer of Calu-3 cells. This study confirms the long-term stability of spray dried and subsequently dried LNPs after 90 days at 4 °C and 25 °C raising its importance as a therapy option targeting pulmonary diseases.

1. Introduction

In the last decade, nucleic acid-based drugs have demonstrated to treat diseases by targeting their genetic construction plan. Nucleic acid therapeutics can accomplish long-term or curative effects through gene addition, inhibition, editing or replacement. [377] The nucleic acid carriers consisted of polymers, lipids or hybrid combinations. [300] Among those, lipid nanoparticles have become one of the most promising drug delivery systems for nucleic acids, driven by several FDA approvals and the mRNA-based COVID-19 vaccines. [313, 378, 379] The storage of drugs and vaccines is an ongoing debate and logistical problem. The latest updates from the European Medicines Agency (EMA) estimate the shelf life for mRNA vaccines from BioNTech/Pfizer and Moderna to a maximum of 2.5 months and 1 months at 4 °C. At storage temperatures of −80 °C and −20 °C, the shelf life increases to a 9-month and 6-month period, respectively. However, once opened the vaccines needed to be used up within 24 hours. [380-383] This discrepancy in storage life gives a hint of the difficulty in creating the ideal product conditions for long-term storage on a global supply level. Onpattro®, which is the first FDA-approved siRNA drug based on a LNP system, shows a three-year shelf life when kept between 2 °C and 8 °C, provided that the drug vials are kept closed. [384] Further studies demonstrated that siRNA-LNPs remained stable at 2 -4 °C for 6 to 18 months keeping their initial particle size and siRNA encapsulation efficiency. [385, 386] However, long-term storage on an aqueous basis can lead to microbial growth and chemical degradation. Hence, drying procedures are favorable of transferring the drug substance in a water-reduced storage environment. Lyophilization is one way of drying, performing a gentle procedure. In a freeze-dried form, mRNA-LNP vaccines could be conveniently shipped worldwide without the need for cooling or freezing. Ball et al. studied the impact of freeze drying on siRNA-LNPs maintaining the bioactivity of the siRNA after 11-months storage at -80°C. [385] In another study, Shirane et al. lyophilized ethanol-containing siRNA-LNPs maintaining the gene knockdown efficiency of the freshly prepared (ethanol removed by ultrafiltration) and the reconstituted lyophilized formulations in vivo. [387] The approach of lyophilization helped to prolong the shelf life. However, lyophilization of LNPs is not straightforward due to the complex composition of various lipids at certain ratios and the freezing

process which can alter the LNP composition. In addition, it is very cost-intensive and time-consuming process. Therefore, other drying approaches, such as spray drying, can help overcoming them. [388] Spray drying is a widely used method for improving shelf-life conditions of drugs. It works on the principle of converting a liquid material into a dry powder offering multiple advantages for industrial use, such as up-concentration and encapsulation of bioactive ingredients into sugar matrix, extended storage stability due to less molecular mobility, shorter production time, and reduced production, transportation and storage costs. [389] The drying effect mainly relies on the sugar spray dried. Crystalline sugars, such as mannitol, tend to reach residual moisture levels of <1%, whereas amorphous sugars, such as lactose, obtained moisture levels of 4 - 5%. [189, 347] Despite the higher moisture level in amorphous matrices, they result in higher product stability and are preferred over crystalline sugars. Independend of the sugar matrix, the lower the moisture level in the product, the less susceptible it is to alterations or decline. [358] Thus, the spray drying parameters need to be adapted to the delivery system being spray dried. Due to the higher melting point, polymer-based systems can be spray dried at higher temperatures as lipid-based particle systems. The spray drying parameters need to find the balance between having the biggest drying impact and keeping the products integrity. One approach of reducing the residual moisture would be the implementation of a subsequent drying step to an amorphous sugar. A constant heat supply in the spray drying tower and the turbulence conditions in the collecting vessel, would dry the product in a gentle way. The most common application of dry powders is the use of dry powder inhalers, such as a Handihaler®.

Various nanoparticle systems have been spray dried focusing on the spray drying process itself, keeping the cargo intact and maintaining nucleic acid bioactivity. [189, 303, 366, 390] Unfortunately, none of those studies evaluated the impact of a subsequent drying step or the long-term storage influence on the product. In a previous study, we have shown a successful spray drying procedure of LNP-siRNA formulations in 5% lactose solution (m/V). The LNP formulation was based on an updated Onpattro® composition maintaining its integrity and mediating strong gene silencing efficiency on protein and mRNA levels both *in vitro* and *ex vivo*. [303] However, long-term assessments of spray dried LNPs were not performed and need to be observed.

The aim of this study was to evaluate the long-term stability of spray dried and subsequently dried LNPs at 3-month storing conditions of 4 °C and 25 °C. The LNPs consisted of an updated Onpattro® composition using a positively charged helper lipid, DOTAP ((+)LNP). Subsequent drying was applied for 20 min within the collection vessel, immediately following the spray drying process. Powders were analyzed and compared for physicochemical properties, siRNA losses, aerodynamic performance and siRNA integrity. The target range was set based on previous studies to obtain sizes after redispersion of around 150 nm, RNA losses below 15% and residual moisture levels below 5%, which should be reduced by to at least 4% after subsequent drying. [303] Furthermore, aerodynamic sizes should range between 3-7 µm and maintain RNA bioactivity. The LNPs' performance and siRNA integrity were tested in vitro in H1299 adenocarcinoma cells expressing enhanced green fluorescent protein (H1299-GFP). Moreover, in a more sophisticated in vitro setup, spray dried and subsequently dried powders were added to mucus excreting Calu-3 cells and tested for gene silencing targeting the house-keeping gene GAPDH. The findings of this study were compared to the previously found data and between the different storage conditions. Unique insights on the performance of long-term stored spray dried LNPs could be made keeping and improving microparticle properties as a pulmonary delivery system.

2. Materials & Methods

2.1 Materials

Dicer substrate double-stranded siRNA targeting green fluorescent protein (DsiRNA EGFP, 25/27) (siGFP), dicer substrate double-stranded siRNA targeting the house-keeping gene GAPDH (DsiRNA

GAPDH) (siGAPDH) and scrambled, non-specific control (siNC) were purchased from IDT (Integrated DNA Technologies, Inc., Leuven, Belgium). [186, 237, 270, 302] Tris-EDTA buffer solution 100x (T9285), RPMI-1640 medium (R8758), EMEM medium, fetal bovine serum (FBS) (F9665), penicillin-streptomycin (P/S) (P4333), G418 disulfate salt solution (G8168), Dulbecco's phosphate buffered saline (D-PBS) (D8537), methylthiazolyldiphenyl-tetrazoliumbromid (MTT), Triton X-100 were purchased from Sigma-Aldrich, a subsidiary of Merck KGaA (Darmstadt, Germany). PEG-DMG, DSPC, DSPG and DOTAP were bought from Avanti Polar Lipids, Alabaster, USA. The ionizable cationic lipid is a sulfur-containing analog of DLin-MC3-DMA (pKa 6.3-6.6). [186, 391] InhaLac®230, lactose monohydrate for dry powder inhalers, was purchased from Meggle Group (Wasserburg, Germany). Quant-it™ RiboGreen DNA reagent, black 96-well plates (10307451), power SYBR™ green PCR master mix and Aquastar® water standard oven 1% were bought from Thermo Fisher Scientific (Schwerte, Germany). Pumpsil® tubings were bought from Watson-Marlow GmbH (Rommerskirchen, Germany) and had an inner diameter and a thickness of 1.6 mm. White 96 well PCR plate and 0.2 mL PCR tubes were purchased from Biozym Scientific GmbH (Hessisch Oldendorf, Germany). PneumaCult ALI differentiation medium, hydrocortisone and heparin were purchased from Stemcell Technologies (Vancouver, Canada). Transwell® polyester membrane cell culture inserts were purchased from Corning (New York, USA).

2.2 Preparation of lipid nanoparticles (LNPs) entrapping siRNA

LNP-siRNA formulations had a lipid composition based on the clinically approved Onpattro formulation and were prepared as previously described [29, 297, 313]. Briefly, lipid components (ionizable cationic lipid, helper lipid, cholesterol, and PEG-DMG) at molar ratios of 50:10:38.5:1.5 mol% were dissolved in ethanol to a concentration of 10 mM total lipid. 1,2-dioleoyl-3-trimethylammonium-propane (DOTAP) was used to enable formation of LNP-siRNA systems with positive [(+)LNP] zeta potential. Purified siRNA (siNC, siGFP and siGAPDH) was dissolved in 25 mM sodium acetate pH 4 buffer to achieve an N/P ratio of 3, which is the charge ratio between the ionizable cationic head group on the lipid to the anionic phosphate in the RNA backbone. The two solutions were mixed through a T-junction mixer at a total flow rate of 20 mL/min, and a flow rate ratio of 3:1 v/v (aqueous:organic phase). The resulting LNP suspension was subsequently dialyzed overnight against PBS pH 7.4, sterile filtered (0.2 µm), and concentrated to 1.0 mg/mL siRNA measured via Ribogreen assay [340].

2.3 Spray drying and subsequent drying of LNPs

For production of spray dried and subsequently dried LNPs, the same method was chosen as described earlier. [186] Briefly, a B-290 spray drying tower (Büchi Labortechnik, Flawil, Schweiz) was used to spray dry siRNA-LNP formulations in a specified solvent (highly purified water (HPW) with lactose (InhaLac), 5% m/V, sterile filtered), at a pump rate of 1.4 mL/min and an inlet-temperature (T-In) of 100 °C resulting in measured outlet-temperatures (T-Out) of accordingly 62 °C ± 2 °C. Each individual stock solution of LNP-siRNA formulations had a concentration of 30 µg siRNA in 5mL5% lactose solution (w/V). This resulted in an siRNA to sugar concentration of 0.12 µg siRNA/mg lactose. Subsequent drying of spray dried powder was achieved by switching of the liquid feed and keeping the heat supply on for 20 min. Spray dried and subsequently dried powders were filled in 20R vials, sealed, and wrapped with parafilm. Samples were stored at 4 °C and 25 °C for 3 months (Table 1).

Table 1 Spray drying and subsequent drying plan of various LNPs. Spray drying was performed using 5% lactose solution (m/V) at 62 °C outlet temperature. Storage temperatures consisted of 4 °C and 25°C and lasted for 3 months.

Name	Drying Time (min)	Storage temperature (°C)	Storage Time (months)
siGFP - (+)LNP siNC - (+)LNP siGAPDH - (+)LNP	0	4	3
siGFP - (+)LNP siNC - (+)LNP siGAPDH - (+)LNP		25	
siGFP - (+)LNP siNC - (+)LNP siGAPDH - (+)LNP	20	4	
siGFP - (+)LNP siNC - (+)LNP siGAPDH - (+)LNP		25	

2.4 siRNA quantification after spray drying of LNPs

The Quant-IT™ Ribogreen assay was adapted as described in Walsh et al. [340] Briefly, LNPs were either freshly prepared or redispersed as described above. For each reading, 50 µL of samples was transferred in a black 96-well plate and filled to 100 µL with 2% Triton X-100 solution. A siRNA standard curve was pipetted at 10.0, 5.0, 2.5 and 1.0 µL of a stock solution (20 µg/mL) resulting in final concentration of 1.0, 0.5, 0.25 and 0.1 µg/mL, respectively. The plate was incubated at 37 °C for 60 min in a shaking incubator. Upon the addition of the Ribogreen reagent at a 1:100 dilution, the fluorescence intensities were measured at an excitation wavelength of 480 nm and an emission wavelength of 525 nm. The siRNA loss was quantified by normalizing the siRNA amount of spray dried and subsequently dried samples to the siRNA amount of fresh LNP samples.

2.5 Hydrodynamic diameter and zeta (ζ) potential measurements of spray dried LNPs

Hydrodynamic diameters and polydispersity indices (PDI) were measured in disposable cuvettes (Brand GmbH, Wertheim, Germany) using the Zetasizer Nano ZS instrument (Malvern Instruments Inc., Malvern, U.K.). To measure the size and PDI of spray dried and subsequently dried formulations at different storage conditions after redispersal, approximately 0.833 mg of spray dried LNP powder was dissolved in 100 µL HPW. This equates to 0.1 µg of siRNA (1 µg siRNA/mL). For comparison, fresh LNPs (c = 1 mg/mL) were diluted in 5% lactose to reach a concentration of 1 µg siRNA/mL. All samples were detected at a backscatter angle of 173°. Results are presented as average size (nm) ± SD. Zeta potentials were measured by Laser Doppler Anemometry (LDA) using a Zeta Cell (Zetasizer Nano series, Malvern, UK) containing a 6.5X dilution of the same 100 µL sample of LNP suspension. For each LNP formulation, measurements were presented as an average charge (mV) ± SD.

2.6 Residual water content – Karl Fischer titration

The residual water content for spray dried and subsequently dried LNPs powders at different storage conditions was determined by weighing 10 mg sample into 2R vials. A 1% water standard was prepared with approximately 40-50 mg powder. Empty vials served as blank values. For coulometric measurements, an Aqua 40.00 Karl Fischer Autosampler-Titrator with corresponding software from Analytik Jena AG (Jena, Germany) was used. The oven was heated to 100°C, and the final drift was set to less than 10.0 µg/min. Blank measurements were run and automatically subtracted from the standards and samples. Residual moisture measurements were considered valid if the 1% water standard measurement resulted in a value between 0.9 and 1.1%. Results are presented as mean residual moisture (%) ± SD.

2.7 Scanning Electron Microscopy (SEM)

A small amount of spray dried and subsequently dried LNPs at various storage conditions was placed on top of a stub covered with double-sided carbon tape. The stub was then coated with carbon under vacuum for 40 s. The microparticles were examined imaged using a FEI Helios G3 UC (Thermo Fisher Scientific, Schwerte, Germany).

2.8 Aerodynamic properties of spray dried LNPs

For the analysis of the aerodynamic properties of spray dried and subsequently dried powders after storage at 4 °C and 25 °C, procedures specified in the monograph 2.9.18, apparatus E, of the European Pharmacopoeia was performed using a next generation impactor (NGI) from Copley Scientific (Nottingham, UK). The measurement procedure was adapted as previously described. [186] Briefly, spray dried, or subsequently dried LNP powder was transferred into 2-3 hydroxypropylmethylcellulose capsules. Each capsule was loaded into a Handihaler® (Boehringer Ingelheim Pharma GmbH & Co. KG, Ingelheim, Germany), hole-punched and discharged twice. Subsequently, the same procedure as in 2.4. was performed. Every stage of the NGI was washed with 2% Triton-X buffer. The induction port (IP) was washed with 5 mL, the pre-separator (PS) was pre-filled with 15 mL, small cups were filled with 2 mL and bigger cups were filled with 4 mL 2% Triton-X buffer solution. All parts were cautiously shaken and placed on a horizontal shaker for 20 min. A standard curve of fresh siRNA was prepared and topped up to 100 µL with 2% Triton-X buffer. As a control, fresh LNPs, at siRNA concentration of 1.0 µg/mL, similar to the redispersed samples, were prepared in 2% Triton-X buffer. Three aliquots of 100 µL from each stage were used for further analysis. All samples were pipetted to a black 96-well plate and put into a shaking incubator for 60 min at 37 °C. Upon the addition of Ribogreen reagent at a 1:100 dilution, the fluorescence intensities were measured at an excitation wavelength of 480 nm and an emission wavelength of 525 nm. The mass median aerodynamic diameter (MMAD), geometric standard deviation (GSD), fine particle dose (FPD), fine particle fraction (FPF) and powder recovery (%) were calculated as described in the European Pharmacopoeia considering fine particles at sizes below 5 µm MMAD.

2.9 *In vitro* characterization of spray dried LNPs

2.9.1 Cell Culture

The human non-small cell lung carcinoma cell line H1299 (ATCC CRL-5803) stably expressing enhanced green fluorescence protein (eGFP) was cultured in RPMI 1640 medium supplemented with 10% FBS, 1% P/S and 0.4% G418. Cells, starting from passage 9, were passaged every 3 days with 0.05% v/v trypsin and subcultured in 75 cm^2 flasks. Calu-3 cells were obtained from LGC Standards GmbH (Wesel, Germany). Cells were maintained in EMEM medium supplemented with 10% FBS and 1% P/S. Cells were passaged once 80% confluence was reached and subcultured in 75 cm^2 flasks. H1299-GFP and Calu-3 cells were kept in a humidified atmosphere at 37 °C with 5% CO_2.All cell lines were mycoplasma-free and tested for mycoplasm every 3 months.

2.9.2 *In vitro* GFP protein downregulation in H1299 cells

To evaluate the *in vitro* gene silencing efficiency of siRNA-LNPs after spray drying and subsequent drying, H1299-GFP cells were seeded in a 24-well plate at a density of 25,000 cells per well in 500 µL medium at 37 °C and 5% CO_2 and incubated for 24 h. Powder samples were weighed at 0.833 mg, resuspended in 100 µL HPW, resulting in concentrations of 1 µg/mL, and added to 400 µL of fresh culture medium left for 24 h incubation at 37 °C and 5% CO_2. The medium was then discarded and replaced with 500 µL of fresh medium, and the plates were further incubated for another 24 h. At the end of the incubation time, cells were washed with PBS, trypsinized and collected. After centrifugation at 400 rcf for 5 min, the supernatant was discarded, and the cell pellet was washed two times in PBS

before being resuspended in PBS with 2 mM EDTA. Samples were analyzed by flow cytometry (Attune® NxT, Thermo Fischer Scientific, Waltham, Massachusetts, USA), and the median fluorescence intensity (MFI) of GFP protein expression was measured by using a 488 nm excitation laser and the emitted light passing through a 530/30 nm band pass emission filter set was detected. All LNPs samples were gated by morphology for a minimum of 10,000 viable cells. Results are displayed as mean MFI values (%) ± SD.

2.9.3 *In vitro* cytotoxicity of spray dried LNPs in H1299 cells

Cell viability after transfection with spray dried and subsequently dried LNPs was tested via an MTT assay as described previously.[392, 393] Briefly, 5,000 H1299-GFP cells per well were seeded in 100 µL medium onto a transparent 96-well plate (BioLite 96 well multidish, Thermo Fisher Scientific, Rochester, New York, USA). The samples were prepared by redispersing 0.833 mg (1 µg siRNA) of powders in 100 µL of HPW. After 24 h, 90 µL of pre-warmed medium was added to each well and supplemented with 10 µL of sample, respectively. The plate was incubated for 24 h at 37 °C and 5% CO_2. As a full viability control, cells were incubated in 100 µL consisting of 10 µL sterile 5% lactose solution (m/V) and 90 µL medium. After 24 h, the media was aspirated and 200 µL of MTT containing medium (0.5 mg/ml in serum-free RPMI-1640 medium) was added to each well. Cells were incubated for another 3 h at 37 °C and 5% CO_2. Subsequently, the cell culture medium was completely removed, and insoluble purple formazan crystals were dissolved in 200 µL DMSO. The plate was set on a horizontal shaker for 20 min for all crystals to dissolve. The absorbance was measured at 570 nm, corrected with background values measured at 680 nm, using a microplate reader (TECAN Spark, TECAN, Maennedorf, Switzerland). The data are shown as mean ± SD as percentage of viable cells in comparison to untreated cells representing 100% viability.

2.9.4 *In vitro* GAPDH knockdown in Calu-3 cells

Calu-3 cells were seeded at a density of 250,000 cells onto uncoated Transwell® polyester cell culture inserts (6.5 mm, 0.4 µm pore size) in 100 µL medium (apical side), while 600 µL medium were added to the basolateral chamber. After 72 h, the apical medium was removed to obtain airliquid interface conditions, while the medium from the basolateral chamber was replaced with 200 µL of PneumaCult™ ALI medium (STEMcell technology, Vancouver, Canada) and replaced every two days. Experiments were performed once TEER values ≥300 Ω*cm^2 were reached and a stable polarized epithelial layer was formed, as measured with an EVOM epithelial volt/Ω meter (World Precision Instruments, Sarasota, USA). For transfection of spray dried and subsequently dried LNPs (siGAPDH-(+)LNP and siNC-(+)LNP) stored at different conditions, 8.33 mg (10 µg/mL) powder was directly poured on top of the mucus layer. The basal compartment consisted of 200 µL of PneumaCult™ ALI medium. Calu-3 cells were incubated for 48 hours at 37 °C and 5% CO_2. Harvesting the cells was done by washing the apical compartment with PBS. Subsequently, the cells were scraped carefully without breaking the membrane and transferred into Eppendorf tubes. The RNA extraction protocol was carried out by using the PureLink RNA mini kit according to the manufacturer's protocol. The RNA concentration and purity were quantified by RT-qPCR. In brief, cDNA was synthesized from total RNA using high-capacity cDNA synthesis kit (Applied Biosystems, Waltham, Massachusetts, USA). The obtained cDNA was then diluted 1:10, and a qPCR was performed using the SYBR™ Green PCR Master Mix (Thermo Fischer Scientific, Waltham, Massachusetts, USA) with primers for human GAPDH and β-actin (Qiagen, Hilden, Germany) for normalization. Cycle thresholds were acquired by auto setting within qPCRsoft software (Analytic Jena AG, Jena, Germany). Three individual batches of spray dried and subsequently dried LNPs (siGAPDH and siNC) were examined. The GAPDH silencing results are reported in the mean percentages (%) normalized to siNC values ± SD.

2.10 Statistics, data analysis and presentation

All experiments were run in independent triplicates. Experimental data passed the D'Agostino-Pearson normality test and were analyzed for statistical significance using the One Way ANOVA repeated measurements on the GraphPad Prism 5 software with Tukey's post-hoc test with $p>0.05$ considered not significant (ns), * $p<0.05$, ** $p<0.01$, *** $p<0.001$. Data presentation was performed using GraphPad Prism 5 data science packages.

3. Results and Discussion

3.1 Characterization of spray dried and subsequently dried LNPs

3.1.1 RNA quantification and physicochemical properties of spray dried and subsequently dried LNPs

One of the most important quality criteria for all drug substances is the quantification of cargo loss after processing. Spray drying of LNPs and subsequent drying of the powder create additional stress on the nanoparticle system. In order to ascertain if the spray drying and subsequent drying process results in siRNA losses, an RNA quantification assay was performed. When spray drying at 62 °C outlet temperature, applying a subsequent drying step at the same temperature for 20 min and storing the samples at 4 °C and 25 °C for 3 months, not more than 10% of siRNA losses were detected (Figure 1).

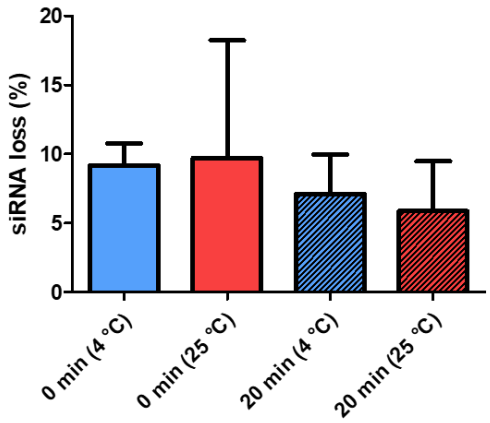

Figure 1 Quantification of siRNA losses after spray drying and subsequent drying for 20 min at storage temperatures of 4 °C and 25 °C after 3 months. Spray drying of LNPs in 5% lactose solution (m/V) at an outlet temperature of 62°C. Each bar shown as mean ± SEM, n=3.

These results are independent of drying time and storage conditions. Subsequently dried LNP samples even show a slight reduction in siRNA losses to 7-8%, however, the difference to freshly spray dried LNPs is non-significant. The standard deviation of spray dried powders stored for 3 months at 25°C exceeded all other values indicating that individual measurements did not show similar results. The spray-drying procedure itself and the storage conditions could have been responsible for the preparation of a malign batch. Overall, spray drying and subsequent drying of LNPs kept the loss of siRNA to a maximum of 10% making the spray drying process a suitable method to be stored for a longer period at temperatures of 4 °C and 25 °C.

Another important aspect to look at are the physicochemical properties of spray dried and subsequently dried LNPs being stored for 3 months. DLS measurements determine the nanoparticle sizes and quantify the size distribution. LNP microparticle powders were redispersed in HPW to prepare for measurements. All LNPs showed sizes of 180-200 nm after spray drying, subsequent drying and storage at 4 °C and 25 °C (Figure 2A). The PDIs varied between 0.1 and 0.15 indicating a narrow size distribution after storage. Furthermore, a 5% PDI increase was seen comparing the spray dried powder without subsequent drying stored at 4 °C and 25 °C. However, this trend can be neglected resulting in similar sizes and PDIs after

3-month storage for all LNP powders. Freshly spray dried (+)LNPs have shown sizes of about 200 nm. [303] The subsequent drying and storage conditions of 4 °C and 25 °C for 90 days did not have an influence on the particle size or PDI. Looking at the zeta potential, all samples showed values between +2 - +3 mV (Figure 2B). As seen and explained before, the lactose matrix is acting as a shield for charges and needing some time to dissolve properly. [303] Comparing drying times and storage conditions to each other, no variance in zeta potential was apparent. A disruption or change in LNP formulation would show obvious changes in zeta potential. After seeing no obvious siRNA losses and no changes in zeta potential after spray drying, subsequent drying and storage at 4 °C and 25 °C for 3 months, the LNP structure seems to be intact keeping the siRNA encapsulated.

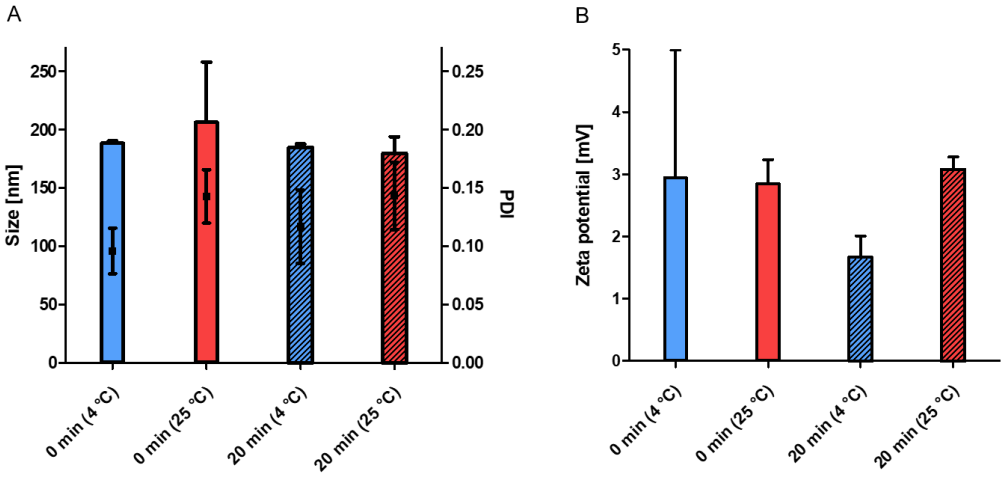

Figure 2 Physicochemical properties of spray dried (0 min) and subsequently dried (20 min, shaded) LNPs stored for 3 months at 4 °C (blue bars) and 25 °C (red bars) A) DLS measurements showing sizes and PDIs. B) Zeta potential measured via LDA. pray-dried (0 min) and subsequently dried (20 min) L Samples were redispersed in HPW. Spray drying temperature was set to 62 °C outlet temperature. Mean ± standard deviation, n=3.

Storage conditions are one way of influencing a products' quality. Residual moisture can favor micropartcle aggregation and microbial growth, a phenomen to be prevented, especially during storage at room temperature. It is pivotal thus to determine the powder's residual moisture before packaging and sotring. [358] In Figure 3, spray drying 5% lactose solution (m/V) resulted in a residual moisture level of 5% which is in line with literature values. [347] Spray drying LNPs in 5% lactose solution (m/V) reduced the residual moisture to 3.6%. This level was kept storing the samples at 4 °C. Applying a subsequent drying of 20 min reduced the residual moisture to 2.8% showing a slight increase in moisture to 3.1% after storage at 25 °C. This increase was neglectable because no statistical significant difference was observed.

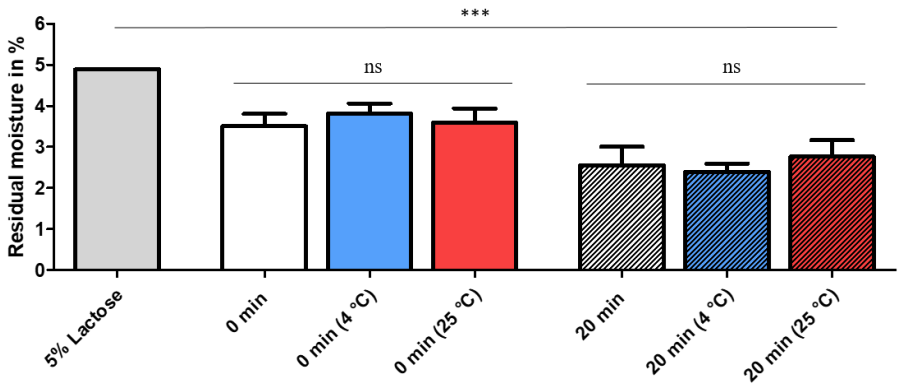

Figure 3 Residual moisture of spray dried and subsequently dried LNPs. Subsequent drying lasted for 20 min. White bars show spray dried samples directly analyzed, blue bars show samples stored at 4°C and red bars show samples stored at 25 °C. All stored samples were kept sealed for 3 months. Mean ± standard deviation, n=3.

As discussed before, the amorphous state of spray drying lactose is favorable for LNP preservation. Moreover, a high glass transition temperature Tg value is necessary to keep the product stable at a longer storage time. The Tg value is oppositely linked to the residual moisture level, meaning that the higher the residual moisture level, the lower the Tg value. [303, 358] In conclusion, storing the spray dried LNP powder in a 20R vial, sealing it and keeping it for 3 months at 4 °C and 25 °C, the moisture levels of spray dried and subsequently dried LNPs were reduced in comparison to spray dried 5% lactose solution. The decrease in residual moisture level favors to maintain the amorphous state of LNP powders, prolonging stability and avoiding nucleation and degradation processes over a longer storage time.

3.1.2 Geometric and aerodynamic performance of spray dried and subsequently dried LNPs

Spray dried powders that are administered to the lungs need to fulfill size requirements in order to be delivered to the bronchioles or alveoli. A first indication can be drawn by measuring the geometric median diameter (GMD) via SEM. Information about the particles' surface and composition can be obtained. Prior measurements have shown spray dried LNP sizes of 2-9 µm. [303] Subsequent drying of those powders and storing at 4°C and 25°C for 3 months led to geometric sizes of 3-8 µm (Figure 4). Therefore, the additional heat impact of subsequent drying did not form microparticle aggregates or merged powder particles. The sizes were kept, and the surface still appeared smooth keeping the subsequently dried powders in ideal conditions for pulmonary administration.

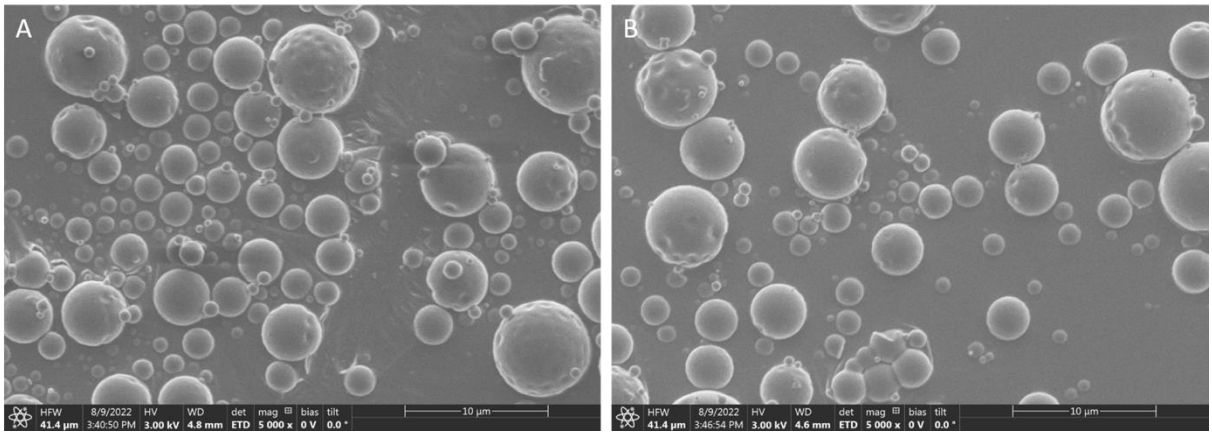

Figure 4 SEM pictures of spray dried A) siGFP-(+)LNP after 20 min subsequent drying at 4 °C storage, B) siGFP-(+)LNP after 20 min subsequent drying at 25 °C storage. Storage time was set for 3 months. All samples were spray dried in 5% lactose solution at 62°C outlet temperature.

Although the GMD provides a good impression about the actual sizes of spray dried powders, the mass median aerodynamic diameters (MMAD) of porous materials commonly falls below the GMD. [362] For pulmonary application, ideal particle sizes of 3-7 µm are required. [359, 360] A next generation impactor (NGI) was used to measure the aerodynamic performance of spray dried and subsequently dried LNPs after storage at 4 °C and 25 °C for 90 days. In Table 2, various comparisons between drying time and storage temperature can be drawn. Spray dried LNPs that were stored at 4 °C resulted in an MMAD of 2.73 µm at a geometric standard deviation (GSD) of 1.85 µm. The fine particle fraction (FPF), which represents the mass percentage of spray dried LNPs with an aerodynamic diameter below 5 µm, was detected at 30.1% at a recovery rate of 98%. Previous results reported a similar MMAD of 2.85 µm and a FPF value of 28.1%. [303] In comparison, spray dried LNP powders that were subsequently dried and stored at 4 °C reported an increased MMAD of 3.78 µm. The FPF was reduced to 21.5% but the recovery rate remained at 99%. The subsequent drying at 62 °C outlet temperature could have caused the increase in MMAD by merging microparticles leading to a reduced FPF value. The residual moisture cannot be a reason because subsequent drying reduced the residual moisture level preventing the microparticles to aggregate. Nevertheless, sugar matrices tend to melt and merge if the

Tg is exceeded. Determining the aerodynamic properties of spray dried LNPs resulted in MMAD of 4.98 µm, the highest MMAD value of all spray dried samples. Even though the residual moisture level remained at 4% when samples were stored at 4 °C, a dominant increase in MMAD of more than 2 µm changed the characteristics of the spray dried powder. The FPF was reduced to 15.9% and the recovery rate sank to 71.3%. The reduction in recovery can be explained by microparticle aggregates that keep the LNPs in their sugar matrix making it harder to quantify all siRNA. Furthermore, a bigger particle is more likely to get stuck in the handihaler application device lowering the amount of siRNA detected. In addition, a big standard deviation for samples at 25 °C storage (0 min) implied batch to batch varieties which could have worsened because of the storage conditions. However, a subsequent drying step improved the powders characteristics after storage at 25 °C. The MMAD was downsized to 3.60 µm, the FPF was increased to 22.4% and the recovery rate was enhanced to 83.9%. Therefore, applying a subsequent drying step for products that are intended to be stored at 25°C is advisable.

Table 2 Microparticle characteristics of spray dried and subsequently dried LNP formulations in 5% lactose solution at an outlet temperature of 62 °C using a Next Generation Impactor (NGI). Subsequent drying lasted for 20 min. Samples were stored for 3 months at 4 °C and 25 °C. DD: dose delivered, FPD: fine particle dose, FPF: fine particle fraction, MMAD: mass median aerodynamic diameter, GSD: geometric standard deviation.

	0 min, 4°C	20 min, 4°C	0 min, 25 °C	20 min, 25 °C
DD	3.19 ± 0.34	3.80 ± 0.67	2.67 ± 0.38	1.96 ± 0.16
FPD (<=µm)	0.96 ± 0.08	0.80 ± 0.06	0.41 ± 0.21	0.43 ± 0.18
FPF (<=µm)	30.1 % ± 0.7 %	21.5 % ± 5.3 %	15.9 % ± 10.0 %	22.4 % ± 11.3 %
MMAD [µm]	2.73 ± 0.30	3.78 ± 0.49	4.98 ± 1.71	3.60 ± 0.70
GSD [µm]	1.89 ± 0.01	2.55 ± 0.66	2.03 ± 0.26	3.67 ± 2.55
Recovery	98.0 % ± 25.2 %	99.9 % ± 10.5 %	71.3 % ± 6.5 %	83.9 % ± 4.9 %

If the results are not compared in regard to their storage conditions, but against drying conditions and times, the data revel that aerodynamic properties of powders that underwent subsequent drying did not differ from each other. Solely, the recovery rate was 16% lower after 25 °C storage in comparison to 4 °C storage. In contrast, the comparison of spray dried powders without subsequent drying resulted in an increased MMAD of almost 2-fold, a 2-fold reduction in FPF and a decrease of powder recovery by almost 27% stored at 25 °Cover storage conditions of 4 °C. Nevertheless, the optimal MMAD range of microparticles was fulfilled target sizes of 3 - 7 µm. All powders stayed within that size range facilitating ideal microparticle characteristics for dry powder pulmonary applications.

3.2 In vitro characterization of spray dried LNPs

Present results have established no severe losses of siRNA after spray drying and storage, as well as establishing the aerodynamic properties of all spray dried microparticles as ideal for pulmonary application. Hence, the bioactivity of spray dried and subsequently dried LNPs after 3 months storage was assessed. Prior to any cell targeted experiments, a MTT study revealed cytotoxic effects of not more than 20% for all spray dried and subsequently dried powders (Figure 5A). This effect could result from lactose which can influence the osmotic pressure on cells resulting in cell death

A gene silencing experiment targeting the enhanced green fluorescent protein expressing H1299 (H1299-GFP) cells was performed using spray dried and subsequently dried LNPs having scramble, negative-control siRNA (siNC) and siRNA against GFP (siGFP) encapsulated (Figure 5B). The storage conditions differed from freshly prepared samples (white bars), over 3-month storage at 4 °C (blue bars), to 3-month storage at 25 °C (red bars). As established in a previous study, the siRNA concentration

chosen to be transfected remained at 1 µg/mL (55.7 nM siGFP/siNC). Throughout all samples and independent of the storage conditions, a highly significant GFP-knockdown of >95% was obtained. This matches previous results for gene silencing of spray dried (+)LNPs. [303] Hence, the subsequent drying and storage for 90 days at 4 °C and 25 °C did not influence the bioactivity of siRNA maintaining a very high potency of gene silencing.

Following the investigation of successful protein knockdown, a mucus excreting cell line, Calu-3, was used to evaluate the gene knockdown efficiency on the mRNA level targeting the house-keeping gene GAPDH. Calu-3 cells were transfected by spreading spray dried LNP powder, having either siNC or siGAPDH encapsulated, on the mucus layer that was grown in air liquid interface inserts. The knockdown efficiency was determined after 48 h incubation time. Figure 5C shows the %-values of GAPDH mRNA by the β-actin mRNA levels being normalized against LNP-siNC values. Comparing the storing conditions and keeping the drying parameters the same, storing spray dried LNPs at 4 °C resulted in a GAPDH/β-actin expression of 55.9%, meaning a mRNA knockdown of 44.1% was achieved. However, a 25 °C storage revealed a mRNA knockdown of only 29.2%. This reduction can be explained by the previous results of batch variety after storage at 25 °C. The bigger microparticle MMAD and lower FPF tend to get stuck in the mucus layer not releasing the same amount of siRNA as for a MMAD of 3 µm as seen after 4 °C storage. Furthermore, a lower recovery rate will automatically transfect a lower amount of siRNA adding to the discrepancy in mRNA knockdown levels. Subsequently dried LNP powders resulted in a mRNA knockdown of 50.7% and 44.3% for 4°C and 25°C storage, respectively.

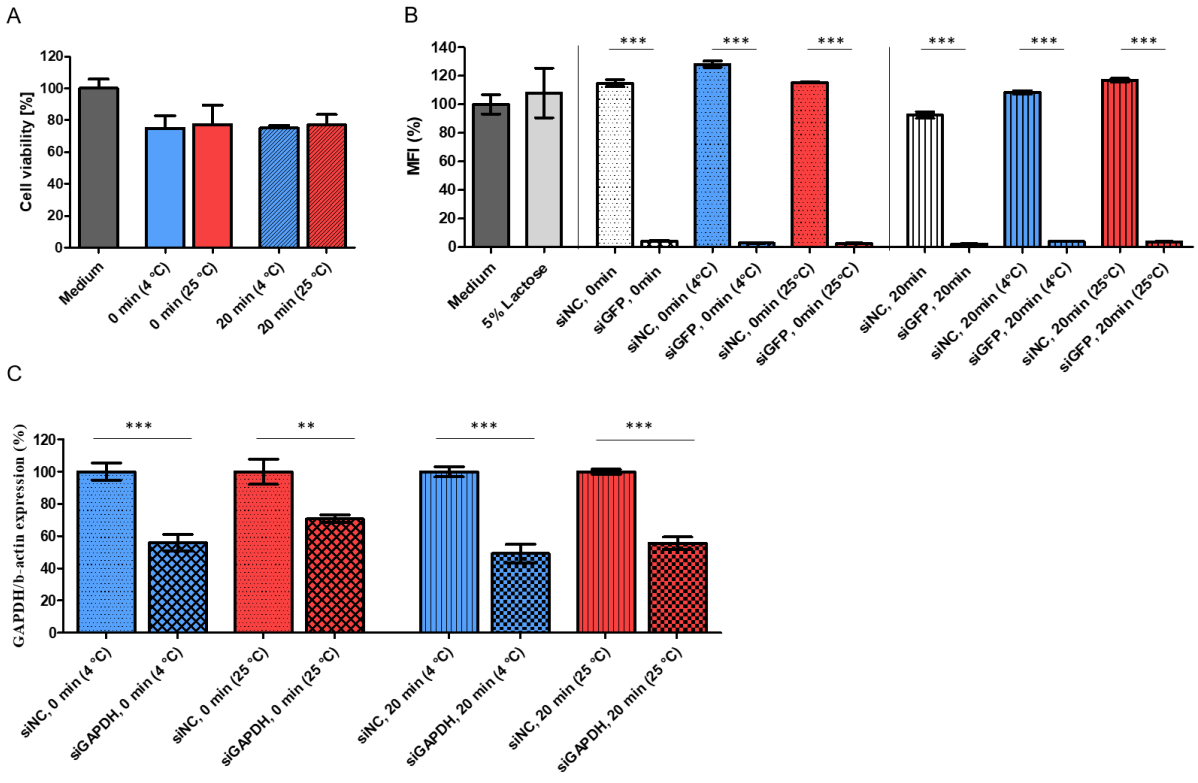

Figure 5 *In vitro* evaluation of spray dried and subsequently dried LNPs. **A**) *In vitro* cytotoxicity evaluation via a MTT assay in H1299 cells.**B**) Gene silencing effect of enhanced green fluorescent protein (eGFP) within a H1299-eGFP expressing cell line. siRNA concentration was set to 1 µg/mL. **C**) Gene silencing effect of house keeping gene GAPDH in mucus expressing Calu-3 cells. siRNA concentrations were set to 10 µg/mL.White samples were freshly spray dried. Blue samples were stored for 3 months at 4°C and red samples were stored for 3 months at 25 °C. Mean ± standard deviation, n=3.

As already seen for the aerodynamic performance of the spray dried powders, LNP powder stored at 4°C and subsequently dried powders stored at both temperatures do not differ in their performance. Only

the spray dried powders stored at 25 °C performed less than others. Comparing samples stored at the same temperature, it could be appreciated that a subsequent drying improved the GAPDH knockdown performance of LNPs at 25 °C, whereas the mRNA silencing effect remained unchanged for samples stored at 4 °C. This novel approach was implemented to imitate real life dry powder administration to the lungs, usually performed by dry powder inhalers. Here, powders must overcome natural barriers, such as lung mucus, before reaching the targeted cells. The lungs' mucus is constantly excreted acting as a protective shield. Hence, any particle or drug that targets the lungs' cells needs to pass the mucus layer and a certain level of drug loss is expected. [280, 303, 363] Reaching GAPDH knockdown levels of 30-50% show the immense potential of LNPs to be used as pulmonary drugs. Even a storage time of 90 days and severe storage conditions of up to 25 °C did not harm the performance and kept the LNP activity intact.

4. Conclusion

In the various phases of product development identifying the conditions for long-term storage it is pivotal to properly conceive a scale-up of the manufacturing process. The aim of this study was to compare the long-term stability of spray dried and subsequently dried LNPs at storage conditions of 4 °C and 25 °C. Our previously established spray drying method for LNPs in 5% lactose solution (m/V) served as a starting point for the spray drying setup, parameters and powder characterization. [303] Neither the spray drying, nor the subsequent drying or the different storage temperatures resulted in siRNA losses <10%, underlining the preservation of siRNA inside the LNPs, and measured nanoparticle sizes of about 180 nm. Furthermore, the size distribution maintained narrow at 0.1 - 0.15 keeping a positive zeta potential of +3 mV. The spray dried microparticles showed residual moisture levels of about 4%, which was reduced to 3% applying the subsequent drying for 20 min. Storage at different temperatures did not lead to an increase in moisture levels. The spray dried powder demonstrated optimal aerodynamic properties for pulmonary administration. Apart for the spray dried powder stored at 25 °C, all samples' MMAD of 2.8-3.6 µm would qualify for administration to the lower respiratory tract. When storing spray dried LNPs at 25 °C, a subsequent drying step can improve the MMAD and FPF. This improvement was not observed when stored at 4 °C. All samples resulted in efficient protein silencing of >95% targeting a lung adenocarcinoma cell line. As demonstrated before, LNPs successfully passed an artificial mucus layer. Therefore, the GAPDH knockdown in mucus excreting Calu-3 cells was observed and resulted in a 50% silencing effect. In summary, our 90-days research on spray dried and subsequently dried LNPs confirms the conservation of LNP structure, cargo integrity and siRNA bioactivity, independent of storage temperatures of 4 °C or 25 °C, maintaining ideal properties for pulmonary delivery.

Acknowledgements

The authors thank Prof Pieter Cullis and Dr Dominik Witzigmann for supporting this collaborative project and for providing the LNP formulations. The authors acknowledge Prof Marco Ciufolini and Dr. Fariba Saadati for providing the sulfur-containing lipid. This project was funded by the European Research Council (ERC-StG 637830 and ERC-PoC-101069308 to O.M.M)

Chapter VIII – Summary and Prospects

This thesis consisted of two parts. The first section investigated whether the modification of existing polyplexes or the synthesis of a novel amphiphilic polymer can overcome the endosomal escape problem. The second part established a spray drying method for a variety of charged LNPs and evaluated the powders characterization after long-term storage as a pulmonary delivery system.

In **Chapter I**, I started the thesis with a brief introduction of RNA interference, the concept of endosomal escape and spray drying. This served as an introduction to people that are new to the topic of pulmonary delivery of nucleic acid-based drugs and combine the concepts, obstacles and solutions that must be considered for a successful delivery system

Chapter II, served as an overview of several nanoparticle systems which are produced by microfluidic mixing. The reader got a list that ranged from nanoemulsions, liposomes and lipid nanoparticles, to polymeric nanoparticles, hybrid lipid-polymer nanoparticles and theranostic nanoparticles. All formulations were linked to research studies with the aim of being nanoparticle drug delivery systems for pharmaceutical applications.

I then moved to **Chapter III**, where the first part of the thesis regarding the endosomal release problem of polyplexes started. I presented a formulation study of several triblock copolymers, PEG-PCL-PEI, using microfluidic mixing for the encapsulation of siRNA. Our group modified the polymer which had struggled with an endosomal release problem. We adapted the composition by varying PCL and PEG weights and grafting densities. I demonstrated that the adaption in block composition led to a more monodisperse size distribution by maintaining acceptable physicochemical properties compared to prior studies. Despite the improvement in uptake behavior, the gene silencing effect did not improve significantly meaning the endosomal escape problem was not resolved by chemical modification.

Not solving the endosomal release problem meant we changed the approach by synthesizing a novel amphiphilic spermine-based polymer which should facilitate endosomal release and nucleic acid drug delivery. In **Chapter IV**, I characterized siRNA polyplexes made from several variants of an amphiphilic poly(spermine acrylamide) polymer. I studied the physicochemical properties of polyplexes and tested nanoparticle stability at physiological pH and acidic pH mimicking the lysosomal compartment. I showed that the novel polyplexes outperformed PEI-based nanoparticles in vitro and our group detected in vivo gene silencing effects in mice. I concluded that the novel amphiphilic poly(spermine acrylamide) polymers enable endosomal release and were established as non-viral vector for siRNA delivery.

Encouraged by the success in gene silencing and endosomal release, as well as participating in a collaboration on lipids, I started **Chapter V** with the intention to solve the endosomal escape problem of polyplexes by forming hybrid lipid polyplex nanoparticles through lipid coating. I started this study with the hypothesis that the combination of polymers and lipids will use their synergies to overcome the endosomal release problem. Three different lipids, DOPC, DOTAP and DLIN-MC3-DMA, were used in a microfluidic mixing setup as a coating agent for PEI-PCL-PEI-based siRNA polyplexes. I performed a full nanoparticle characterization consisting of physicochemical properties, morphology and size detection via microscopy, nanoparticle stability and in vitro performance. I showed that DOPC- and DOTAP coated hybrid nanoparticles did not improve the gene silencing effect compared to their polyplex precursors. A chloroquine addition revealed that the nanoparticles were stuck in the endosome. I switched to the ionizable lipid DLIN-MC3-DMA which protonates upon acidification. I performed the same characterization steps and I observed a significant improvement in gene silencing to its polyplex precursor while maintaining all other parameters.

The second part of my thesis dealt with spray drying and long-term storage of LNP encapsulating siRNA. In **Chapter VI**, I established a spray drying platform for several LNPs which were based on an adapted formulation of Onpattro®. I used the knowledge of a novel dual emssion fluorescence method that prescreened the use of various sugars and temperatures on LNP integrity. The results paved the choice of a lactose solution and a spray drying temperature of 100° C inlet temperature which was established in my spray drying method. I tried to find the highest possible drying temperature to enable ideal powder characteristics without destroying the LNP composition and the siRNA bioactivity. I performed powder characterization after redispersion, similar to testing nanoparticles. I intended to use the spray drying powder for pulmonary application, therefore, I tested the mucus penetration ability and the aerodynamic properties using a next generation impactor. After obtaining successful characteristics for pulmonary delivery, I tested the spray dried LNPs in vitro in lung cells and ex vivo in human precision cut lung slices. I observed hardly any cytotoxic effects at full gene silencing in vitro and the highest detected RNA silencing ex vivo. In summary, I was able to establish a method to transfer LNPs into a dry powder formulation for pulmonary application.

Following the successful method of spray drying LNPs, I decided to analyze long-term storage conditions of spray dried LNPs and compare them to a subsequent drying step, in **Chapter VII**. I followed the idea of a subsequent drying step because I saw that spray drying of lactose led to an amorphous sugar matrix with residual moisture levels of 4-5% which can facilitate microbial growth and accelerate product decay. I set the storage conditions to 4 °C and 25 °C for 3 months to generate comparable storage conditions of dry powders that are on the market. I performed the same powder characterization as in Chapter VI and compared all values with each other. I showed that the long-term storage did not affect physicochemical conditions and led to siRNA losses of no more than 10%. I performed in vitro performance studies on adenocarcinoma cells and mucus excreting lung cancer cells. I chose a mucus excreting cell line to mimic the impact of powders after inhalation. The protein silencing effect remained at almost 100% and the RNA was silenced by more than 50%. All results were independent of the different storage conditions. This long-term storage study concluded the successful spray drying approach of LNPs which can be classified as effective pulmonary nucleic acid delivery systems.

This thesis is relevant to research groups tackling the endosomal release problem of polyplex nanoparticles and implementing a spray drying method for lipid nanoparticles. Most of the techniques I used are important for characterization of siRNA-based nanoparticle systems and spray dried nano-in-microparticle systems. The main focus and choice of methods created an almost real-life comparison, i.e. the use of an mucus excreting cell line and an ex vivo gene silencing in human precision cut lung slices. The study of spray drying LNPs

As new findings raise new questions, I would like to list a few observations in regards to my research that could be pursued in the future. I see big potential in using ionizable lipids to improve the endosomal release ability of polymeric nanoparticles. My approach has shown a satisfying improvement, however, the performance of HLPNP systems can still be enhanced. Adapting the flow rate ratio or increasing the amount of lipid could help. Once changes are applied, the nanoparticle systems need to be characterized again. Another important aspect that should be tested, is the stability of HLPNPs. A long-term study can verify if the nanoparticles maintain their structure and if the siRNA is still encapsulated. Furthermore, particle stability should be tested in the presence of acidity to mimic the endosomal compartment and in the presence of serum proteins. The latter is especially important for *in vitro* and *in vivo* experiments, as proteins could interact with the nanoparticles and reduce their effectiveness.

The establishment of a spray drying platform for LNPs has opened up the opportunity for a wide range of drugs to be administered via the pulmonary route. However, the spray drying procedure can still be optimized. Ideally, a continuous setup, in which the nanoparticle formation is directly navigated into the

spray drying tower, would simplify the spray dried powder production. An implementation of on-line quality tests would enable a high standard of production. In addition, *in vivo* experiments could confirm the promising status of a powerful pulmonary drug which has the potential to reach clinical trials. The long-term storage and the subsequent drying of LNPs can be improved by changing some method parameters, such as changing the bottom area of the collection vessel which is the contact point between heated glass and spray dried powder. The larger the area, the better and more evenly the powder can dry. Furthermore, I noticed that the air turbulence of the cyclone did not reach the powder in the collection vessel, hence, the drying had only an impact on the top layer of the powder. Increasing the air volume could create turbulences and dry the particles more evenly. However, exercise caution, as the siRNA cargo should not get affected and loose bioactivity. Finally, the long-term study should be expanded to at least 12 months and harsher storage conditions following ICH guidelines should be considered. These approaches should be considered for all nanoparticle characterization and efficiency studies.

Chapter IX – Appendix

A1 - Amphiphilic poly(spermine acrylamides): A new class of sophisticated non-viral vectors for pulmonary siRNA delivery

"Supplementary information"

Titration curve

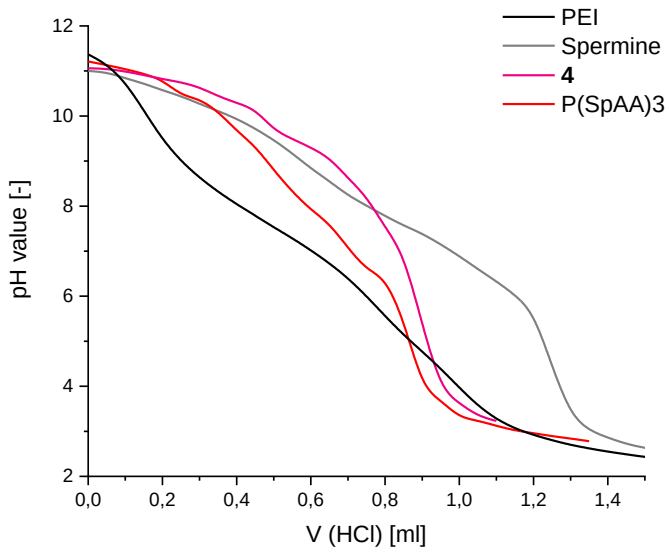

Figure S1 Titration curves of PEI, Spermine, 4 and P(SpAA)3.

CMC calculations

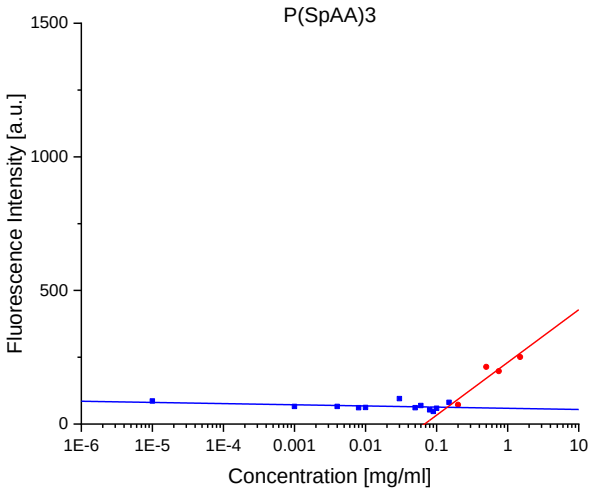

Figure S2 Determination of critical micelle concentration (CMC) of P(SpAA)3 with Nile red.

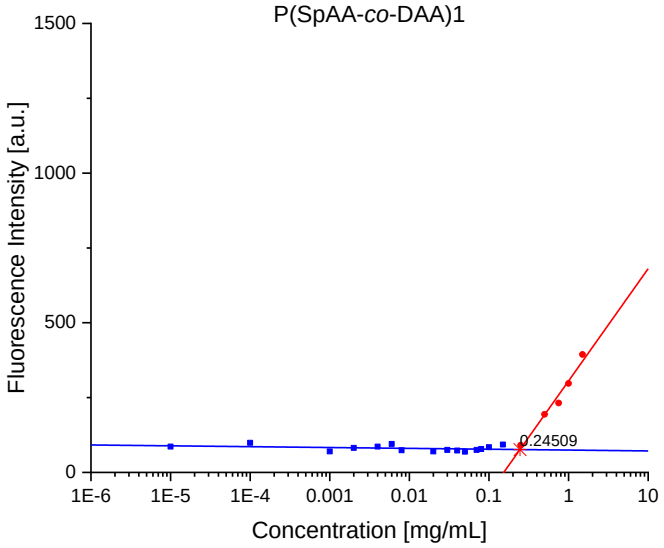

Figure S3 Determination of critical micelle concentration (CMC) of P(SpAA-co-DAA)1 with Nile red.

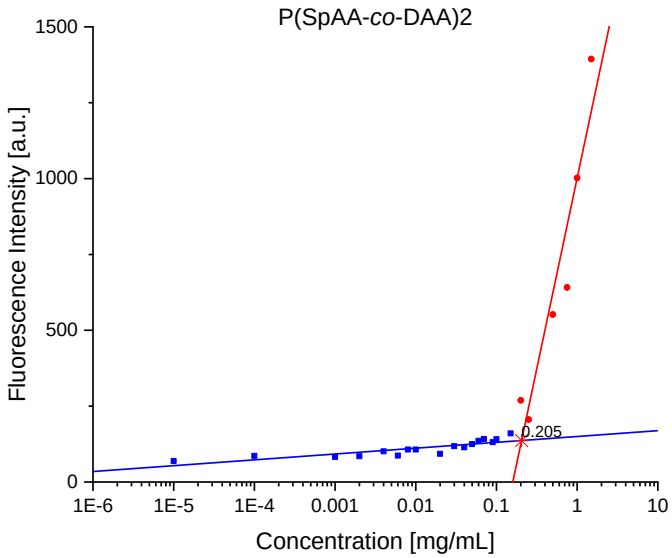

Figure S4 Determination of critical micelle concentration (CMC) of P(SpAA-co-DAA)2 with Nile red.

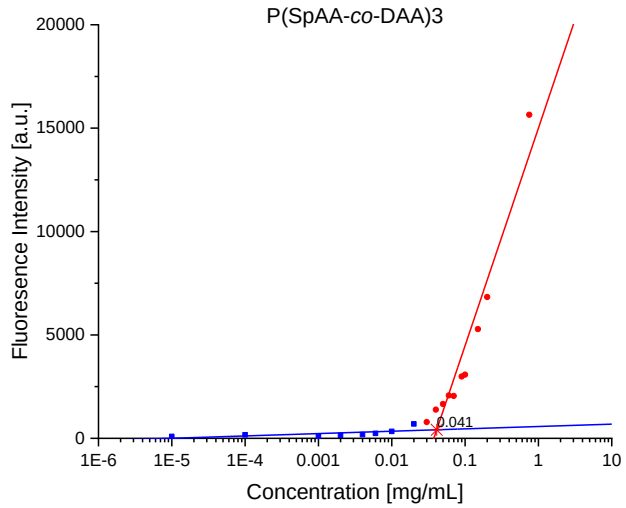

Figure S5 Determination of critical micelle concentration (CMC) of P(SpAA-co-DAA)3 with Nile red.

SYBR gold assay

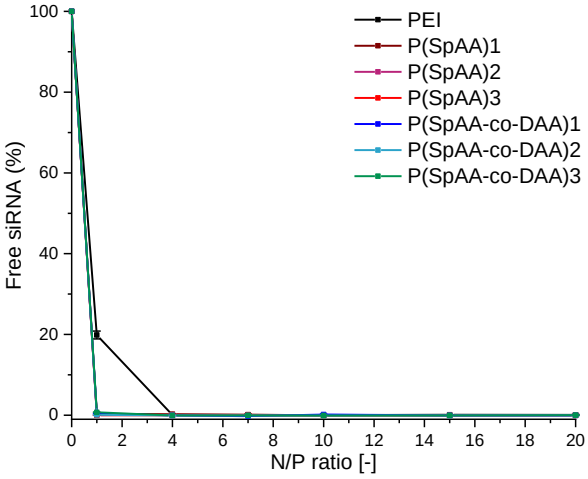

Figure S6 siRNA encapsulation profiles of polyplexes as measured by SYBR Gold assay at various N/P ratios. 100% values are represented by the determined fluorescence of uncondensed siRNA (data points indicate mean ± SD, n = 3).

Size and Zeta Potential

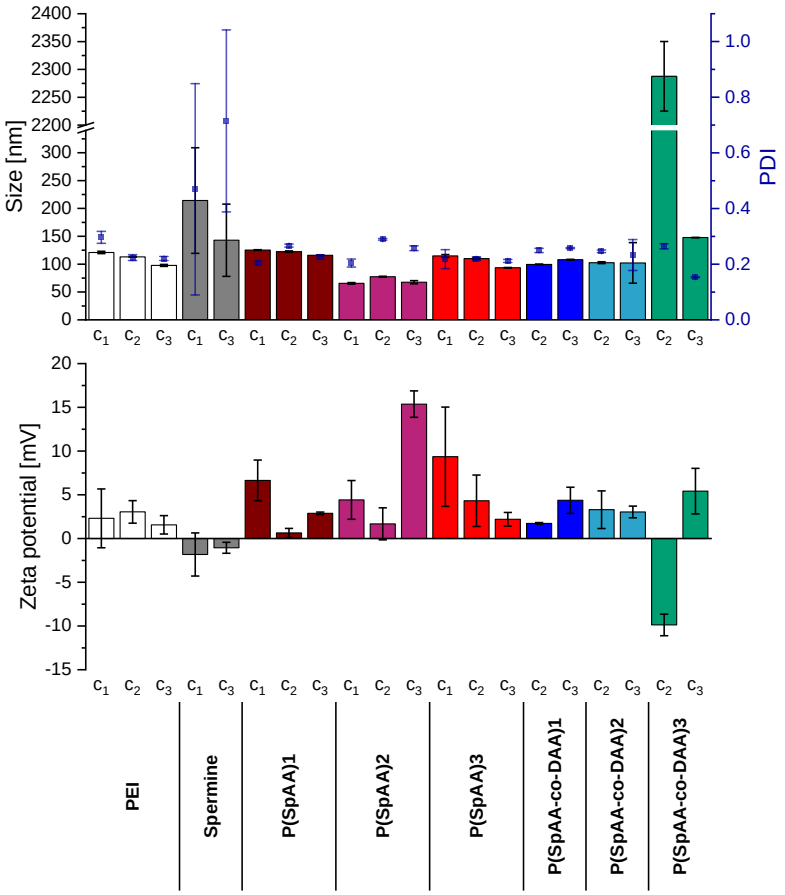

Figure S7 Dynamic light scattering and laser Doppler anemometry measurements of polyplexes formed with PEI, Spermine, P(SpAA)1-3 and P(SpAA-co-DAA)1-3. (Top) Hydrodynamic diameters (left y-axis), polydispersity indices (PDI, right y-axis) and (Bottom) zeta potentials of polyplexes at concentrations of c_1 = 5.603 µg/mL, c_2 = 7.844 µg/mL, c_3 = 11.206 µg/mL polymer representing $\mu g_{polymer}/\mu g_{siRNA}$ weight ratios of 0.67, 0.93 and 1.33 assigned to N/P ratios of 5, 7 and 10 for PEI (data points indicate mean ± SD, n = 3).

eGFP Knockdown experiments

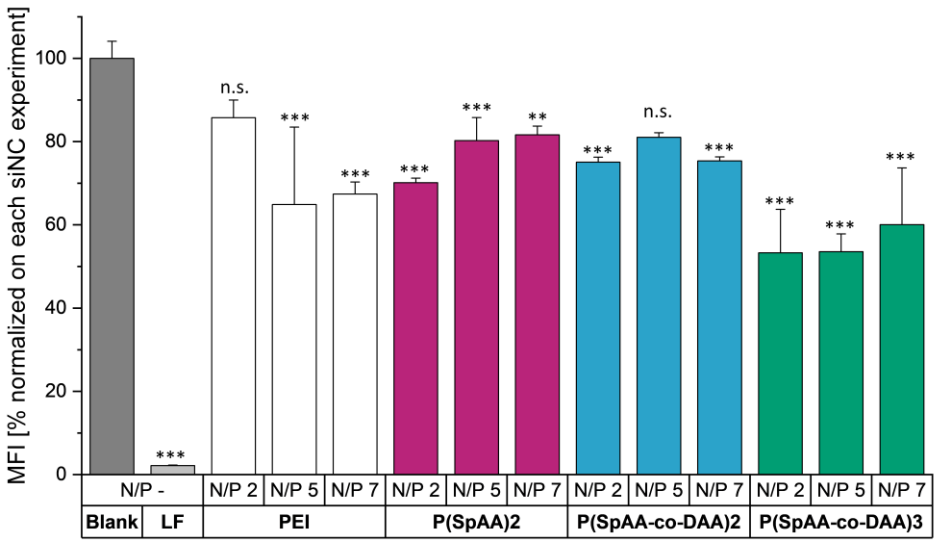

Figure S8: Enhanced green fluorescent protein (eGFP) knockdown of PEI, P(SpAA)2, P(SpAA-co-DAA)2 and P(SpAA-co-DAA)3 polyplexes in human non-small cell lung carcinoma cells expressing eGFP (H1299/eGFP) quantified by flow cytometry as median fluorescence intensity (MFI) of eGFP after transfection with polyplexes at N/P 2, 5 and 7 with eGFP siRNA (siGFP) or scrambled control siRNA (siNC) for 48 h. Blank samples consisted of H1299/eGFP untreated cells. The positive control consisted of Lipofectamine (LF) 2000 lipoplexes formulated with eGFP siRNA or scrambled control siRNA. Data given as MFI in %, normalized to each polymer/siNC experiment.

Phalloidin staining of Calu3 cells at ALI

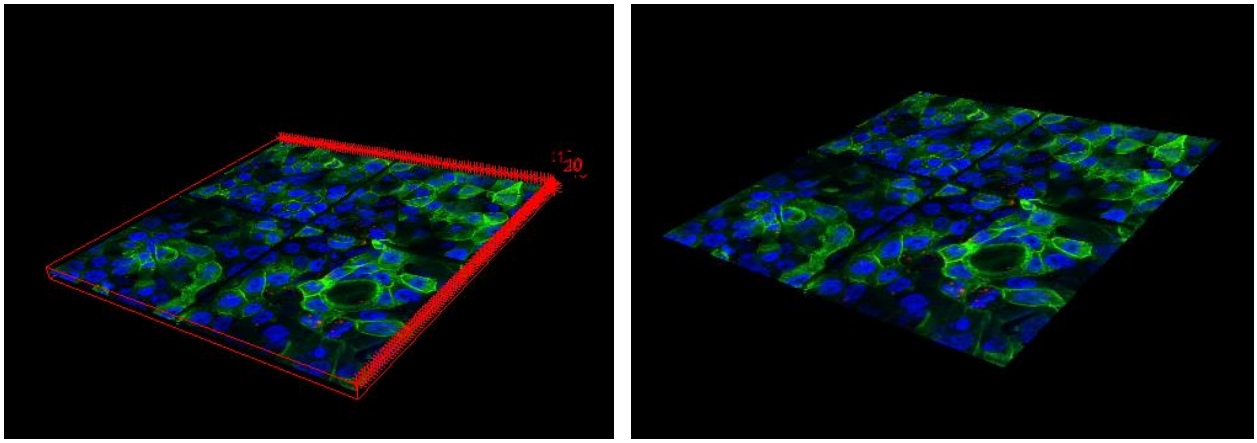

Figure S9 3D view/orthoslice of phalloidin staining of Calu3 cells at ALI. Incubation time: 24 h; Blue: DAPI (nuclei); Green: Phalloidin (cytoskeleton); Red: AF647-siRNA.

Mucus staining of Calu3 cells at ALI

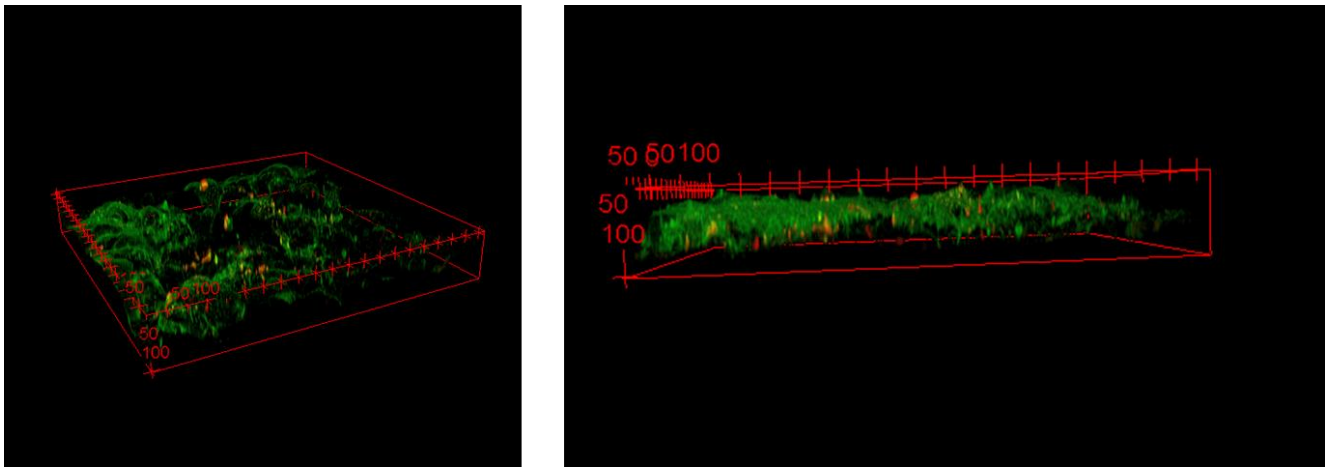

Figure S10 3D orthoslice (same picture from different angles) of mucus staining of Calu3 cells at ALI. Incubation time: 24 h; Green: WGA-AF488 staining of mucus layer; Red: AF647-siRNA.

MTT Assay

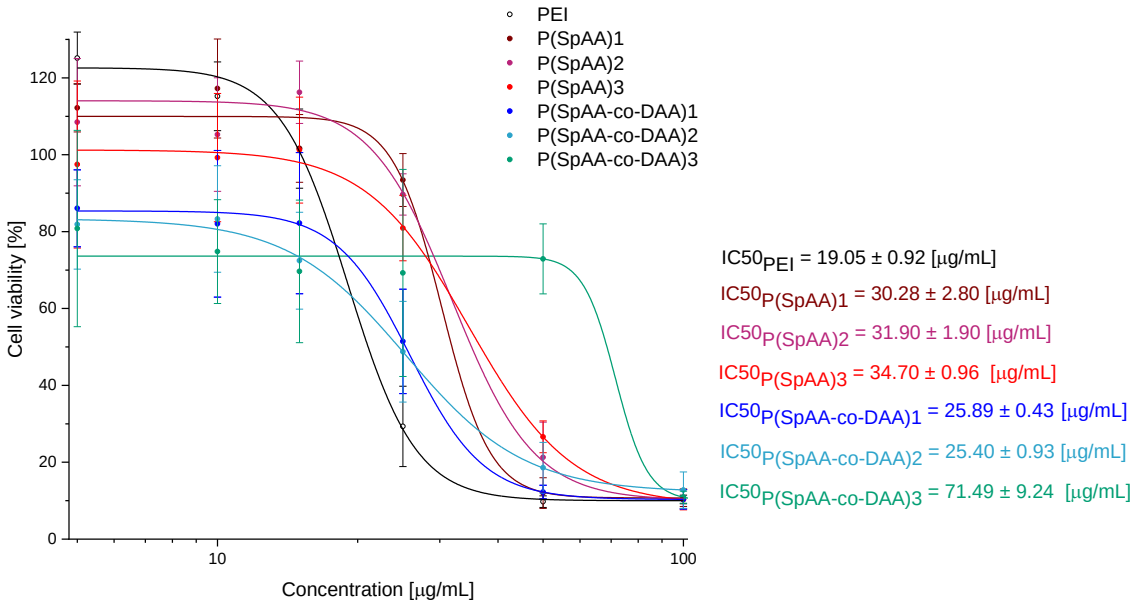

Figure S11 IC50 values of PEI, P(SpAA)1-3 and P(SpAA-co-DAA)1-3 determined by MTT assay. Cell viabilities are plotted as a function of polymer concentration. IC50 values were calculated by a sigmoidal fit. [177]

"Additional information of polymer synthesis"

General Homopolymerization Procedures:

After dissolving the calculated amount of monomer in toluene (monomer concentrations of 10 wt./vol.%), the respective equivalents of AIBN (2-10 wt.%) were added. The solution was purged with nitrogen for 20 min and then immersed in an oil bath at 65 °C. At the end of the reaction time, polymerization was stopped by cooling the reaction mixture in an ice bath. The polymers were either washed with toluene if they already precipitated during reaction or were isolated by addition of the reaction mixture to a solvent (hexane or acetonitrile), centrifugation and then the solution was decanted off, if necessary, followed by a washing step and afterwards the sample was dried in a vacuum oven at 50 °C. The structure and purity of the polymers were analyzed *via* ^{1}H NMR spectroscopy and SEC analysis in DMF or chloroform.

General Copolymerization Procedures:

After dissolving a calculated amount of NAS and DAA in toluene to obtain a concentration of 10 wt./vol.%, 10 wt.% of AIBN were added. The solution was purged with nitrogen for 20 min and then immersed in an oil bath at 65 °C. At the end of the reaction time, polymerization was stopped by cooling the reaction mixture in an ice bath. The polymers were either washed with toluene if they already precipitated during reaction (P(NAS-co-DAA)1, P(NAS-co-DAA)2) or precipitated and washed by addition of the reaction mixture to hexane ((P(NAS-co-DAA)3) followed by centrifugation and an additional washing step. The solvent was decanted off and the sample was dried in a vacuum oven at 50 °C. The structure, purity, and ratio of the two monomer units were analyzed *via* ^{1}H NMR spectroscopy. In case of P(NAS-co-DAA)1 and P(NAS-co-DAA)2 deuterated DMSO was used as solvent, due to insolubility of the NAS subunit in deuterated chloroform. The ratio of NAS/DAA was calculated by using the methyl group signal of DAA (δ = 0.8 ppm) and the signal at 2.8 ppm assigned to 4 protons of NAS (see ^{1}H NMR spectra of P(NAS) homopolymers). NMR spectra for P(NAS-co-DAA)3 were measured in $CDCl_3$ and the ratio of NAS/DAA was calculated by using the methyl group signal of DAA (δ = 0.8 ppm) and the signal at 2.8 ppm assigned to 4 protons of NAS (see ^{1}H NMR spectra of P(NAS) homopolymers). The number average molecular weight (M_n) and molecular weight distribution (Đ) were determined by GPC analysis in DMF relative to PMMA standards.

General Post-Polymerization Procedures:

Synthesis of P(Tri-Boc spermine acrylamide)

To a solution of one equivalent of the obtained P(NAS) in DMF (4 mL) at 60 °C, one equivalent of tri-Boc spermine dissolved in DMF (2 mL) was added dropwise and stirred overnight. The solvent was removed *in vacuo*, then chloroform (20 mL) and concentrated NH_3 (aq.) (20 mL) were added to the residue and the reaction mixture was stirred for 2 h at room temperature. The separation of the phases was performed *via* centrifugation and the aqueous phase was decanted off. The organic phase was washed with water (1 x 40 mL) and brine (1 x 40 mL), dried over magnesium sulfate, and filtered. The solvent was removed *in vacuo* until about 4 mL of reaction mixture were left. The polymers were precipitated by addition of the reaction mixture to hexane, followed by centrifugation. The solvent was decanted off, if necessary, followed by a washing step. The product was further dried in a vacuum oven at 50 °C and if necessary, residual solvent was removed by freeze-drying from benzene overnight. The structure and purity of the polymers were analyzed *via* ^{1}H NMR spectroscopy. The number average molecular weight (M_n) and molecular weight distribution (Đ) were determined by GPC in DMF.

Synthesis of P(TBSpAA-co-DAA).

To a solution of the obtained P(NAS-co-DAA) in DMF (5 mL) at 40 °C, Tri-boc spermine (TBSp) (one equivalent with regard to the NAS repeating unit) dissolved in DMF (4 mL) was added dropwise and the reaction mixture was stirred overnight. The solvent was removed *in vacuo*, then chloroform (20 mL) and concentrated NH_3 (aq.) (20 mL) were added to the residue and the reaction mixture was stirred for 2 h at room temperature. The separation of the phases was performed *via* centrifugation and the aqueous phase was decanted off. The organic phase was washed with water (1 x 40 mL) and brine (1 x 40 mL), dried over magnesium sulfate and filtered. The solvent was removed *in vacuo* until about 4 mL of solvent were left. The polymers were isolated by addition of the reaction mixture to hexane, centrifugation and then the solvent was decanted off. The product was dried in a vacuum oven at 50 °C and if necessary, residual solvent was removed by freeze-drying from benzene overnight. The structure, purity and subunit ratio were analyzed *via* ^{1}H NMR spectroscopy in $CDCl_3$. The ratio of TBSpAA/DAA was calculated by using the methyl group signal of DAA (δ = 0.8 ppm) and the broad signal at 3.0 ppm consisting of 2 protons of DAA and 12 protons of TBSpAA (see ^{1}H NMR spectra of P(TBSpAA) homopolymers). Number average molecular weights (M_n) and molecular weight distributions (Đ) were determined by GPC in DMF relative to PMMA standards.

General Deprotection Procedures:

Deprotection of P(Tri-Boc spermine acrylamide).

Trifluoro acetic acid (2 mL) was added at room temperature to the respective Boc-protected polymer in one portion. The reaction mixture was stirred for 2 h at room temperature. The polymers were isolated by addition of the reaction mixture to hexane or diethyl ether, centrifugation and then the solution was decanted off, if necessary, followed by a washing step. Subsequently, the polymers were dissolved in water, filtered (1 µm PES-syringe filter) and freeze-dried from water. The structure and purity of the TFA-salts of the polymers were analyzed *via* ^{1}H NMR spectroscopy in D_2O.

Deprotection of P(TBSpAA-co-DAA).

TFA (2 mL) was added to the obtained P(TBSpAA-co-DAA) polymers at room temperature. The reaction mixture was stirred for 2 h at room temperature. The polymers were precipitated by addition of the reaction mixture to diethyl ether followed by centrifugation. The solvent was decanted off and the polymers were dissolved in water and filtered (1 µm PES syringe filter). After freeze-drying from water, the structure and purity and ratio of SpAA/DAA were calculated *via* ^{1}H NMR spectroscopy in D_2O of the TFA salts of the polymers. The ratio of SpAA/DAA was calculated by using the methyl group signal of DAA (δ = 0.8 ppm) and the broad signal at 3.0 ppm consisting of 2 protons of DAA and 12 protons of SpAA (see ^{1}H NMR spectra of P(SpAA) homopolymers).

Calculation of the Protonable Unit:

The protonable unit of the homopolymers was calculated by dividing the mass of the repeating unit by the number of protonable primary and secondary amines present in the polymer.

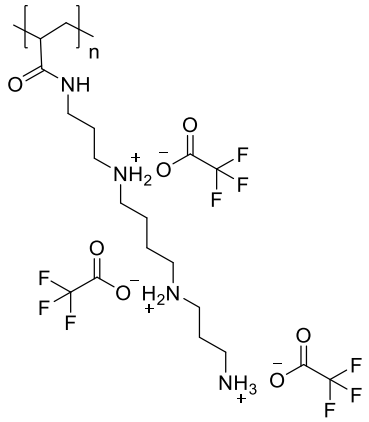

P(SpAA)

M_n = 598.46 g/mol
$M_{protonable\ unit}$ = 199.49 g/mol

Figure A1 Structure and protonable unit of P(SpAA) 1-3.

The protonable unit of the different copolymers is calculated using the ratio of the two repeating units and the number of protonable primary and secondary amines present in the polymer.

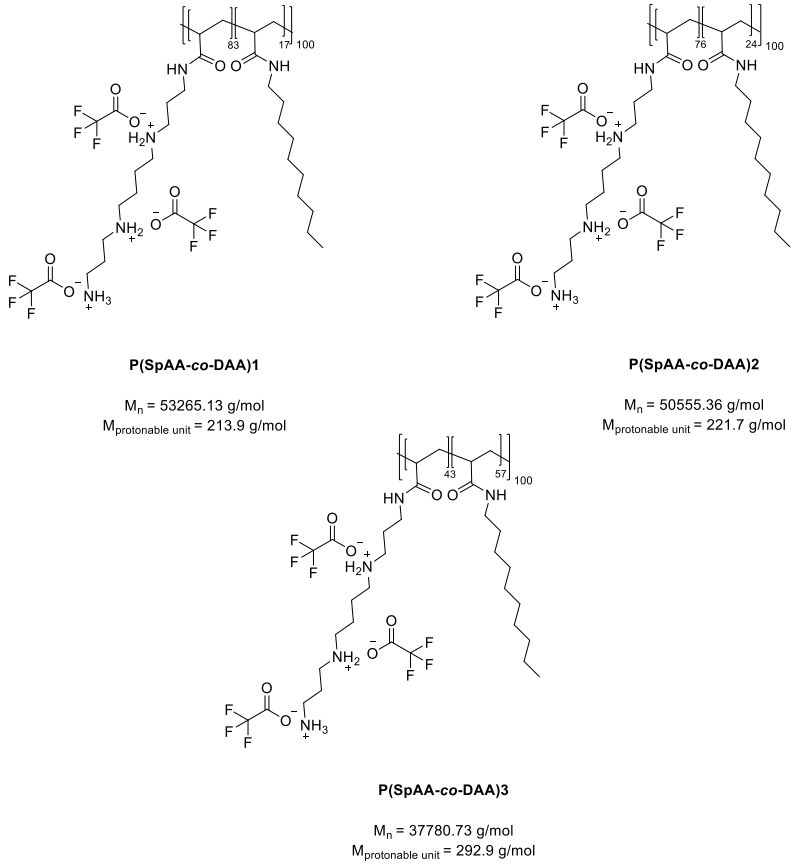

P(SpAA-*co*-DAA)1

M_n = 53265.13 g/mol
$M_{protonable\ unit}$ = 213.9 g/mol

P(SpAA-*co*-DAA)2

M_n = 50555.36 g/mol
$M_{protonable\ unit}$ = 221.7 g/mol

P(SpAA-*co*-DAA)3

M_n = 37780.73 g/mol
$M_{protonable\ unit}$ = 292.9 g/mol

Figure A2 Structure and protonable unit of P(SpAA-co-DAA) 1-3.

Monomer reactivity ratios of NAS and DAA.

After dissolving varying ratios of NAS and DAA (10:90 → 90:10; overall 0.594 mmol) in toluene (0.5 mL), AIBN (0.2 M in toluene; 17.8 µL, 0.6 mol%) was added. Each reaction mixture was stirred for 2 min at 60 °C, then the polymerization was stopped by adding hydroquinone as a radical scavenger. The conversion of both monomers was determined *via* ^{1}H NMR spectroscopy in $CDCl_3$. If conversion was below 10%, polymerization time, initial feed monomer composition, and final copolymer composition were used for determination of reactivity ratios by Fineman−Ross technique. [394]

The Fineman-Ross equations (*Equation (1)* and *Equation (2)*) were used to calculate the reactivity ratios of a NAS or DAA-polymer chain ends towards reaction with an NAS or DAA monomer,

$$\frac{F}{f}(f-1) = r_1\frac{F^2}{f} - r_2 \quad (1)$$

$$\frac{f-1}{F} = -r_2\frac{f}{F^2} + r_1 \quad (2)$$

in which F is the monomer ratio in feed ($F = M_1/M_2$; NAS (M_1) and DAA (M_2)) and f is the monomer ratio in the polymer ($f = m_1/m_2$; NAS (m_1) and DAA (m_2)). Furthermore, r_1 and r_2 are the reactivity ratios of NAS and DAA, respectively. The monomer reactivity ratios are given by $r_1 = k_{11}/k_{12}$ and $r_2 = k_{22}/k_{21}$.

The reactivity ratios are obtained from calculating the slopes by plotting (F^2/f) against ($F/f)(f-1$) and (f/F^2) against ($f-1)/F$ for the determination of r_1 and r_2, respectively (Figure 1). [395]

Characterization and synthesis of 1-4

N-Acryloxysuccinimide (NAS) (1): [396]

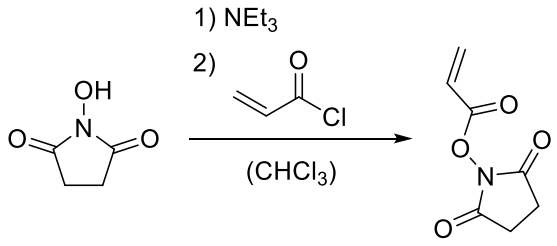

1

$C_7H_7NO_4$
169.14 g/mol

N-Hydroxysuccinimide (5.30 g, 46.0 mmol, 1.00 eq.) was dissolved in 60 ml chloroform. Triethylamine (7.30 mL, 52.6 mmol, 1.15 eq.) was added, the solution was cooled to 0 °C and acryloyl chloride (4.25 mL, 52.6 mmol, 1.15 eq.) was added dropwise. After stirring for 4 h at room temperature, the resulting reaction mixture was extracted with water (2 x 50 mL), the organic phase was dried over anhydrous $MgSO_4$, filtered and concentrated *in vacuo*. After recrystallization from hexane/EtOAc (8:1), the product was obtained as a colorless crystalline substance (5.26 g, 71%).

^{1}H NMR (400 MHz, $CDCl_3$, 298 K): δ (ppm) = 6.69 (dd, J = 17.3, 0.9 Hz, 1H, H_{Alkene}), 6.32 (dd, J = 17.3, 10.7 Hz, 1H, H_{Alkene}), 6.16 (dd, J = 10.7, 0.9 Hz, 1H, H_{Alkene}), 2.85 (s, 4H, H_{NHS}).

^{13}C NMR (101 MHz, $CDCl_3$, 298 K): δ (ppm) = 169.2, 161.2, 136.3, 123.1, 25.7.

EA: calculated: C 49.71 H 4.17 N 8.29

found: C 49.65 H 4.19 N 8.34

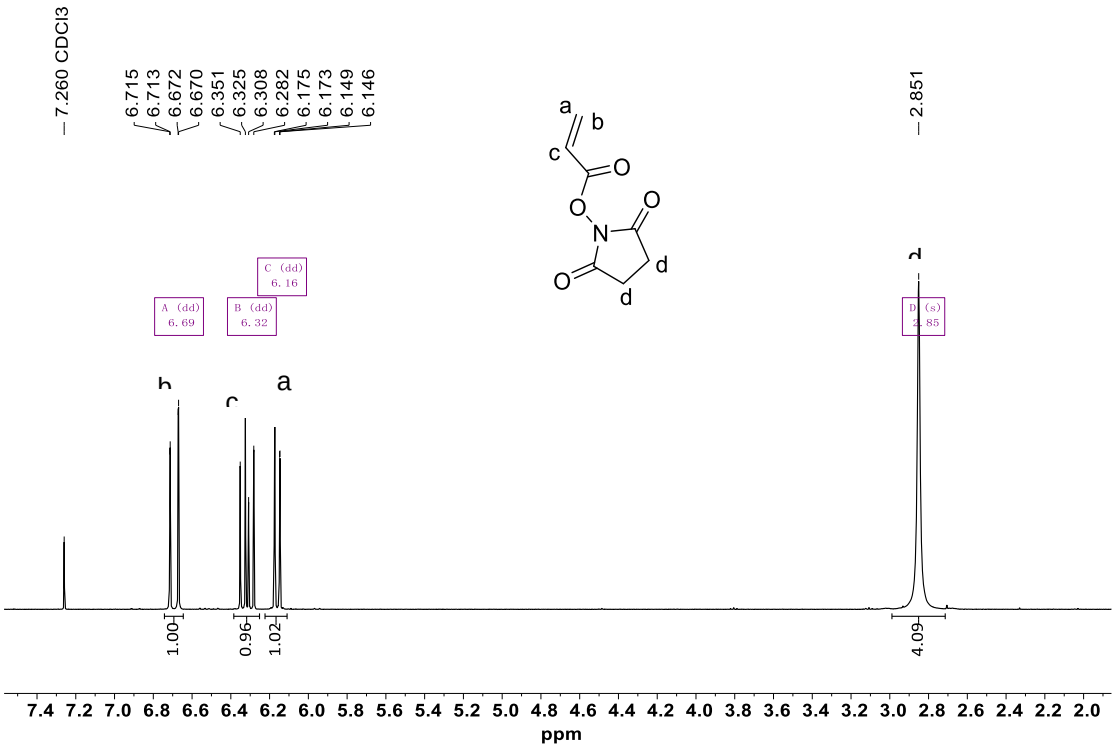

Figure A3 ^{1}H-NMR spectrum of NAS (1) in $CDCl_3$ (400 MHz).

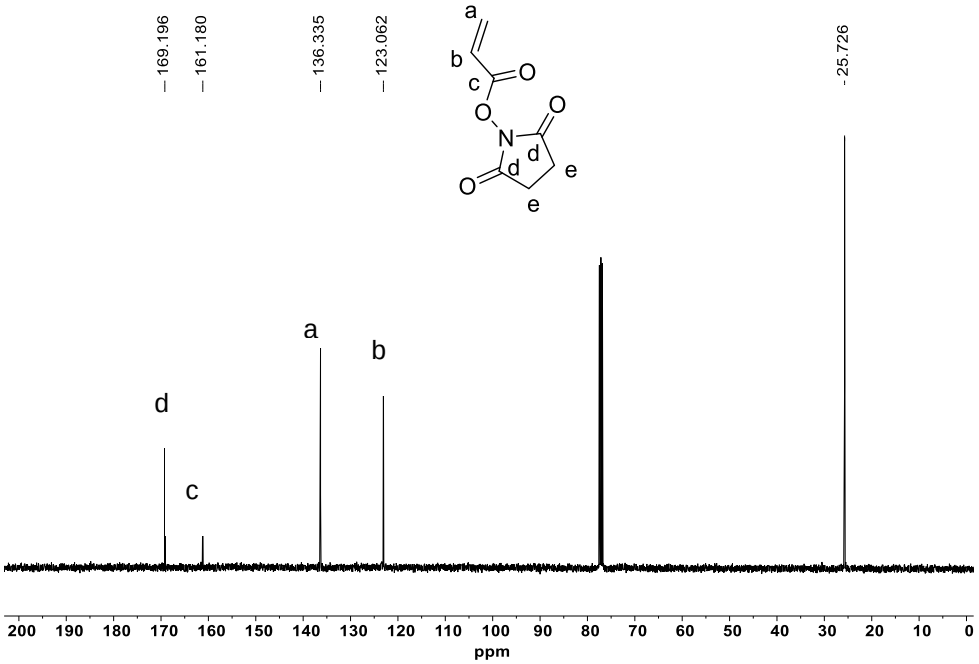

Figure A4 ^{13}C-NMR spectrum of NAS (1) in $CDCl_3$ (101 MHz).

N-Decylacrylamide (DAA)(2): [256]

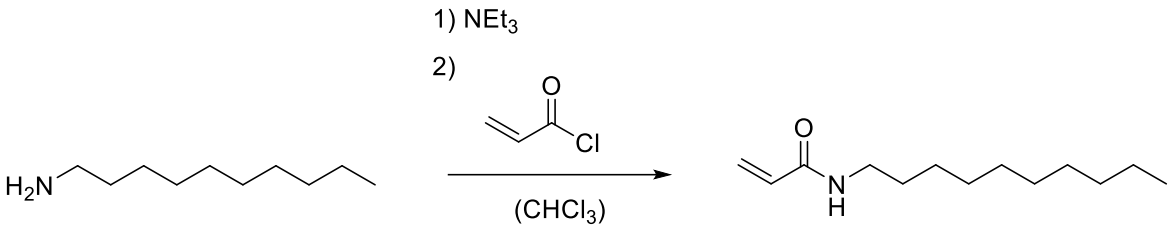

2
$C_{13}H_{25}NO$
211.35 g/mol

N-Decylamine (8.00 g, 50.9 mmol, 1.00 eq.) was dissolved in 50 ml chloroform. Triethylamine (7.75 mL, 55.9 mmol, 1.10 eq.) was added, the solution was cooled to 0 °C and acryloyl chloride (4.52 mL, 55.9 mmol, 1.10 eq.) was added dropwise. After stirring for 1 h at 0 °C and 4 h at room temperature, the resulting reaction mixture was extracted with saturated NH_4Cl aqueous solution (1 x 40 mL) and saturated NaCl aqueous solution (1 x 40 mL), the organic phase was dried over anhydrous $MgSO_4$, filtered and concentrated *in vacuo*. After recrystallization from heptane, the product was obtained as a colorless crystalline substance (7.02 g, 65%).

^{1}H NMR (400 MHz, $CDCl_3$, 298 K): δ (ppm) = 6.25 (dd, J = 17.0, 1.5 Hz, 1H, H_{Alkene}), 6.08 (dd, J = 17.0, 10.3 Hz, 1H, H_{Alkene}), 5.81 – 5.68 (broad, 1H, NH), 5.61 (dd, J = 10.3, 1.5 Hz, 1H, H_{Alkene}), 3.34 – 3.28 (m, 2H, C*H*$_2$-NH-C(O)), 1.52 (p, 2H, CH_2), 1.32 – 1.21 (m, 14H, CH_2), 0.87 (t, 3H, CH_3).

^{13}C NMR (101 MHz, $CDCl_3$, 298 K): δ (ppm) = 165.7 (C=O), 131.1 (CH=), 126.2 (CH_2=), 39.8 (CH_2N), 32.0 (CH_2), 29.6 (2xCH_2), 29.4 (2xCH_2), 27.1 (CH_2), 22.7 (CH_2), 14.2 (CH_3).

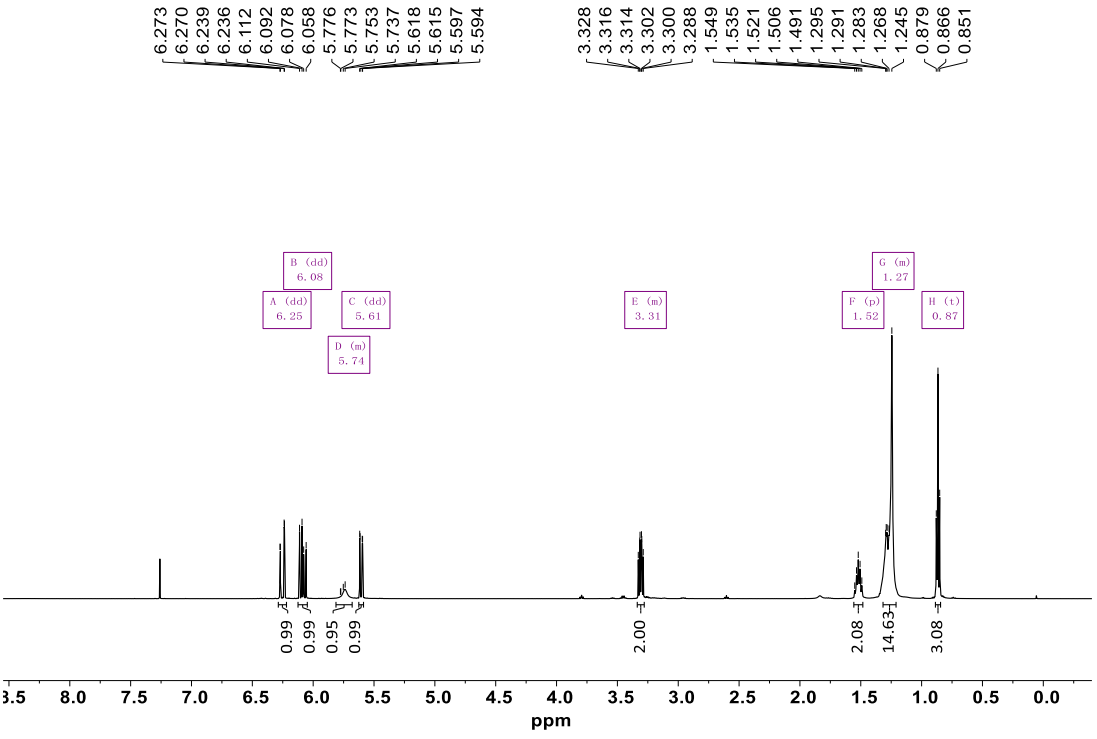

Figure A5 ^{1}H-NMR spectrum of DAA (2) in $CDCl_3$ (400 MHz).

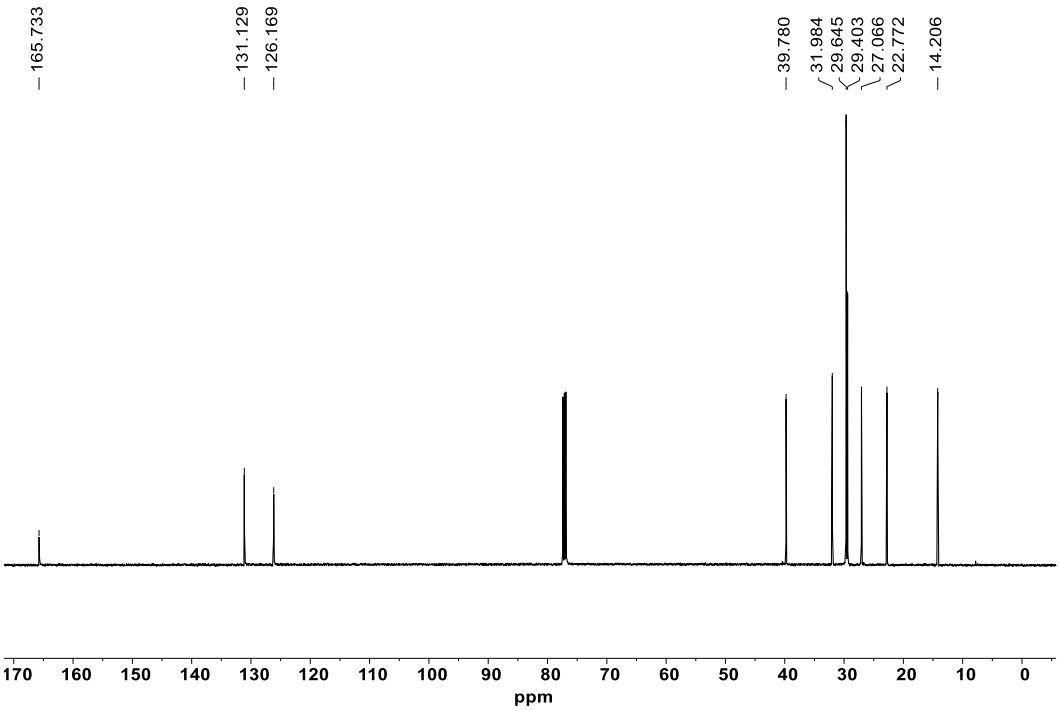

Figure A6 ^{13}C-NMR spectrum of DAA (2) in $CDCl_3$ (101 MHz).

Tri-boc spermine (TBSp) (3): [397]

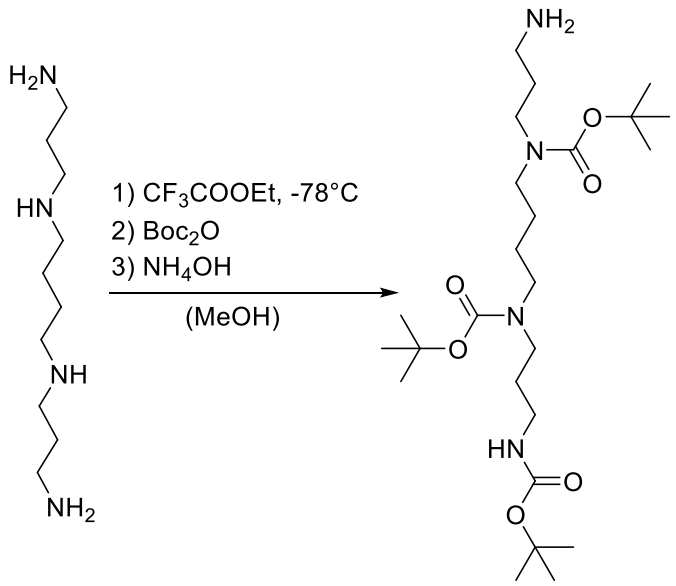

3

$C_{25}H_{50}N_4O_6$
502.70 g/mol

Spermine (4.00 g, 19.8 mmol, 1.0 eq) was dissolved in anhydrous MeOH (250 mL). The solution was cooled down to –78°C and 2.81 g Ethyltrifluoroacetate (2.35 mL, 19.8 mmol, 1.0 eq) were added dropwise. Afterwards, the reaction mixture was stirred at –78°C for 1 h and then at 0°C for 1 h. Di-tert-butyl dicarbonate (17.3 g, 79.1 mmol, 4.0 eq) was dissolved in 50 mL MeOH and added to the solution. After stirring for one day at room temperature, the pH was increased to 11 with concentrated aqueous ammonia and the solution was stirred at room temperature overnight. The solvent was removed under reduced pressure and the crude was purified via column chromatography (SiO_2, CH_2Cl_2/MeOH/$NH_{3,aq}$ = 70:10:1 to 50:10:1) to obtain the desired tri-boc spermine **3** as a colorless viscous oil (4.80 g, 9.54 mmol, 48%).

R_f = 0.27 (SiO_2, $KMnO_4$, CH_2Cl_2/MeOH/NH_3 = 10:1:0.1).

^{1}H NMR (500 MHz, $CDCl_3$, 298 K): δ (ppm) = 3.32 – 2.90 (m, 10H, 5xCH_2N), 2.80 (s, 2H, CH_2), 1.78 (s, 2H, CH_2), 1.55 (s, 2H, CH_2), 1.49 – 1.19 (m, 31H, 2xCH_2, 9x$CH_{3,Boc}$).

HR-MS (ESI+): Calculated: m/z 503.38086 ($C_{25}H_{51}O_6N_4$ $[M+H]^+$)

Found: m/z 503.38026

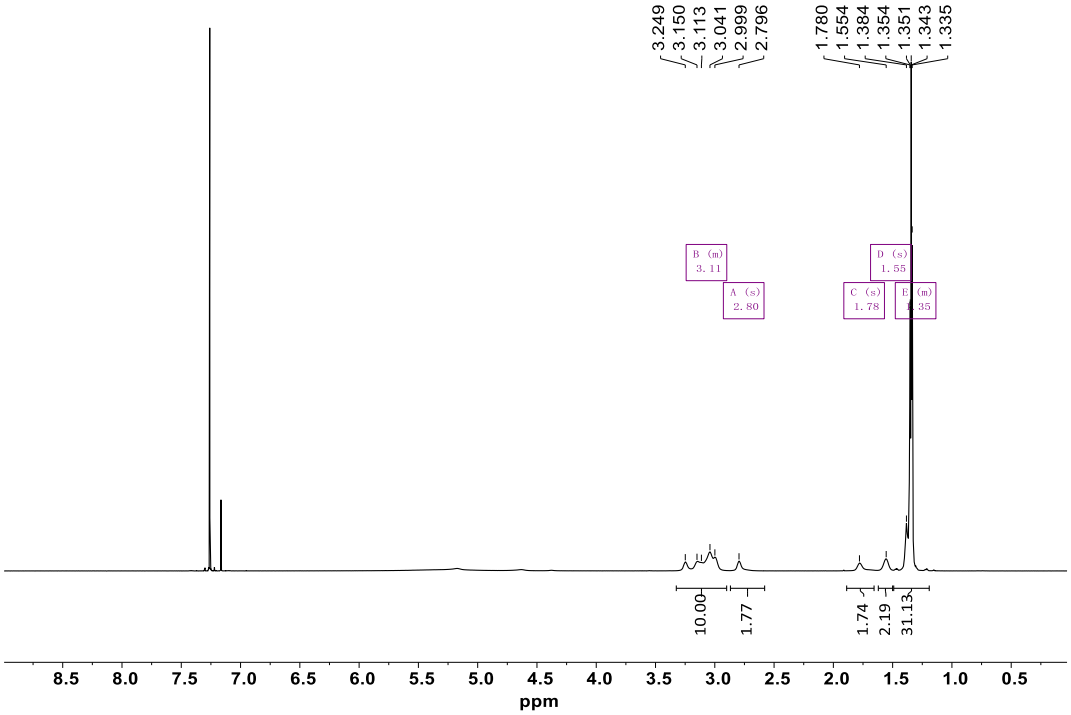

Figure A7 ^{1}H-NMR spectrum of TBSp (3) in $CDCl_3$ (400 MHz).

Propionyl-spermine TFA-salt (4)

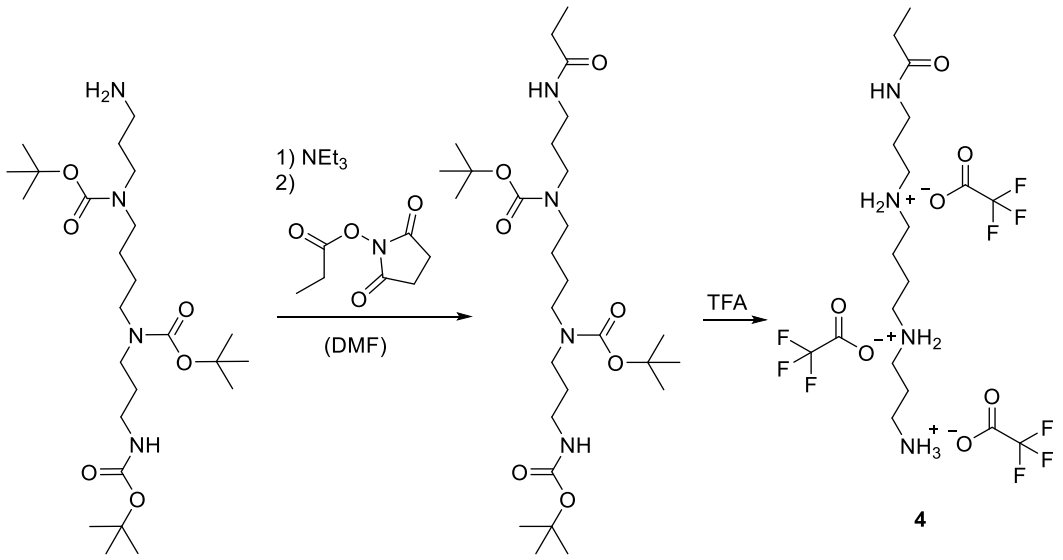

Tri-boc spermine **3** (410 mg, 0.82 mmol, 1.0 eq.) was dissolved in 5 ml anhydrous dimethylformamide and 0.32 mL triethylamine (330 mg, 3.26 mmol, 4.0 eq.) were added. 140 mg propionyl-NHS ester (0.82 mmol, 1.0 eq.) in 0.8 mL dimethylformamide were slowly added to the reaction mixture at room temperature. After stirring for 4 h, the solvent was evaporated and the crude product was purified via column-chromatography (SiO_2, CH_2Cl_2/MeOH/$NH_{3,aq}$ = 4:1:0.1) to obtain propionyl tri-boc spermine.

^{1}H NMR (500 MHz, $CDCl_3$, 298 K): δ (ppm) = 3.28 – 2.94 (m, 12H), 2.15 (q, J = 7.6 Hz, 2H), 1.58 (s, 4H), 1.38 (m, 31H), 1.09 (t, J = 7.6 Hz, 3H).

ESI-MS (Acetonitrile/H_2O): 581.4 $[M+Na]^+$

Propionyl tri-boc spermine is treated with 2 mL trifluoroacetic acid for 2 hours at room temperature. The reaction mixture is precipitated from diethyl ether and freeze-dried from water to give propionyl spermine **4** as a colorless powder.

^{1}H NMR (400 MHz, D_2O, 298 K): δ (ppm) = 3.28 (t, J = 6.7 Hz, 2H), 3.18 – 2.97 (m, 10H), 2.25 (q, J = 7.7 Hz, 2H), 2.14 – 2.01 (m, 2H), 1.88 (dq, J = 8.4, 6.9 Hz, 2H), 1.76 (p, J = 3.5 Hz, 4H), 1.09 (t, J = 7.7 Hz, 3H).

^{13}C NMR (101 MHz, D_2O, 298 K): δ (ppm) = 178.6 (NH-C=O), 162.9 (q, J = 35.6 Hz, F_3CC(O)=O), 116.3 (q, J = 291.5 Hz, F_3CC(O)=O), 46.9, 46.8, 44.9, 44.4, 36.4, 35.8, 29.0, 25.6, 23.7, 22.7, 9.5.

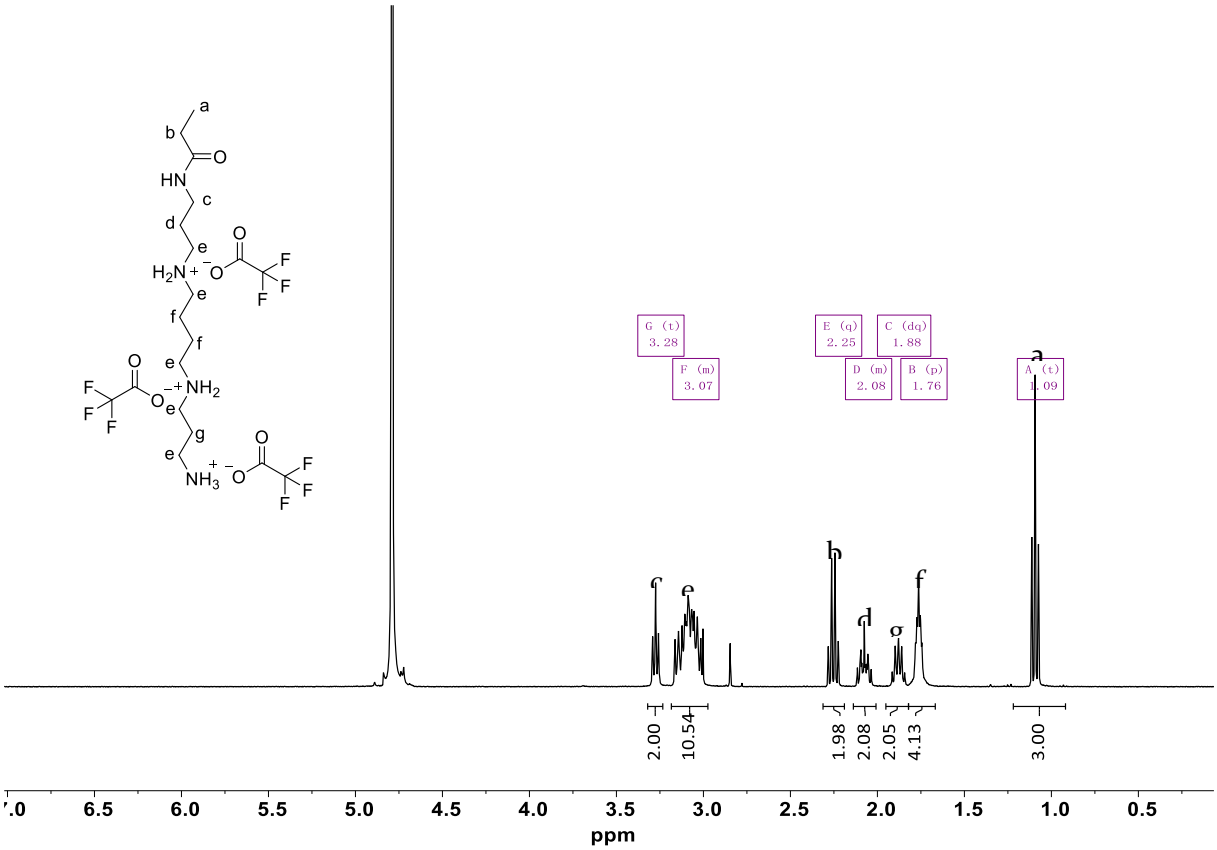

Figure A8: ^{1}H-NMR spectrum of 4 in D_2O (400 MHz).

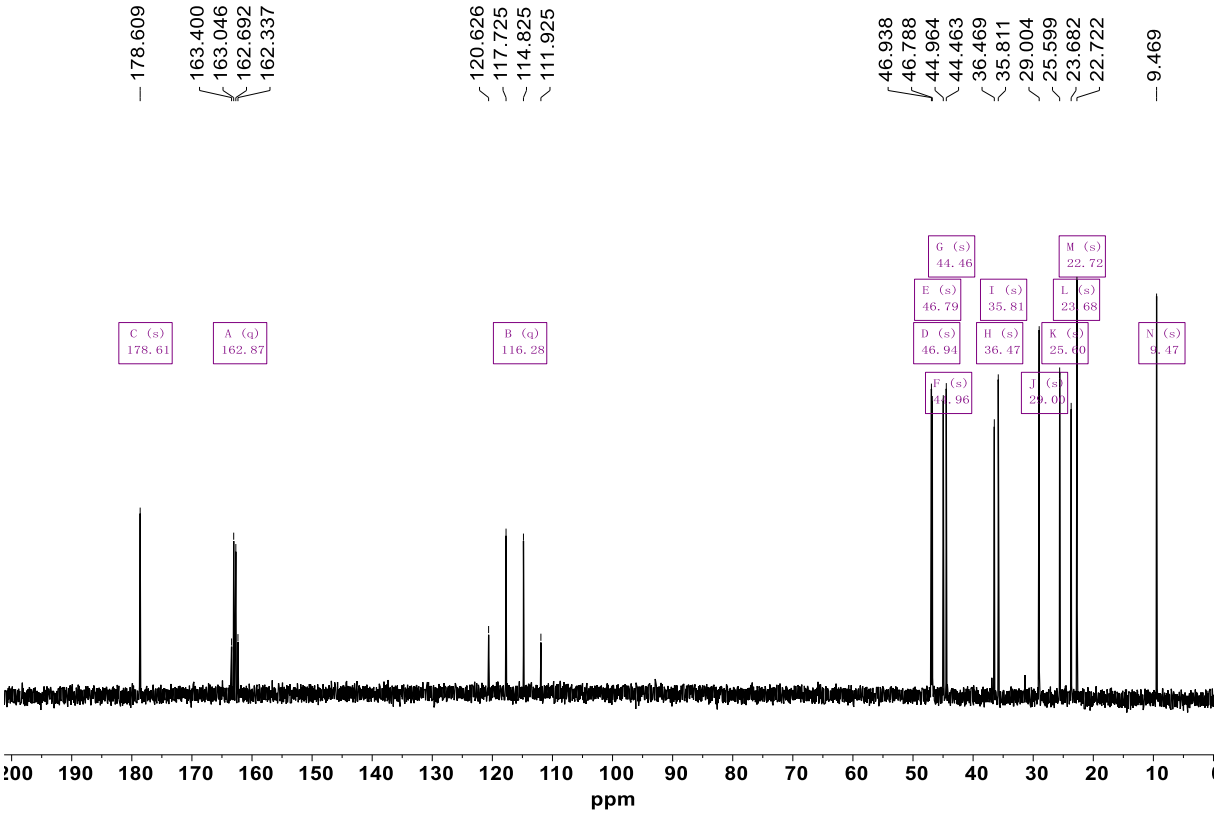

Figure A9 ^{13}C-NMR spectrum of 4 in D_2O (101 MHz)

(Co)polymerization of NAS and DAA

Synthesis of 1-3

Monomers N-acryloxysuccinimide 1 (NAS) and N-decylacrylamide 2 (DAA) were synthesized starting from acryloyl chloride, triethylamine and N-hydroxysuccinimide or N-decylamine, respectively, using modified literature procedures. [256, 396] Both monomers were isolated as pure products in good yields (71% NAS, 65% DAA, see Supporting Information).

To use spermine as a functional molecule, tri-boc spermine 3 (TBSp) which bears only one reactive primary amine was synthesized using orthogonal protection group chemistry in an adapted literature procedure. [397] Such a complex synthesis route is mandatory to prevent possible unwanted side reactions and to facilitate reaction of solely one amine group per spermine during post-polymerization functionalization. In brief, the first step selectively protected one of the primary amines with ethyl trifluoroacetate at -78 °C. The remaining free amine groups were protected using di-tert-butyl dicarbonate (Boc2O). Increasing the pH of the reaction mixture to 11 led to selective deprotection of the acetate-protected amine followed by purification via column chromatography resulting in pure 3 as a colorless oil in moderate yield (48% yield).

Free radical polymerization of NAS and DAA

Polymerization studies

The endogenous molecule spermine seems to have great potential in encapsulating siRNA and therefore, presents a promising non-viral gene delivery agent. In order to increase its molecular weight, spermine homo- and copolymers were synthesized via free radical polymerization (FRP). Using NAS as a precursor monomer and DAA as the hydrophobic unit, these monomers were employed in FRP using azobisisobutyronitrile (AIBN) as polymerization initiator to evaluate the general activities, yields, molar masses, polydispersities, and microstructures of the isolated poly(N-acryloxysuccinimide) (P(NAS)) and poly(N-decylacrylamide) (P(DAA)) homo- and copolymers (Scheme A1). NAS polymerization was conducted over night at 65 °C in toluene using monomer concentrations of 10 wt./vol.% in the presence of varying amounts of AIBN (2-10 wt.%) as the radical starter. No clear correlation between weight ratio of AIBN and molecular weight during polymerization was observed (Table A1). As expected for FRP and due to precipitation of the polymer during polymerization, the obtained P(NAS) polymers 1-3 showed molar masses between 12.6 kg/mol and 20.0 kg/mol and broad molecular weight distributions ($3.43 \leq Đ \leq 3.57$) measured via size-exclusion chromatography (SEC). All polymers were isolated in good yields (84 – 97%). A similar procedure was used for DAA polymerization. Using 2 wt.% AIBN, P(DAA) with a molar mass of 23.7 kg/mol and a polydispersity of 2.02 was synthesized. Additionally, copolymers with varying ratios of NAS and DAA were synthesized by simple modulation of the monomer feed by preaddition mixing of different NAS/DAA ratios using 10 wt.% AIBN and a total monomer concentration of 10 wt./vol.%. Different ratios of NAS and DAA contents were obtained in the copolymers P(NAS-co-DAA) 1-3 ranging from 90 mol% NAS to 50 mol% NAS (Table A1). 1H NMR spectroscopy verified the successful polymerization since all signals of the NAS and DAA repeating units agree with those of the obtained homopolymers P(NAS) and P(DAA) (Figures A10 and A15). It was possible to exactly tune the composition of the copolymer through the monomer feed as the ratios of the two monomers in the feed and in the polymer were nearly identical (Table A1). DOSY NMR studies were used to confirm the successful linkage between the NAS and the DAA monomers and to exclude the formation of two separate homopolymers. DOSY NMR spectra of P(NAS-co-DAA)2 showed only one set of signals assigned to the diffusion coefficient for the copolymer (Figure A18). Molar masses and polydispersities were calculated via SEC in DMF relative to polystyrene standards. Compared to homopolymerizations, the shift in molecular weight of the copolymers with increasing DAA content can either be attributed to higher molecular weights or to different hydrodynamic radii of

DAA containing polymers. To further understand the comonomer sequence distribution and the compositional drift of the copolymers, since material properties strongly correlate to the molecular structure of copolymers, a series of reactions with different monomer feed ratios was performed. Fineman-Ross technique was used to determine the monomer reactivity ratios of NAS (r1 (rNAS)) and DAA (r2 (rDAA)) in copolymerizations (Figure A10). [394]

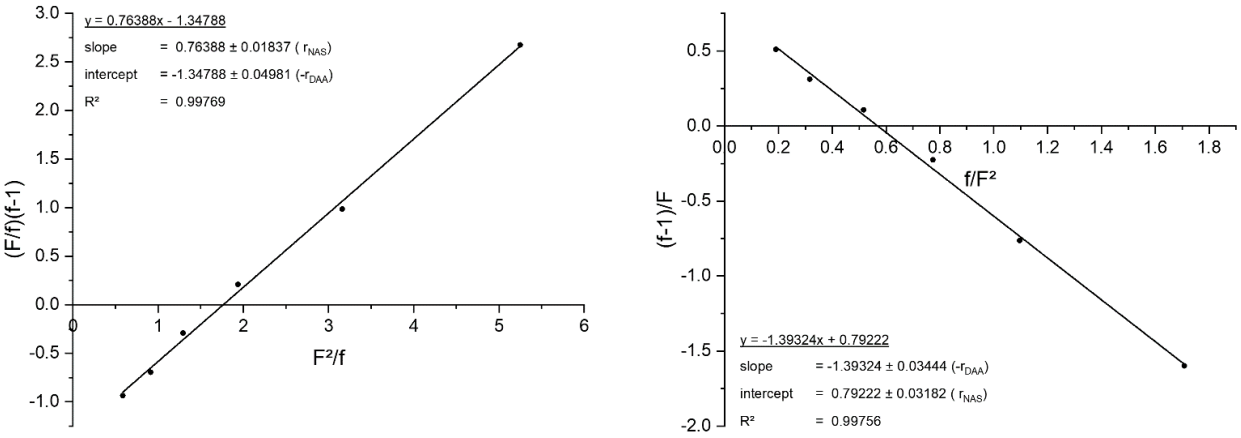

Figure A10 Determination of copolymerization reactivity ratios according to Fineman-Ross technique

r1 (rNAS) was calculated as 0.76, showing a minor preference for cross-propagation, whereas r2 (rDAA) had a value of 1.39, indicating a preference for homopropagation. As a consequence, a compositional drift from DAA to NAS occurred. If higher fractions of DAA are incorporated in the initial stage of the copolymerization, this molecular structure could be beneficial for amphiphilic material properties.

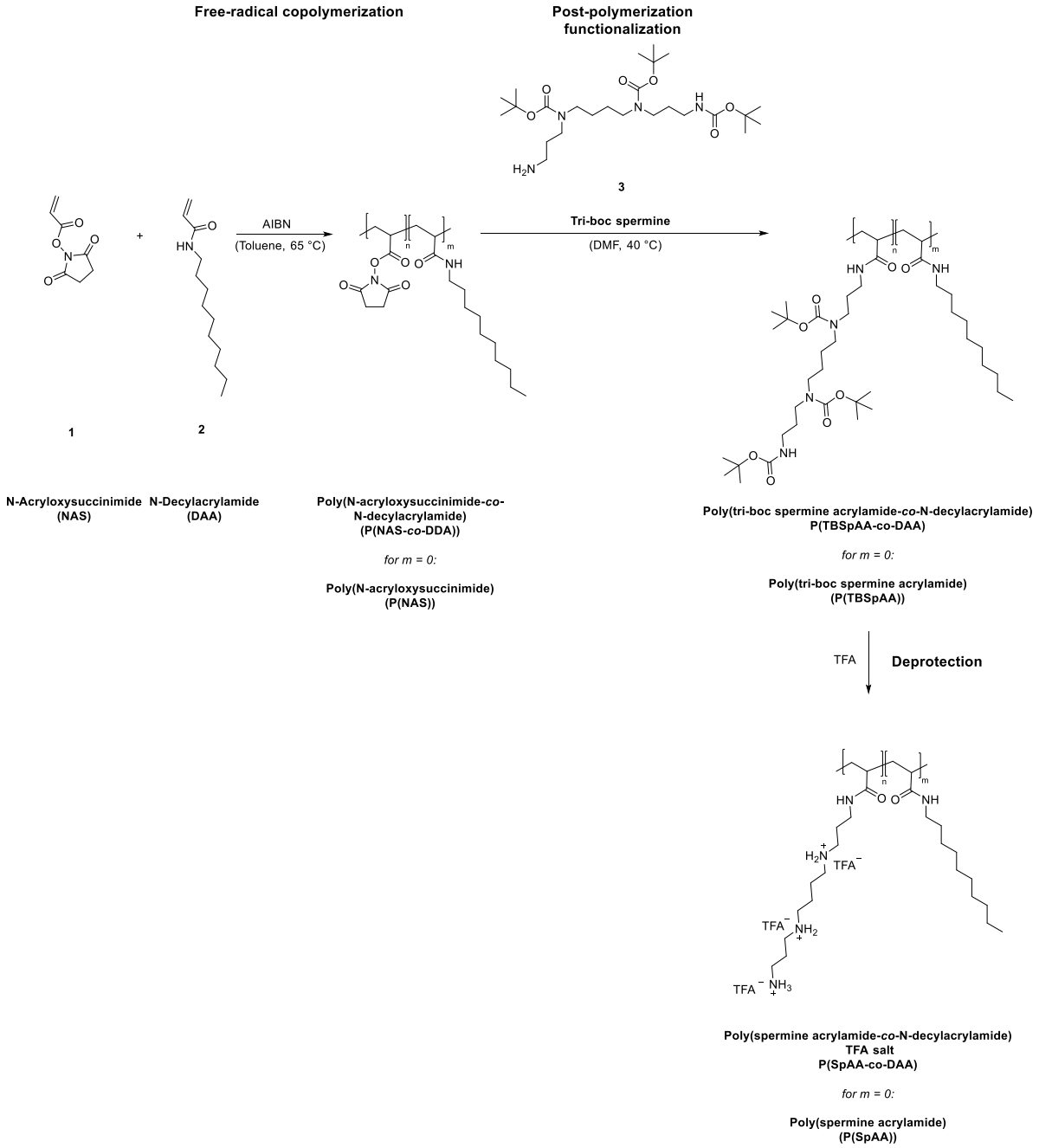

Scheme A1: Synthesis of poly(spermine acrylamide) (P(SpAA)) and poly(spermine acrylamide-co-N-decylacrylamide) (P(SpAA-co-DAA) via radical (co)polymerization of N-Acryloxysuccinimide (NAS) and N-Decylacrylamide (DAA), followed by post-polymerization with tri-boc spermine and deprotection using tri fluoro acetic acid (TFA).

Table A1: Free radical polymerization of NAS and DAA and copolymerizations of NAS and DAA.[a]

Entry	Name	NAS/ DAA_{Feed} [mol%]	wt.% AIBN	Time [h]	Yield [%]	M_n [kg mol^{-1}][b]	Đ[b]	NAS/ DAA [mol%][c]	Name Postpoly.	M_n [kg mol^{-1}][b]	Đ[b]	TBSpAA/DAA [mol%][d]	Name Deprot.	SpAA/DAA [mol%][e]
1	P(NAS)1-3	100/0	2	16.5	84	16.9	3.43	100/0	P(TBSpAA)1-3	104.9	2.75	100/0	P(SpAA)1-3	100/0
2		100/0	5	17	97	20.0	3.46	100/0		115.2	2.55	100/0		100/0
3		100/0	10	19	93	12.6	3.57	100/0		97.8	2.11	100/0		100/0
4	P(DAA)	0/100	2	16.5	80	23.7[f]	2.02[f]	0/100	-	-	-	-	-	-
5	P(NAS-co-DAA)1-3	90/10	10	22	80	20.0	3.40	91/9	P(TBSpAA-co-DAA)1-3	53.1	3.5	83/17	P(SpAA-co-DAA)1-3	83/17
6		80/20	10	21	72	29.3	2.8	83/17		82.5	2.61	72/28		76/24
7		50/50	10	20	87	35.3	3.69	49/51		129.5	1.74	40/60		43/57

[a] Polymerization in toluene at 65 °C with monomer concentrations of 10 wt./vol.% over night [b] M_n as obtained via SEC in DMF relative to poly(methyl methacrylate) (PMMA) standards. Đ = M_w/M_n calculated via SEC in DMF.[c] Ratio between NAS/DAA calculated via ^{1}H NMR spectroscopy in DMSO or $CDCl_3$ (see Supporting Information). [d] Ratio between TBSpAA/DAA calculated via ^{1}H NMR spectroscopy in $CDCl_3$ (see Supporting Information). [e] Ratio between SpAA/DAA calculated via ^{1}H NMR spectroscopy in D_2O (see Supporting Information). [f] M_n as obtained via SEC in chloroform relative to polystyrene standards. Đ = M_w/M_n calculated via SEC in chloroform.

Synthesis of P(SpAA) 1-3 and P(SpAA-co-DAA) 1-3

Post-polymerization functionalization

Post-polymerization functionalization is a facile tool for access to pendant groups that are not easily accessible as monomers themselves. N-acryloxysuccinimide, an active ester of acrylic acid, was chosen as a monomer, because active esters are reactive towards nucleophiles in a straightforward addition-elimination reaction without generating toxic by-products. After polymerization of NAS or copolymerization with DAA, the obtained homo- and copolymers were treated with one equivalent of tri-boc spermine 3 per NAS-repeating unit to convert NAS units to tri-boc spermine acrylamide (TBSpAA). To ensure full removal of active esters to prevent side reactions during in vivo and in vitro evaluations, the reaction mixture was treated with ammonia to convert unreacted NAS units to water-soluble acrylamides. Full conversion was proven by an absence of NAS signals in 1H NMR spectra. Signals could be assigned to either tri-boc spermine pendant group, DAA, or backbone protons. Additionally, no residual N-hydroxysuccinimide, which is formed during modification of P(NAS), is intercalated in the polymer, which was often observed if ammonia was not added. SEC analysis in DMF showed a shift in retention time towards higher molecular weights for all polymers. Molecular weights were not comparable between P(NAS) and P(TBSpAA) homo- and copolymers, due to potentially different hydrodynamic radii in the SEC solvent and broad polydispersities. 1H NMR spectroscopy was also used to determine the percentage of the tri-boc spermine TBSpAA and DAA in the obtained copolymers. The calculated ratio of spermine in P(TBSpAA-co-DAA) 1-3 showed slightly divergent values than the NAS/DAA ratios (Table 1). This is explained by the low amount of NAS groups that was converted into acrylamides instead of being functionalized by spermine.

Deprotection of polymers

Deprotection of all Boc-protected polymers was performed in trifluoroacetic acid (TFA) to obtain the TFA salts of the desired poly(spermine acrylamide) (P(SpAA)) and poly(spermine acrylamide-co-DAA) (P(SpAA-co-DAA)) polymers.

To be able to compare the polymers to a small molecule with a similar structure (one primary and two secondary amines), tri-boc spermine 3 was converted to a propionyl-spermine amide species 4 in a two-step reaction, i.e., coupling to an activated propionyl-group followed by deprotection with trifluoroacetic acid. The resulting propionyl-spermine TFA-salt 4 was characterized via 1H and 13C NMR spectroscopy to assist with signal assignment of the similar poly(spermine acrylamide) polymers. 1H NMR spectra of the polymer TFA-salts showed similar chemical shifts of the spermine proton signals as 4 with a strong broadening of the peaks attributed to the polymeric structure (Figure A8 and A13). Additionally, the methylene group signal of 4 showed a similar chemical shift as the backbone protons of the isolated P(SpAA) polymers 1-3. 13C NMR spectra of the polymers reflected the presence of TFA salt in the polymers, substantiating the assumption of polymer TFA-salts (Figure A14).

After deprotection, a final cationic to hydrophobic ratio (SpAA:DAA) of 83:17, 76:24 and 43:57 was obtained for the copolymers P(SpAA-co-DAA)1, P(SpAA-co-DAA)2 and P(SpAA co-DAA)3 as determined via 1H NMR spectroscopy. These values are in accordance with the ones before deprotection, showing that TFA treatment does not lead to any alteration of the polymer composition.

NMR spectra of polymers

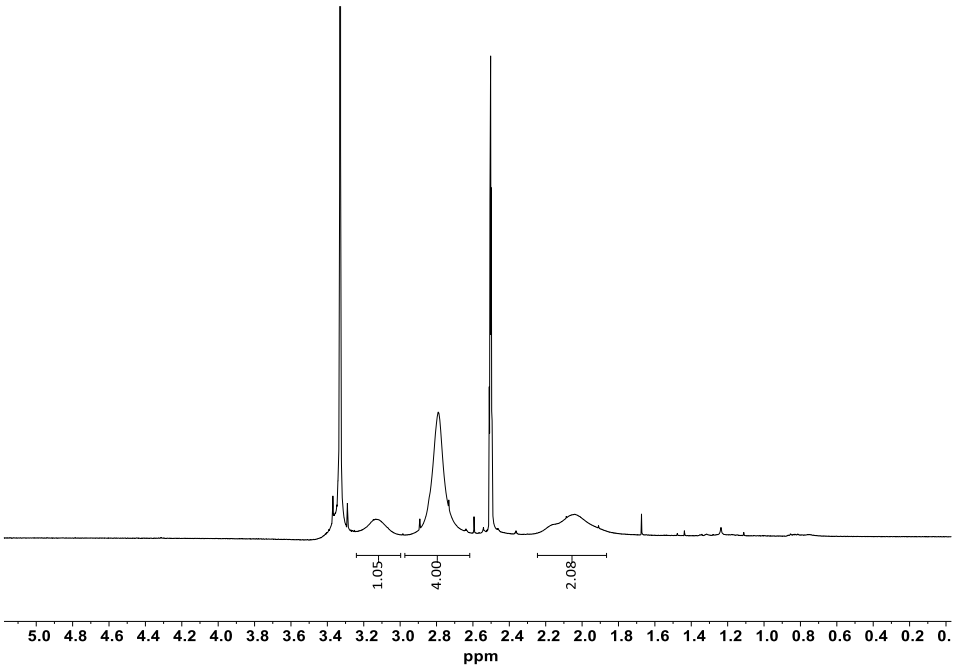

Figure A11 ^{1}H-NMR spectrum of P(NAS) in DMSO (500 MHz).

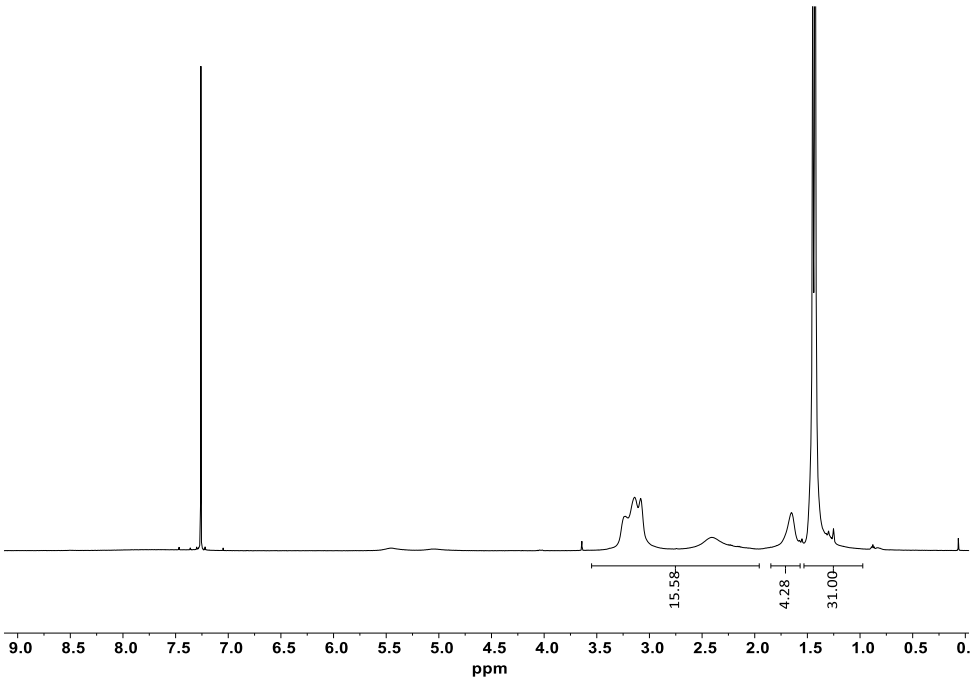

Figure A12 ^{1}H-NMR spectrum of P(TBSpAA) in $CDCl_3$ (500 MHz).

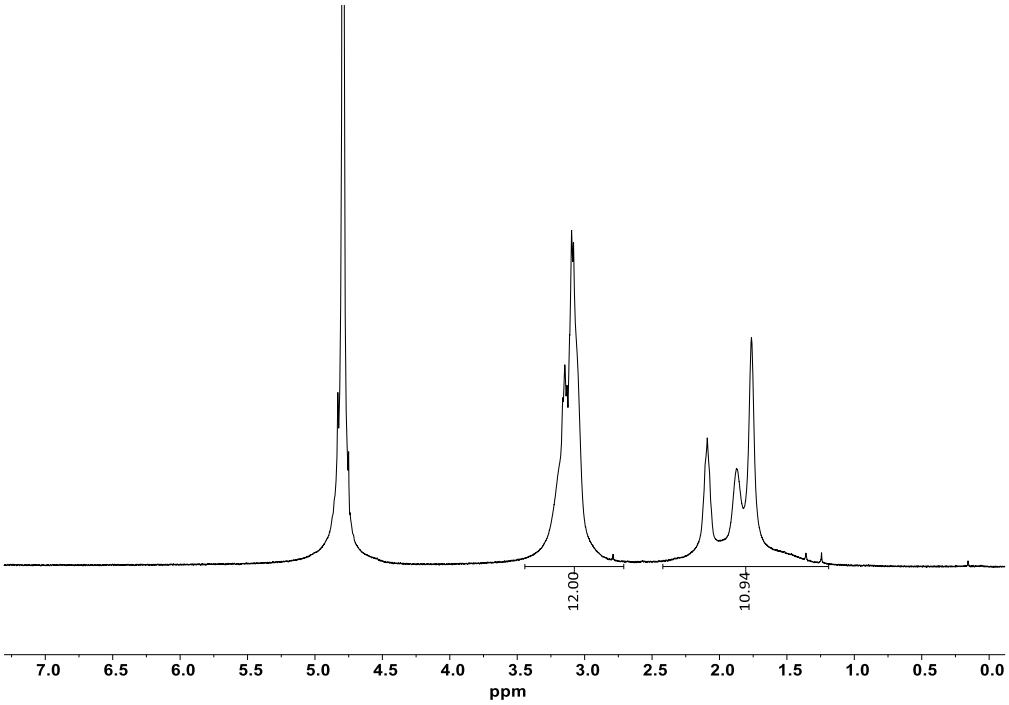

Figure A13 ^{1}H-NMR spectrum of P(SpAA) TFA salt in D_2O (500 MHz).

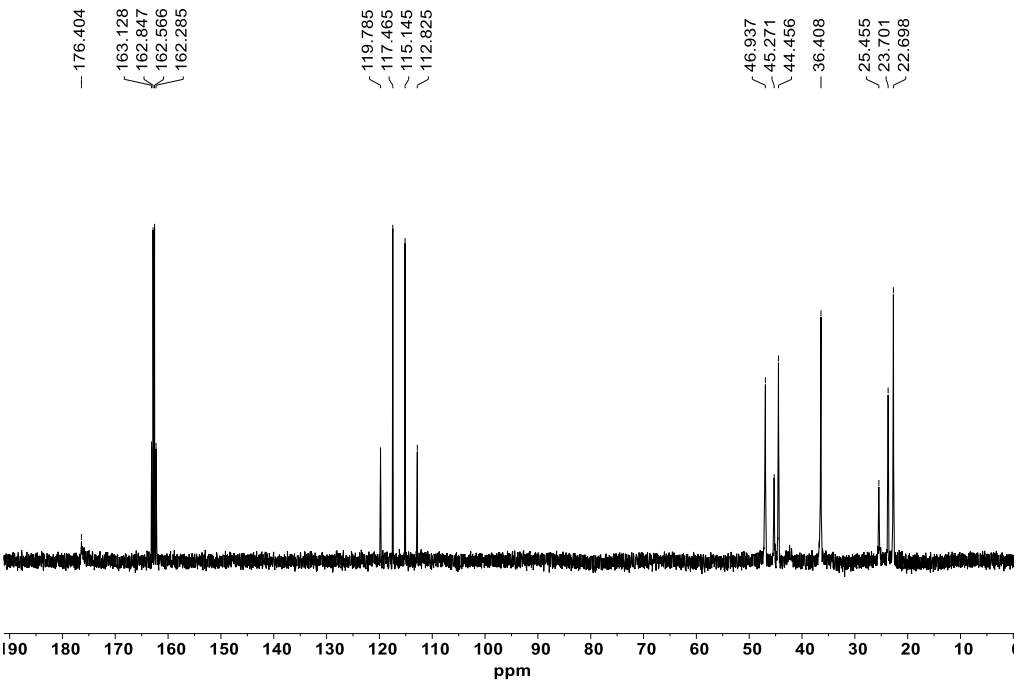

Figure A14 ^{13}C-NMR spectrum of P(SPAA) TFA salt in D_2O (101 MHz).

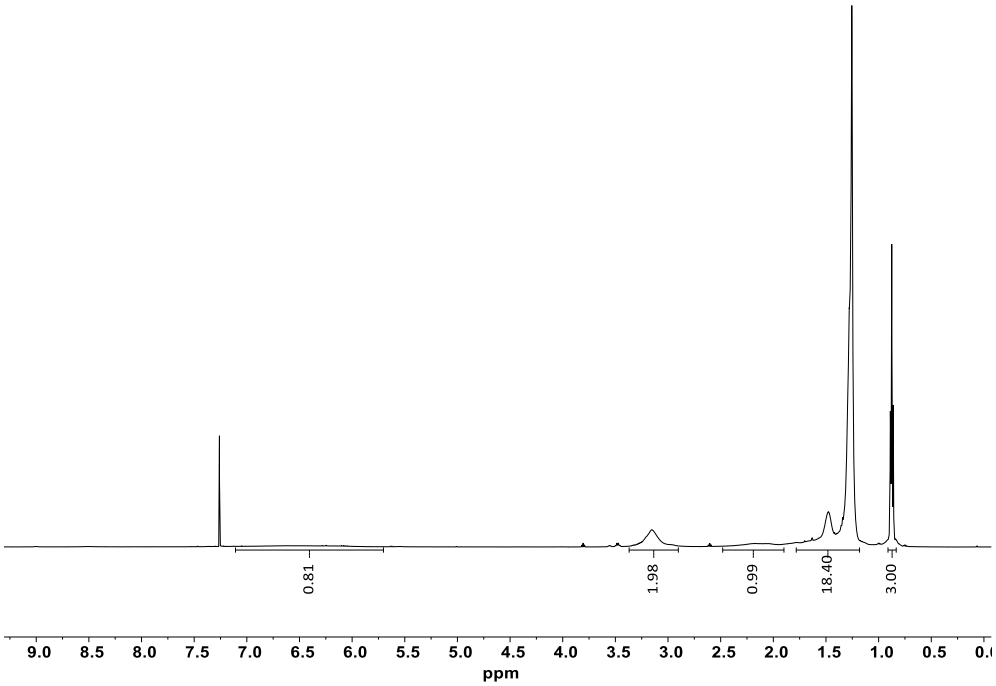

Figure A15 ^{1}H-NMR spectrum of P(DAA) in $CDCl_3$ (500 MHz).

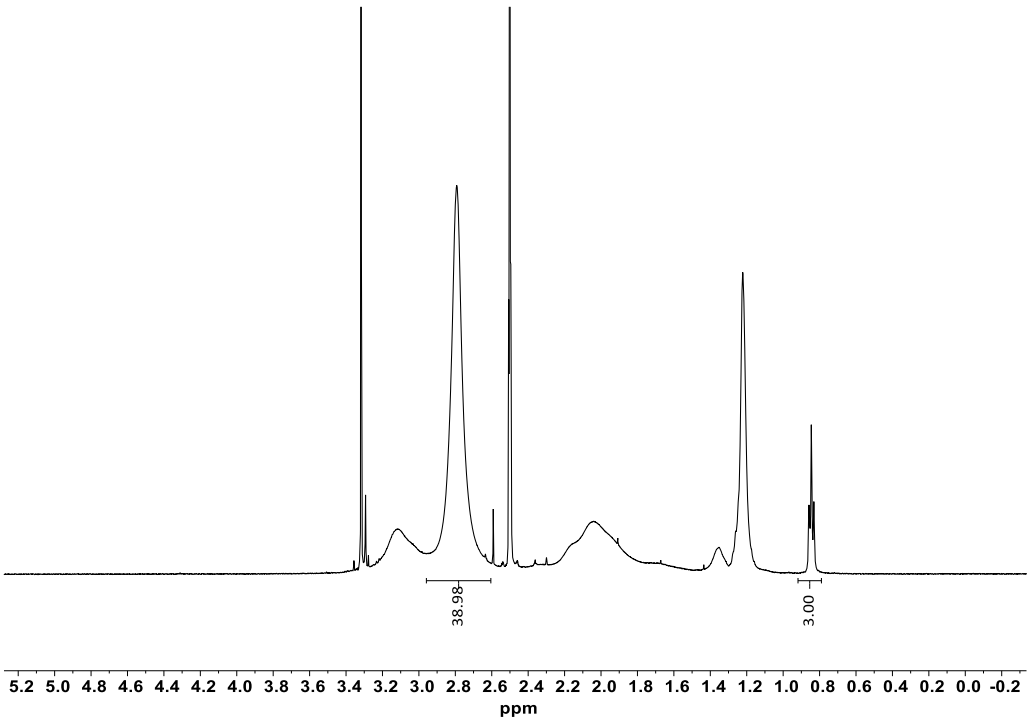

Figure A16 ^{1}H-NMR spectrum of P(NAS-co-DAA)1 in DMSO (500 MHz).

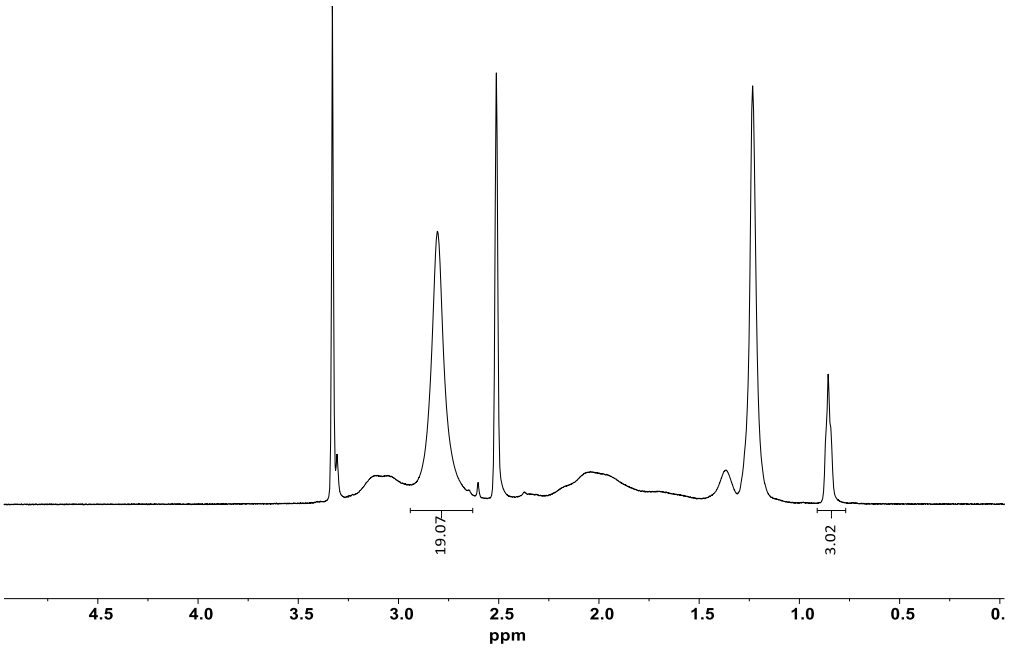

Figure A17 ^{1}H-NMR spectrum of P(NAS-co-DAA)2 in DMSO (500 MHz).

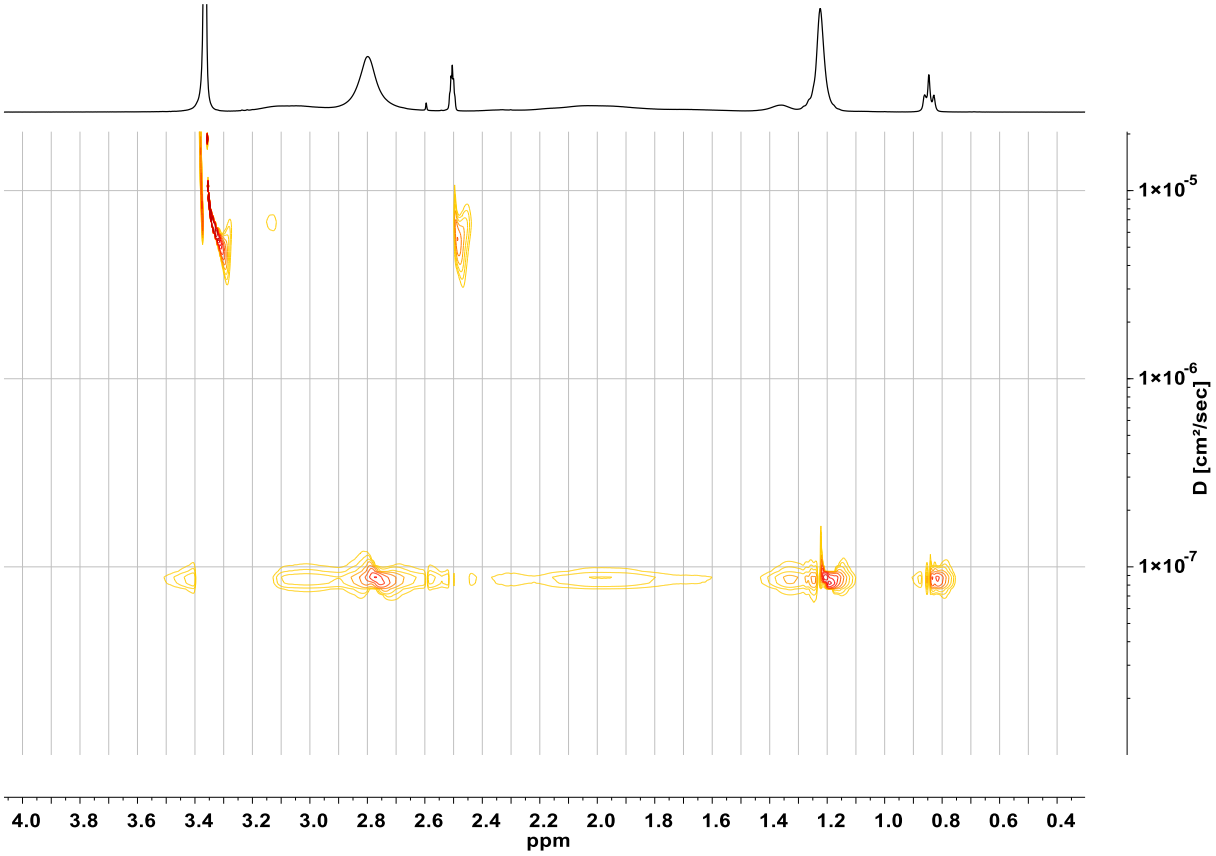

Figure A18 DOSY-NMR spectrum of P(NAS-co-DAA)2 in DMSO (400 MHz, 32 scans, resolution factor; 1, repetitions:1, points in diffusion dimension: 128).

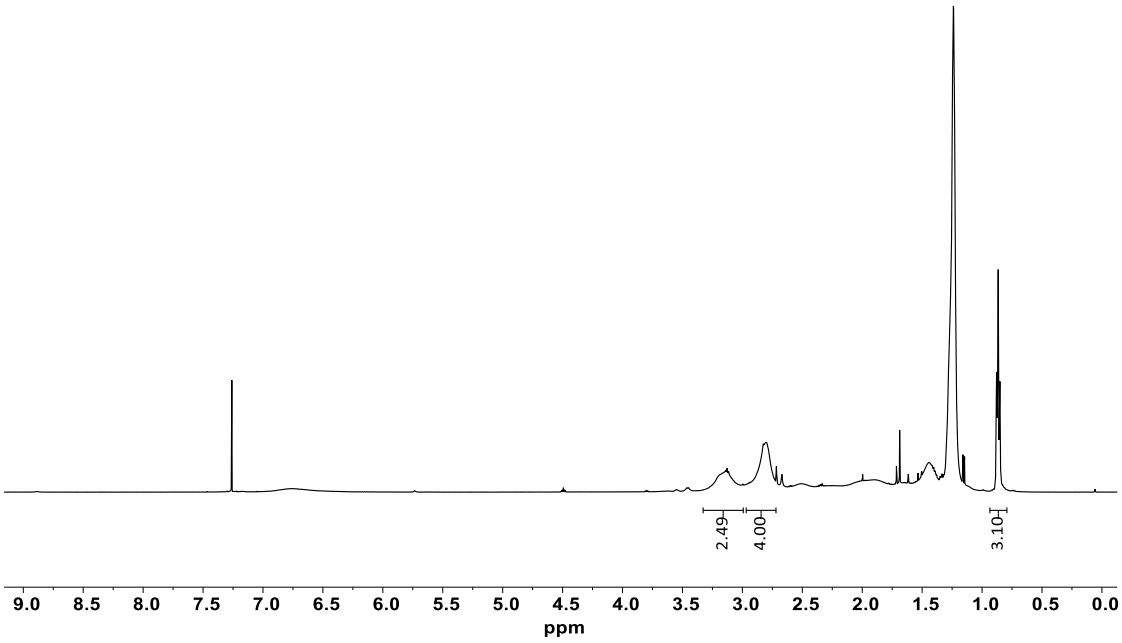

Figure A19 ^{1}H-NMR spectrum of P(NAS-co-DAA)3 in $CDCl_3$ (500 MHz).

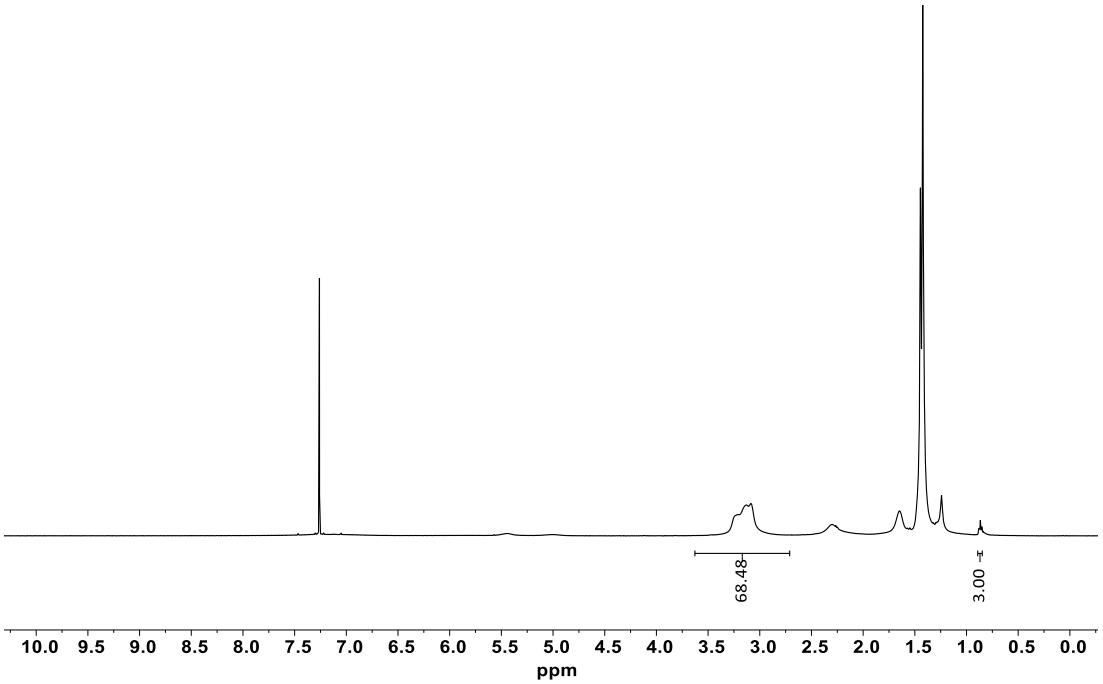

Figure A20 ^{1}H-NMR spectrum of P(TBSpAA-co-DAA)1 in $CDCl_3$ (500 MHz).

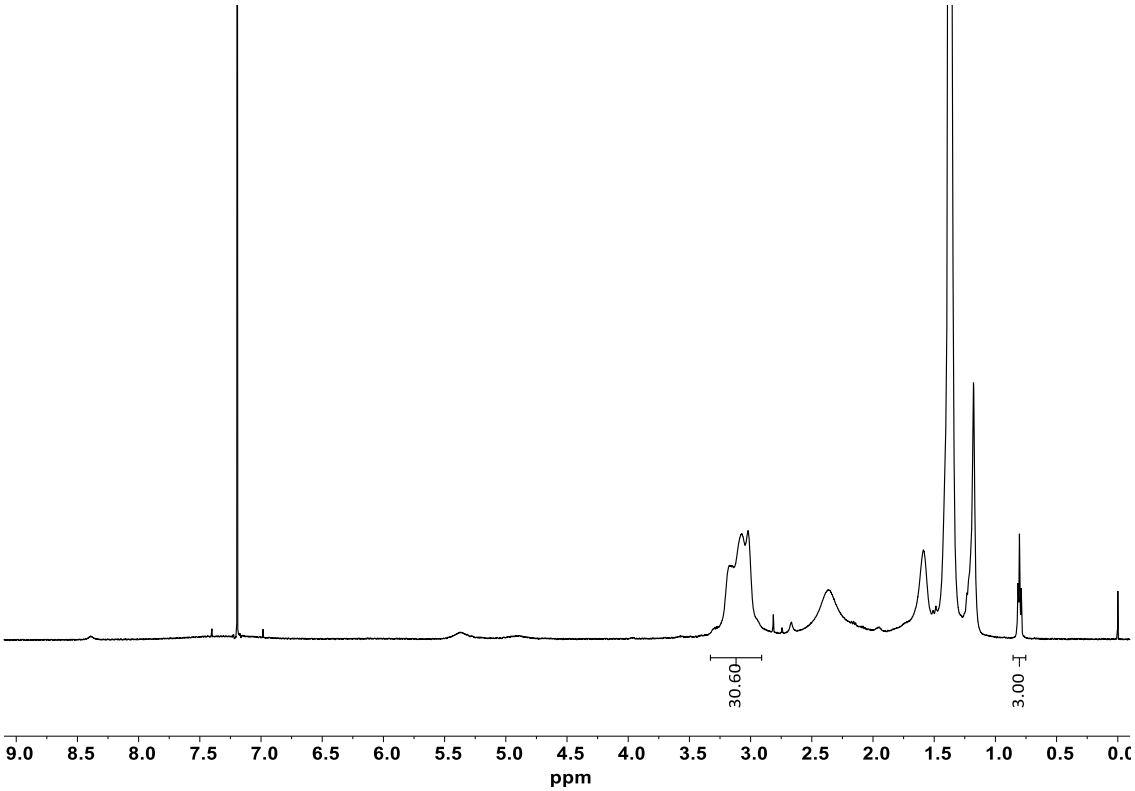

Figure A21 ^{1}H-NMR spectrum of P(TBSpAA-co-DAA)2 in $CDCl_3$ (500 MHz).

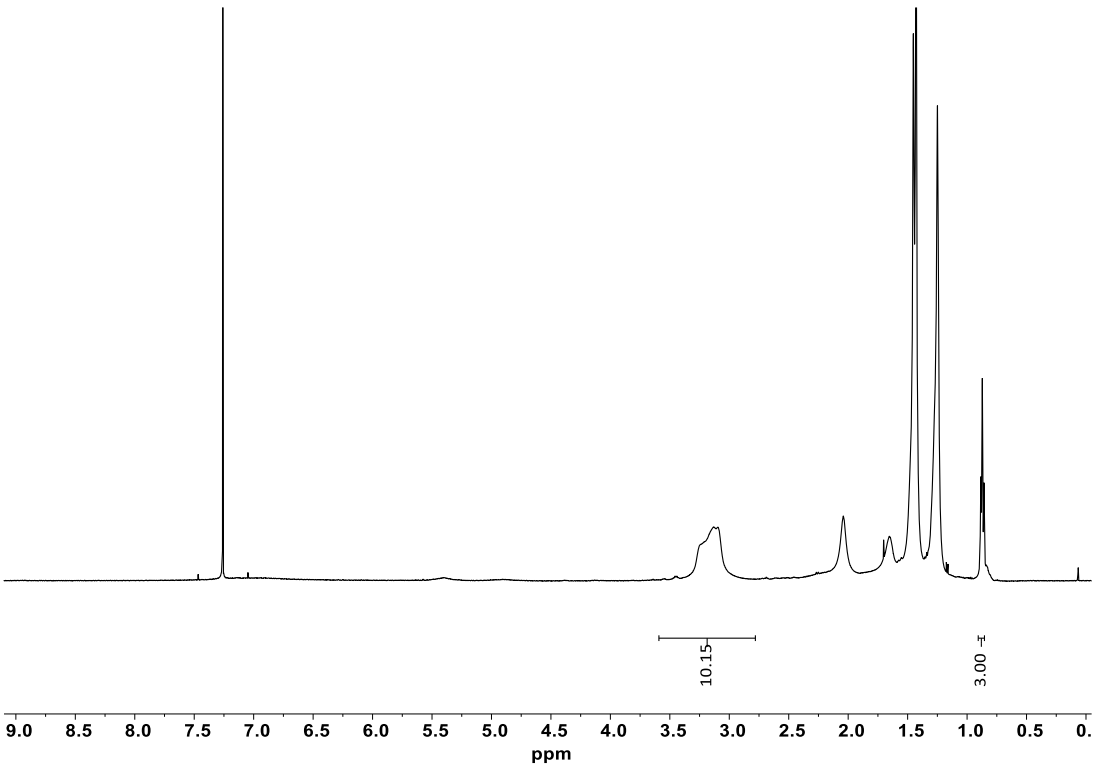

Figure A22 ^{1}H-NMR spectrum of P(TBSpAA-co-DAA)3 in $CDCl_3$ (500 MHz).

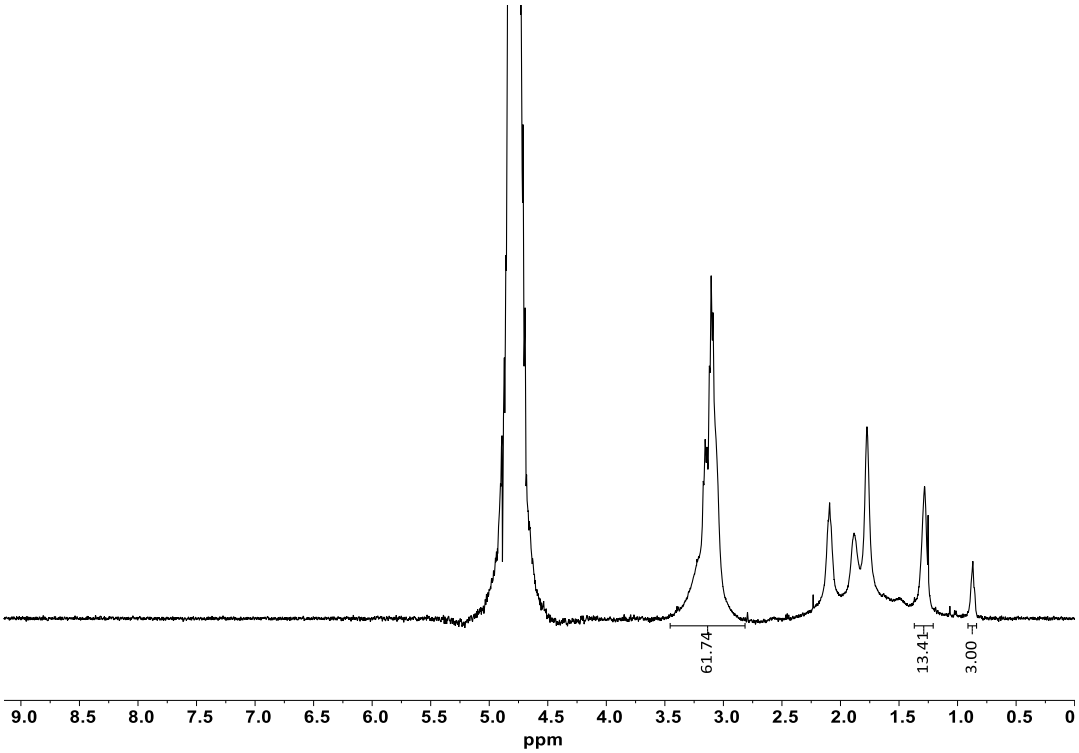

Figure A23 ^{1}H-NMR spectrum of P(SpAA-co-DAA)1 TFA salt in D_2O (500 MHz).

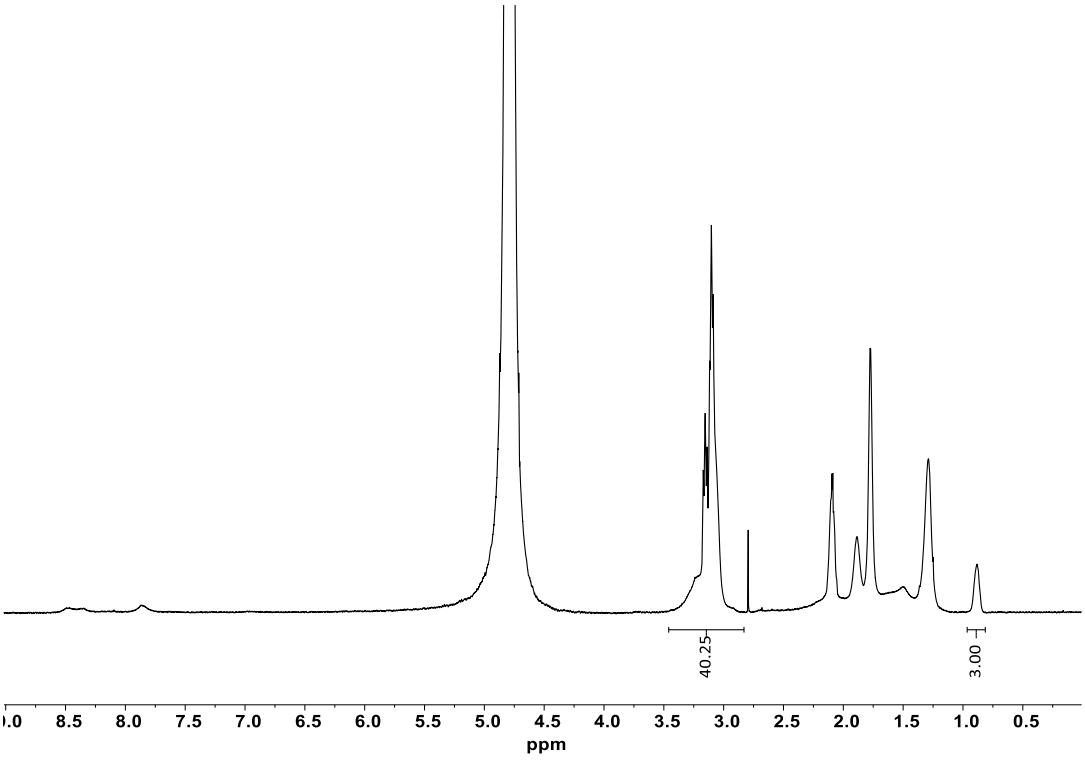

Figure A24 ^{1}H-NMR spectrum of P(SpAA-co-DAA)2 TFA salt in D_2O (500 MHz).

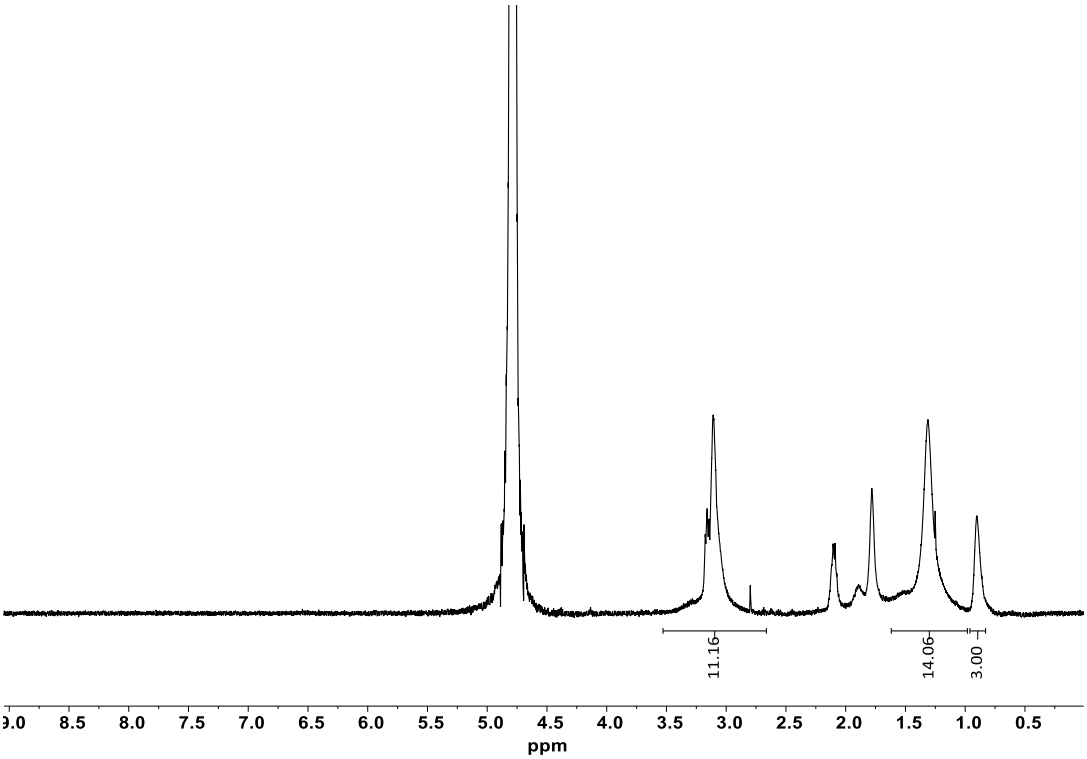

Figure A25 ^{1}H-NMR spectrum of P(SpAA-co-DAA)3 TFA salt in D_2O (500 MHz).

GPC-traces

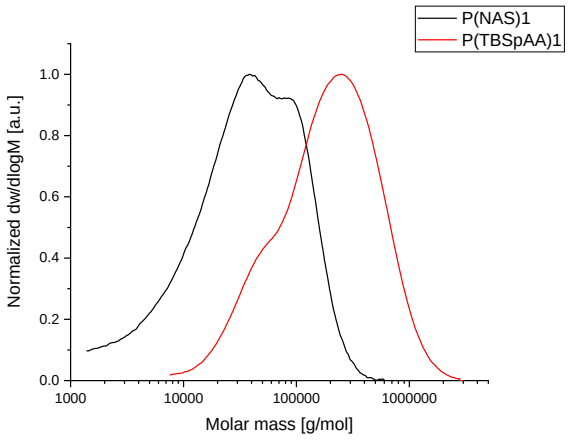

Figure A26 GPC traces of P(NAS)1 and P(TBSpAA)1 measured via SEC in DMF.

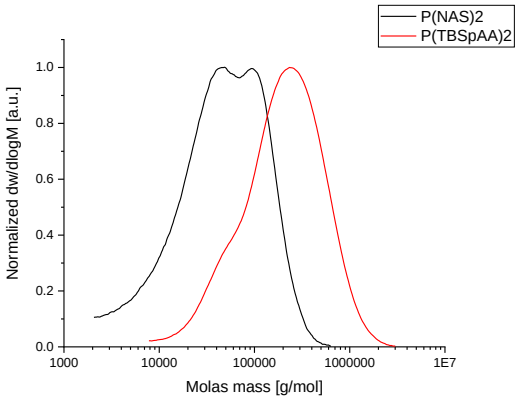

Figure A27 GPC traces of P(NAS)2 and P(TBSpAA)2 measured via SEC in DMF.

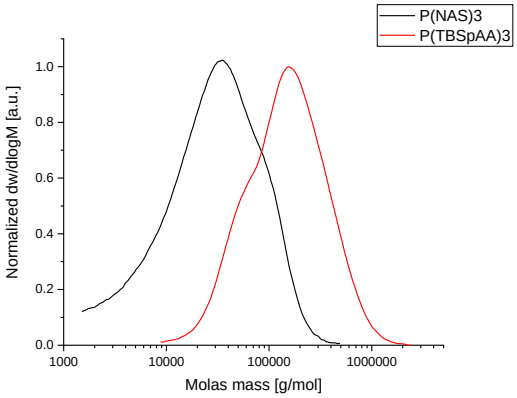

Figure A28 GPC traces of P(NAS)3 and P(TBSpAA)3 measured via SEC in DMF.

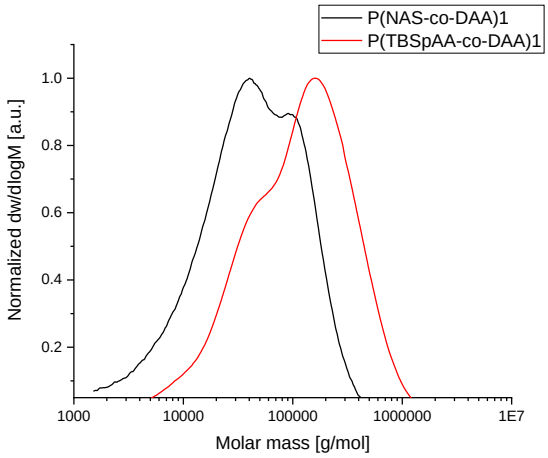

Figure A29 GPC traces of P(NAS-co-DAA)1 and P(TBSpAA-co-DAA)1 measured via SEC in DMF.

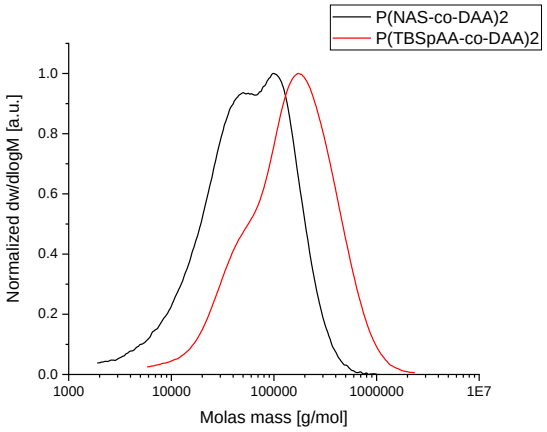

Figure A30 GPC traces of P(NAS-co-DAA)2 and P(TBSpAA-co-DAA)2 measured via SEC in DMF.

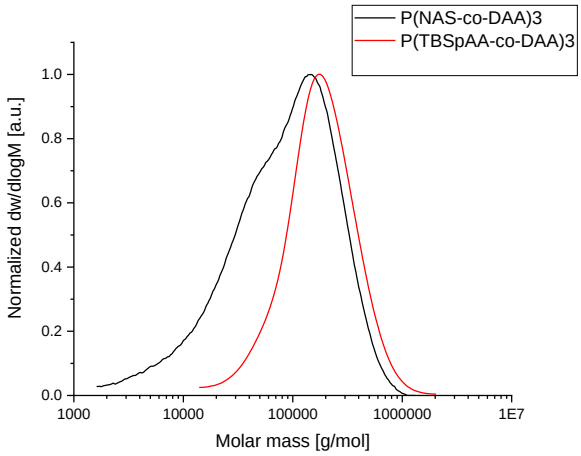

Figure A31 GPC traces of P(NAS-co-DAA)3 and P(TBSpAA-co-DAA)3 measured via SEC in DMF.

A2 - Design and characterization of lipid-polyplex hybrid nanoparticles for siRNA delivery

"Supplementary information"

Table S1 Sequences of siRNAs used in the study. Nt = nucleotides; GFP = green fluorescence protein; NC = negative control; A = Adenine; C = Cytosine; G = Guanine; U = Uracil; T = Thymine; p = phosphate residue; lower case bold letters = 2´-deoxyribonucleotides; capital letters = ribonucleotides; underlined capital letters = 2´-O-methylribonucleotides.

Name	Sense strand (5'-3')	Antisense strand (3'-5')	Length (nt)	
			Sense	Antisense
siGFP	pACCCUGAAGUUCAUCUGCA CCACcg	ACUGGGACUUCAAGUAGACGU GGUGGC	25	27
siNC	pCGUUAAUCGCGUAUAAUAC GCGUat	CAGCAAUUAGCGCAUAUUAUG CGCAUAp	25	27
siAF488	pACCCUGAAGUUCAUCUGCA CCACcg	ACUGGGACUUCAAGUAGACGU GGUGGCC6MA	25	27

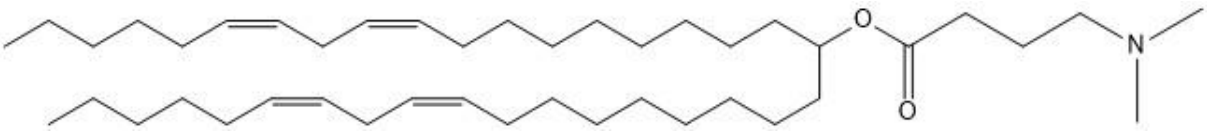

Figure S1 Chemical structure of DLin-MC3-DMA.

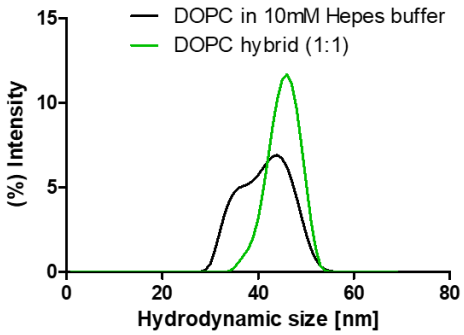

Figure S2 Size distribution comparison between DOPC in 10 mM HEPES buffer solution and DOPC coated HLPNPs prepared via microfluidic mixing.

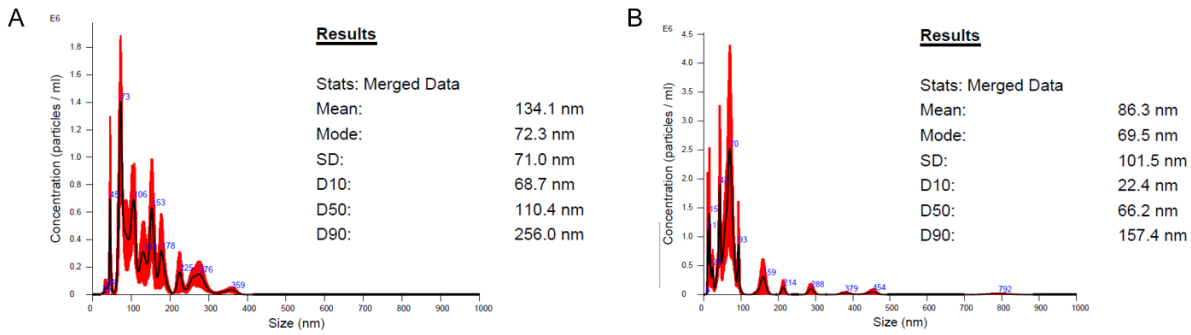

Figure S3 NTA size and zeta potential measurement of DOTAP HLPNPS at N/P ratios 7 and 14.

A3 - Spray drying siRNA-lipid nanoparticles for dry powder pulmonary delivery

"Supplementary information"

Table S1 Sequences of siRNAs used in the study. Nt = nucleotides; GFP = green fluorescence protein; NC = negative control; GAPDH = housekeeping gene GAPDH; A = Adenine; C = Cytosine; G = Guanine; U = Uracil; T = Thymine; p = phosphate residue; lower case bold letters = 2´-deoxyribonucleotides; capital letters = ribonucleotides; underlined capital letters = 2´-O-methylribonucleotides.

Name	Sense strand (5'-3')	Antisense strand (3'-5')	Length (nt)	
			Sense	Antisense
siGFP	pACCCUGAAGUUCAUCUG CACCAC**cg**	ACUGGGACUUCAAGUAGAC GUGGUGGC	**25**	**27**
siNC	pCGUUAAUCGCGUAUAAU ACGCGU**at**	CAGCAAUUAGCGCAUAUUA UGCGCAUAp	**25**	**27**
siGAPDH	pGGUCGGAGUCAACGGAU UUGGUC**gt**	UUCCAGCCUCAGUUGCCUA AACCAGCA	**25**	**27**

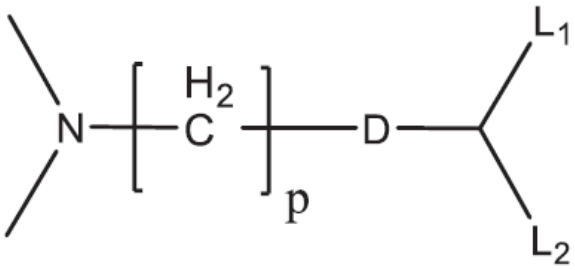

Figure S1 Chemical structure of sulfur-containing analog of DLin-MC3-DMA.

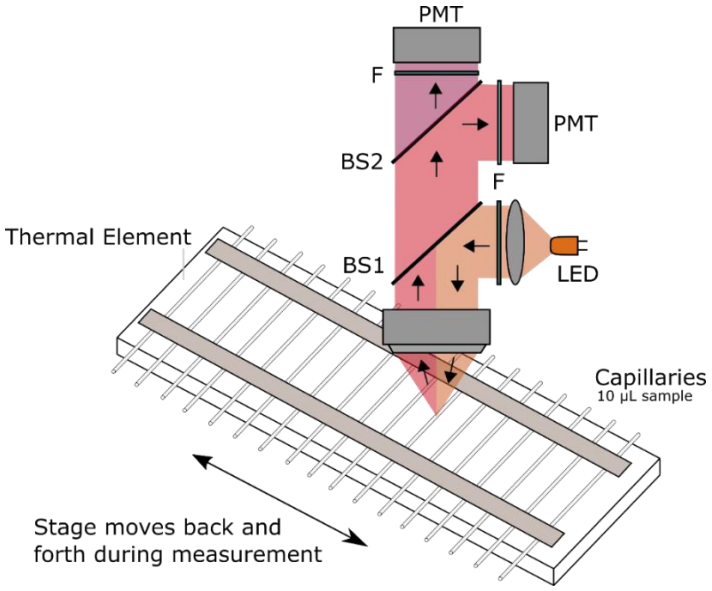

Figure S2 Experimental epifluorescence setup. An amber LED produces excitation light that matches the secondary, shorter absorption peak of a suitable near-infrared fluorophore attached to siRNA. The light is reflected on a beam splitter (BS1) and excites fluorescence within a capillary. The red-shifted emission then passes BS1 and is divided by a second beam splitter

(BS2) into a lower and higher wavelength component. Filters (F) further clean up the emission light before being collected in photo-multiplier tubes (PMT).

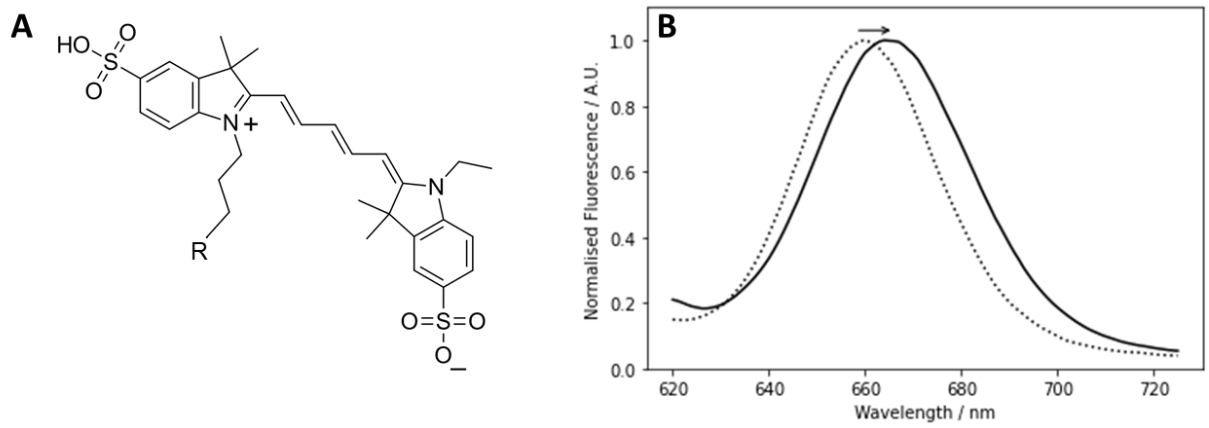

Figure S3 A) Chemical structure of the Cyanine 5 dye, R group is attachment site to protein or nucleic acid. B) Cy5-siRNA (dashed line) displays a 6 nm bathochromic peak shift after encapsulation within an LNP (solid line). Cy5-siRNA was encapsulated within (-)LNP and diluted in PBS before excitation at 590 ± 20 nm, with emission recorded from 620 – 725 nm with a 10 nm band gap. Spectra were recorded in a temperature-controlled sample chamber at 20 °C.

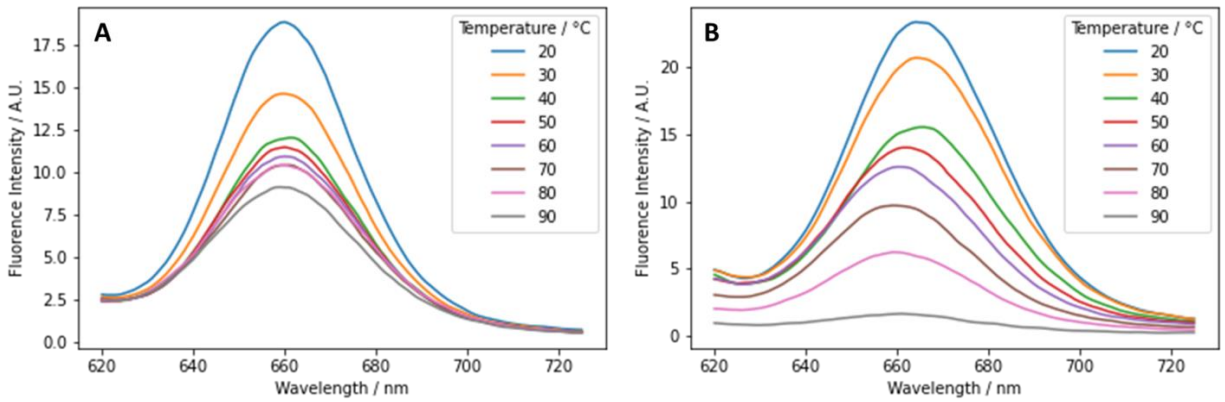

Figure S4 Temperature Interval Fluorescence Emission Spectroscopy of A) Cy-siRNA and B) Cy-siRNA encapsulated in (-) LNP. Fluorescence emission scans were performed every 10 °C with a heating rate of 2 °C per min.

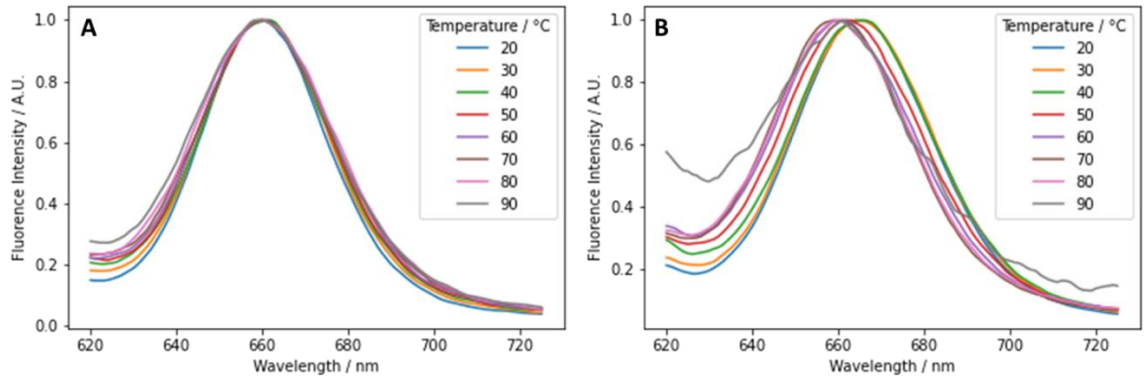

Figure S5 Hypsochromic peak shift, normalized Spectra from Figure S3. Temperature Interval Fluorescence Emission Spectroscopy of A) Cy-siRNA and B) Cy-siRNA encapsulated in LNP5. Fluorescence emission scans were performed every 10 °C with a heating rate of 2 °C per min.

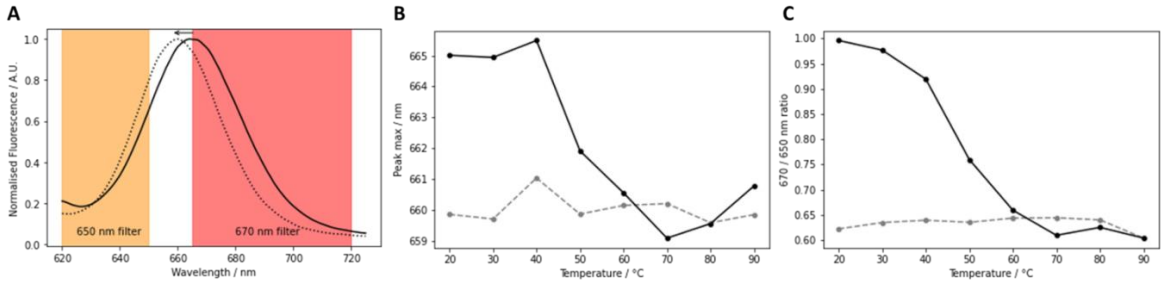

Figure S6 Fluorescence based measurements. A) Fluorescence emission spectra of Cy5-siRNA encapsulated within (-)LNP (black solid line) and Cy5-siRNA (dashed line) in PBS. Arrow indicates the shift in peak between the two samples, with coloured shading indicating the two spectra windows used for 650 nm and 670 nm ratio measurements. B) Peak shift and C) 670 nm / 650 nm ratio plotted against sample temperature of (-)LNP (black markers) and Cy5-siRNA (grey markers).

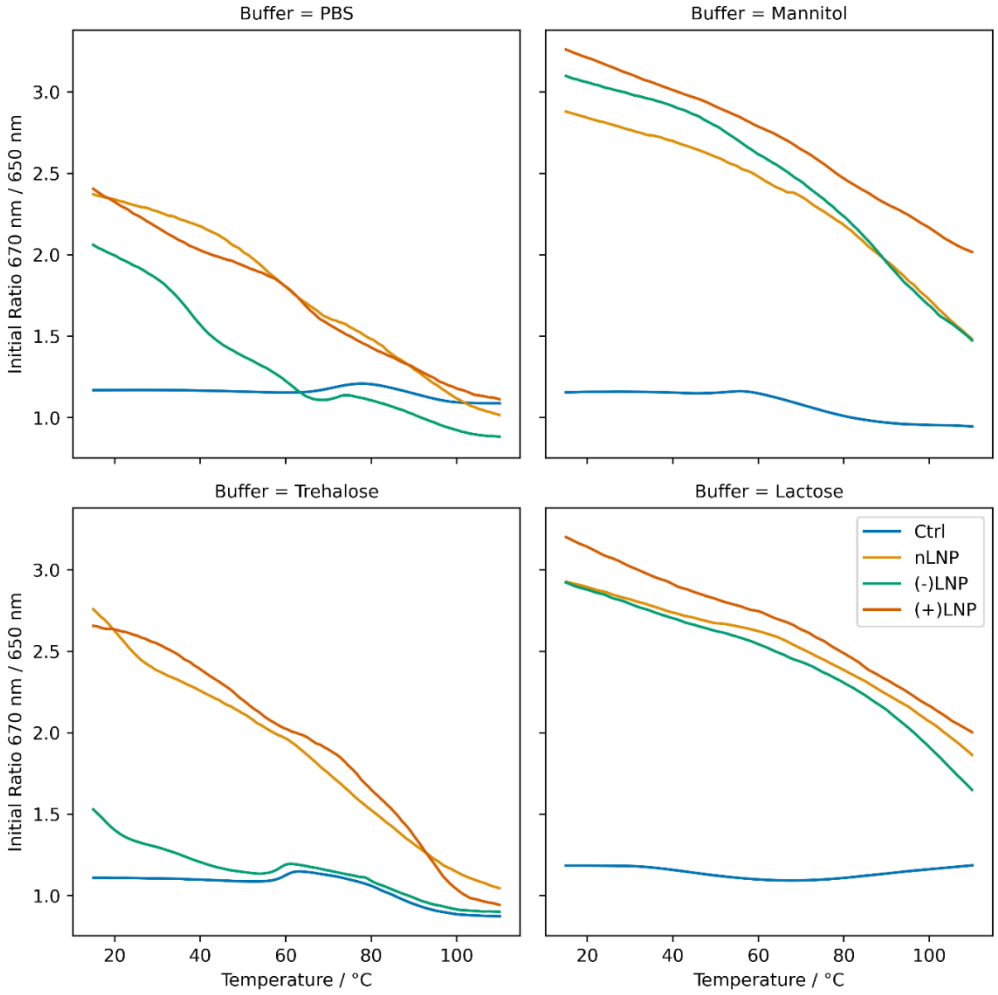

Figure S7 670 nm / 650 nm ratio of LNP samples in different excipient solutions (PBS, mannitol, trehalose and lactose) plotted against temperature of sample. Samples were loaded into high sensitivity capillaries and subjected to a temperature ramp rate of 1 °C/min.

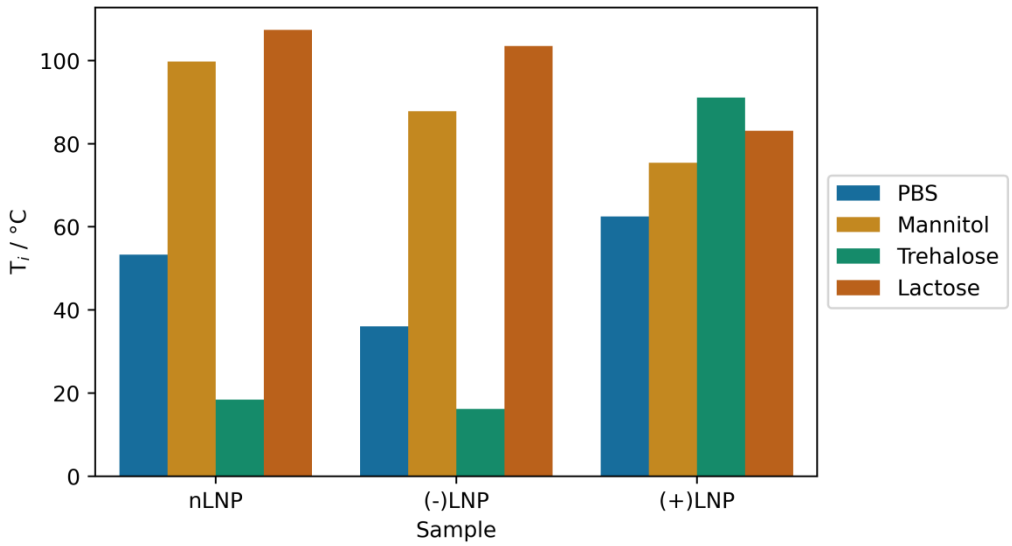

Figure S8 Category plot of inflection point temperatures for LNP samples. The maximum slope of the melting curves shown over an 8-degree temperature range in Figure S6 was calculated and the center temperature of that slope recorded.

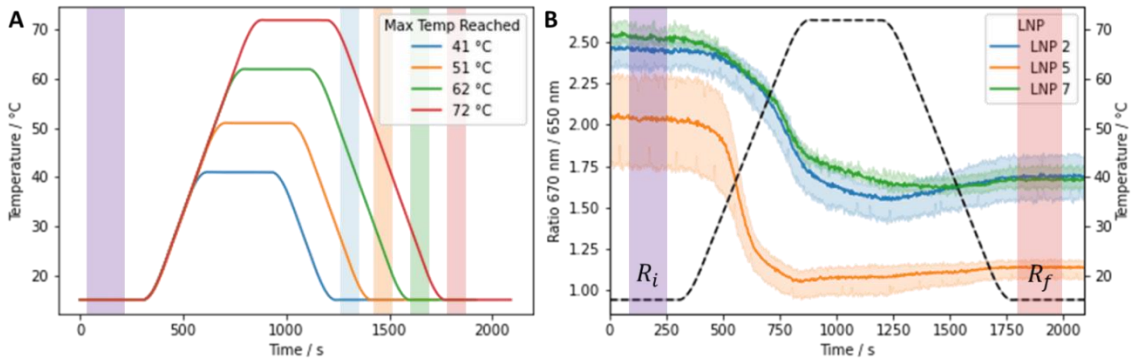

Figure S9 A) Plot to show the temperature vs time of each stress testing experiment. B) Example traces for LNPs in PBS heated to 72 °C, with the regions for calculating Δ indicated.

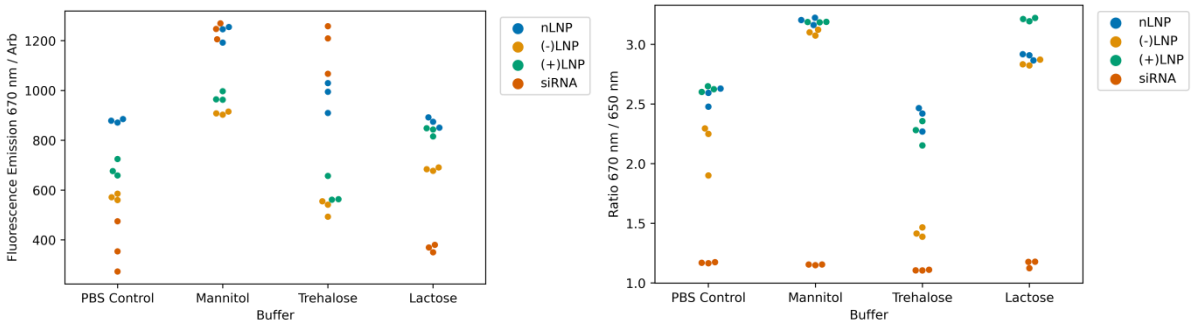

Figure S10 Swarm plots of A) Initial Fluorescence and B) Initial Ratio of LNPs and Cy5-siRNA controls in buffers, as indicated. Data collected at 15 °C prior to heating the samples.

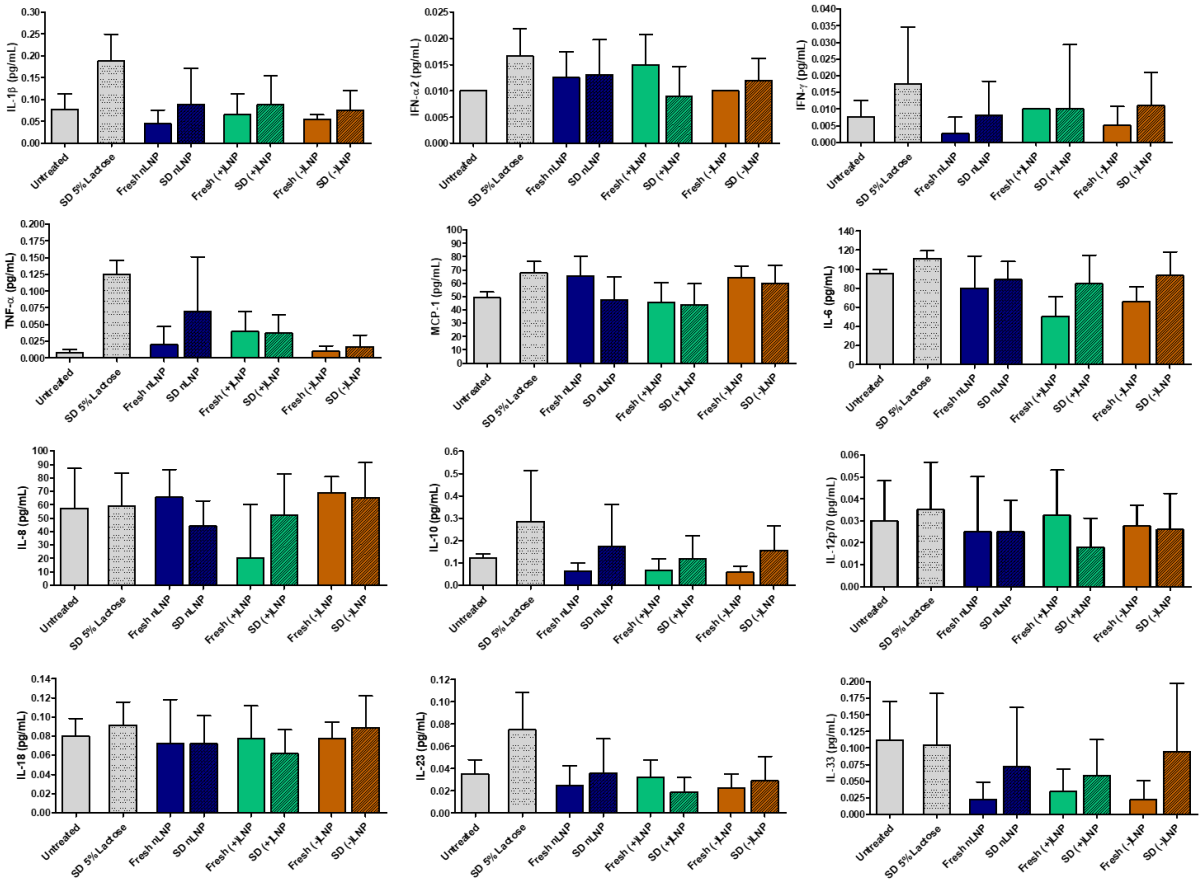

Figure S11 Ex vivo cytokine secretion from hPCLS transfected at 10 µg siRNA / mL with spray dried LNPs. Comparison of different cytokines after transfection with fresh and spray dried (SD) LNPs. Mean ± standard deviation, n=3.

References

[1] A. Fire, D. Albertson, S.W. Harrison, D.G. Moerman, Production of antisense RNA leads to effective and specific inhibition of gene expression in C. elegans muscle, Development, 113 (1991) 503-514.

[2] C.C. Mello, D. Conte, Jr., Revealing the world of RNA interference, Nature, 431 (2004) 338-342.

[3] K.A. Whitehead, R. Langer, D.G. Anderson, Knocking down barriers: advances in siRNA delivery, Nat Rev Drug Discov, 8 (2009) 129-138.

[4] B. Hu, L. Zhong, Y. Weng, L. Peng, Y. Huang, Y. Zhao, X.J. Liang, Therapeutic siRNA: state of the art, Signal Transduct Target Ther, 5 (2020) 101.

[5] R. Kandil, Y. Xie, R. Heermann, L. Isert, K. Jung, A. Mehta, O.M. Merkel, Coming in and Finding Out: Blending Receptor-Targeted Delivery and Efficient Endosomal Escape in a Novel Bio-Responsive siRNA Delivery System for Gene Knockdown in Pulmonary T Cells, Adv Ther (Weinh), 2 (2019).

[6] F. Czauderna, M. Fechtner, S. Dames, H. Aygun, A. Klippel, G.J. Pronk, K. Giese, J. Kaufmann, Structural variations and stabilising modifications of synthetic siRNAs in mammalian cells, Nucleic Acids Res, 31 (2003) 2705-2716.

[7] F. Mainini, M.R. Eccles, Lipid and Polymer-Based Nanoparticle siRNA Delivery Systems for Cancer Therapy, Molecules, 25 (2020).

[8] N.D. Donahue, H. Acar, S. Wilhelm, Concepts of nanoparticle cellular uptake, intracellular trafficking, and kinetics in nanomedicine, Adv Drug Deliv Rev, 143 (2019) 68-96.

[9] I. Wrobel, D. Collins, Fusion of cationic liposomes with mammalian cells occurs after endocytosis, Biochim Biophys Acta, 1235 (1995) 296-304.

[10] I.M.S. Degors, C. Wang, Z.U. Rehman, I.S. Zuhorn, Carriers Break Barriers in Drug Delivery: Endocytosis and Endosomal Escape of Gene Delivery Vectors, Acc Chem Res, 52 (2019) 1750-1760.

[11] L.I. Selby, C.M. Cortez-Jugo, G.K. Such, A.P.R. Johnston, Nanoescapology: progress toward understanding the endosomal escape of polymeric nanoparticles, Wiley Interdiscip Rev Nanomed Nanobiotechnol, 9 (2017).

[12] K.I. Cupic, J.J. Rennick, A.P.R. Johnston, G.K. Such, Controlling endosomal escape using nanoparticle composition: current progress and future perspectives, Nanomedicine, 14 (2019) 215-223.

[13] T. Lubke, P. Lobel, D.E. Sleat, Proteomics of the lysosome, Biochim Biophys Acta, 1793 (2009) 625-635.

[14] E.C. Freeman, L.M. Weiland, W.S. Meng, Modeling the proton sponge hypothesis: examining proton sponge effectiveness for enhancing intracellular gene delivery through multiscale modeling, J Biomater Sci Polym Ed, 24 (2013) 398-416.

[15] T. Bus, A. Traeger, U.S. Schubert, The great escape: how cationic polyplexes overcome the endosomal barrier, J Mater Chem B, 6 (2018) 6904-6918.

[16] R.A. Jones, C.Y. Cheung, F.E. Black, J.K. Zia, P.S. Stayton, A.S. Hoffman, M.R. Wilson, Poly(2-alkylacrylic acid) polymers deliver molecules to the cytosol by pH-sensitive disruption of endosomal vesicles, Biochem J, 372 (2003) 65-75.

[17] G. Tamura, Y. Shinohara, A. Tamura, Y. Sanada, M. Oishi, I. Akiba, Y. Nagasaki, K. Sakurai, Y. Amemiya, Dependence of the swelling behavior of a pH-responsive PEG-modified nanogel on the cross-link density, Polymer Journal, 44 (2011) 240-244.

[18] F. Wan, A. Bohr, M.J. Maltesen, S. Bjerregaard, C. Foged, J. Rantanen, M. Yang, Critical solvent properties affecting the particle formation process and characteristics of celecoxib-loaded plga microparticles via spray-drying, Pharm Res, 30 (2013) 1065-1076.

[19] A. Sosnik, K.P. Seremeta, Advantages and challenges of the spray-drying technology for the production of pure drug particles and drug-loaded polymeric carriers, Adv Colloid Interface Sci, 223 (2015) 40-54.

[20] K. Cal, K. Sollohub, Spray drying technique. I: Hardware and process parameters, J Pharm Sci, 99 (2010) 575-586.

[21] J. Berggren, G. Frenning, G. Alderborn, Compression behaviour and tablet-forming ability of spray-dried amorphous composite particles, Eur J Pharm Sci, 22 (2004) 191-200.

[22] T. Bhowmik, B. D'Souza, R. Shashidharamurthy, C. Oettinger, P. Selvaraj, M.J. D'Souza, A novel microparticulate vaccine for melanoma cancer using transdermal delivery, J Microencapsul, 28 (2011) 294-300.

[23] C. Anish, A.K. Upadhyay, D. Sehgal, A.K. Panda, Influences of process and formulation parameters on powder flow properties and immunogenicity of spray dried polymer particles entrapping recombinant pneumococcal surface protein A, Int J Pharm, 466 (2014) 198-210.

[24] B.L. AG, Spray drying, (2022).

[25] P.M. Valencia, O.C. Farokhzad, R. Karnik, R. Langer, Microfluidic technologies for accelerating the clinical translation of nanoparticles, Nature Nanotechnology, 7 (2012) 623-629.

[26] A. Jahn, J.E. Reiner, W.N. Vreeland, D.L. DeVoe, L.E. Locascio, M. Gaitan, Preparation of nanoparticles by continuous-flow microfluidics, Journal of Nanoparticle Research, 10 (2008) 925-934.

[27] J. deMello, A. deMello, Microscale reactors: nanoscale products, Lab Chip, 4 (2004) 11N-15N.

[28] R. Karnik, F. Gu, P. Basto, C. Cannizzaro, L. Dean, W. Kyei-Manu, R. Langer, O.C. Farokhzad, Microfluidic platform for controlled synthesis of polymeric nanoparticles, Nano Lett, 8 (2008) 2906-2912.

[29] J.A. Kulkarni, D. Witzigmann, S. Chen, P.R. Cullis, R. van der Meel, Lipid Nanoparticle Technology for Clinical Translation of siRNA Therapeutics, Acc Chem Res, 52 (2019) 2435-2444.

[30] S. Damiati, U.B. Kompella, S.A. Damiati, R. Kodzius, Microfluidic Devices for Drug Delivery Systems and Drug Screening, Genes (Basel), 9 (2018).

[31] D. Liu, H. Zhang, F. Fontana, J.T. Hirvonen, H.A. Santos, Current developments and applications of microfluidic technology toward clinical translation of nanomedicines, Advanced Drug Delivery Reviews, 128 (2018) 54-83.

[32] T. Sun, Y.S. Zhang, B. Pang, D.C. Hyun, M. Yang, Y. Xia, Engineered nanoparticles for drug delivery in cancer therapy, Angew Chem Int Ed Engl, 53 (2014) 12320-12364.

[33] J.M.L.a.J.H. BAERT, Alveolar Clearance and the Role of the Pulmonary Lymphatics, AMERICAN REVIEW OF RESPIRATORY DISEASE, 115 (1977) 625-683.

[34] D.P. Feldmann, Y. Xie, S.K. Jones, D. Yu, A. Moszczynska, O.M. Merkel, The impact of microfluidic mixing of triblock micelleplexes on in vitro / in vivo gene silencing and intracellular trafficking, Nanotechnology, 28 (2017) 224001.

[35] M.L. Immordino, F. Dosio, L. Cattel, Stealth liposomes: review of the basic science, rationale, and clinical applications, existing and potential, Int J Nanomed, 1 (2006) 297-315.

[36] C.H. T.M. Allen, F. Martin, C. Redemann and A. Yau-Young Liposomes containing synthetic lipid derivatives of poly(ethylene glycol) show prolonged circulation half-lives in vivo, Biochimica et Biophysica Acta, 1066 (1991) 29-36.

[37] A. Gupta, H.B. Eral, T.A. Hatton, P.S. Doyle, Nanoemulsions: formation, properties and applications, Soft Matter, 12 (2016) 2826-2841.

[38] Y. Singh, J.G. Meher, K. Raval, F.A. Khan, M. Chaurasia, N.K. Jain, M.K. Chourasia, Nanoemulsion: Concepts, development and applications in drug delivery, J Control Release, 252 (2017) 28-49.

[39] H. Cobas Gomez, R. Mansini Cardoso, J. de Novais Schianti, A. Marim de Oliveira, M.R. Gongora-Rubio, Fab on a Package: LTCC Microfluidic Devices Applied to Chemical Process Miniaturization, Micromachines (Basel), 9 (2018).

[40] N. Anton, T.F. Vandamme, The universality of low-energy nano-emulsification, International Journal of Pharmaceutics, 377 (2009) 142-147.

[41] L. Bai, D.J. McClements, Development of microfluidization methods for efficient production of concentrated nanoemulsions: Comparison of single- and dual-channel microfluidizers, J Colloid Interface Sci, 466 (2016) 206-212.

[42] S.M. Jafari, Y. He, B. Bhandari, Optimization of nano-emulsions production by microfluidization, European Food Research and Technology, 225 (2006) 733-741.

[43] Y. Zhang, Y.P. Ho, Y.L. Chiu, H.F. Chan, B. Chlebina, T. Schuhmann, L. You, K.W. Leong, A programmable microenvironment for cellular studies via microfluidics-generated double emulsions, Biomaterials, 34 (2013) 4564-4572.

[44] Y. Wang, R. Deng, L. Yang, C.D. Bain, Fabrication of monolayers of uniform polymeric particles by inkjet printing of monodisperse emulsions produced by microfluidics, Lab Chip, 19 (2019) 3077-3085.

[45] S.L. Anna, N. Bontoux, H.A. Stone, Formation of dispersions using “flow focusing” in microchannels, Applied Physics Letters, 82 (2003) 364-366.

[46] P.K.C. Zenon Toprakcioglu, David B. Morse, Tuomas Knowles, Attoliter protein nanogels from droplet nanofluidics for intracellular delivery, Sci Adv, 6 (2020).

[47] T.A. Nguyen, Q.D. Tang, D.C.T. Doan, M.C. Dang, Micro and nano liposome vesicles containing curcumin for a drug delivery system, Advances in Natural Sciences: Nanoscience and Nanotechnology, 7 (2016).

[48] T.G. Tomohiro Imura, Katsuto Otake,, Satoshi Yoda, Yoshihiro Takebayashi, Shoko Yokoyama, Hitoshi Takebayashi, Hideki Sakai, Makoto Yuasa and Masahiko Abe†, Control of Physicochemical Properties of Liposomes Using a Supercritical Reverse Phase Evaporation Method, American Chemical Society, 19 (2003) 2021-2025.

[49] S.P.a.A.K.S. Himanshu Anwekar*, Liposome-as Drug Carriers, INTERNATIONAL JOURNAL OF PHARMACY & LIFE SCIENCES, 2 (2011).

[50] R.R.-S. Abolfazl Akbarzadeh, Soodabeh Davaran, Sang Woo Joo, Nosratollah Zarghami, Younes Hanifehpour, Mohammad Samiei, Mohammad Kouhi and Kazem Nejati-Koshki, Liposome: classification, preparation, and application, Nanoscale Research Letters 8(2013).

[51] D. Yadav, K. Sandeep, D. Pandey, R.K. Dutta, Liposomes for Drug Delivery, Journal of Biotechnology & Biomaterials, 07 (2017).

[52] T. Ishida, H. Harashima, H. Kiwada, Liposome clearance, Bioscience Rep, 22 (2002) 197-224.

[53] C. Kelly, C. Jefferies, S.A. Cryan, Targeted liposomal drug delivery to monocytes and macrophages, J Drug Deliv, 2011 (2011) 727241.

[54] J.Y. Hwang, Z. Li, X.J. Loh, Small molecule therapeutic-loaded liposomes as therapeutic carriers: from development to clinical applications, RSC Advances, 6 (2016) 70592-70615.

[55] J.R. Hoffman, E. Tasciotti, R. Molinaro, Microfluidic Assembly of Liposomes with Tunable Size and Coloading Capabilities, Methods Mol Biol, 1792 (2018) 205-214.

[56] D. Carugo, E. Bottaro, J. Owen, E. Stride, C. Nastruzzi, Liposome production by microfluidics: potential and limiting factors, Sci Rep, 6 (2016) 25876.

[57] R.R. Hood, W.N. Vreeland, D.L. DeVoe, Microfluidic remote loading for rapid single-step liposomal drug preparation, Lab Chip, 14 (2014) 3359-3367.

[58] M.I.A.a.D.S. Dimitrov, Liposome Electroformation, Faraday Discuss. Chem. SOC., , 81 (1986) 303-311.

[59] K. Kuribayashi, G. Tresset, P. Coquet, H. Fujita, S. Takeuchi, Electroformation of giant liposomes in microfluidic channels, Measurement Science and Technology, 17 (2006) 3121-3126.

[60] Y.-C. Lin, K.-S. Huang, J.-T. Chiang, C.-H. Yang, T.-H. Lai, Manipulating self-assembled phospholipid microtubes using microfluidic technology, Sensors and Actuators B: Chemical, 117 (2006) 464-471.

[61] M.J. Hope, M.B. Bally, G. Webb, P.R. Cullis, Production of Large Unilamellar Vesicles by a Rapid Extrusion Procedure - Characterization of Size Distribution, Trapped Volume and Ability to Maintain a Membrane-Potential, Biochimica Et Biophysica Acta, 812 (1985) 55-65.

[62] P.S. Dittrich, M. Heule, P. Renaud, A. Manz, On-chip extrusion of lipid vesicles and tubes through microsized apertures, Lab Chip, 6 (2006) 488-493.

[63] A. Jahn, W.N. Vreeland, M. Gaitan, L.E. Locascio, Controlled vesicle self-assembly in microfluidic channels with hydrodynamic focusing, Journal of the American Chemical Society, 126 (2004) 2674-2675.

[64] S.M.S. Andreas Jahn, Jennifer S. Hong, Wyatt N. Vreeland, Don L. DeVoe, and Michael Gaitan, Microfluidic Mixing and the Formation ofNanoscale Lipid Vesicles, ACS Nano, 4 (2010) 2077-2087.

[65] W.S. Lin, N. Malmstadt, Liposome production and concurrent loading of drug simulants by microfluidic hydrodynamic focusing, Eur Biophys J, 48 (2019) 549-558.

[66] M. Michelon, D.R.B. Oliveira, G. de Figueiredo Furtado, L. Gaziola de la Torre, R.L. Cunha, High-throughput continuous production of liposomes using hydrodynamic flow-focusing microfluidic devices, Colloids Surf B Biointerfaces, 156 (2017) 349-357.

[67] J.C. Stachowiak, D.L. Richmond, T.H. Li, A.P. Liu, S.H. Parekh, D.A. Fletcher, Unilamellar vesicle formation and encapsulation by microfluidic jetting, P Natl Acad Sci USA, 105 (2008) 4697-4702.

[68] H.C. Shum, D. Lee, I. Yoon, T. Kodger, D.A. Weitz, Double emulsion templated monodisperse phospholipid vesicles, Langmuir, 24 (2008) 7651-7653.

[69] K.H. Yung-Chieh Tan, Maria Siu, Yen-Ru Pan, and Abraham Phillip Lee, Controlled Microfluidic Encapsulation of Cells, Proteins, and Microbeads in Lipid Vesicles, J. AM. CHEM. SOC., 128 (2006) 5656-5658.

[70] S. Sugiura, T. Kuroiwa, T. Kagota, M. Nakajima, S. Sato, S. Mukataka, P. Walde, S. Ichikawa, Novel method for obtaining homogeneous giant vesicles from a monodisperse water-in-oil emulsion prepared with a microfluidic device, Langmuir, 24 (2008) 4581-4588.

[71] S. Ota, S. Yoshizawa, S. Takeuchi, Microfluidic formation of monodisperse, cell-sized, and unilamellar vesicles, Angew Chem Int Ed Engl, 48 (2009) 6533-6537.

[72] S. Matosevic, B.M. Paegel, Stepwise synthesis of giant unilamellar vesicles on a microfluidic assembly line, J Am Chem Soc, 133 (2011) 2798-2800.

[73] D. van Swaay, A. deMello, Microfluidic methods for forming liposomes, Lab Chip, 13 (2013) 752-767.

[74] R. Ran, A.P.J. Middelberg, C.X. Zhao, Microfluidic synthesis of multifunctional liposomes for tumour targeting, Colloids Surf B Biointerfaces, 148 (2016) 402-410.

[75] N. Hamano, R. Bottger, S.E. Lee, Y. Yang, J.A. Kulkarni, S. Ip, P.R. Cullis, S.D. Li, Robust Microfluidic Technology and New Lipid Composition for Fabrication of Curcumin-Loaded Liposomes: Effect on the Anticancer Activity and Safety of Cisplatin, Mol Pharm, 16 (2019) 3957-3967.

[76] P. Anand, A.B. Kunnumakkara, R.A. Newman, B.B. Aggarwal, Bioavailability of curcumin: Problems and promises, Molecular Pharmaceutics, 4 (2007) 807-818.

[77] M.-C.M. Tzeng-Horng Leu, The Molecular Mechanisms for the Antitumorigenic Effect of Curcumin, Curr. Med. Chem. - Anti-Cancer Agents, 2 (2002) 357-370.

[78] P. Kumar, C.C. Barua, K. Sulakhiya, R.K. Sharma, Curcumin Ameliorates Cisplatin-Induced Nephrotoxicity and Potentiates Its Anticancer Activity in SD Rats: Potential Role of Curcumin in Breast Cancer Chemotherapy, Front Pharmacol, 8 (2017) 132.

[79] K. Shahani, S.K. Swaminathan, D. Freeman, A. Blum, L. Ma, J. Panyam, Injectable sustained release microparticles of curcumin: a new concept for cancer chemoprevention, Cancer Res, 70 (2010) 4443-4452.

[80] P. Kumari, M.O. Swami, S.K. Nadipalli, S. Myneni, B. Ghosh, S. Biswas, Curcumin Delivery by Poly(Lactide)-Based Co-Polymeric Micelles: An In Vitro Anticancer Study, Pharm Res, 33 (2016) 826-841.

[81] N.A. Patankar, D. Waterhouse, D. Strutt, M. Anantha, M.B. Bally, Topophore C: a liposomal nanoparticle formulation of topotecan for treatment of ovarian cancer, Invest New Drugs, 31 (2013) 46-58.

[82] P.R. Cullis, M.J. Hope, Lipid Nanoparticle Systems for Enabling Gene Therapies, Mol Ther, 25 (2017) 1467-1475.

[83] N. Pardi, M.J. Hogan, R.S. Pelc, H. Muramatsu, H. Andersen, C.R. DeMaso, K.A. Dowd, L.L. Sutherland, R.M. Scearce, R. Parks, W. Wagner, A. Granados, J. Greenhouse, M. Walker, E. Willis, J.S. Yu, C.E. McGee, G.D. Sempowski, B.L. Mui, Y.K. Tam, Y.J. Huang, D. Vanlandingham, V.M. Holmes, H. Balachandran, S. Sahu, M. Lifton, S. Higgs, S.E. Hensley, T.D. Madden, M.J. Hope, K. Kariko, S. Santra, B.S. Graham, M.G. Lewis, T.C. Pierson, B.F. Haynes, D. Weissman, Zika virus protection by a single low-dose nucleoside-modified mRNA vaccination, Nature, 543 (2017) 248-251.

[84] J.A. Kulkarni, J.L. Myhre, S. Chen, Y.Y.C. Tam, A. Danescu, J.M. Richman, P.R. Cullis, Design of lipid nanoparticles for in vitro and in vivo delivery of plasmid DNA, Nanomedicine, 13 (2017) 1377-1387.

[85] D. Wilbie, J. Walther, E. Mastrobattista, Delivery Aspects of CRISPR/Cas for in Vivo Genome Editing, Acc Chem Res, 52 (2019) 1555-1564.

[86] C.F. Xu, G.J. Chen, Y.L. Luo, Y. Zhang, G. Zhao, Z.D. Lu, A. Czarna, Z. Gu, J. Wang, Rational designs of in vivo CRISPR-Cas delivery systems, Adv Drug Deliv Rev, (2019).

[87] D. Witzigmann, J.A. Kulkarni, J. Leung, S. Chen, P.R. Cullis, R. van der Meel, Lipid nanoparticle technology for therapeutic gene regulation in the liver, Adv Drug Deliv Rev, (2020).

[88] M. Estanqueiro, J. Conceição, M.H. Amaral, J.M. Sousa Lobo, The role of liposomes and lipid nanoparticles in the skin hydration, in: Nanobiomaterials in Galenic Formulations and Cosmetics, 2016, pp. 297-326.

[89] V.A. Duong, T.T. Nguyen, H.J. Maeng, Preparation of Solid Lipid Nanoparticles and Nanostructured Lipid Carriers for Drug Delivery and the Effects of Preparation Parameters of Solvent Injection Method, Molecules, 25 (2020).

[90] K.M. Wolfgang Mehnert, Solid lipid nanoparticles

Production, characterization and applications, Advanced Drug Delivery Reviews 47 (2001) 165-196.

[91] J.A. Kulkarni, M.M. Darjuan, J.E. Mercer, S. Chen, R. van der Meel, J.L. Thewalt, Y.Y.C. Tam, P.R. Cullis, On the Formation and Morphology of Lipid Nanoparticles Containing Ionizable Cationic Lipids and siRNA, ACS Nano, 12 (2018) 4787-4795.

[92] D. Chen, K.T. Love, Y. Chen, A.A. Eltoukhy, C. Kastrup, G. Sahay, A. Jeon, Y. Dong, K.A. Whitehead, D.G. Anderson, Rapid Discovery of Potent siRNA-Containing Lipid Nanoparticles Enabled by Controlled Microfluidic Formulation, Journal of the American Chemical Society, 134 (2012) 6948-6951.

[93] D. Adams, A. Gonzalez-Duarte, W.D. O'Riordan, C.C. Yang, M. Ueda, A.V. Kristen, I. Tournev, H.H. Schmidt, T. Coelho, J.L. Berk, K.P. Lin, G. Vita, S. Attarian, V. Plante-Bordeneuve, M.M. Mezei, J.M. Campistol, J. Buades, T.H. Brannagan, 3rd, B.J. Kim, J. Oh, Y. Parman, Y. Sekijima, P.N. Hawkins, S.D. Solomon, M. Polydefkis, P.J. Dyck, P.J. Gandhi, S. Goyal, J. Chen, A.L. Strahs, S.V. Nochur, M.T. Sweetser, P.P. Garg, A.K. Vaishnaw, J.A. Gollob, O.B. Suhr, Patisiran, an RNAi Therapeutic, for Hereditary Transthyretin Amyloidosis, N Engl J Med, 379 (2018) 11-21.

[94] S. Chen, Y.Y.C. Tam, P.J.C. Lin, M.M.H. Sung, Y.K. Tam, P.R. Cullis, Influence of particle size on the in vivo potency of lipid nanoparticle formulations of siRNA, J Control Release, 235 (2016) 236-244.

[95] N. Jyotsana, A. Sharma, A. Chaturvedi, R. Budida, M. Scherr, F. Kuchenbauer, R. Lindner, F. Noyan, K.W. Suhs, M. Stangel, D. Grote-Koska, K. Brand, H.P. Vornlocher, M. Eder, F. Thol, A. Ganser, R.K. Humphries, E. Ramsay, P. Cullis, M. Heuser, Lipid nanoparticle-mediated siRNA delivery for safe targeting of human CML in vivo, Ann Hematol, 98 (2019) 1905-1918.

[96] Y.Y. Tam, S. Chen, P.R. Cullis, Advances in Lipid Nanoparticles for siRNA Delivery, Pharmaceutics, 5 (2013) 498-507.

[97] N.M. Belliveau, J. Huft, P.J. Lin, S. Chen, A.K. Leung, T.J. Leaver, A.W. Wild, J.B. Lee, R.J. Taylor, Y.K. Tam, C.L. Hansen, P.R. Cullis, Microfluidic Synthesis of Highly Potent Limit-size Lipid Nanoparticles for In Vivo Delivery of siRNA, Mol Ther Nucleic Acids, 1 (2012) e37.

[98] Z. Tang, N. Kong, X. Zhang, Y. Liu, P. Hu, S. Mou, P. Liljestrom, J. Shi, W. Tan, J.S. Kim, Y. Cao, R. Langer, K.W. Leong, O.C. Farokhzad, W. Tao, A materials-science perspective on tackling COVID-19, Nat Rev Mater, (2020) 1-14.

[99] A.K. Blakney, P.F. McKay, B.I. Yus, Y. Aldon, R.J. Shattock, Inside out: optimization of lipid nanoparticle formulations for exterior complexation and in vivo delivery of saRNA, Gene Ther, 26 (2019) 363-372.

[100] T. Demoulins, P. Milona, P.C. Englezou, T. Ebensen, K. Schulze, R. Suter, C. Pichon, P. Midoux, C.A. Guzman, N. Ruggli, K.C. McCullough, Polyethylenimine-based polyplex delivery of self-replicating RNA vaccines, Nanomedicine, 12 (2016) 711-722.

[101] J. Siepmann, A. Faham, S.D. Clas, B.J. Boyd, V. Jannin, A. Bernkop-Schnurch, H. Zhao, S. Lecommandoux, J.C. Evans, C. Allen, O.M. Merkel, G. Costabile, M.R. Alexander, R.D. Wildman, C.J. Roberts, J.C. Leroux, Lipids and polymers in pharmaceutical technology: Lifelong companions, Int J Pharm, 558 (2019) 128-142.

[102] R.H. Prabhu, V.B. Patravale, M.D. Joshi, Polymeric nanoparticles for targeted treatment in oncology: current insights, Int J Nanomedicine, 10 (2015) 1001-1018.

[103] P. Grossen, D. Witzigmann, S. Sieber, J. Huwyler, PEG-PCL-based nanomedicines: A biodegradable drug delivery system and its application, J Control Release, 260 (2017) 46-60.

[104] C. Vauthier, K. Bouchemal, Methods for the preparation and manufacture of polymeric nanoparticles, Pharm Res, 26 (2009) 1025-1058.

[105] C. Martins, B. Sarmento, Microfluidic Manufacturing of Multitargeted PLGA/PEG Nanoparticles for Delivery of Taxane Chemotherapeutics, Methods Mol Biol, 2059 (2020) 213-224.

[106] M.C. Operti, Y. Dolen, J. Keulen, E.A.W. van Dinther, C.G. Figdor, O. Tagit, Microfluidics-Assisted Size Tuning and Biological Evaluation of PLGA Particles, Pharmaceutics, 11 (2019).

[107] X. Li, X. Jiang, Microfluidics for producing poly (lactic-co-glycolic acid)-based pharmaceutical nanoparticles, Adv Drug Deliv Rev, 128 (2018) 101-114.

[108] A.S. Jong-Min Lim, Laura M. Gilson, Sunandini Chopra, Sungyoung Choi, Jun Wu, Robert Langer, Rohit Karnik, and Omid C. Farokhzad, Ultra-High Throughput Synthesis of Nanoparticles with Homogeneous Size Distribution Using a Coaxial Turbulent Jet Mixer, ACS Nano, 8 (2014) 6056–6065.

[109] S.H. Au, P. Kumar, A.R. Wheeler, A new angle on pluronic additives: advancing droplets and understanding in digital microfluidics, Langmuir, 27 (2011) 8586-8594.

[110] Z. Chen, K.W. Pulsipher, R. Chattaraj, D.A. Hammer, C.M. Sehgal, D. Lee, Engineering the Echogenic Properties of Microfluidic Microbubbles Using Mixtures of Recombinant Protein and Amphiphilic Copolymers, Langmuir, 35 (2019) 10079-10086.

[111] L. Capretto, S. Mazzitelli, E. Brognara, I. Lampronti, D. Carugo, M. Hill, X. Zhang, R. Gambari, C. Nastruzzi, Mithramycin encapsulated in polymeric micelles by microfluidic technology as novel therapeutic protocol for beta-thalassemia, Int J Nanomedicine, 7 (2012) 307-324.

[112] F.S. Majedi, M.M. Hasani-Sadrabadi, S.H. Emami, M.A. Shokrgozar, J.J. VanDersarl, E. Dashtimoghadam, A. Bertsch, P. Renaud, Microfluidic assisted self-assembly of chitosan based nanoparticles as drug delivery agents, Lab Chip, 13 (2013) 204-207.

[113] D. Liu, S. Cito, Y. Zhang, C.-F. Wang, T.M. Sikanen, H.A. Santos, A Versatile and Robust Microfluidic Platform Toward High Throughput Synthesis of Homogeneous Nanoparticles with Tunable Properties, Advanced Materials, 27 (2015) 2298-2304.

[114] D. Essa, Y.E. Choonara, P.P.D. Kondiah, V. Pillay, Comparative Nanofabrication of PLGA-Chitosan-PEG Systems Employing Microfluidics and Emulsification Solvent Evaporation Techniques, Polymers (Basel), 12 (2020).

[115] E. Chiesa, A. Greco, F. Riva, E.M. Tosca, R. Dorati, S. Pisani, T. Modena, B. Conti, I. Genta, Staggered Herringbone Microfluid Device for the Manufacturing of Chitosan/TPP Nanoparticles: Systematic Optimization and Preliminary Biological Evaluation, Int J Mol Sci, 20 (2019).

[116] J. Chen, K. Huang, Q. Chen, C. Deng, J. Zhang, Z. Zhong, Tailor-Making Fluorescent Hyaluronic Acid Microgels via Combining Microfluidics and Photoclick Chemistry for Sustained and Localized Delivery of Herceptin in Tumors, ACS Appl Mater Interfaces, 10 (2018) 3929-3937.

[117] F. Bongiovi, C. Fiorica, F.S. Palumbo, G. Pitarresi, G. Giammona, Hyaluronic acid based nanohydrogels fabricated by microfluidics for the potential targeted release of Imatinib: Characterization and preliminary evaluation of the antiangiogenic effect, Int J Pharm, 573 (2020) 118851.

[118] C. Martino, C. Statzer, D. Vigolo, A.J. deMello, Controllable generation and encapsulation of alginate fibers using droplet-based microfluidics, Lab Chip, 16 (2016) 59-64.

[119] T. Sun, X. Li, Q. Shi, H. Wang, Q. Huang, T. Fukuda, Microfluidic Spun Alginate Hydrogel Microfibers and Their Application in Tissue Engineering, Gels, 4 (2018).

[120] D. Ragab, S. Sabra, Y. Xia, D. Goodale, A.L. Allan, S. Rohani, On-Chip Preparation of Amphiphilic Nanomicelles-in-Sodium Alginate Spheroids as a Novel Platform Against Triple-Negative Human Breast Cancer Cells: Fabrication, Study of Microfluidics Flow Hydrodynamics and Proof of Concept for Anticancer and Drug Delivery Applications, J Pharm Sci, 108 (2019) 3528-3539.

[121] F.S. Majedi, M.M. Hasani-Sadrabadi, J.J. VanDersarl, N. Mokarram, S. Hojjati-Emami, E. Dashtimoghadam, S. Bonakdar, M.A. Shokrgozar, A. Bertsch, P. Renaud, On-Chip Fabrication of Paclitaxel-Loaded Chitosan Nanoparticles for Cancer Therapeutics, Advanced Functional Materials, 24 (2014) 432-441.

[122] J.M. Lim, N. Bertrand, P.M. Valencia, M. Rhee, R. Langer, S. Jon, O.C. Farokhzad, R. Karnik, Parallel microfluidic synthesis of size-tunable polymeric nanoparticles using 3D flow focusing towards in vivo study, Nanomedicine, 10 (2014) 401-409.

[123] Jong-Min Lim, ‡,§ Archana Swami,‡ Laura M. Gilson,† Sunandini Chopra,† Sungyoung Choi,†,^ Jun Wu,‡ Robert Langer,§,, Rohit Karnik, * and Omid C. Farokhzad‡,#,*, Ultra-High Throughput Synthesis of Nanoparticles with Homogeneous Size Distribution Using a Coaxial Turbulent Jet Mixer, ACS Nano, 8 (2014) 6056-6065.

[124] N. Anton, F. Bally, C.A. Serra, A. Ali, Y. Arntz, Y. Mely, M. Zhao, E. Marchioni, A. Jakhmola, T.F. Vandamme, A new microfluidic setup for precise control of the polymer nanoprecipitation process and lipophilic drug encapsulation, Soft Matter, 8 (2012).

[125] H. Debus, M. Beck-Broichsitter, T. Kissel, Optimized preparation of pDNA/poly(ethylene imine) polyplexes using a microfluidic system, Lab Chip, 12 (2012) 2498-2506.

[126] J.D. Ziebarth, D.R. Kennetz, N.J. Walker, Y. Wang, Structural Comparisons of PEI/DNA and PEI/siRNA Complexes Revealed with Molecular Dynamics Simulations, J Phys Chem B, 121 (2017) 1941-1952.

[127] W.F. Lai, M.C. Lin, Nucleic acid delivery with chitosan and its derivatives, J Control Release, 134 (2009) 158-168.

[128] D.R. Wilson, A. Mosenia, M.P. Suprenant, R. Upadhya, D. Routkevitch, R.A. Meyer, A. Quinones-Hinojosa, J.J. Green, Continuous microfluidic assembly of biodegradable poly(beta-amino ester)/DNA nanoparticles for enhanced gene delivery, J Biomed Mater Res A, 105 (2017) 1813-1825.

[129] Y.P. Ho, C.L. Grigsby, F. Zhao, K.W. Leong, Tuning physical properties of nanocomplexes through microfluidics-assisted confinement, Nano Lett, 11 (2011) 2178-2182.

[130] M. Lu, Y.P. Ho, C.L. Grigsby, A.A. Nawaz, K.W. Leong, T.J. Huang, Three-dimensional hydrodynamic focusing method for polyplex synthesis, ACS Nano, 8 (2014) 332-339.

[131] J.Y. Cherng, H. Talsma, R. Verrijk, D.J. Crommelin, W.E. Hennink, The effect of formulation parameters on the size of poly-((2-dimethylamino)ethyl methacrylate)-plasmid complexes, Eur J Pharm Biopharm, 47 (1999) 215-224.

[132] J.Y. Cherng, P. van de Wetering, H. Talsma, D.J. Crommelin, W.E. Hennink, Effect of size and serum proteins on transfection efficiency of poly ((2-dimethylamino)ethyl methacrylate)-plasmid nanoparticles, Pharm Res, 13 (1996) 1038-1042.

[133] S. Asayama, M. Sudo, S. Nagaoka, H. Kawakami, Carboxymethyl poly(L-histidine) as a new pH-sensitive polypeptide to enhance polyplex gene delivery, Molecular Pharmaceutics, 5 (2008) 898-901.

[134] A.V. Kabanov, I.V. Astafieva, I.V. Maksimova, E.M. Lukanidin, G.P. Georgiev, V.A. Kabanov, Efficient Transformation of Mammalian-Cells Using DNA Interpolyelectrolyte Complexes with Carbon-Chain Polycations, Bioconjugate Chemistry, 4 (1993) 448-454.

[135] H. Wang, K. Liu, K.J. Chen, Y. Lu, S. Wang, W.Y. Lin, F. Guo, K. Kamei, Y.C. Chen, M. Ohashi, M. Wang, M.A. Garcia, X.Z. Zhao, C.K. Shen, H.R. Tseng, A rapid pathway toward a superb gene delivery system: programming structural and functional diversity into a supramolecular nanoparticle library, ACS Nano, 4 (2010) 6235-6243.

[136] D.P. Feldmann, J. Heyza, C.M. Zimmermann, S.M. Patrick, O.M. Merkel, Nanoparticle-Mediated Gene Silencing for Sensitization of Lung Cancer to Cisplatin Therapy, Molecules, 25 (2020).

[137] Z. He, J.L. Santos, H. Tian, H. Huang, Y. Hu, L. Liu, K.W. Leong, Y. Chen, H.Q. Mao, Scalable fabrication of size-controlled chitosan nanoparticles for oral delivery of insulin, Biomaterials, 130 (2017) 28-41.

[138] H.L. Gordon L Amidon, Vinod P Shah, John R Crison, A theoretical basis for a biopharmaceutical drug classification, Pharmaceutical Research, 12 (1995).

[139] M. Lindenberg, S. Kopp, J.B. Dressman, Classification of orally administered drugs on the World Health Organization Model list of Essential Medicines according to the biopharmaceutics classification system, Eur J Pharm Biopharm, 58 (2004) 265-278.

[140] M. Murakami, K. Nishina, C. Watanabe, K. Yoshida-Tanaka, W. Piao, H. Kuwahara, Y. Horikiri, K. Miyata, N. Nishiyama, K. Kataoka, M. Yoshida, H. Mizusawa, T. Yokota, Enteral siRNA delivery technique for therapeutic gene silencing in the liver via the lymphatic route, Sci Rep, 5 (2015) 17035.

[141] G.R. Valicherla, K.M. Dave, A.A. Syed, M. Riyazuddin, A.P. Gupta, A. Singh, Wahajuddin, K. Mitra, D. Datta, J.R. Gayen, Formulation optimization of Docetaxel loaded self-emulsifying drug delivery system to enhance bioavailability and anti-tumor activity, Sci Rep, 6 (2016) 26895.

[142] Y. Jiang, R. Tang, B. Duncan, Z. Jiang, B. Yan, R. Mout, V.M. Rotello, Direct cytosolic delivery of siRNA using nanoparticle-stabilized nanocapsules, Angew Chem Int Ed Engl, 54 (2015) 506-510.

[143] L. Zhang, Q. Feng, J. Wang, J. Sun, X. Shi, X. Jiang, Microfluidic synthesis of rigid nanovesicles for hydrophilic reagents delivery, Angew Chem Int Ed Engl, 54 (2015) 3952-3956.

[144] L.I. Zhang, L. Zhang, Lipid–Polymer Hybrid Nanoparticles: Synthesis, Characterization and Applications, Nano LIFE, 01 (2012) 163-173.

[145] V. Dave, K. Tak, A. Sohgaura, A. Gupta, V. Sadhu, K.R. Reddy, Lipid-polymer hybrid nanoparticles: Synthesis strategies and biomedical applications, J Microbiol Methods, 160 (2019) 130-142.

[146] R.X. Zhang, T. Ahmed, L.Y. Li, J. Li, A.Z. Abbasi, X.Y. Wu, Design of nanocarriers for nanoscale drug delivery to enhance cancer treatment using hybrid polymer and lipid building blocks, Nanoscale, 9 (2017) 1334-1355.

[147] R.J. Bose, S.H. Lee, H. Park, Lipid-based surface engineering of PLGA nanoparticles for drug and gene delivery applications, Biomater Res, 20 (2016) 34.

[148] S. Krishnamurthy, R. Vaiyapuri, L. Zhang, J.M. Chan, Lipid-coated polymeric nanoparticles for cancer drug delivery, Biomater Sci, 3 (2015) 923-936.

[149] B. Mandal, H. Bhattacharjee, N. Mittal, H. Sah, P. Balabathula, L.A. Thoma, G.C. Wood, Core-shell-type lipid-polymer hybrid nanoparticles as a drug delivery platform, Nanomedicine, 9 (2013) 474-491.

[150] R. Jc Bose, S.-H. Lee, H. Park, Lipid polymer hybrid nanospheres encapsulating antiproliferative agents for stent applications, J. Ind. Eng. Chem., 36 (2016) 284-292.

[151] L. Zhang, J.M. Chan, F.X. Gu, J.W. Rhee, A.Z. Wang, A.F. Radovic-Moreno, F. Alexis, R. Langer, O.C. Farokhzad, Self-assembled lipid--polymer hybrid nanoparticles: a robust drug delivery platform, ACS Nano, 2 (2008) 1696-1702.

[152] N. Tahir, A. Madni, W. Li, A. Correia, M.M. Khan, M.A. Rahim, H.A. Santos, Microfluidic fabrication and characterization of Sorafenib-loaded lipid-polymer hybrid nanoparticles for controlled drug delivery, Int J Pharm, 581 (2020) 119275.

[153] L. Zhang, Q. Feng, J. Wang, S. Zhang, B. Ding, Y. Wei, M. Dong, J.-Y. Ryu, T.-Y. Yoon, X. Shi, J. Sun, X. Jiang, Microfluidic Synthesis of Hybrid Nanoparticles with Controlled Lipid Layers: Understanding Flexibility-Regulated Cell–Nanoparticle Interaction, ACS Nano, 9 (2015) 9912-9921.

[154] W. Wei, J. Sun, X.Y. Guo, X. Chen, R. Wang, C. Qiu, H.T. Zhang, W.H. Pang, J.C. Wang, Q. Zhang, Microfluidic-Based Holonomic Constraints of siRNA in the Kernel of Lipid/Polymer Hybrid Nanoassemblies for Improving Stable and Safe In Vivo Delivery, ACS Appl Mater Interfaces, 12 (2020) 14839-14854.

[155] E.T. Sarcan, M. Silindir-Gunay, A.Y. Ozer, Theranostic polymeric nanoparticles for NIR imaging and photodynamic therapy, Int J Pharm, 551 (2018) 329-338.

[156] W.L. Tang, W.H. Tang, S.D. Li, Cancer theranostic applications of lipid-based nanoparticles, Drug Discov Today, 23 (2018) 1159-1166.

[157] M.M. Hasani-Sadrabadi, E. Dashtimoghadam, G. Bahlakeh, F.S. Majedi, H. Keshvari, J.J. Van Dersarl, A. Bertsch, A. Panahifar, P. Renaud, L. Tayebi, M. Mahmoudi, K.I. Jacob, On-chip synthesis of fine-tuned bone-seeking hybrid nanoparticles, Nanomedicine (Lond), 10 (2015) 3431-3449.

[158] P.M. Valencia, P.A. Basto, L. Zhang, M. Rhee, R. Langer, O.C. Farokhzad, R. Karnik, Single-step assembly of homogenous lipid-polymeric and lipid-quantum dot nanoparticles enabled by microfluidic rapid mixing, ACS Nano, 4 (2010) 1671-1679.

[159] F.R. Maia, R.L. Reis, J.M. Oliveira, Finding the perfect match between nanoparticles and microfluidics to respond to cancer challenges, Nanomedicine, 24 (2019) 102139.

[160] J. Mosayebi, M. Kiyasatfar, S. Laurent, Synthesis, Functionalization, and Design of Magnetic Nanoparticles for Theranostic Applications, Adv Healthc Mater, 6 (2017).

[161] J.P. Martins, G. Torrieri, H.A. Santos, The importance of microfluidics for the preparation of nanoparticles as advanced drug delivery systems, Expert Opin Drug Deliv, 15 (2018) 469-479.

[162] R.L. Juliano, The delivery of therapeutic oligonucleotides, Nucleic Acids Res, 44 (2016) 6518-6548.

[163] K. Paunovska, D. Loughrey, J.E. Dahlman, Drug delivery systems for RNA therapeutics, Nat Rev Genet, 23 (2022) 265-280.

[164] S. Han, R.I. Mahato, Y.K. Sung, S.W. Kim, Development of biomaterials for gene therapy, Mol Ther, 2 (2000) 302-317.

[165] D. Luo, W.M. Saltzman, Synthetic DNA delivery systems, Nat Biotechnol, 18 (2000) 33-37.

[166] H. Lee, J.H. Jeong, T.G. Park, A new gene delivery formulation of polyethylenimine/DNA complexes coated with PEG conjugated fusogenic peptide, J Control Release, 76 (2001) 183-192.

[167] L. Zhou, M. Emenuga, S. Kumar, Z. Lamantia, M. Figueiredo, T. Emrick, Designing Synthetic Polymers for Nucleic Acid Complexation and Delivery: From Polyplexes to Micelleplexes to Triggered Degradation, Biomacromolecules, (2022).

[168] B.D. Monnery, Polycation-Mediated Transfection: Mechanisms of Internalization and Intracellular Trafficking, Biomacromolecules, 22 (2021) 4060-4083.

[169] R. Kumar, C.F. Santa Chalarca, M.R. Bockman, C.V. Bruggen, C.J. Grimme, R.J. Dalal, M.G. Hanson, J.K. Hexum, T.M. Reineke, Polymeric Delivery of Therapeutic Nucleic Acids, Chem Rev, 121 (2021) 11527-11652.

[170] Y. Liu, J. Nguyen, T. Steele, O. Merkel, T. Kissel, A new synthesis method and degradation of hyper-branched polyethylenimine grafted polycaprolactone block mono-methoxyl poly (ethylene glycol) copolymers (hy-PEI-g-PCL-b-mPEG) as potential DNA delivery vectors, Polymer, 50 (2009) 3895-3904.

[171] R. Jiang, X. Lu, M. Yang, W. Deng, Q. Fan, W. Huang, Monodispersed brush-like conjugated polyelectrolyte nanoparticles with efficient and visualized siRNA delivery for gene silencing, Biomacromolecules, 14 (2013) 3643-3652.

[172] R.J. Dalal, R. Kumar, M. Ohnsorg, M. Brown, T.M. Reineke, Cationic Bottlebrush Polymers Outperform Linear Polycation Analogues for pDNA Delivery and Gene Expression, ACS Macro Lett, 10 (2021) 886-893.

[173] Y. Jiang, T.P. Lodge, T.M. Reineke, Packaging pDNA by Polymeric ABC Micelles Simultaneously Achieves Colloidal Stability and Structural Control, J Am Chem Soc, 140 (2018) 11101-11111.

[174] X. Yang, Y. Wang, Y. Zhou, J. Chen, Q. Wan, The Application of Polycaprolactone in Three-Dimensional Printing Scaffolds for Bone Tissue Engineering, Polymers (Basel), 13 (2021).

[175] G.P. Tang, J.M. Zeng, S.J. Gao, Y.X. Ma, L. Shi, Y. Li, H.P. Too, S. Wang, Polyethylene glycol modified polyethylenimine for improved CNS gene transfer: effects of PEGylation extent, Biomaterials, 24 (2003) 2351-2362.

[176] S. Akhtar, Non-viral cancer gene therapy: beyond delivery, Gene Ther, 13 (2006) 739-740.

[177] O.M. Merkel, A. Beyerle, D. Librizzi, A. Pfestroff, T.M. Behr, B. Sproat, P.J. Barth, T. Kissel, Nonviral siRNA delivery to the lung: investigation of PEG-PEI polyplexes and their in vivo performance, Mol Pharm, 6 (2009) 1246-1260.

[178] T. Endres, M. Zheng, A. Kilic, A. Turowska, M. Beck-Broichsitter, H. Renz, O.M. Merkel, T. Kissel, Amphiphilic biodegradable PEG-PCL-PEI triblock copolymers for FRET-capable in vitro and in vivo delivery of siRNA and quantum dots, Mol Pharm, 11 (2014) 1273-1281.

[179] S. Mishra, P. Webster, M.E. Davis, PEGylation significantly affects cellular uptake and intracellular trafficking of non-viral gene delivery particles, Eur J Cell Biol, 83 (2004) 97-111.

[180] O.M. Merkel, D. Librizzi, A. Pfestroff, T. Schurrat, K. Buyens, N.N. Sanders, S.C. De Smedt, M. Behe, T. Kissel, Stability of siRNA polyplexes from poly(ethylenimine) and poly(ethylenimine)-g-poly(ethylene glycol) under in vivo conditions: effects on pharmacokinetics and biodistribution measured by Fluorescence Fluctuation Spectroscopy and Single Photon Emission Computed Tomography (SPECT) imaging, J Control Release, 138 (2009) 148-159.

[181] M. Zheng, D. Librizzi, A. Kilic, Y. Liu, H. Renz, O.M. Merkel, T. Kissel, Enhancing in vivo circulation and siRNA delivery with biodegradable polyethylenimine-graft-polycaprolactone-block-poly(ethylene glycol) copolymers, Biomaterials, 33 (2012) 6551-6558.

[182] M. Zheng, Y. Liu, O. Samsonova, T. Endres, O. Merkel, T. Kissel, Amphiphilic and biodegradable hy-PEI-g-PCL-b-PEG copolymers efficiently mediate transgene expression depending on their graft density, Int J Pharm, 427 (2012) 80-87.

[183] H. Petersen, P.M. Fechner, A.L. Martin, K. Kunath, S. Stolnik, C.J. Roberts, D. Fischer, M.C. Davies, T. Kissel, Polyethylenimine-graft-poly(ethylene glycol) copolymers: Influence of copolymer block structure on DNA complexation and biological activities as gene delivery system, Bioconjugate Chemistry, 13 (2002) 845-854.

[184] C.L. Grigsby, Y.-P. Ho, C. Lin, J.F.J. Engbersen, K.W. Leong, Microfluidic Preparation of Polymer-Nucleic Acid Nanocomplexes Improves Nonviral Gene Transfer, Scientific Reports, 3 (2013) 3155.

[185] T. Endres, M. Zheng, M. Beck-Broichsitter, O. Samsonova, H. Debus, T. Kissel, Optimising the self-assembly of siRNA loaded PEG-PCL-lPEI nano-carriers employing different preparation techniques, J Control Release, 160 (2012) 583-591.

[186] C.M. Zimmermann, D. Baldassi, K. Chan, N.B.P. Adams, A. Neumann, D.L. Porras-Gonzalez, X. Wei, N. Kneidinger, M.G. Stoleriu, G. Burgstaller, D. Witzigmann, P. Luciani, O.M. Merkel, Spray drying siRNA-lipid nanoparticles for dry powder pulmonary delivery, J Control Release, (2022).

[187] L. Liu, M. Zheng, D. Librizzi, T. Renette, O.M. Merkel, T. Kissel, Efficient and Tumor Targeted siRNA Delivery by Polyethylenimine-graft-polycaprolactone-block-poly(ethylene glycol)-folate (PEI–PCL–PEG–Fol), Molecular Pharmaceutics, 13 (2015) 134-143.

[188] Y. Xie, N.H. Kim, V. Nadithe, D. Schalk, A. Thakur, A. Kilic, L.G. Lum, D.J.P. Bassett, O.M. Merkel, Targeted delivery of siRNA to activated T cells via transferrin-polyethylenimine (Tf-PEI) as a potential therapy of asthma, J Control Release, 229 (2016) 120-129.

[189] T.W.M. Keil, C. Zimmermann, D. Baldassi, F. Adams, W. Friess, A. Mehta, O.M. Merkel, Impact of Crystalline and Amorphous Matrices on Successful Spray Drying of siRNA Polyplexes for Inhalation of Nano-in-Microparticles, Adv Ther, (2021) 1-15.

[190] R. Singh, J.W. Lillard, Jr., Nanoparticle-based targeted drug delivery, Exp Mol Pathol, 86 (2009) 215-223.

[191] O.M. Merkel, T. Kissel, Quo vadis polyplex?, J Control Release, 190 (2014) 415-423.

[192] M. Danaei, M. Dehghankhold, S. Ataei, F. Hasanzadeh Davarani, R. Javanmard, A. Dokhani, S. Khorasani, M.R. Mozafari, Impact of Particle Size and Polydispersity Index on the Clinical Applications of Lipidic Nanocarrier Systems, Pharmaceutics, 10 (2018).

[193] R. Li, Wang, X., Z. Ji, B. Sun, H. Zhang, C.H. Chang, S. Lin, H. Meng, Y.P. Liao, M. Wang, Z. Li, A.A. Hwang, T.B. Song, R. Xu, Y. Yang, J.I. Zink, A.E. Nel, T. Xia, Surface charge and cellular processing of covalently functionalized multiwall carbon nanotubes determine pulmonary toxicity, ACS Nano, 7 (2013) 2352-2368.

[194] I. Canton, G. Battaglia, Endocytosis at the nanoscale, Chem Soc Rev, 41 (2012) 2718-2739.

[195] D. Pei, M. Buyanova, Overcoming Endosomal Entrapment in Drug Delivery, Bioconjug Chem, 30 (2019) 273-283.

[196] O. Boussif, F. Lezoualch, M.A. Zanta, M.D. Mergny, D. Scherman, B. Demeneix, J.P. Behr, A Versatile Vector for Gene and Oligonucleotide Transfer into Cells in Culture and in-Vivo - Polyethylenimine, P Natl Acad Sci USA, 92 (1995) 7297-7301.

[197] S. Hong, P.R. Leroueil, E.K. Janus, J.L. Peters, M.M. Kober, M.T. Islam, B.G. Orr, J.R. Baker, Jr., M.M. Banaszak Holl, Interaction of polycationic polymers with supported lipid bilayers and cells: nanoscale hole formation and enhanced membrane permeability, Bioconjug Chem, 17 (2006) 728-734.

[198] P.R. Leroueil, S.A. Berry, K. Duthie, G. Han, V.M. Rotello, D.Q. McNerny, J.R. Baker, Jr., B.G. Orr, M.M. Holl, Wide varieties of cationic nanoparticles induce defects in supported lipid bilayers, Nano Lett, 8 (2008) 420-424.

[199] M.T. McManus, P.A. Sharp, Gene silencing in mammals by small interfering RNAs, Nat Rev Genet, 3 (2002) 737-747.

[200] O.M. Merkel, I. Rubinstein, T. Kissel, siRNA delivery to the lung: what's new?, Adv Drug Deliv Rev, 75 (2014) 112-128.

[201] I.G. Medeiros, A.S. Khayat, B. Stransky, S. Santos, P. Assumpcao, J.E.S. de Souza, A small interfering RNA (siRNA) database for SARS-CoV-2, Sci Rep, 11 (2021) 8849.

[202] A. Idris, A. Davis, A. Supramaniam, D. Acharya, G. Kelly, Y. Tayyar, N. West, P. Zhang, C.L.D. McMillan, C. Soemardy, R. Ray, D. O'Meally, T.A. Scott, N.A.J. McMillan, K.V. Morris, A SARS-CoV-2 targeted siRNA-nanoparticle therapy for COVID-19, Mol Ther, 29 (2021) 2219-2226.

[203] A. Mehta, T. Michler, O.M. Merkel, siRNA Therapeutics against Respiratory Viral Infections-What Have We Learned for Potential COVID-19 Therapies?, Adv Healthc Mater, 10 (2021) e2001650.

[204] M.I. Sajid, M. Moazzam, Y. Cho, S. Kato, A. Xu, J.J. Way, S. Lohan, R.K. Tiwari, siRNA Therapeutics for the Therapy of COVID-19 and Other Coronaviruses, Mol Pharm, 18 (2021) 2105-2121.

[205] Y. Xie, O.M. Merkel, Pulmonary Delivery of siRNA via Polymeric Vectors as Therapies of Asthma, Arch Pharm (Weinheim), 348 (2015) 681-688.

[206] K. Dua, R. Wadhwa, G. Singhvi, V. Rapalli, S.D. Shukla, M.D. Shastri, G. Gupta, S. Satija, M. Mehta, N. Khurana, R. Awasthi, P.K. Maurya, L. Thangavelu, R. S, M.M. Tambuwala, T. Collet, P.M. Hansbro, D.K. Chellappan, The potential of siRNA based drug delivery in respiratory disorders: Recent advances and progress, Drug Dev Res, 80 (2019) 714-730.

[207] F. Apparailly, C. Jorgensen, siRNA-based therapeutic approaches for rheumatic diseases, Nat Rev Rheumatol, 9 (2013) 56-62.

[208] N. Feng, F. Guo, Nanoparticle-siRNA: A potential strategy for rheumatoid arthritis therapy?, J Control Release, 325 (2020) 380-393.

[209] M. Grzelinski, B. Urban-Klein, T. Martens, K. Lamszus, U. Bakowsky, S. Hobel, F. Czubayko, A. Aigner, RNA interference-mediated gene silencing of pleiotrophin through polyethylenimine-complexed small interfering RNAs in vivo exerts antitumoral effects in glioblastoma xenografts, Hum Gene Ther, 17 (2006) 751-766.

[210] M.J. Gomes, S. Martins, B. Sarmento, siRNA as a tool to improve the treatment of brain diseases: Mechanism, targets and delivery, Ageing Res Rev, 21 (2015) 43-54.

[211] M. Zheng, W. Tao, Y. Zou, O.C. Farokhzad, B. Shi, Nanotechnology-Based Strategies for siRNA Brain Delivery for Disease Therapy, Trends Biotechnol, 36 (2018) 562-575.

[212] G. Rassu, E. Soddu, A.M. Posadino, G. Pintus, B. Sarmento, P. Giunchedi, E. Gavini, Nose-to-brain delivery of BACE1 siRNA loaded in solid lipid nanoparticles for Alzheimer's therapy, Colloids Surf B Biointerfaces, 152 (2017) 296-301.

[213] T. Kanazawa, F. Akiyama, S. Kakizaki, Y. Takashima, Y. Seta, Delivery of siRNA to the brain using a combination of nose-to-brain delivery and cell-penetrating peptide-modified nano-micelles, Biomaterials, 34 (2013) 9220-9226.

[214] M.G. Kaplitt, A. Feigin, C. Tang, H.L. Fitzsimons, P. Mattis, P.A. Lawlor, R.J. Bland, D. Young, K. Strybing, D. Eidelberg, M.J. During, Safety and tolerability of gene therapy with an adeno-associated virus (AAV) borne GAD gene for Parkinson's disease: an open label, phase I trial, Lancet, 369 (2007) 2097-2105.

[215] F. Zahir-Jouzdani, F. Mottaghitalab, M. Dinarvand, F. Atyabi, siRNA delivery for treatment of degenerative diseases, new hopes and challenges, Journal of Drug Delivery Science and Technology, 45 (2018) 428-441.

[216] M. Thomas, J.J. Lu, J. Chen, A.M. Klibanov, Non-viral siRNA delivery to the lung, Adv Drug Deliv Rev, 59 (2007) 124-133.

[217] S.M. Elbashir, J. Harborth, W. Lendeckel, A. Yalcin, K. Weber, T. Tuschl, Duplexes of 21-nucleotide RNAs mediate RNA interference in cultured mammalian cells, Nature, 411 (2001) 494-498.

[218] S.M. Elbashir, W. Lendeckel, T. Tuschl, RNA interference is mediated by 21- and 22-nucleotide RNAs, Genes Dev, 15 (2001) 188-200.

[219] S.M. Elbashir, J. Martinez, A. Patkaniowska, W. Lendeckel, T. Tuschl, Functional anatomy of siRNAs for mediating efficient RNAi in Drosophila melanogaster embryo lysate, EMBO J, 20 (2001) 6877-6888.

[220] A. Fire, S. Xu, M.K. Montgomery, S.A. Kostas, S.E. Driver, C.C. Mello, Potent and specific genetic interference by double-stranded RNA in Caenorhabditis elegans, Nature, 391 (1998) 806-811.

[221] G.J. Hannon, RNA interference, Nature, 418 (2002) 244-251.

[222] J.Y. Jeon, V.S. Ayyar, A. Mitra, Pharmacokinetic and Pharmacodynamic Modeling of siRNA Therapeutics - a Minireview, Pharm Res, 39 (2022) 1749-1759.

[223] A. Paul, A. Muralidharan, A. Biswas, B.V. Kamath, A. Joseph, A.T. Alex, siRNA therapeutics and its challenges: Recent advances in effective delivery for cancer therapy, OpenNano, 7 (2022).

[224] M. Gunther, J. Lipka, A. Malek, D. Gutsch, W. Kreyling, A. Aigner, Polyethylenimines for RNAi-mediated gene targeting in vivo and siRNA delivery to the lung, Eur J Pharm Biopharm, 77 (2011) 438-449.

[225] A. de Fougerolles, T. Novobrantseva, siRNA and the lung: research tool or therapeutic drug?, Curr Opin Pharmacol, 8 (2008) 280-285.

[226] O.M. Merkel, M. Zheng, H. Debus, T. Kissel, Pulmonary gene delivery using polymeric nonviral vectors, Bioconjug Chem, 23 (2012) 3-20.

[227] J.K. Lam, W. Liang, H.K. Chan, Pulmonary delivery of therapeutic siRNA, Adv Drug Deliv Rev, 64 (2012) 1-15.

[228] N. Ernst, S. Ulrichskotter, W.A. Schmalix, J. Radler, R. Galneder, E. Mayer, S. Gersting, C. Plank, D. Reinhardt, J. Rosenecker, Interaction of liposomal and polycationic transfection complexes with pulmonary surfactant, J Gene Med, 1 (1999) 331-340.

[229] M.A. Mintzer, E.E. Simanek, Nonviral vectors for gene delivery, Chem Rev, 109 (2009) 259-302.

[230] D.W. Pack, A.S. Hoffman, S. Pun, P.S. Stayton, Design and development of polymers for gene delivery, Nat Rev Drug Discov, 4 (2005) 581-593.

[231] C.E. Thomas, A. Ehrhardt, M.A. Kay, Progress and problems with the use of viral vectors for gene therapy, Nat Rev Genet, 4 (2003) 346-358.

[232] H.M. Wallace, A.V. Fraser, Inhibitors of polyamine metabolism: review article, Amino Acids, 26 (2004) 353-365.

[233] C.W. Tabor, H. Tabor, Polyamines in microorganisms, Microbiol Rev, 49 (1985) 81-99.

[234] H. Tabor, C.W. Tabor, Spermidine, Spermine, and Related Amines, Pharmacol Rev, 16 (1964) 245-300.

[235] T. Thomas, T.J. Thomas, Polyamines in cell growth and cell death: molecular mechanisms and therapeutic applications, Cell Mol Life Sci, 58 (2001) 244-258.

[236] E.H. Szybalska, W. Szybalski, Genetics of human cell line. IV. DNA-mediated heritable transformation of a biochemical trait, Proc Natl Acad Sci U S A, 48 (1962) 2026-2034.

[237] M. Elsayed, V. Corrand, V. Kolhatkar, Y. Xie, N.H. Kim, R. Kolhatkar, O.M. Merkel, Influence of oligospermines architecture on their suitability for siRNA delivery, Biomacromolecules, 15 (2014) 1299-1310.

[238] L. Nuhn, L. Braun, I. Overhoff, A. Kelsch, D. Schaeffel, K. Koynov, R. Zentel, Degradable cationic nanohydrogel particles for stimuli-responsive release of siRNA, Macromol Rapid Commun, 35 (2014) 2057-2064.

[239] S.Y. Duan, X.M. Ge, N. Lu, F. Wu, W. Yuan, T. Jin, Synthetic polyspermine imidazole-4, 5-amide as an efficient and cytotoxicity-free gene delivery system, Int J Nanomedicine, 7 (2012) 3813-3822.

[240] S. Duan, W. Yuan, F. Wu, T. Jin, Polyspermine imidazole-4,5-imine, a chemically dynamic and biologically responsive carrier system for intracellular delivery of siRNA, Angew Chem Int Ed Engl, 51 (2012) 7938-7941.

[241] M.S. Shim, Y.J. Kwon, Dual mode polyspermine with tunable degradability for plasmid DNA and siRNA delivery, Biomaterials, 32 (2011) 4009-4020.

[242] D. Jere, J.E. Kim, R. Arote, H.L. Jiang, Y.K. Kim, Y.J. Choi, C.H. Yun, M.H. Cho, C.S. Cho, Akt1 silencing efficiencies in lung cancer cells by sh/si/ssiRNA transfection using a reductable polyspermine carrier, Biomaterials, 30 (2009) 1635-1647.

[243] Y. Shen, Q. Li, J. Tu, J. Zhu, Synthesis and characterization of low molecular weight hyaluronic acid-based cationic micelles for efficient siRNA delivery, Carbohydrate Polymers, 77 (2009) 95-104.

[244] X.B. Xiong, H. Uludag, A. Lavasanifar, Biodegradable amphiphilic poly(ethylene oxide)-block-polyesters with grafted polyamines as supramolecular nanocarriers for efficient siRNA delivery, Biomaterials, 30 (2009) 242-253.

[245] S.H. Bhang, K. Kim, W.J. Rhee, M.S. Shim, Bioreducible Polyspermine-Based Gene Carriers for Efficient siRNA Delivery: Effects of PEG Conjugation on Gene Silencing Efficiency, Macromolecular Research, 26 (2018) 1135-1142.

[246] R.L. Xie, Y.J. Jang, L. Xing, B.F. Zhang, F.Z. Wang, P.F. Cui, M.H. Cho, H.L. Jiang, A novel potential biocompatible hyperbranched polyspermine for efficient lung cancer gene therapy, Int J Pharm, 478 (2015) 19-30.

[247] Z. Du, M. Chen, Q. He, Y. Zhou, T. Jin, Polymerized spermine as a novel polycationic nucleic acid carrier system, Int J Pharm, 434 (2012) 437-443.

[248] H.L. Jiang, S.H. Hong, Y.K. Kim, M.A. Islam, H.J. Kim, Y.J. Choi, J.W. Nah, K.H. Lee, K.W. Han, C. Chae, C.S. Cho, M.H. Cho, Aerosol delivery of spermine-based poly(amino ester)/Akt1 shRNA complexes for lung cancer gene therapy, Int J Pharm, 420 (2011) 256-265.

[249] A.R. Lote, V.R. Kolhatkar, T. Insley, P. Kral, R. Kolhatkar, Oligospermines and Nucleic Acid Interaction: A Structure Property Relationship Study, ACS Macro Lett, 3 (2014) 829-833.

[250] N. Hartl, F. Adams, G. Costabile, L. Isert, M. Doblinger, X. Xiao, R. Liu, O.M. Merkel, The Impact of Nylon-3 Copolymer Composition on the Efficiency of siRNA Delivery to Glioblastoma Cells, Nanomaterials (Basel), 9 (2019).

[251] Z. Liu, Z. Zhang, C. Zhou, Y. Jiao, Hydrophobic modifications of cationic polymers for gene delivery, Progress in Polymer Science, 35 (2010) 1144-1162.

[252] M. Thomas, A.M. Klibanov, Enhancing polyethylenimine's delivery of plasmid DNA into mammalian cells, P Natl Acad Sci USA, 99 (2002) 14640-14645.

[253] A. Neamnark, O. Suwantong, R.K. Bahadur, C.Y. Hsu, P. Supaphol, H. Uludag, Aliphatic lipid substitution on 2 kDa polyethylenimine improves plasmid delivery and transgene expression, Mol Pharm, 6 (2009) 1798-1815.

[254] T.J.V. Prazeres, M. Beija, F.V. Fernandes, P.G.A. Marcelino, J.P.S. Farinha, J.M.G. Martinho, Determination of the critical micelle concentration of surfactants and amphiphilic block copolymers using coumarin 153, Inorganica Chimica Acta, 381 (2012) 181-187.

[255] G. Marcelo, T. J. V. Prazeres, M.-T. Charreyre, J.M.G. Martinho, J.P.S. Farinha, Thermoresponsive Micelles of Phenanthrene-α-end-labeled Poly(N-decylacrylamide-b-N,N-diethylacrylamide) in Water, Macromolecules, 43 (2009) 501-510.

[256] T.J.V. Prazeres, M. Beija, M.-T. Charreyre, J.P.S. Farinha, J.M.G. Martinho, RAFT polymerization and self-assembly of thermoresponsive poly(N-decylacrylamide-b-N,N-

diethylacrylamide) block copolymers bearing a phenanthrene fluorescent α-end group, Polymer, 51 (2010) 355-367.

[257] A.M. Peterson, Z. Tan, E.M. Kimbrough, J.M. Heemstra, 3,3′-Dioctadecyloxacarbocyanine perchlorate (DiO) as a fluorogenic probe for measurement of critical micelle concentration, Analytical Methods, 7 (2015) 6877-6882.

[258] P.R. Twentyman, M. Luscombe, A study of some variables in a tetrazolium dye (MTT) based assay for cell growth and chemosensitivity, Br J Cancer, 56 (1987) 279-285.

[259] O.M. Merkel, A. Beyerle, B.M. Beckmann, M. Zheng, R.K. Hartmann, T. Stoger, T.H. Kissel, Polymer-related off-target effects in non-viral siRNA delivery, Biomaterials, 32 (2011) 2388-2398.

[260] Y. Liu, D.A. Peterson, H. Kimura, D. Schubert, Mechanism of cellular 3-(4,5-dimethylthiazol-2-yl)-2,5-diphenyltetrazolium bromide (MTT) reduction, J Neurochem, 69 (1997) 581-593.

[261] O.M. Merkel, L.M. Marsh, H. Garn, T. Kissel, Flow cytometry-based cell type-specific assessment of target regulation by pulmonary siRNA delivery, Methods Mol Biol, 948 (2013) 263-273.

[262] A. Akinc, M. Thomas, A.M. Klibanov, R. Langer, Exploring polyethylenimine-mediated DNA transfection and the proton sponge hypothesis, J Gene Med, 7 (2005) 657-663.

[263] S.M. Moghimi, P. Symonds, J.C. Murray, A.C. Hunter, G. Debska, A. Szewczyk, A two-stage poly(ethylenimine)-mediated cytotoxicity: implications for gene transfer/therapy, Mol Ther, 11 (2005) 990-995.

[264] G.J.M. Koper, M. Borkovec, Proton binding by linear, branched, and hyperbranched polyelectrolytes, Polymer, 51 (2010) 5649-5662.

[265] H. Kim, H.A. Kim, Y.M. Bae, J.S. Choi, M. Lee, Dexamethasone-conjugated polyethylenimine as an efficient gene carrier with an anti-apoptotic effect to cardiomyocytes, J Gene Med, 11 (2009) 515-522.

[266] O. Gusachenko Simonova, Y. Kravchuk, D. Konevets, V. Silnikov, V.V. Vlassov, M.A. Zenkova, Transfection efficiency of 25-kDa PEI-cholesterol conjugates with different levels of modification, J Biomater Sci Polym Ed, 20 (2009) 1091-1110.

[267] R.R. Sawant, S.K. Sriraman, G. Navarro, S. Biswas, R.A. Dalvi, V.P. Torchilin, Polyethyleneimine-lipid conjugate-based pH-sensitive micellar carrier for gene delivery, Biomaterials, 33 (2012) 3942-3951.

[268] D.A. Wang, A.S. Narang, M. Kotb, A.O. Gaber, D.D. Miller, S.W. Kim, R.I. Mahato, Novel branched poly(ethylenimine)-cholesterol water-soluble lipopolymers for gene delivery, Biomacromolecules, 3 (2002) 1197-1207.

[269] L.-Y. Su, T.-Y. Fang, W.-C. Tseng, The effect of pendant hydrophobicity on the biological efficacy of polyethylenimine conjugate, Biochemical Engineering Journal, 49 (2010) 21-27.

[270] O.M. Merkel, M.A. Mintzer, D. Librizzi, O. Samsonova, T. Dicke, B. Sproat, H. Garn, P.J. Barth, E.E. Simanek, T. Kissel, Triazine dendrimers as nonviral vectors for in vitro and in vivo RNAi: the effects of peripheral groups and core structure on biological activity, Mol Pharm, 7 (2010) 969-983.

[271] T.C. Klauber, R.V. Sondergaard, R.R. Sawant, V.P. Torchilin, T.L. Andresen, Elucidating the role of free polycations in gene knockdown by siRNA polyplexes, Acta Biomater, 35 (2016) 248-259.

[272] L. Liu, M. Zheng, D. Librizzi, T. Renette, O.M. Merkel, T. Kissel, Efficient and Tumor Targeted siRNA Delivery by Polyethylenimine-graft-polycaprolactone-block-poly(ethylene glycol)-folate (PEI-PCL-PEG-Fol), Mol Pharm, 13 (2016) 134-143.

[273] G. Guo, L. Zhou, Z. Chen, W. Chi, X. Yang, W. Wang, B. Zhang, Alkane-modified low-molecular-weight polyethylenimine with enhanced gene silencing for siRNA delivery, Int J Pharm, 450 (2013) 44-52.

[274] H.M. Aliabadi, B. Landry, R.K. Bahadur, A. Neamnark, O. Suwantong, H. Uludag, Impact of lipid substitution on assembly and delivery of siRNA by cationic polymers, Macromol Biosci, 11 (2011) 662-672.

[275] W.J. Kim, C.W. Chang, M. Lee, S.W. Kim, Efficient siRNA delivery using water soluble lipopolymer for anti-angiogenic gene therapy, J Control Release, 118 (2007) 357-363.

[276] A. Alshamsan, A. Haddadi, V. Incani, J. Samuel, A. Lavasanifar, H. Uludag, Formulation and delivery of siRNA by oleic acid and stearic acid modified polyethylenimine, Mol Pharm, 6 (2009) 121-133.

[277] J. Chen, H. Tian, Z. Guo, J. Xia, A. Kano, A. Maruyama, X. Jing, X. Chen, A highly efficient siRNA carrier of PBLG modified hyperbranched PEI, Macromol Biosci, 9 (2009) 1247-1253.

[278] N. Hartl, F. Adams, G. Costabile, L. Isert, M. Döblinger, X. Xiao, R. Liu, M.O. Merkel, The Impact of Nylon-3 Copolymer Composition on the Efficiency of siRNA Delivery to Glioblastoma Cells, Nanomaterials, 9 (2019).

[279] D.P. Feldmann, Y. Cheng, R. Kandil, Y. Xie, M. Mohammadi, H. Harz, A. Sharma, D.J. Peeler, A. Moszczynska, H. Leonhardt, S.H. Pun, O.M. Merkel, In vitro and in vivo delivery of siRNA via VIPER polymer system to lung cells, J. Control. Release, 276 (2018) 50-58.

[280] D. Baldassi, S. Ambike, M. Feuerherd, C.C. Cheng, D.J. Peeler, D.P. Feldmann, D.L. Porras-Gonzalez, X. Wei, L.A. Keller, N. Kneidinger, M.G. Stoleriu, A. Popp, G. Burgstaller, S.H. Pun, T. Michler, O.M. Merkel, Inhibition of SARS-CoV-2 replication in the lung with siRNA/VIPER polyplexes, J Control Release, 345 (2022) 661-674.

[281] R. Scherliess, The MTT assay as tool to evaluate and compare excipient toxicity in vitro on respiratory epithelial cells, Int J Pharm, 411 (2011) 98-105.

[282] Z. Guo, H. Tian, L. Lin, J. Chen, C. He, Z. Tang, X. Chen, Hydrophobic polyalanine modified hyperbranched polyethylenimine as high efficient pDNA and siRNA carrier, Macromol Biosci, 14 (2014) 1406-1414.

[283] B.D. Monnery, M. Wright, R. Cavill, R. Hoogenboom, S. Shaunak, J.H.G. Steinke, M. Thanou, Cytotoxicity of polycations: Relationship of molecular weight and the hydrolytic theory of the mechanism of toxicity, Int J Pharm, 521 (2017) 249-258.

[284] A. Beyerle, A. Braun, O. Merkel, F. Koch, T. Kissel, T. Stoeger, Comparative in vivo study of poly(ethylene imine)/siRNA complexes for pulmonary delivery in mice, J Control Release, 151 (2011) 51-56.

[285] M.E. Davis, J.E. Zuckerman, C.H. Choi, D. Seligson, A. Tolcher, C.A. Alabi, Y. Yen, J.D. Heidel, A. Ribas, Evidence of RNAi in humans from systemically administered siRNA via targeted nanoparticles, Nature, 464 (2010) 1067-1070.

[286] Y. Liu, O. Samsonova, B. Sproat, O. Merkel, T. Kissel, Biophysical characterization of hyper-branched polyethylenimine-graft-polycaprolactone-block-mono-methoxyl-poly(ethylene glycol) copolymers (hy-PEI-PCL-mPEG) for siRNA delivery, J Control Release, 153 (2011) 262-268.

[287] T.W.M. Keil, D. Baldassi, O.M. Merkel, T-cell targeted pulmonary siRNA delivery for the treatment of asthma, Wiley Interdiscip Rev Nanomed Nanobiotechnol, 12 (2020) e1634.

[288] D.P. Feldmann, S. Jones, K. Douglas, A.F. Shields, O.M. Merkel, Microfluidic Assembly of siRNA-Loaded Micelleplexes for Tumor Targeting in an Orthotopic Model of Ovarian Cancer, Methods Mol Biol, 1974 (2019) 355-369.

[289] C. Tros de Ilarduya, Y. Sun, N. Duzgunes, Gene delivery by lipoplexes and polyplexes, Eur J Pharm Sci, 40 (2010) 159-170.

[290] D.E. Owens, 3rd, N.A. Peppas, Opsonization, biodistribution, and pharmacokinetics of polymeric nanoparticles, Int J Pharm, 307 (2006) 93-102.

[291] H. Otsuka, Y. Nagasaki, K. Kataoka, PEGylated nanoparticles for biological and pharmaceutical applications, Advanced Drug Delivery Reviews, 55 (2003) 403-419.

[292] E. Samaridou, J. Heyes, P. Lutwyche, Lipid nanoparticles for nucleic acid delivery: Current perspectives, Adv Drug Deliv Rev, (2020).

[293] R. Tenchov, R. Bird, A.E. Curtze, Q. Zhou, Lipid Nanoparticles-From Liposomes to mRNA Vaccine Delivery, a Landscape of Research Diversity and Advancement, ACS Nano, (2021).

[294] C.D. Siewert, H. Haas, V. Cornet, S.S. Nogueira, T. Nawroth, L. Uebbing, A. Ziller, J. Al-Gousous, A. Radulescu, M.A. Schroer, C.E. Blanchet, D.I. Svergun, M.P. Radsak, U. Sahin, P. Langguth, Hybrid Biopolymer and Lipid Nanoparticles with Improved Transfection Efficacy for mRNA, Cells, 9 (2020).

[295] P. Garcia-Garcia, E. Briffault, M. Landin, C. Evora, P. Diaz-Rodriguez, A. Delgado, Tailor-made oligonucleotide-loaded lipid-polymer nanosystems designed for bone gene therapy, Drug Deliv Transl Res, 11 (2021) 598-607.

[296] M.A. Maier, M. Jayaraman, S. Matsuda, J. Liu, S. Barros, W. Querbes, Y.K. Tam, S.M. Ansell, V. Kumar, J. Qin, X. Zhang, Q. Wang, S. Panesar, R. Hutabarat, M. Carioto, J. Hettinger, P. Kandasamy, D. Butler, K.G. Rajeev, B. Pang, K. Charisse, K. Fitzgerald, B.L. Mui, X. Du, P. Cullis, T.D. Madden, M.J. Hope, M. Manoharan, A. Akinc, Biodegradable lipids enabling rapidly eliminated lipid nanoparticles for systemic delivery of RNAi therapeutics, Mol Ther, 21 (2013) 1570-1578.

[297] J.A. Kulkarni, D. Witzigmann, J. Leung, Y.Y.C. Tam, P.R. Cullis, On the role of helper lipids in lipid nanoparticle formulations of siRNA, Nanoscale, (2019) 1-7.

[298] S.S. Aboelela, M. Ibrahim, A.Z.M. Badruddoza, V. Tran, J.K. Ferri, T.D. Roper, Encapsulation of a highly hydrophilic drug in polymeric particles: A comparative study of batch and microfluidic processes, Int J Pharm, 606 (2021) 120906.

[299] A. Mukherjee, A.K. Waters, P. Kalyan, A.S. Achrol, S. Kesari, V.M. Yenugonda, Lipid-polymer hybrid nanoparticles as a next-generation drug delivery platform: state of the art, emerging technologies, and perspectives, Int J Nanomedicine, 14 (2019) 1937-1952.

[300] Y. Liu, G. Yang, Y. Hui, S. Ranaweera, C.X. Zhao, Microfluidic Nanoparticles for Drug Delivery, Small, 18 (2022) e2106580.

[301] G.H. Zhu, A.B.C. Gray, H.K. Patra, Nanomedicine: controlling nanoparticle clearance for translational success, Trends Pharmacol Sci, 43 (2022) 709-711.

[302] S.K. Jones, V. Lizzio, O.M. Merkel, Folate Receptor Targeted Delivery of siRNA and Paclitaxel to Ovarian Cancer Cells via Folate Conjugated Triblock Copolymer to Overcome TLR4 Driven Chemotherapy Resistance, Biomacromolecules, 17 (2016) 76-87.

[303] C.M. Zimmermann, D. Baldassi, K. Chan, N.B.P. Adams, A. Neumann, D.L. Porras-Gonzalez, X. Wei, N. Kneidinger, M.G. Stoleriu, G. Burgstaller, D. Witzigmann, P. Luciani, O.M. Merkel, Spray drying siRNA-lipid nanoparticles for dry powder pulmonary delivery, J Control Release, 351 (2022) 137-150.

[304] G. Costabile, K.I. Gasteyer, V. Nadithe, K. Van Denburgh, Q. Lin, S. Sharma, J.J. Reineke, S.M. Firestine, O.M. Merkel, Physicochemical and In Vitro Evaluation of Drug Delivery of an Antibacterial Synthetic Benzophenone in Biodegradable PLGA Nanoparticles, AAPS PharmSciTech, 19 (2018) 3561-3570.

[305] S.A.A. Rizvi, A.M. Saleh, Applications of nanoparticle systems in drug delivery technology, Saudi Pharm J, 26 (2018) 64-70.

[306] A.J. Shnoudeh, I. Hamad, R.W. Abdo, L. Qadumii, A.Y. Jaber, H.S. Surchi, S.Z. Alkelany, Synthesis, Characterization, and Applications of Metal Nanoparticles, in: Biomaterials and Bionanotechnology, 2019, pp. 527-612.

[307] D. Dey, S. Kumar, R. Banerjee, S. Maiti, D. Dhara, Polyplex formation between PEGylated linear cationic block copolymers and DNA: equilibrium and kinetic studies, J Phys Chem B, 118 (2014) 7012-7025.

[308] L. statistics, Pearson Product-Moment Correlation, https://statistics.laerd.com/statistical-guides/pearson-correlation-coefficient-statistical-guide.php, (2022).

[309] T. Patino, J. Soriano, L. Barrios, E. Ibanez, C. Nogues, Surface modification of microparticles causes differential uptake responses in normal and tumoral human breast epithelial cells, Sci Rep, 5 (2015) 11371.

[310] W.-d. Tian, Y.-q. Ma, Insights into the endosomal escape mechanism via investigation of dendrimer–membrane interactions, Soft Matter, 8 (2012).

[311] M. Hajimolaali, H. Mohammadian, A. Torabi, A. Shirini, M. Khalife Shal, H. Barazandeh Nezhad, S. Iranpour, R. Baradaran Eftekhari, F. Dorkoosh, Application of chloroquine as an endosomal escape enhancing agent: new frontiers for an old drug, Expert Opin Drug Deliv, 18 (2021) 877-889.

[312] L. Schoenmaker, D. Witzigmann, J.A. Kulkarni, R. Verbeke, G. Kersten, W. Jiskoot, D.J.A. Crommelin, mRNA-lipid nanoparticle COVID-19 vaccines: Structure and stability, Int J Pharm, 601 (2021) 120586.

[313] A. Akinc, M.A. Maier, M. Manoharan, K. Fitzgerald, M. Jayaraman, S. Barros, S. Ansell, X. Du, M.J. Hope, T.D. Madden, B.L. Mui, S.C. Semple, Y.K. Tam, M. Ciufolini, D. Witzigmann, J.A. Kulkarni, R. van der Meel, P.R. Cullis, The Onpattro story and the clinical translation of nanomedicines containing nucleic acid-based drugs, Nat Nanotechnol, 14 (2019) 1084-1087.

[314] M. Jayaraman, S.M. Ansell, B.L. Mui, Y.K. Tam, J. Chen, X. Du, D. Butler, L. Eltepu, S. Matsuda, J.K. Narayanannair, K.G. Rajeev, I.M. Hafez, A. Akinc, M.A. Maier, M.A. Tracy, P.R. Cullis, T.D. Madden, M. Manoharan, M.J. Hope, Maximizing the potency of siRNA lipid nanoparticles for hepatic gene silencing in vivo, Angew Chem Int Ed Engl, 51 (2012) 8529-8533.

[315] M. Schlich, R. Palomba, G. Costabile, S. Mizrahy, M. Pannuzzo, D. Peer, P. Decuzzi, Cytosolic delivery of nucleic acids: The case of ionizable lipid nanoparticles, Bioeng Transl Med, 6 (2021) e10213.

[316] E.R. Society, The Global Impact of Respiratory Disease, https://www.who.int/gard/publications/The_Global_Impact_of_Respiratory_Disease.pdf, (2017).

[317] W.W. Labaki, M.K. Han, Chronic respiratory diseases: a global view, Lancet Respir Med, 8 (2020) 531-533.

[318] J.E. Michalski, J.S. Kurche, D.A. Schwartz, From ARDS to pulmonary fibrosis: the next phase of the COVID-19 pandemic?, Transl Res, 241 (2022) 13-24.

[319] M. Agnoletti, A. Bohr, K. Thanki, F. Wan, X. Zeng, J.P. Boetker, M. Yang, C. Foged, Inhalable siRNA-loaded nano-embedded microparticles engineered using microfluidics and spray drying, Eur J Pharm Biopharm, 120 (2017) 9-21.

[320] M. Choi, J. Gu, M. Lee, T. Rhim, A new combination therapy for asthma using dual-function dexamethasone-conjugated polyethylenimine and vitamin D binding protein siRNA, Gene Ther, 24 (2017) 727-734.

[321] T.W.M. Keil, D. Baldassi, O.M. Merkel, T-cell targeted pulmonary siRNA delivery for the treatment of asthma, Wiley Interdiscip Rev Nanomed Nanobiotechnol, 12 (2020) 1-11.

[322] L.D. Kumar, A.R. Clarke, Gene manipulation through the use of small interfering RNA (siRNA): from in vitro to in vivo applications, Adv Drug Deliv Rev, 59 (2007) 87-100.

[323] C. Sheridan, A reprieve from hemophilia A, but for how long?, Nat Biotechnol, 38 (2020) 1107-1109.

[324] S. Ambike, C.-C. Cheng, S. Afridi, M. Feuerherd, P. Hagen, V. Grass, O. Merkel, A. Pichlmair, C. Ko, T. Michler, Systematic analysis of RNAi-accessible SARS-CoV2 replication steps identifies ORF1 as promising targets, Res Squ, (2020) 1-23.

[325] R. Kandil, O.M. Merkel, Pulmonary delivery of siRNA as a novel treatment for lung diseases, Ther Deliv, 10 (2019) 203-206.

[326] P. Hofemeier, J. Sznitman, Revisiting pulmonary acinar particle transport: convection, sedimentation, diffusion, and their interplay, J Appl Physiol, 118 (2015) 1375-1385.

[327] M. Bassetti, A. Vena, A. Russo, M. Peghin, Inhaled Liposomal Antimicrobial Delivery in Lung Infections, Drugs, 80 (2020) 1309-1318.

[328] L.R. Baden, H.M. El Sahly, B. Essink, K. Kotloff, S. Frey, R. Novak, D. Diemert, S.A. Spector, N. Rouphael, C.B. Creech, J. McGettigan, S. Khetan, N. Segall, J. Solis, A. Brosz, C. Fierro, H. Schwartz, K. Neuzil, L. Corey, P. Gilbert, H. Janes, D. Follmann, M. Marovich, J. Mascola, L. Polakowski, J. Ledgerwood, B.S. Graham, H. Bennett, R. Pajon, C. Knightly, B. Leav, W. Deng, H. Zhou, S. Han, M. Ivarsson, J. Miller, T. Zaks, C.S. Group, Efficacy and Safety of the mRNA-1273 SARS-CoV-2 Vaccine, N Engl J Med, 384 (2021) 403-416.

[329] S.C. Semple, A. Akinc, J. Chen, A.P. Sandhu, B.L. Mui, C.K. Cho, D.W. Sah, D. Stebbing, E.J. Crosley, E. Yaworski, I.M. Hafez, J.R. Dorkin, J. Qin, K. Lam, K.G. Rajeev, K.F. Wong, L.B. Jeffs, L. Nechev, M.L. Eisenhardt, M. Jayaraman, M. Kazem, M.A. Maier, M. Srinivasulu, M.J. Weinstein, Q. Chen, R. Alvarez, S.A. Barros, S. De, S.K. Klimuk, T. Borland, V. Kosovrasti, W.L. Cantley, Y.K. Tam, M. Manoharan, M.A. Ciufolini, M.A. Tracy, A. de Fougerolles, I. MacLachlan, P.R. Cullis, T.D. Madden, M.J. Hope, Rational design of cationic lipids for siRNA delivery, Nat Biotechnol, 28 (2010) 172-176.

[330] R. van der Meel, S. Chen, J. Zaifman, J.A. Kulkarni, X.R.S. Zhang, Y.K. Tam, M.B. Bally, R.M. Schiffelers, M.A. Ciufolini, P.R. Cullis, Y.Y.C. Tam, Modular Lipid Nanoparticle Platform Technology for siRNA and Lipophilic Prodrug Delivery, Small, 17 (2021) 1-12.

[331] S.A. Cryan, N. Sivadas, L. Garcia-Contreras, In vivo animal models for drug delivery across the lung mucosal barrier, Adv Drug Deliv Rev, 59 (2007) 1133-1151.

[332] N. Durcan, C. Murphy, S.A. Cryan, Inhalable siRNA: Potential as a therapeutic agent in the lungs, Mol Pharm, 5 (2008) 559-566.

[333] U.S.D.o.H.a.H.S.F.a.D. Administration, Metered Dose Inhaler (MDI) and Dry Powder Inhaler (DPI) Products Quality Considerations Guidance for Industry, Pharmaceutical Quality/CMC, (2018) 1-50.

[334] E.M. Agency, Bronchitol, (2012) 1-126.

[335] T.W.M. Keil, D.P. Feldmann, G. Costabile, Q. Zhong, S. da Rocha, O.M. Merkel, Characterization of spray dried powders with nucleic acid-containing PEI nanoparticles, Eur J Pharm Biopharm, 143 (2019) 61-69.

[336] M. Odziomek, T.R. Sosnowski, L. Gradon, Conception, preparation and properties of functional carrier particles for pulmonary drug delivery, Int J Pharm, 433 (2012) 51-59.

[337] Y. Eygeris, S. Patel, A. Jozic, G. Sahay, Deconvoluting Lipid Nanoparticle Structure for Messenger RNA Delivery, Nano Lett, 20 (2020) 4543-4549.

[338] Y. Xu, A. Thakur, Y. Zhang, C. Foged, Inhaled RNA Therapeutics for Obstructive Airway Diseases: Recent Advances and Future Prospects, Pharmaceutics, 13 (2021) 1-35.

[339] C.M.C.F.M.L. (CA), SULFUR-CONTAINING LIPIDS, in: U.B.C. (CA) (Ed.), 2022.

[340] C. Walsh, K. Ou, N.M. Belliveau, T.J. Leaver, A.W. Wild, J. Huft, P.J. Lin, S. Chen, A.K. Leung, J.B. Lee, C.L. Hansen, R.J. Taylor, E.C. Ramsay, P.R. Cullis, Microfluidic-based manufacture of siRNA-lipid nanoparticles for therapeutic applications, Methods Mol Biol, 1141 (2014) 109-120.

[341] B. Casciaro, I. d'Angelo, X. Zhang, M.R. Loffredo, G. Conte, F. Cappiello, F. Quaglia, Y.P. Di, F. Ungaro, M.L. Mangoni, Poly(lactide- co-glycolide) Nanoparticles for Prolonged Therapeutic Efficacy of Esculentin-1a-Derived Antimicrobial Peptides against Pseudomonas aeruginosa Lung Infection: in Vitro and in Vivo Studies, Biomacromolecules, 20 (2019) 1876-1888.

[342] O.R. Moss, Simulants of lung interstitial fluid, Health Phys., 36 (1979) 447−448.

[343] M. Gerckens, H.N. Alsafadi, D.E. Wagner, M. Lindner, G. Burgstaller, M. Konigshoff, Generation of Human 3D Lung Tissue Cultures (3D-LTCs) for Disease Modeling, J Vis Exp, 144 (2019) 1-8.

[344] H.N. Alsafadi, C.A. Staab-Weijnitz, M. Lehmann, M. Lindner, B. Peschel, M. Konigshoff, D.E. Wagner, An ex vivo model to induce early fibrosis-like changes in human precision-cut lung slices, Am J Physiol Lung Cell Mol Physiol, 312 (2017) L896-L902.

[345] S. Ambike, C.-C. Cheng, M. Feuerherd, S. Velkov, D. Baldassi, S.Q. Afridi, D. Porras-Gonzalez, X. Wei, P. Hagen, N. Kneidinger, Mircea G. Stoleriu, V. Grass, G. Burgstaller, A. Pichlmair, Olivia M. Merkel, C. Ko, T. Michler, Targeting genomic SARS-CoV-2 RNA with siRNAs allows efficient inhibition of viral replication and spread, Nucleic Acids Res, (2021) 1-17.

[346] A.P. Lipids, Phase Transition Temperatures for Glycerophospholipids, https://avantilipids.com/tech-support/physical-properties/phase-transition-temps, (2022).

[347] M.K.H.a.Y.H. Roos, Water Plasticization and Crystallization of Lactose in Spray-dried Lactose/Protein Mixtures, J Food Sci, 69 (2008) 23-29.

[348] M. Maury, K. Murphy, S. Kumar, L. Shi, G. Lee, Effects of process variables on the powder yield of spray-dried trehalose on a laboratory spray-dryer, Eur J Pharm Biopharm, 59 (2005) 565-573.

[349] M. Adler, G. Lee, Stability and Surface Activity of Lactate Dehydrogenase in Spray-Dried Trehalose, J Pharm Sci, 88 (1998) 199-208.

[350] C. Freitas, R.H. Müller, Spray-drying of solid lipid nanoparticles (SLNTM), Eur J Pharm Biopharm, 46 (1998) 145–151.

[351] D. Weinbuch, J.K. Cheung, J. Ketelaars, V. Filipe, A. Hawe, J. den Engelsman, W. Jiskoot, Nanoparticulate Impurities in Pharmaceutical-Grade Sugars and their Interference with Light Scattering-Based Analysis of Protein Formulations, Pharm Res, 32 (2015) 2419-2427.

[352] B. AG, Sprühtrocknungs- & Verkapselungslösungen, Partikelerzeugung im Labormassstab, https://assets.buchi.com/image/upload/v1629464620/pdf/Brochures/SB_11592838_Spray_Drying_Encapsulation_de.pdf, (2022).

[353] M. Munir, L. Jena, V.L. Kett, N.J. Dunne, H.O. McCarthy, Spray drying: Inhalable powders for pulmonary gene therapy, Mater Sci Eng C, (2021) 1-14.

[354] O.C. Chidavaenzi, G. Buckton, F. Koosha, R. Pathak, The use of thermal techniques to assess the impact of feed concentration on the amorphous content and polymorphic forms present in spray dried lactose, Int J Pharm, 159 (1997) 67-74.

[355] L. Wu, X. Miao, Z. Shan, Y. Huang, L. Li, X. Pan, Q. Yao, G. Li, C. Wu, Studies on the spray dried lactose as carrier for dry powder inhalation, Asian J Pharm Sci, 9 (2014) 336-341.

[356] M.K. Haque, Y.H. Roos, Differences in the physical state and thermal behavior of spray-dried and freeze-dried lactose and lactose/protein mixtures, Innovative Food Science & Emerging Technologies, 7 (2006) 62-73.

[357] K.J. Geh, M. Hubert, G. Winter, Progress in formulation development and sterilisation of freeze-dried oligodeoxynucleotide-loaded gelatine nanoparticles, Eur J Pharm Biopharm, 129 (2018) 10-20.

[358] G.Z. Evgenyi Y. Shalaev, How Does Residual Water Affect the Solid-State Degradation of Drugs in the Amorphous State?, J Pharm Sci, 85 (1996) 1137-1141.

[359] L.T.G. Pieter Zanen, Jan-Willem J Lammers, Optimal particle size for b2 agonist and anticholinergic aerosols in patients with severe airflow obstruction, Thorax, 51 (1996) 977-980.

[360] J.S. Patton, Mechanisms of macromolecule absorption by the lungs, Adv Drug Deliv Rev, 19 (1996) 3-36.

[361] N.R. Labiris, M.B. Dolovich, Pulmonary drug delivery. Part I: physiological factors affecting therapeutic effectiveness of aerosolized medications, Br J Clin Pharmacol, 56 (2003) 588-599.

[362] I. Gonda, A.F. Abd El Khalik, On the Calculation of Aerodynamic Diameters of Fibers, Aerosol Science and Technology, 4 (2011) 233-238.

[363] G. Conte, G. Costabile, D. Baldassi, V. Rondelli, R. Bassi, D. Colombo, G. Linardos, E.V. Fiscarelli, R. Sorrentino, A. Miro, F. Quaglia, P. Brocca, I. d'Angelo, O.M. Merkel, F. Ungaro, Hybrid

Lipid/Polymer Nanoparticles to Tackle the Cystic Fibrosis Mucus Barrier in siRNA Delivery to the Lungs: Does PEGylation Make the Difference?, ACS Appl Mater Interfaces, 14 (2022) 7565-7578.

[364] M. Mahmoudi, I. Lynch, M.R. Ejtehadi, M.P. Monopoli, F.B. Bombelli, S. Laurent, Protein-nanoparticle interactions: opportunities and challenges, Chem Rev, 111 (2011) 5610-5637.

[365] Y. Sato, H. Hatakeyama, Y. Sakurai, M. Hyodo, H. Akita, H. Harashima, A pH-sensitive cationic lipid facilitates the delivery of liposomal siRNA and gene silencing activity in vitro and in vivo, J Control Release, 163 (2012) 267-276.

[366] D.K. Jensen, L.B. Jensen, S. Koocheki, L. Bengtson, D. Cun, H.M. Nielsen, C. Foged, Design of an inhalable dry powder formulation of DOTAP-modified PLGA nanoparticles loaded with siRNA, J Control Release, 157 (2012) 141-148.

[367] L.A.S. Shrirang Karve; Frank DeRosa; Michael Heartlein; Zarna Patel Dry powder formulations for messenger RNA, United States Patent Application Publication, US 2020/0022921A1 (2020) 1-66.

[368] A. Nagy, A. Steinbruck, J. Gao, N. Doggett, J.A. Hollingsworth, R. Iyer, Comprehensive analysis of the effects of CdSe quantum dot size, surface charge, and functionalization on primary human lung cells, ACS Nano, 6 (2012) 4748-4762.

[369] O. Danov, L. Lasswitz, H. Obernolte, C. Hesse, A. Braun, S. Wronski, K. Sewald, Rupintrivir reduces RV-induced TH-2 cytokine IL-4 in precision-cut lung slices (PCLS) of HDM-sensitized mice ex vivo, Respir Res, 20 (2019) 1-9.

[370] F.E. Uhl, S. Vierkotten, D.E. Wagner, G. Burgstaller, R. Costa, I. Koch, M. Lindner, S. Meiners, O. Eickelberg, M. Konigshoff, Preclinical validation and imaging of Wnt-induced repair in human 3D lung tissue cultures, Eur Respir J, 46 (2015) 1150-1166.

[371] H. Maarsingh, C.M. Bidan, B.S. Brook, A.B. Zuidhof, C.R.S. Elzinga, M. Smit, A. Oldenburger, R. Gosens, W. Timens, H. Meurs, Small airway hyperresponsiveness in COPD: relationship between structure and function in lung slices, Am J Physiol Lung Cell Mol Physiol, 316 (2019) L537-L546.

[372] P.F. Mercer, H.V. Woodcock, J.D. Eley, M. Plate, M.G. Sulikowski, P.F. Durrenberger, L. Franklin, C.B. Nanthakumar, Y. Man, F. Genovese, R.J. McAnulty, S. Yang, T.M. Maher, A.G. Nicholson, A.D. Blanchard, R.P. Marshall, P.T. Lukey, R.C. Chambers, Exploration of a potent PI3 kinase/mTOR inhibitor as a novel anti-fibrotic agent in IPF, Thorax, 71 (2016) 701-711.

[373] M.C. Rosales Gerpe, J.P. van Vloten, L.A. Santry, J. de Jong, R.C. Mould, A. Pelin, J.C. Bell, B.W. Bridle, S.K. Wootton, Use of Precision-Cut Lung Slices as an Ex Vivo Tool for Evaluating Viruses and Viral Vectors for Gene and Oncolytic Therapy, Mol Ther Methods Clin Dev, 10 (2018) 245-256.

[374] G. Liu, C. Betts, D.M. Cunoosamy, P.M. Aberg, J.J. Hornberg, K.B. Sivars, T.S. Cohen, Use of precision cut lung slices as a translational model for the study of lung biology, Respir Res, 20 (2019) 1-14.

[375] F. Viana, C.M. O'Kane, G.N. Schroeder, Precision-cut lung slices: A powerful ex vivo model to investigate respiratory infectious diseases, Mol Microbiol, (2021) 1-11.

[376] M.J.R. Ruigrok, J.L. Xian, H.W. Frijlink, B.N. Melgert, W.L.J. Hinrichs, P. Olinga, siRNA-mediated protein knockdown in precision-cut lung slices, Eur J Pharm Biopharm, 133 (2018) 339-348.

[377] J.A. Kulkarni, D. Witzigmann, S.B. Thomson, S. Chen, B.R. Leavitt, P.R. Cullis, R. van der Meel, The current landscape of nucleic acid therapeutics, Nat Nanotechnol, 16 (2021) 630-643.

[378] B. Wire, Alnylam Announces Approval of GIVLAARI (givosiran) by the U.S. Food and Drug Administration (FDA, (2019) 1-6.

[379] J. Kim, Y. Eygeris, M. Gupta, G. Sahay, Self-assembled mRNA vaccines, Adv Drug Deliv Rev, 170 (2021) 83-112.

[380] M.N. Uddin, M.A. Roni, Challenges of Storage and Stability of mRNA-Based COVID-19 Vaccines, Vaccines (Basel), 9 (2021).

[381] M.R. Holm, G.A. Poland, Critical aspects of packaging, storage, preparation, and administration of mRNA and adenovirus-vectored COVID-19 vaccines for optimal efficacy, Vaccine, 39 (2021) 457-459.

[382] D.J.A. Crommelin, T.J. Anchordoquy, D.B. Volkin, W. Jiskoot, E. Mastrobattista, Addressing the Cold Reality of mRNA Vaccine Stability, J Pharm Sci, 110 (2021) 997-1001.

[383] Z. Kis, Stability Modelling of mRNA Vaccine Quality Based on Temperature Monitoring throughout the Distribution Chain, Pharmaceutics, 14 (2022).

[384] EMA, Onpattro - Product information, (2022) 1-31.

[385] R.L. Ball, P. Bajaj, K.A. Whitehead, Achieving long-term stability of lipid nanoparticles: examining the effect of pH, temperature, and lyophilization, Int J Nanomedicine, 12 (2017) 305-315.

[386] Y. Suzuki, K. Hyodo, Y. Tanaka, H. Ishihara, siRNA-lipid nanoparticles with long-term storage stability facilitate potent gene-silencing in vivo, J Control Release, 220 (2015) 44-50.

[387] D. Shirane, H. Tanaka, Y. Nakai, H. Yoshioka, H. Akita, Development of an Alcohol Dilution-Lyophilization Method for Preparing Lipid Nanoparticles Containing Encapsulated siRNA, Biol Pharm Bull, 41 (2018) 1291-1294.

[388] S. Ramachandran, S.R. Satapathy, T. Dutta, Delivery Strategies for mRNA Vaccines, Pharmaceut Med, 36 (2022) 11-20.

[389] H. Salminen, J. Ankenbrand, B. Zeeb, G. Badolato Bonisch, C. Schafer, R. Kohlus, J. Weiss, Influence of spray drying on the stability of food-grade solid lipid nanoparticles, Food Res Int, 119 (2019) 741-750.

[390] C. Dormenval, A. Lokras, G. Cano-Garcia, A. Wadhwa, K. Thanki, F. Rose, A. Thakur, H. Franzyk, C. Foged, Identification of Factors of Importance for Spray Drying of Small Interfering RNA-Loaded Lipidoid-Polymer Hybrid Nanoparticles for Inhalation, Pharm Res, 36 (2019) 142.

[391] M. Ciufolini, M.L. Ferguson, Sulfur-containing lipids, in: T.U.o.B. Columbia (Ed.), Canada, 2021.

[392] O.M. Merkel, A. Beyerle, B.M. Beckmann, M. Zheng, R.K. Hartmann, T. Stöger, T.H. Kissel, Polymer-related off-target effects in non-viral siRNA delivery, Biomaterials, 32 (2011) 2388-2398.

[393] P.R. Twentyman, M. Luscombe, A study of some variables in a tetrazolium dye (MTT) based assay for cell growth and chemosensitivity, British journal of cancer, 56 (1987) 279-285.

[394] M. Fineman, S.D. Ross, Linear method for determining monomer reactivity ratios in copolymerization, Journal of Polymer Science, 5 (1950) 259-262.

[395] J.C. Lai, T. Rounsfell, C.U. Pittman, Free-radical homopolymerization and copolymerization of vinylferrocene, Journal of Polymer Science Part A-1: Polymer Chemistry, 9 (1971) 651-662.

[396] S. Sharma, K.C. Basavaraju, A.K. Singh, D.P. Kim, Continuous recycling of homogeneous Pd/Cu catalysts for cross-coupling reactions, Org Lett, 16 (2014) 3974-3977.

[397] A.J. Geall, I.S. Blagbrough, Rapid and sensitive ethidium bromide fluorescence quenching assay of polyamine conjugate-DNA interactions for the analysis of lipoplex formation in gene therapy, J Pharm Biomed Anal, 22 (2000) 849-859.